

A CRYSTAL ENGINEERING APPROACH FOR THE DESIGN OF MULTICOMPONENT
CRYSTALS AND ASSEMBLY OF NANO-SCALE ARCHITECTURES

by

EVAN PATRICK HURLEY

BS, Hobart College, 2004
MS, University of Nebraska-Lincoln, 2007

AN ABSTRACT OF A DISSERTATION

submitted in partial fulfillment of the requirements for the degree

DOCTOR OF PHILOSOPHY

Department of Chemistry
College of Arts and Sciences

KANSAS STATE UNIVERSITY
Manhattan, Kansas

2013

Abstract

The work presented in this thesis has demonstrated that supramolecular synthons can be used to make multicomponent crystals, and various synthons can be combined to make supermolecules. The synthons can also be used to construct nanoscale assemblies.

Molecules containing single and multiple hydrogen-bond (HB) and halogen-bond (XB) acceptor sites have been synthesized in an effort to carry out supramolecular synthesis in order to establish a reliable hierarchy for intermolecular interactions. Pyrazole-based molecules have been made, combined with various carboxylic acids, and characterized using infrared (IR) spectroscopy to give a success rate of 55-70%. Reactions that gave a positive result were converted to solution experiments, and crystals were grown and characterized using single-crystal X-ray diffraction (XRD). The co-crystals display infinite 1-D chains with the intended stoichiometry and structural landscape on 6/6 occasions. The salts, on the other hand, display unpredictable stoichiometry and structural landscape on 5/5 occasions. Furthermore, the electrostatic charge on the primary hydrogen-bond acceptor, N(pyz), can be altered by adding a nitro, R-NO₂, covalent handle to the backbone of the pyrazole molecule. Addition of a strongly electron withdrawing group significantly lowered the charge on the pyrazole nitrogen atom and, in turn, lowered the supramolecular yield to 10%.

Ditopic molecules containing pyrazole and pyridine on the same molecular backbone were synthesized and characterized using ¹H NMR. The molecules were co-crystallized with carboxylic acids, and the resulting solids were characterized using IR spectroscopy. The solids could then be classified as co-crystal or salt using specific markers in the IR spectrum. Single-crystal XRD was used to observe the intermolecular interactions in the co-crystals and salts, and the co-crystals were assigned to two groups: Group 1 (2) and Group 2 (2). The salts (4) show more unpredictability with stoichiometry and structural landscape.

A library of ditopic molecules containing triazole and pyridine acceptor sites were synthesized and characterized using ¹H and ¹³C NMR. The molecules were co-crystallized with carboxylic acids and the resulting solids were characterized using IR spectroscopy which demonstrated a 100% supramolecular yield whenever a pyridine moiety was present, consistent with results from Chapter 3. Single-crystal XRD was used to identify the intermolecular

interactions in the co-crystals (2) and salt (1), and the results show that triazole can compete with pyridine for hydrogen bond donors.

A library of ditopic molecules was also used for halogen-bonding (XB) studies with a series of activated iodine and bromine-based donors. The results show that iodine donors have a higher success rate range (12.5-75%) compared to bromine donors (16.7-50%) based on results obtained from IR spectra. Furthermore, the results from the XRD show that pyrazole nitrogen atoms can compete with pyridine for forming XB, and two groups of supramolecular synthons were observed.

Finally, relatively weak non-covalent interactions, HB and XB, can influence the assembly of nanoparticles based on IR spectroscopy and TEM images. The assembly of the particles is influenced by specific capping ligands, which were synthesized and characterized using ^1H , ^{13}C and ^{19}F NMR. The results demonstrate that relatively weak non-covalent interactions based on HB and XB interactions can influence nanoparticle assembly.

A CRYSTAL ENGINEERING APPROACH FOR THE DESIGN OF ORGANIC CO-
CRYSTALS AND NANO-SCALE ARCHITECTURES

by

EVAN PATRICK HURLEY

BS, Hobart College, 2004
MS, University of Nebraska-Lincoln, 2007

A DISSERTATION

submitted in partial fulfillment of the requirements for the degree

DOCTOR OF PHILOSOPHY

Department of Chemistry
College of Arts and Sciences

KANSAS STATE UNIVERSITY
Manhattan, Kansas

2013

Approved by:

Major Professor
Christer B. Aakeröy

Abstract

The work presented in this thesis has demonstrated that supramolecular synthons can be used to make multicomponent crystals, and various synthons can be combined to make supermolecules. The synthons can also be used to construct nanoscale assemblies.

Molecules containing single and multiple hydrogen-bond (HB) and halogen-bond (XB) acceptor sites have been synthesized in an effort to carry out supramolecular synthesis in order to establish a reliable hierarchy for intermolecular interactions. Pyrazole-based molecules have been made, combined with various carboxylic acids, and characterized using infrared (IR) spectroscopy to give a success rate of 55-70%. Reactions that gave a positive result were converted to solution experiments, and crystals were grown and characterized using single-crystal X-ray diffraction (XRD). The co-crystals display infinite 1-D chains with the intended stoichiometry and structural landscape on 6/6 occasions. The salts, on the other hand, display unpredictable stoichiometry and structural landscape on 5/5 occasions. Furthermore, the electrostatic charge on the primary hydrogen-bond acceptor, N(pyz), can be altered by adding a nitro, R-NO₂, covalent handle to the backbone of the pyrazole molecule. Addition of a strongly electron withdrawing group significantly lowered the charge on the pyrazole nitrogen atom and, in turn, lowered the supramolecular yield to 10%.

Ditopic molecules containing pyrazole and pyridine on the same molecular backbone were synthesized and characterized using ¹H NMR. The molecules were co-crystallized with carboxylic acids, and the resulting solids were characterized using IR spectroscopy. The solids could then be classified as co-crystal or salt using specific markers in the IR spectrum. Single-crystal XRD was used to observe the intermolecular interactions in the co-crystals and salts, and the co-crystals were assigned to two groups: Group 1 (2) and Group 2 (2). The salts (4) show more unpredictability with stoichiometry and structural landscape.

A library of ditopic molecules containing triazole and pyridine acceptor sites were synthesized and characterized using ¹H and ¹³C NMR. The molecules were co-crystallized with carboxylic acids and the resulting solids were characterized using IR spectroscopy which demonstrated a 100% supramolecular yield whenever a pyridine moiety was present, consistent with results from Chapter 3. Single-crystal XRD was used to identify the intermolecular

interactions in the co-crystals (2) and salt (1), and the results show that triazole can compete with pyridine for hydrogen bond donors.

A library of ditopic molecules was also used for halogen-bonding (XB) studies with a series of activated iodine and bromine-based donors. The results show that iodine donors have a higher success rate range (12.5-75%) compared to bromine donors (16.7-50%) based on results obtained from IR spectra. Furthermore, the results from the XRD show that pyrazole nitrogen atoms can compete with pyridine for forming XB, and two groups of supramolecular synthons were observed.

Finally, relatively weak non-covalent interactions, HB and XB, can influence the assembly of nanoparticles based on IR spectroscopy and TEM images. The assembly of the particles is influenced by specific capping ligands, which were synthesized and characterized using ^1H , ^{13}C and ^{19}F NMR. The results demonstrate that relatively weak non-covalent interactions based on HB and XB interactions can influence nanoparticle assembly.

Table of Contents

List of Figures	xvi
List of Tables	xxii
Acknowledgements.....	xxiv
Dedication.....	xxv
Chapter 1 - Introduction.....	1
1.1 Supramolecular chemistry	1
1.1.1 Self-assembly.....	1
1.1.1.1 Self-assembly using metal ions and organic ligands	2
1.1.1.2 Self-assembly using organic molecules driven by hydrogen bonds	2
1.1.2 Molecular recognition.....	3
1.2 Crystal Engineering	4
1.3 The tools of crystal engineering.....	5
1.3.1 Hydrogen bonds	5
1.3.2 Halogen bonds	5
1.3.3 Supramolecular synthons	6
1.3.4 Graph set notation	7
1.4 Multicomponent crystals (co-crystals).....	8
1.4.1 Examples of multicomponent crystals (co-crystals)	9
1.4.2 Applications of multicomponent crystals	10
1.5 Goals	13
1.6 References:.....	14
Chapter 2 - Is the pyrazole···carboxylic acid synthon robust enough for driving co-crystal synthesis?.....	17
2.1 Introduction.....	17
2.2 Experimental.....	19
2.2.1 Charge calculations	19
2.2.2 Covalent synthesis	19
2.2.2.1 Synthesis of 4-chloro-1H-pyrazole, 1.Cl	19

2.2.2.2	Synthesis of 4-bromo-1H-pyrazole, 1.Br	20
2.2.2.3	Synthesis of 4-iodo-1H-pyrazole, 1.I	20
2.2.2.4	Synthesis of 4-chloro-(3,5-dimethyl)-1H-pyrazole, 2.Cl	21
2.2.2.5	Synthesis of 4-bromo-(3,5-dimethyl)-1H-pyrazole, 2.Br	21
2.2.2.6	Synthesis of 4-iodo-(3,5-dimethyl)-1H-pyrazole, 2.I	22
2.2.2.7	Synthesis of 4-bromo-1H-pyrazole:3,5-dinitrobenzoic acid (1:1), 1.Br:N	22
2.2.2.8	Synthesis of 4-iodo-1H-pyrazole:4-cyanobenzoic acid (1:1), 1.I:H	22
2.2.2.9	Synthesis of 4-iodo-1H-pyrazole:3,5-dinitrobenzoic acid (1:1), 1.I:N	23
2.2.2.10	Synthesis of 4-chloro-3,5-dimethyl-1H-pyrazole:4-hydroxy-3-methoxybenzoic acid (1:1), 2.Cl:B	23
2.2.2.11	Synthesis of 4-chloro-3,5-dimethyl-1H-pyrazole:3,5-dinitrobenzoic acid (1:1), 2.Cl:N	23
2.2.2.12	Synthesis of 4-bromo-3,5-dimethyl-1H-pyrazole:3,5-dinitrobenzoic acid (1:1), 2.Br:N	23
2.2.2.13	Synthesis of 4-chloro-3,5-dimethyl-1H-pyrazolium:2,4-dinitrobenzoate:4-chloro-3,5-dimethyl-1H-pyrazole (1:1:1), 2.Cl:T	24
2.2.2.14	Synthesis of 4-iodo-3,5-dimethyl-1H-pyrazolium:3,5-dinitrobenzoate (1:1), 2.I:N	24
2.2.2.15	Synthesis of 1H-pyrazolium:3,5-dinitrobenzoate:3,5-dinitrobenzoic acid (1:1:1), 1.H:N	24
2.2.2.16	Synthesis of 3,5-dimethyl-1H-pyrazolium:3,5-dinitrobenzoate hydrate (1:1:1), 2.H:N:H ₂ O	24
2.2.2.17	Synthesis of 1H-pyrazolium:2,6-dichlorobenzoate:2,6-dichlorobenzoic acid (1:1:1), 1.H:R	25
2.2.3	IR	25
2.3	Results	25
2.3.1	MEP surface calculations	25
2.3.2	Covalent synthesis	26
2.3.3	Infrared data	26
2.3.4	Crystal structure of 4-bromo-1H-pyrazole:3,5-dinitrobenzoic acid (1:1), 1.Br:N	28
2.3.5	Crystal structure of 4-iodo-1H-pyrazole:4-cyanobenzoic acid (1:1), 1.I:H	29

2.3.6	Crystal structure of 4-iodo-1H-pyrazole: 3,5-dinitrobenzoic acid (1:1), 1.I:N.....	29
2.3.7	Crystal structure of 4-chloro-3,5-dimethyl-1H-pyrazole:4-hydroxy-3-methoxybenzoic acid (1:1), 2.Cl:B	30
2.3.8	Crystal structure of 4-chloro-3,5-dimethyl-1H-pyrazole:3,5-dinitrobenzoic acid (1:1), 2.Cl:N	30
2.3.9	Crystal structure of 4-bromo-3,5-dimethyl-1H-pyrazole:3,5-dinitrobenzoic acid (1:1), 2.Br:N.....	31
2.3.10	Crystal structure of 4-chloro-3,5-dimethyl-1H-pyrazolium:2,4-dinitrobenzoate:4-chloro-3,5-dimethyl-1H-pyrazole (1:1:1), 2.Cl:T	31
2.3.11	Crystal structure of 4-iodo-3,5-dimethyl-1H-pyrazolium:3,5-dinitrobenzoate (1:1), 2.I:N	32
2.3.12	Crystal structure of 1H-pyrazolium:3,5-dinitrobenzoate:3,5-dinitrobenzoic acid (1:1:1), 1.H:N.....	33
2.3.13	Crystal structure of 3,5-dimethyl-1H-pyrazolium:3,5-dinitrobenzoate hydrate (1:1), 2.H:N:H ₂ O.....	33
2.3.14	Crystal structure of 1H-pyrazolium:2,6-dichlorobenzoate:2,6-dichlorobenzoic acid (1:1:1), 1.H:R	34
2.4	Discussion.....	36
2.4.1	Can the charge on the pyrazole backbone be altered by adding covalent ‘handles’?	36
2.4.2	Do the results from the screening experiment corroborate the charge calculations?	36
2.4.3	Co-crystals	37
2.4.4	Salts.....	37
2.4.5	Do other nitrogen-based heterocycles display structural unpredictability when proton transfer occurs?.....	37
2.4.3	Is the pyrazole···carboxylic acid synthon robust enough for driving co-crystal synthesis?	37
2.5	References:.....	38
Chapter 3 - Structural competition between carboxylic acid···pyridine and carboxylic acid···pyrazole: is there a difference?		40

3.1	Introduction.....	40
3.2	Experimental.....	43
3.2.1	Charge calculations.....	43
3.2.2	Covalent synthesis.....	44
3.2.2.1	Synthesis of 2-(1H-pyrazol-4-yl)pyridine, 2.....	44
3.2.2.2	Synthesis of 3-(1H-pyrazol-4-yl)pyridine, 3.....	45
3.2.2.3	Synthesis of 4-(1H-pyrazol-4-yl)pyridine, 4.....	46
3.2.2.4	Synthesis of 2-(1H-pyrazol-4-yl)pyridine:4-cyanobenzoic acid (1:1), 2:H.....	46
3.2.2.5	Synthesis of 2-(1H-pyrazol-4-yl)pyridine:4-nitrobenzoic acid (1:1), 2:K.....	47
3.2.2.6	Synthesis of 3-(1H-pyrazol-4-yl)pyridine:2,4-difluorobenzoic acid (1:2), 3:M ₂	47
3.2.2.7	Synthesis of 4-(1H-pyrazol-4-yl)pyridine:4-nitrobenzoic acid (1:2), 4:K ₂	47
3.2.2.8	Synthesis of 2-(1H-pyrazol-4-yl)pyridinium:2,4-dinitrobenzoate (1:1), 2:U.....	47
3.2.2.9	Synthesis of 3-(1H-pyrazol-4-yl)pyridinium:2,4-dinitrobenzoate (1:1), 3:U.....	47
3.2.2.10	Synthesis of 4-(1H-pyrazol-4-yl)pyridinium:4-cyanobenzoate (1:1), 4:H.....	47
3.2.2.11	Synthesis of 4-(1H-pyrazol-4-yl)pyridinium:2,4-dinitrobenzoate dihydrate (1:1:2), 4:U:(H ₂ O) ₂	48
3.2.3	IR spectroscopy.....	48
3.3	Results.....	48
3.3.1	MEP surface calculations.....	48
3.3.2	Covalent synthesis.....	49
3.3.3	Infrared data.....	49
3.3.4	Determining co-crystal formation by infra-red (IR) spectroscopy.....	50
	Co-crystals:.....	52
3.3.5	Crystal structure of 2-(1H-pyrazol-4-yl)pyridine:4-cyanobenzoic acid (1:1), 2:H.....	52
3.3.6	Crystal structure of 2-(1H-pyrazol-4-yl)pyridine:4-nitrobenzoic acid (1:1), 2:K.....	52
3.3.7	Crystal structure of 3-(1H-pyrazol-4-yl)pyridine:bis-2,4-difluorobenzoic acid (1:2), 3:M ₂	53
3.3.8	Crystal structure of 4-(1H-pyrazol-4-yl)pyridine:bis-4-nitrobenzoic acid (1:2), 4:K ₂	54
	Salts:.....	55
3.3.9	Crystal structure of 2-(1H-pyrazol-4-yl)pyridinium:2,4-dinitrobenzoate (1:1), 2:U... ..	55
3.3.10	Crystal structure of 3-(1H-pyrazol-4-yl)pyridinium:2,4-dinitrobenzoate (1:1), 3:U.....	55

3.3.11 Crystal structure of 4-(1H-pyrazol-4-yl)pyridinium:4-cyanobenzoate (1:1), 4:H.....	56
3.3.12 Crystal structure of 4-(1H-pyrazol-4-yl)pyridinium:2,4-dinitrobenzoate dihydrate (1:1:2), 4:U:(H ₂ O) ₂	57
3.4 Discussion	57
3.4.1 What do the AM1 charge calculations tell us about where binding should take place?	57
3.4.2 Can we determine co-crystal or salt formation from the IR data?	58
3.4.3 Can we group the interactions in the co-crystals and salts obtained from the single crystal data?	61
3.4.3.1 Co-crystals	61
3.4.3.2 Salts	61
3.5 References:	62
Chapter 4 - Are triazoles competitive with pyridine for hydrogen bonds?	64
4.1 Introduction	64
4.2 Experimental	70
4.2.1 Charge calculations	70
4.2.2 Covalent synthesis and characterization of products	70
4.2.2.1 Synthesis of 3-((2H-1,2,3-triazol-2-yl)methyl)pyridine and 3-((1H-1,2,3-triazol-1-yl)methyl)pyridine, IV _a and IV _b	71
4.2.2.2 Synthesis of 4-((2H-1,2,3-triazol-2-yl)methyl)pyridine and 4-((1H-1,2,3-triazol-1-yl)methyl)pyridine, V _a and V _b	72
4.2.2.3 Synthesis of 3-((1H-1,2,4-triazol-1-yl)methyl)pyridine, VI	73
4.2.2.4 Synthesis of 4-((1H-1,2,4-triazol-1-yl)methyl)pyridine, VII	73
4.2.2.5 Synthesis of 4-((1H-1,2,4-triazol-1-yl)methyl)pyridine:bis(3-nitrobenzoic) acid (1:2), VII:I ₂	74
4.2.2.6 Synthesis of 4-((1H-1,2,4-triazol-1-yl)methyl)pyridine:bis(4-nitrobenzoic) acid (1:2), VII:K ₂	74
4.2.2.7 Synthesis of 4-((1H-1,2,3-triazol-1-yl)methyl)pyridinium:3,5-dinitrobenzoate:3,5-dinitrobenzoic acid hydrate (1:2:1), V:N ₂ :H ₂ O	75
4.2.3 IR	75
4.3 Results	75

4.3.1	MEP surface calculations.....	75
4.3.2	Covalent synthesis	76
4.3.3	Infrared data	76
	Co-crystals:	79
4.3.4	Crystal structure of 4-((1H-1,2,4-triazol-1-yl)methyl)pyridine:bis(3-nitrobenzoic acid (1:2), VII:I ₂).....	79
4.3.5	Crystal structure of 4-((1H-1,2,4-triazol-1-yl)methyl)pyridine:bis(4-nitrobenzoic acid (1:2), VII:K ₂)	79
	Salt:	80
4.3.6	Crystal structure of 4-((1H-1,2,3-triazol-1-yl)methyl)pyridinium:3,5-dinitrobenzoate:3,5-dinitrobenzoic acid hydrate (1:2:1), V:N ₂ :H ₂ O	80
4.4	Discussion	81
4.4.1	What do charge calculations tell us about where binding preferences should be?	81
4.4.2	Can we determine co-crystal or salt formation from the IR data?.....	82
4.4.3	Can we group the interactions in the co-crystals and salts from the single crystal data?	84
4.4.3.1	Co-crystals	84
4.4.3.2	Salt	84
4.5	References:.....	86
Chapter 5 - Halogen-bonding (XB) with ditopic pyridine/pyrazole: Are halogen-bonds competitive with hydrogen-bonds?.....		
5.1	Introduction.....	88
5.2	Experimental	94
5.2.1	Charge calculations	94
5.2.2	Synthesis of 3-(1H-pyrazol-4-yl)pyridine:1,4-diiodooctafluorobutane (4:1), 3 ₄ :1,4-DIOFB.....	94
5.2.3	Synthesis of 3-(1H-pyrazol-4-yl)pyridine:1,6-diiodoperfluorohexane (4:1), 3 ₄ :1,6-DIPFH	94
5.2.4	Synthesis of 4-(1H-pyrazol-4-yl)pyridine:1,2-diiodotetrafluoroethane (2:1), 4 ₂ :1,2-DITFE	94

5.2.5 Synthesis of 4-(1H-pyrazol-4-yl)pyridine:1,4-diiodooctafluorobutane (5:3), 4 ₅ :1,4-DIOFB ₃	94
5.2.6 Synthesis of 2-(1H-pyrazol-4-yl)pyridine:1,4-diiodotetrafluorobenzene (1:1), 2:1,4-DITFB	95
5.2.7 Synthesis of 3-(1H-pyrazol-4-yl)pyridine:1,4-diiodotetrafluorobenzene (1:1), 3:1,4-DITFB	95
5.2.8 Synthesis of 4-(1H-pyrazol-4-yl)pyridine:1,4-diiodotetrafluorobenzene (2:1), 4 ₂ :1,4-DITFB	95
5.2.7 IR spectroscopy	95
5.3 Results	95
5.3.1 DFT calculations	95
5.3.2 IR spectroscopy	97
5.3.3 Crystal structure of 3-(1H-pyrazol-4-yl)pyridine:1,4-diiodooctafluorobutane (4:1), 3 ₄ :1,4-DIOFB	99
5.3.4 Crystal structure of 3-(1H-pyrazol-4-yl)pyridine:1,6-diiodoperfluorohexane (4:1), 3 ₄ :1,6-DIPFH	99
5.3.5 Crystal structure of 4-(1H-pyrazol-4-yl)pyridine:1,2-diiodotetrafluoroethane (2:1), 4 ₂ :1,2-DITFE	100
5.3.6 Crystal structure of 4-(1H-pyrazol-4-yl)pyridine:1,4-diiodooctafluorobutane (5:3), 4 ₅ :1,4-DIOFB ₃	100
5.3.7 Crystal structure of 2-(1H-pyrazol-4-yl)pyridine:1,4-diiodotetrafluorobenzene (1:1), 2:1,4-DITFB	101
5.3.8 Crystal structure of 3-(1H-pyrazol-4-yl)pyridine:1,4-diiodotetrafluorobenzene (1:1), 3:1,4-DITFB	102
5.3.9 Crystal structure of 4-(1H-pyrazol-4-yl)pyridine:1,4-diiodotetrafluorobenzene (2:1), 4 ₂ :1,4-DITFB	102
5.4 Discussion	103
5.4.1 What do the DFT calculations tell us about ranking the acceptors and donors?	103
5.4.2 Does iodine show a higher success rate than bromine from the IR spectra results? ..	104
5.4.3 Is the pyrazole nitrogen atom suitable for forming XB's based on the single crystal results?	106

5.5	References:.....	107
Chapter 6 - Can hydrogen-bonds (HB) and halogen-bonds (XB) influence nanoparticle assembly?..... 110		
6.1	Introduction.....	110
6.2	Experimental.....	114
6.2.1	Synthesis.....	114
6.2.1.1	Synthesis of 1-bromooctan-8-ol, 6.1.....	114
6.2.1.2	Synthesis of 1-mercaptooctan-8-ol, 6.2.....	115
6.2.1.3	Synthesis of bis(8-hydroxyoctyl)disulfide, 6.3.....	115
6.2.1.4	Synthesis of bis(8-bromooctyl)disulfide, 6.4.....	116
6.2.1.5	Synthesis of bis(8-imidazol-1-yloctyl)disulfide, 6.5.....	116
6.2.1.6	Synthesis of bis(8-(2,3,5,6-tetrafluoro-4-iodophenoxy)octyl)disulfide, 6.6.....	117
6.2.1.7	Synthesis of dodecylamine functionalised gold nanoparticles, 7.....	117
6.2.1.8	Digestive ripening of gold nanoparticles, 8.....	118
6.2.1.9	Ligand exchange of gold nanoparticles, 9.....	118
6.3	Results.....	118
6.3.1	TEM image of dodecylamine functionalized AuNP's.....	118
6.3.2	TEM image of 11-mercaptoundecanoic acid (MUA) functionalized AuNP's.....	119
6.3.3	TEM image of bis(8-imidazol-1-yloctyl)disulfide functionalized AuNP's.....	120
6.3.4	TEM image of bis(8-(2,3,5,6-tetrafluoro-4-iodophenoxy)octyl)disulfide functionalized AuNP's.....	121
6.3.6	TEM image of 11-mercaptoundecanoic acid (MUA) functionalized AuNP's + bis(8-imidazol-1-yloctyl)disulfide functionalized AuNP's.....	122
6.3.7	TEM image of bis(8-(2,3,5,6-tetrafluoro-4-iodophenoxy)octyl)disulfide functionalized AuNP's + bis(8-imidazol-1-yloctyl)disulfide functionalized AuNP's.....	123
6.3.7	Determining nanoparticle 'communication' using infra-red (IR) spectroscopy.....	124
6.4	Discussion.....	126
6.4.1	Examining the effect of digestive ripening.....	126
6.4.2	Examining the effect of ligand exchange.....	126
6.4.3	Examining interparticle distances.....	127
6.4.4	Examining interparticle 'communication'.....	128

6.5	References:.....	130
Appendix A	- ^1H , ^{13}C and ^{19}F NMR.....	132

List of Figures

Figure 1-1 Self-assembly of three units into one.	1
Figure 1-2 Self-assembly of Pd(II) and pyridine linker to form a supramolecular cage (figure adapted from reference).	2
Figure 1-3 Self-assembly of 5,10,15,20-tetra-4-pyridyl porphyrin (TPP) and benzene-1,2,4,5-tetracarboxylic acid (B4CA) to form a 2D sheet (figure adapted from reference).	3
Figure 1-4 Molecular recognition of a substrate for an enzyme binding pocket.	3
Figure 1-5 Two molecular recognition events: the carboxylic acid recognizes and binds to the amide, followed by iodine interacting with the pyrazine heterocycle (iodine atoms are purple; nitrogen atoms are blue; oxygen atoms are red; hydrogen atoms are white).	4
Figure 1-6 A simple flowchart highlighting the importance of crystal engineering.	4
Figure 1-7 Base pairs of DNA with hydrogen bonds shown as dashed lines. T = Thymine; A = Adenine; C = Cytosine; G = Guanine.	5
Figure 1-8 Number of Scifinder hits for the term ‘halogen bonding’ (figure adapted from reference).	6
Figure 1-9 Combination of hydrogen and halogen bonds in the Itraconazole:succinic acid (2:1) co-crystal.	6
Figure 1-10 Examples of synthons. (A) Homomeric acid···acid. (B) Heteromeric acid···pyridine.	7
Figure 1-11 R22(8) graph set notation for a benzoic acid dimer.	7
Figure 1-12 Two possible outcomes from slow evaporation of a saturated solution of two molecular species, re-crystallization or co-crystallization.	8
Figure 1-13 Example of a <i>homomeric</i> synthon.	9
Figure 1-14 Example of a <i>heteromeric</i> synthon.	9
Figure 1-15 Example of a trimeric supermolecule containing acid···amide and acid···pyridine <i>heterosynthons</i>	10
Figure 1-16 API (A) and co-formers (1,2,3,4,5) used to generate co-crystals.	11
Figure 1-17 2D sheet generated via O-H···N and C=O···H-N synthons between API and diacids. ⁴⁴	11

Figure 1-18 Comparison of the solubility of an API (A) with co-crystals A1-A5 (figure adapted from reference). ⁴⁴	12
Figure 1-19 Molecular structure of Meloxicam®.....	12
Figure 2-1 The carboxylic acid···pyridine heterosynthon, R22(7).....	17
Figure 2-2 The carboxylic acid···pyrazole heterosynthon, R22(7).....	18
Figure 2-3 Infinite 1-D chain in the crystal structure of 1.Br:N driven by O-H···N(py _z) and N-H···O synthons. N-O ⁻ ···Br interactions extend the dimers into 1D chains.	29
Figure 2-4 Infinite 1-D chain in the crystal structure of 1.I:H driven by O-H···N(py _z) and N-H···O synthons. C-N···I interactions extend the dimers into 1-D chains.....	29
Figure 2-5 An overview of the 2-D layer in the crystal structure of 1.I:N	30
Figure 2-6 Infinite 1-D zig-zag chain in the structure of 2.Cl:B	30
Figure 2-7 1-D chain of in the structure of 2.Cl:N	31
Figure 2-8 1-D chain in the crystal structure of 2.Br:N	31
Figure 2-9 A hydrogen-bonded trimer in the crystal structure of 4-chloro-3,5-dimethylpyrazolium:2,4-dinitrobenzoate:4-chloro-3,5-dimethylpyrazole, 1:1:1, 2.Cl:T	32
Figure 2-10 Tetramers (subsequently linked into ribbon) formed in the solid product resulting from a combination of 2.I and N	32
Figure 2-11 A zig-zag chain in the crystal structure of pyrazolium 3,5-dinitrobenzoate 3,5-dinitrobenzoic acid (1:1:1), 1.H:N	33
Figure 2-12 A hydrated ion-pair in the crystal structure of pyrazolium:3,5,-dinitrobenzoate hydrate (1:1), 2.H:N	34
Figure 2-13 Discrete tetramers formed in the crystal structure of 1.H:R	34
Figure 2-14 Summary of the results obtained from co-crystals and salts.....	38
Figure 3-1 Two potential binding sites for an incoming carboxylic acid.	40
Figure 3-2 Potential supramolecular interactions between acid and N(py) and N(py _z).	40
Figure 3-3 Nexium© and potential binding sites for hydrogen bond donors.	41
Figure 3-4 Library of isomeric ditopic molecules 2 , 3 , and 4 . The molecules have been named based on the position of the pyridine nitrogen atom.	41
Figure 3-5 Flowchart for determining a correlation between charge and observed structural motifs.	42
Figure 3-6 The carboxylic acid···pyridine heterosynthon (Synthon 1).	43

Figure 3-7 The carboxylic acid···pyrazole heterosynthon (Synthon 2).....	43
Figure 3-8 MEP surfaces of the ditopic molecules indicating the distribution of charge. Red surfaces indicate hydrogen-bond acceptor sites; blue indicates hydrogen bond donor sites.	49
Figure 3-9 Synthetic routes to obtaining the target molecules 2 , 3 , and 4	49
Figure 3-10 IR spectrum of reaction between 4 and K . Evidence of O-H···N interactions are circled. Change in the carbonyl C=O stretch is 4 cm^{-1} .	51
Figure 3-11 Catemer in the crystal structure of 2:H .	52
Figure 3-12 Catemer in the crystal structure of 2:K .	53
Figure 3-13 Two predominant interactions in the crystal structure of 3:M₂ .	54
Figure 3-14 Supermolecule formed in the crystal structure of 4:K₂ .	54
Figure 3-15 Zig-zag chain formed in 2:U .	55
Figure 3-16 Proton transfer from acid to base in the crystal structure of 3:U .	56
Figure 3-17 Part of the zig-zag chain formed through proton transfer from acid to base in the crystal structure of 4:H .	56
Figure 3-18 Hydrated salt formed in the reaction between 4 and U .	57
Figure 3-19 Interactions observed in the four co-crystals.....	61
Figure 4-1 Two groups of triazole. (I) 1 <i>H</i> -1,2,3-triazole. (II) 1 <i>H</i> -1,2,4-triazole.....	64
Figure 4-2 (I) Fluconazole® and (II) Itraconazole® highlighting the triazole functional group.	64
Figure 4-3 Itraconazole:succinic acid co-crystal (2:1). ⁷	65
Figure 4-4 Triazole nitrogen position relative to the carboxylic acid.....	66
Figure 4-5 Triazole (I-III) and triazole/pyridine asymmetric ditopic molecules (IV-VII).....	66
Figure 4-6 Potential interactions between carboxylic acid and triazole molecules. Potential interactions with 1 <i>H</i> -1,2,3-triazole (I,II,III) and with 1 <i>H</i> -1,2,4-triazole (IV, V, VI) are shown.	67
Figure 4-7 Potential binding sites of two of the four triazole/pyridine asymmetric ditopic molecules. Group I: 4-((1 <i>H</i> -1,2,3-triazol-1-yl)methyl)pyridine. Group II: 4-((1 <i>H</i> -1,2,4-triazol-1-yl)methyl)pyridine.....	68
Figure 4-8 Flowchart for determining a correlation between charge calculations, IR spectroscopy results and single crystal data.	69
Figure 4-9 The four asymmetric ditopic triazole/pyridine molecules (IV-VII) used for screening with carboxylic acids.	76

Figure 4-10 The primary interactions observed in the crystal structure of VII:I₂	79
Figure 4-11 The primary interactions observed in the crystal structure of VII:K₂	80
Figure 4-12 The primary interactions observed in the crystal structure of V:N₂:H₂O	81
Figure 4-13 Triazole (I-III) and triazole/pyridine asymmetric ditopic molecules (IV-VII).....	81
Figure 4-14 Primary interactions observed in the co-crystals obtained.....	84
Figure 4-15 Proton transfer to the N(py) site in the salt formed between V and N	85
Figure 4-16 Two groups of interactions, 1 and 10 , observed from the potential interactions listed in Figure 4.7.....	86
Figure 5-1 Increase in the size of the sigma hole. Red indicates areas of negative charge; blue indicates areas of positive charge (figure adapted from reference).....	89
Figure 5-2 Halogen-bonding (XB) interaction between nitrogen and iodine.....	89
Figure 5-3 Halogen-bonding (XB) interaction between IPFA's and aromatic and aliphatic nitrogen compounds (figure adapted from reference).....	90
Figure 5-4 Flowchart for determining a correlation between charge calculations and single crystal results.....	91
Figure 5-5 Primary interactions in the crystal structure of 3₄:1,4-DIOFB	99
Figure 5-6 Primary interactions in the crystal structure of 3₄:1,6-DIPFH	99
Figure 5-7 Primary interactions in the crystal structure of 4₂:1,2-DITFE	100
Figure 5-8 Primary interactions in the crystal structure of 4₅:1,4-DIOFB₃	101
Figure 5-9 Primary interactions in the crystal structure of 2:1,4-DITFB	101
Figure 5-10 Primary interactions in the crystal structure of 3:1,4-DITFB	102
Figure 5-11 Primary interactions in the crystal structure of 4₂:1,4-DITFB	102
Figure 5-12 The two groups of interactions observed in the crystals.....	106
Figure 5-13 The primary interactions observed in the crystals structure of 2-amino-3,5-dibromopyrazine:1,4-DITFB displaying the hydrogen and halogen bonds.....	107
Figure 6-1 Relative volumes of nanoparticles (~380nm ³) compared to molecules (~20nm ³) and coordination complexes (~80nm ³).....	110
Figure 6-2 Arrangement of nanoparticles observed in dodecylamine functionalised gold nanoparticles.....	111
Figure 6-3 Ligands (1 and 2) and linkers (1 and 2) used in the halogen-bond assembly of nanoparticles.....	112

Figure 6-4 Target ligands (I) bis(8-imidazol-1-yl)octyl)disulfide, (IM); (II) bis(8-(2,3,5,6-tetrafluoro-4-iodophenoxy)octyl)disulfide, (XBD).	113
Figure 6-5 Flowchart for synthesis and characterization of gold nanoparticles.	113
Figure 6-6 TEM image of dodecylamine functionalized AuNP's. (I) magnification = 92,000x; scale = 100nm (II) magnification = 245,000x; scale = 20nm.	119
Figure 6-7 Histogram of dodecylamine functionalized AuNP's.	119
Figure 6-8 TEM image of 11-mercaptopundecanoic acid (MUA) functionalized AuNP's. (I) magnification = 92,000x; scale = 100nm (II) magnification = 130,000x; scale = 100nm.	120
Figure 6-9 Histogram of 11-mercaptopundecanoic acid (MUA) functionalized AuNP's.	120
Figure 6-10 TEM image of bis(8-imidazol-1-yl)octyl)disulfide functionalized AuNP's. (I) magnification = 130,000x; scale = 100nm (II) magnification = 180,000x; scale = 20nm.	121
Figure 6-11 Histogram of bis(8-imidazol-1-yl)octyl)disulfide (DS-IM) functionalized AuNP's.	121
Figure 6-12 TEM image of bis(8-(2,3,5,6-tetrafluoro-4-iodophenoxy)octyl)disulfide functionalized AuNP's. (I) magnification = 130,000x; scale = 100nm (II) magnification = 180,000x; scale = 20nm.	122
Figure 6-13 Histogram of bis(8-(2,3,5,6-tetrafluoro-4-iodophenoxy)octyl)disulfide functionalized AuNP's.	122
Figure 6-14 TEM image of 11-mercaptopundecanoic acid (MUA) functionalized AuNP's combined with bis(8-imidazol-1-yl)octyl)disulfide functionalized AuNP's. (I) magnification = 130,000x; scale = 100nm (II) magnification = 180,000x; (III) magnification = 64,000x; scale = 20nm.	123
Figure 6-15 TEM image of bis(8-(2,3,5,6-tetrafluoro-4-iodophenoxy)octyl)disulfide combined with bis(8-imidazol-1-yl)octyl)disulfide functionalized AuNP's. (I) magnification = 130,000x; scale = 100nm (II) magnification = 180,000x; scale = 20nm.	124
Figure 6-16 IR spectrum of 11-mercaptopundecanoic acid (MUA) capping ligand combined with bis(8-imidazol-1-yl)octyl)disulfide capping ligand (green scan, top). AuIM nanoparticles combined with AuMUA nanoparticles showing the O-H...N hydrogen bonds (red scan, bottom).	125
Figure 6-17 IR spectrum comparison of bis(8-(2,3,5,6-tetrafluoro-4-iodophenoxy)octyl)disulfide neat ligand (red scan, top) versus the combination of bis(8-	

imidazol-1-yloctyl)disulfide and bis(8-(2,3,5,6-tetrafluoro-4-iodophenoxy)octyl)disulfide gold nanoparticles (purple scan, bottom).....	125
Figure 6-18 TEM images of dodecylamine particles. (I) before digestive ripening and (II) after digestive ripening; magnification = 92,000x; scale = 100nm.....	126
Figure 6-19 TEM images of dodecylamine particles before and after ligand exchange. (I) 11-mercaptoundecanoic acid (MUA); (II) bis(8-imidazol-1-yloctyl)disulfide (IM); (III) bis(8-(2,3,5,6-tetrafluoro-4-iodophenoxy)octyl)disulfide (XBD); magnification = 92,000x; scale = 100nm.	127
Figure 6-20 TEM images of the combination of AuIM + AuNH ₂	128
Figure 6-21 TEM images of Van der Boom's particles (A) and the particles obtained in this study (B), both influenced by XB interactions.	129

List of Tables

Table 2.1 Molecular electrostatic surface potential calculations for the various pyrazoles (AM1, PM3, DFT). Values given in kJ/mol.	25
Table 2.2 ¹ H NMR data, yields, and melting points for six pyrazoles synthesized.	26
Table 2.3 Table of aromatic carboxylic acids used in the study.	27
Table 2.4 Summary of prominent IR stretches (cm ⁻¹) from the melt experiments between nine pyrazoles and twenty carboxylic acids.	27
Table 2.5 Hydrogen bond geometries.	35
Table 3.1 AM1 Molecular electrostatic surface potential energies for ditopics 2 , 3 , and 4	48
Table 3.2 Aromatic carboxylic acids used in the study.	50
Table 3.3 Summary of prominent IR stretches (cm ⁻¹) from the grinding experiments between three ditopic molecules and twenty-one carboxylic acids.	51
Table 3.4 Summary of changes in the carbonyl (C=O) after reaction (rxn).	58
Table 3.5 Summary of ΔpK_a and the corresponding structures obtained from the single crystal data. The number of structures is given in parentheses; dash marks indicate no structures.	60
Table 3.6 Groups of primary interactions between the co-crystals and salts.	62
Table 4.1 Molecular electrostatic surface potential (MEP) calculations for the various triazoles and asymmetric ditopic triazole/pyridine molecules. Values are given in kJ/mol.	75
Table 4.2 Table of aromatic carboxylic acids used in the study.	77
Table 4.3 Summary of prominent IR stretches for the triazole molecules combined with various carboxylic acids.	78
Table 4.4 Summary of charges on pyrazole and the triazole molecules.	83
Table 4.5 Summary of the results obtained from different chapters.	83
Table 4.6 Summary of relevant structures.	85
Table 5.1 Library of halogen-bond (XB) acceptors used in the screening.	92
Table 5.2 Library of halogen bond (XB) donors used in the screening.	92
Table 5.3 Summary of DFT charges (kJ/mol) on the pyridine nitrogen atom (N(py), red), pyrazole nitrogen atom (N(py), orange) and pyrazole N-H hydrogen atom (blue).	96
Table 5.4 Summary of charges for the iodine donors.	96

Table 5.5 Summary of charge for the bromine donors	97
Table 5.6 Summary of 84 solvent-assisted grinding experiments. XB donors are listed in the left hand column; XB acceptors are top row.....	98
Table 5.7 Summary of charges on the pyrazole and pyrazole/pyridine XB acceptor molecules.	103
Table 5.8 Range of charges on the iodine and bromine XB donors. IPFB = iodopentafluorobenzene. BPFB = bromopentafluorobenzene.....	104
Table 5.9 Summary of supramolecular yields obtained from the screening experiments.	105
Table 5.10 Summary of hits found in CSD.....	105
Table 5.11 Summary of CSD results for co-crystals of 1,4-diiodobenzene vs. 1,4-diiidotetrafluorobenzene.	105
Table 5.12 Summary of the observed interactions in the crystal structures.....	106
Table 6.1 Comparison of the interparticle distance between gold nanoparticles.....	128

Acknowledgements

I would like to thank my advisor, Professor Christer Aakeröy, for his support and encouragement over the past five years. I admire his strong work ethic, turnaround time and his dedication to the overall well-being and success of his students.

To my committee members, Professors Klabunde, Aikens, Chakrabarti, and Lease, for their time serving on my advisory committee and helpful discussions. I would like to point out the helpful discussions with Professors Klabunde and Chakrabarti during my time working on the Nano Interdisciplinary Research Team (NIRT) grant.

I would especially like to thank Dr. John Desper for solving my crystal structures and refinements. A special thanks to Dr. Leila Maurmann, for all her help with NMR-related questions.

Jim Hodgson, Ron Jackson, Tobe Eggers, and office staff for all the help with glassware and Schlenk lines, monkey bars, computer problems, and financial and administrative paperwork.

Finally, I would like to acknowledge all my friends and family members who have been supportive over the years. I have missed a lot of lake time, but not anymore.

Dedication

I would like to dedicate this dissertation to my mother and father, Lucille and Patrick Hurley. Without their unconditional love, support, and encouragement over the years, I would never have pursued higher education.

Chapter 1 - Introduction

1.1 Supramolecular chemistry

The term ‘supramolecular chemistry’ is used to describe ‘chemistry beyond the molecule’¹ and refers to the self-organization² of small building blocks into larger architectures. The term can, in essence, be applied to any system where individual building blocks undergo some type of self-assembly to give an entirely new structure, which is different from the individual building blocks.

One of the underlying goals of supramolecular chemistry is to control how to bring together two (or more) individual building blocks in a *predictable* and *controllable* way. One may ask how the inherent ‘selfishness’ of molecules³ may be overcome, when molecules would prefer to stick to themselves rather than pair with something else in the same lattice.⁴ In fact, a 2013 Scifinder⁵ search gave 1,900 hits for the term ‘cocrystallization’, and 40,370 for the term ‘recrystallization’, highlighting the differences and the likelihood of a recrystallization event occurring.

It is important for the supramolecular chemist to recognize the factors controlling the process of how molecules recognize and self-assemble with one another. If one can gain control over both processes (molecular recognition and self-assembly), then ultimately control over the entire system may be attained. Controlling the arrangement of molecules leads to control over macroscopic properties of materials.⁶

1.1.1 Self-assembly

What do we mean by self-assembly? There are many examples of systems which undergo self-assembly to give larger ‘superstructures’, or ‘supermolecules’, which are different from their individual building blocks.⁷ To help visualize this, three individual units, labeled A, B, and C, respectively, self-assemble into one discrete unit, D, shown in Figure 1.1.

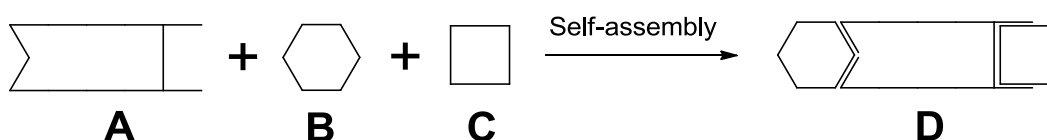


Figure 1-1 Self-assembly of three units into one.

Structure 'D' may have very different properties from either of the individual components, or may be similar as far as physical properties are concerned.

1.1.1.1 Self-assembly using metal ions and organic ligands

An example of self-assembly using metal ions and organic ligands is the construction of molecular cages by Fujita *et al.*⁸ who showed that *cis*-capped Pd(II) metal ions, which act as 90° linkers, can spontaneously self-assemble with a pyridine-based ligand to give an octahedral cage driven by coordination bonds between metal ions and pyridine ligands, Figure 1.2.

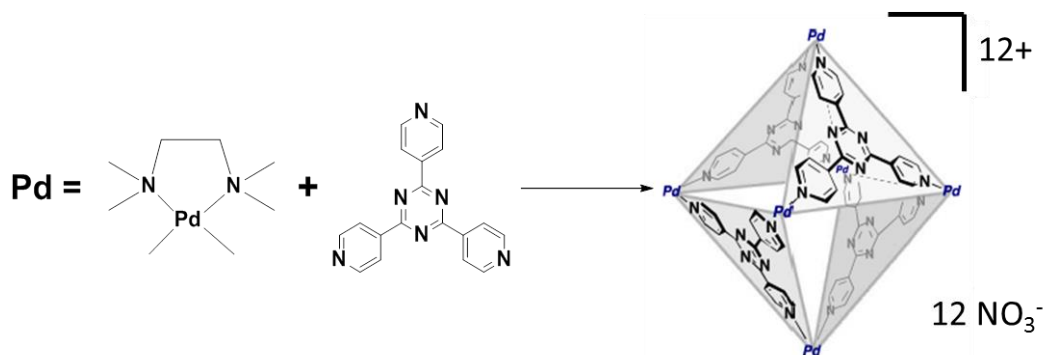


Figure 1-2 Self-assembly of Pd(II) and pyridine linker to form a supramolecular cage (figure adapted from reference).⁸

1.1.1.2 Self-assembly using organic molecules driven by hydrogen bonds

Hydrogen bonds are useful tools for assembling supramolecular structures because they are both strong and directional (in a non-covalent context).⁹ For example, small molecules containing hydrogen bond donors (or acceptors) can be assembled into one-dimensional chains¹⁰, two-dimensional sheets¹¹, or three-dimensional layered materials¹² by forming intermolecular hydrogen bonds.

Hydrogen bonds are not restricted to small molecule assembly; larger molecules, such as cavitands¹³ and porphyrins¹⁴ can also be assembled into predictable structures with unique properties. For example, Goldberg *et al.*¹⁵ have shown that pyridine...carboxylic acid hydrogen bonds are useful for constructing larger architectures. Moreover, molecules containing pendant pyridyl groups with tetra-carboxylic acid molecules can be assembled into 2D sheets, Figure 1.3

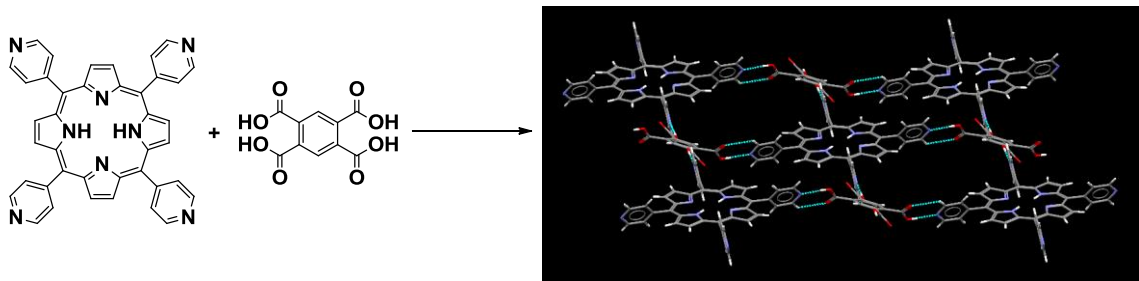


Figure 1-3 Self-assembly of 5,10,15,20-tetra-4-pyridyl porphyrin (TPP) and benzene-1,2,4,5-tetracarboxylic acid (B4CA) to form a 2D sheet (figure adapted from reference).¹⁶

1.1.2 Molecular recognition

Molecular recognition is defined as “the energy and information involved in binding (with a purpose) and selection of substrate by a receptor (ligands with a purpose)”.¹ An illustrative example of molecular recognition occurs when a substrate molecule interacts with an enzyme to make an enzyme-substrate complex, Figure 1.4.

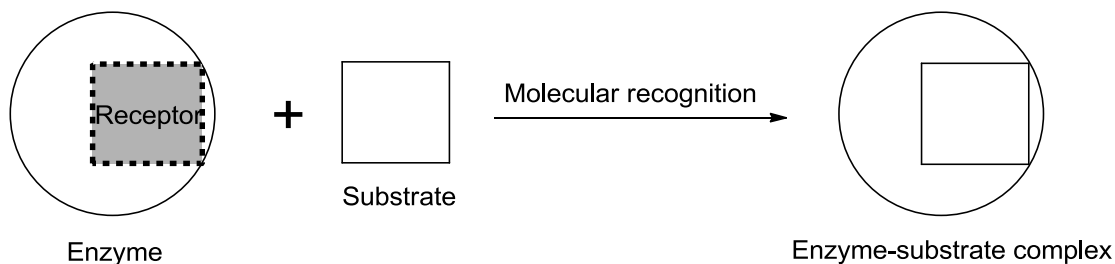


Figure 1-4 Molecular recognition of a substrate for an enzyme binding pocket.

Molecular recognition occurs frequently between small molecules when given the choice between multiple binding sites. For example, molecules with specific hydrogen bond or halogen bond acceptor sites can selectively bind to other molecules when a desirable functional group is present.¹⁷ An example is shown in Figure 1.5, where the carboxylic acid group specifically recognizes the amide group and forms a heteromeric dimer, leaving the iodine to recognize and form an intermolecular halogen bond to the pyrazine.

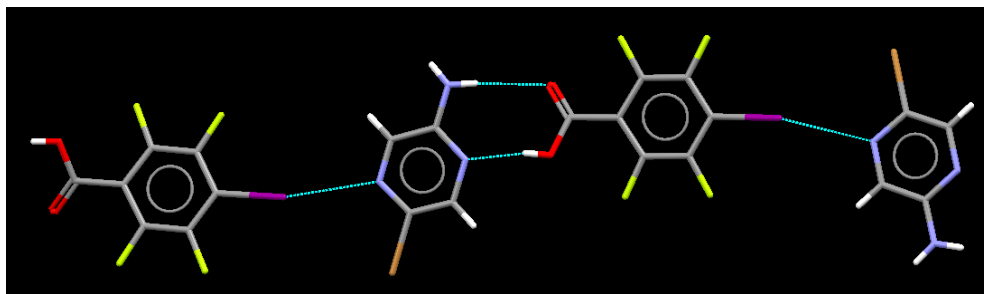


Figure 1-5 Two molecular recognition events: the carboxylic acid recognizes and binds to the amide, followed by iodine interacting with the pyrazine heterocycle (iodine atoms are purple; nitrogen atoms are blue; oxygen atoms are red; hydrogen atoms are white).¹⁷

1.2 Crystal Engineering

Now that we have described two fundamental processes that occur during the recognition and assembly of molecules into ordered structures, it is vital to understand the fundamental interactions occurring *between* the molecules, which allows them to assemble in a predictable and controllable way.

Crystal engineering can be thought of as a sub-section of supramolecular chemistry, and the field has its roots in the work of Gerhardt Schmidt from the 1950's and 1960's.¹⁸ The term 'crystal engineering' was first used by Schmidt in 1971 to describe the photodimerization and packing modes of primary amides and dichlorophenyl derivatives in the solid state.¹⁹ Since then, there has been a significant amount of research conducted to understand how to control the arrangement of molecules in the solid state to achieve the desired supramolecular outcome, or crystal structure.²⁰

So, why is all this important? Control over the molecular arrangement, and hence the crystal structure, ultimately will give a better handle on the physical properties of materials, Figure 1.6.

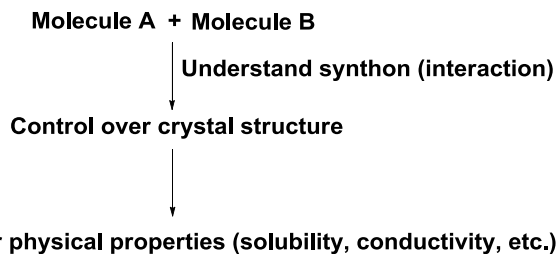


Figure 1-6 A simple flowchart highlighting the importance of crystal engineering.

1.3 The tools of crystal engineering

1.3.1 Hydrogen bonds

Hydrogen bonds are common ‘non-covalent’ interactions used not only in crystal engineering,²¹ but also in biology. Hydrogen bonds are responsible for joining strands of DNA through base-pair complementarity. The four base pairs (and their corresponding hydrogen bonds, denoted as dotted lines) are shown below, Figure 1.7.

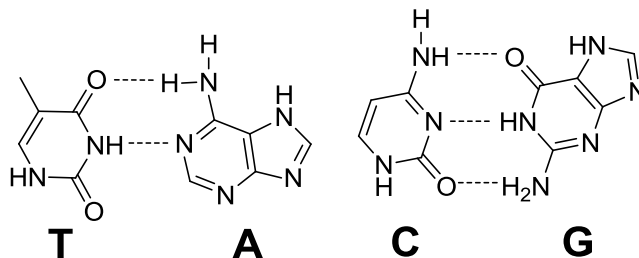


Figure 1-7 Base pairs of DNA with hydrogen bonds shown as dashed lines. T = Thymine; A = Adenine; C = Cytosine; G = Guanine.

Larger architectures based on hydrogen bonds can also be made. For example, Rebek *et al.*²² have shown that cavitands, ‘bowl’ shaped molecules, can be assembled using complementary hydrogen bonds between ‘bowls’ to make ‘capsules’. Furthermore, the ‘bowl’ can be tuned to accommodate a variety of guests²³ and cavitand ‘bowls’ have recently demonstrated the ability to detect small molecules in human urine.²⁴

1.3.2 Halogen bonds

Although halogen bonding (XB) is still a relatively new area in crystal engineering, it has gained a tremendous amount of attention in the past decade. The number of Scifinder hits illustrates that point, where a Scifinder search using the phrase “halogen bonding” doubled from 2009 to 2011, Figure 1.8.

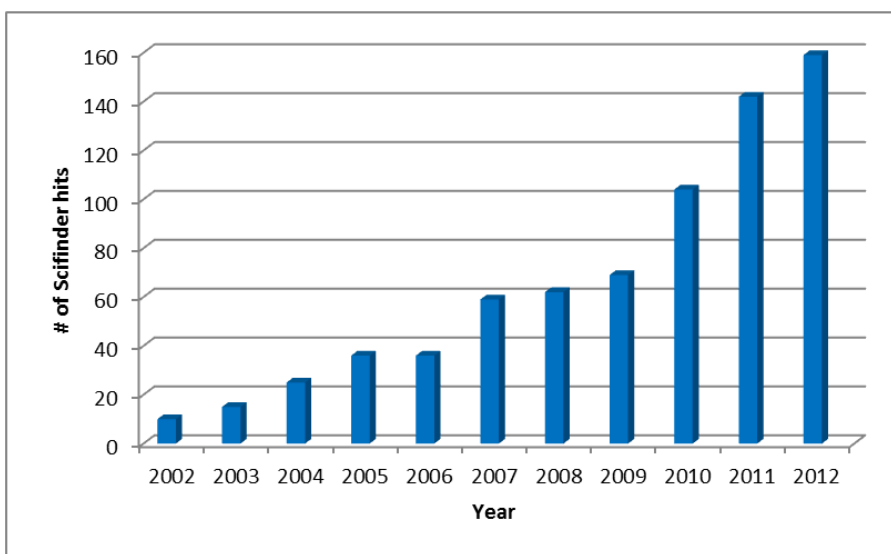


Figure 1-8 Number of Scifinder hits for the term ‘halogen bonding’ (figure adapted from reference).²⁵

Halogen bonds have been used for the assembly of a number of supramolecular structures, ranging from chains²⁶ to liquid crystals²⁷ to pharmaceutical materials.²⁸ For example, co-crystals of Itraconazole® show both halogen and hydrogen bonds present at the same time. O-H···N hydrogen bonds exist between succinic acid and triazole, and C-Cl···O halogen bonds exist between dichlorophenyl and triazolone groups,²⁹ Figure 1.9.

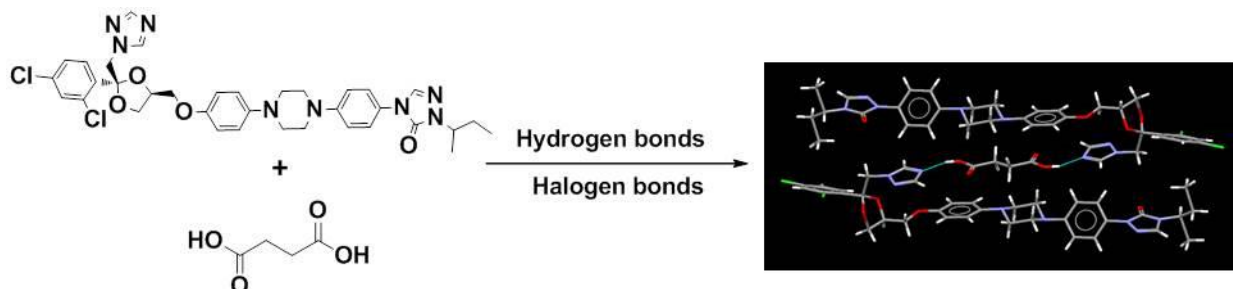


Figure 1-9 Combination of hydrogen and halogen bonds in the Itraconazole:succinic acid (2:1) co-crystal.

1.3.3 Supramolecular synthons

Supramolecular synthons are defined as “*structural units within supermolecules which can be formed and/or assembled by known or conceivable synthetic operations using intermolecular interactions*”³⁰. Synthons can be grouped into different classes, depending on if

the interaction is between the same (homomeric) or different (heteromeric) functional groups, Figure 1.10.

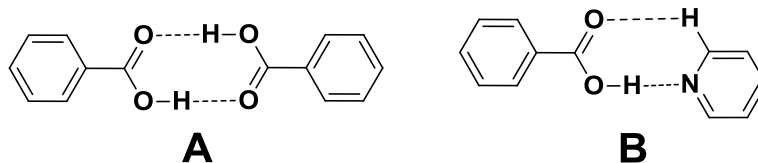


Figure 1-10 Examples of synthons. (A) Homomeric acid···acid. (B) Heteromeric acid···pyridine.

Synthons play an important role in crystal engineering, as they represent the ‘glue’ that holds small (and large) molecules together and allows molecules to communicate with each other. Therefore, a thorough understanding of the nature and binding preferences of any given synthon may allow the crystal engineer to design molecular assemblies in a predictable way.³¹

1.3.4 Graph set notation

Graph-set notation was first introduced by Etter *et al.*³² in the early 1990’s in an effort to understand the patterns of hydrogen bonding in organic solids. The notation is based on the observed patterns from the crystal structure. The graph set notation goes as follows:

$$G_d^a(n)$$

where G is the pattern designator, n is the degree, a is number of acceptors, and d is number of donors. The pattern designator, G, can be either S (for intramolecular bonds), C (for infinite chains), R (for intermolecular rings), or D (for non-cyclic dimers and other finite structures). As an example, take the benzoic acid dimer in Figure 1.9. The acid dimer makes a ring, so we would designate that as R. The ring has two hydrogen bond donors, two hydrogen bond acceptors, and contains eight total atoms in the ring. Therefore, the graph-set notation would be written as $R_2^2(8)$, Figure 1.11.

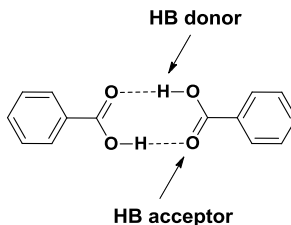


Figure 1-11 $R_2^2(8)$ graph set notation for a benzoic acid dimer.

Graph set notation is useful for decoding hydrogen bond preferences in the organic solid state³³, since there can be many options available for small molecules to choose from.

1.4 Multicomponent crystals (co-crystals)

Multicomponent crystals, also called ‘co-crystals’, are defined as “*structurally homogenous crystalline materials that contain two or more neutral building blocks that are solids under ambient conditions and are present in definite stoichiometric amounts*”.³⁴

How do you make a co-crystal? The most common method of making co-crystals is using solution-based methods, where a suitable solvent is chosen (which gives moderate to good solubility of both components), the components are dissolved in the solvent (usually with heating), and allowed to slowly evaporate under ambient conditions. Other methods exist, such as solid-state grinding³⁵ and melting³⁶, and recently Boese *et al.*³⁷ have shown low-temperature co-crystallization with acetylene.

How do we overcome the natural tendency of molecules to ‘re-crystallize’ instead of ‘co-crystallize’, Figure 1.12?

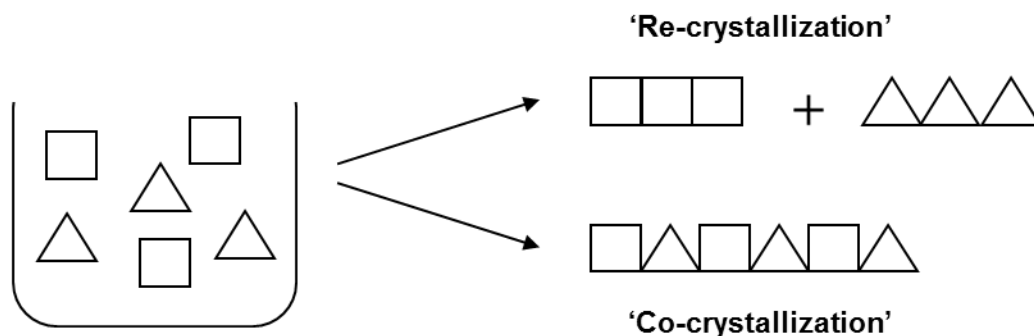


Figure 1-12 Two possible outcomes from slow evaporation of a saturated solution of two molecular species, re-crystallization or co-crystallization.

One way to overcome the problem of re-crystallization is to understand the nature of intermolecular interactions, or how molecules can bind to one another in a predictable and controllable ways. This may be accomplished using a few strategies. First, the electrostatics of any molecule can be fine-tuned to make *intermolecular* interactions more favorable (or less favorable) by adding specific covalent handles. For example, the charge on a nitrogen atom

acceptor site can be lowered by adding a nitro electron-withdrawing group, R-NO₂; the opposite can happen by adding methyl groups, which are electron-donating. Second, in order for a co-crystal to preferentially form, the heteromeric material should have stronger intermolecular interactions than either of the homomeric starting materials.²¹

1.4.1 Examples of multicomponent crystals (co-crystals)

Some examples of two-component (binary) crystals which give 0-D motifs will be addressed in the following examples. First, a 1:1 co-crystal between 4-nitrobenzoic acid and 3-(dimethylamino)benzoic acid³⁸ displays the *homomeric* acid...acid synthon driven by O-H...O hydrogen bonds, Figure 1.13.

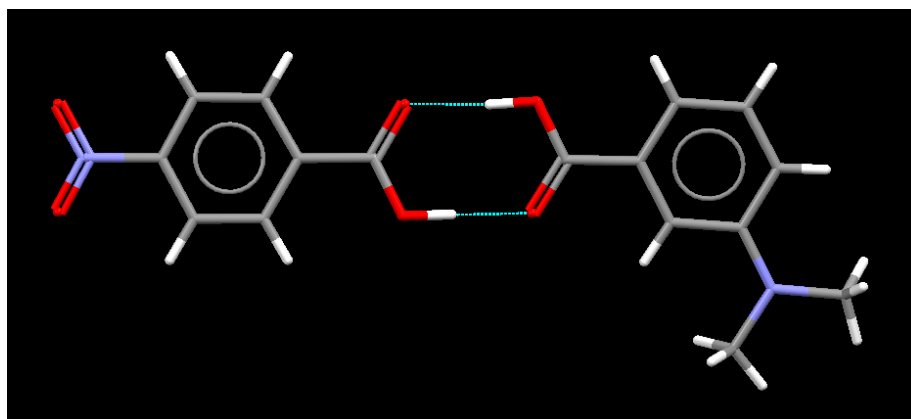


Figure 1-13 Example of a *homomeric* synthon.³⁸

In some cases, depending on which functional groups are present, a *heteromeric* synthon is observed. For example, 3,5-dinitrobenzamide forms a *heteromeric* ‘dimer’ with 4-(dimethylamino)benzoic acid³⁸, Figure 1.14.

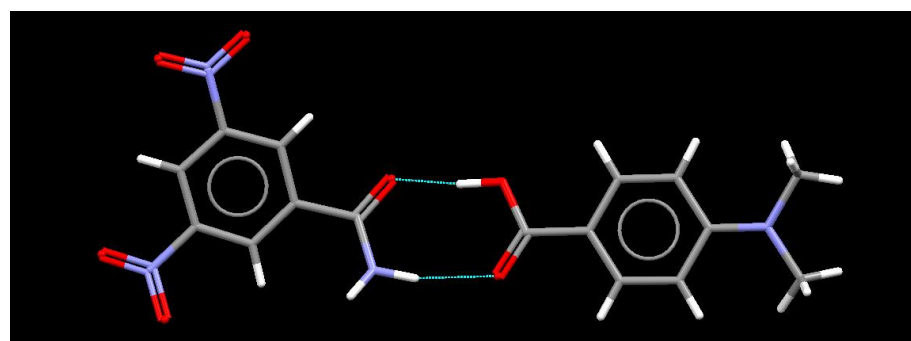


Figure 1-14 Example of a *heteromeric* synthon.³⁸

Not only can *homomeric* and *heteromeric* synthons be used to build binary co-crystals, but both synthons can be combined to build three-component crystals (trimeric supermolecules),³⁹ Figure 1.15.

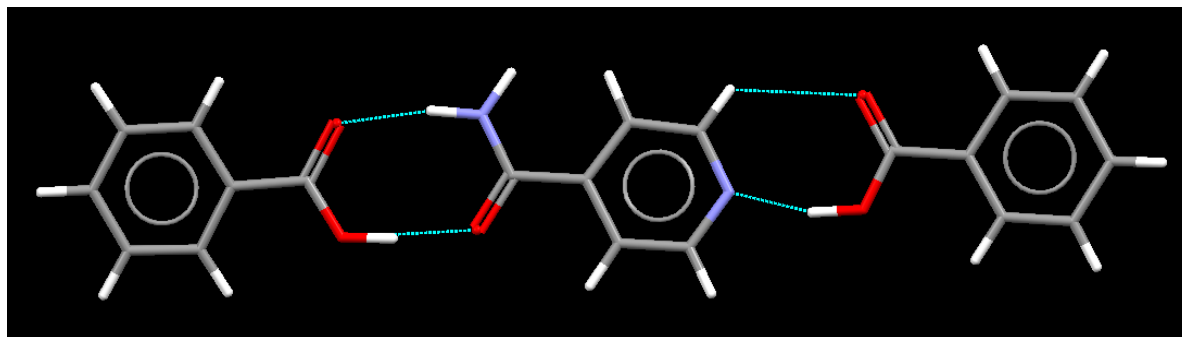


Figure 1-15 Example of a trimeric supermolecule containing acid···amide and acid···pyridine *heterosynthons*.³⁹

1.4.2 Applications of multicomponent crystals

Multicomponent crystals have gained attention, especially in the pharmaceutical industry, where physical properties (*e.g.* solubility, melting behavior, hygroscopicity) of an active pharmaceutical ingredient (API) can, *in some cases*, be modulated by making a new solid form of the drug substance. Common solid forms of API molecules with improved properties include co-crystals,⁴⁰ salts,⁴¹ and amorphous materials.⁴² Only co-crystals containing API will be addressed in the following section.

In 2009, Aakeröy *et al.*⁴⁴ showed that a poorly water soluble cancer drug, bis-hexamethylene-4-pyridineacetamide (A), could be co-crystallized with various dicarboxylic acid cofomers (1,2,3,4,5), Figure 1.16.

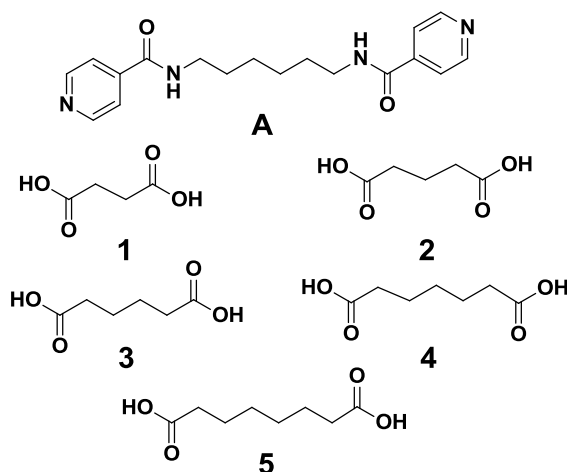


Figure 1-16 API (**A**) and co-formers (**1,2,3,4,5**) used to generate co-crystals.⁴⁴

The reason for choosing a specific co-former have to do with characteristic functional groups which can potentially help improve some physical property of the material it is co-crystallized with (in this case solubility). Short-chain di-carboxylic acids have high aqueous solubility, and therefore make attractive candidates for co-crystallization with something that has poor aqueous solubility.

As anticipated, the structural landscape⁴³ of the crystal displayed primary acid...pyridine O-H...N heterosynthons which joined the drug and coformer to give 1-D chains. The chains were further linked together by carbonyl C=O...H-N acetamide interactions to give 2-D sheets, Figure 1.17.

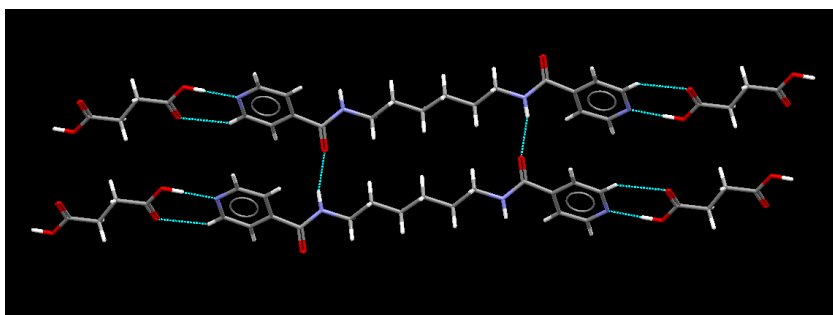


Figure 1-17 2D sheet generated via O-H...N and C=O...H-N synthons between API and diacids.⁴⁴

More importantly, the authors demonstrated the improved aqueous solubility of the new co-crystals, which showed an *increase* (A1, A2, A3) over the drug by itself (A); in two cases (A4, A5) the solubility was *decreased*, Figure 1.18.⁴⁴

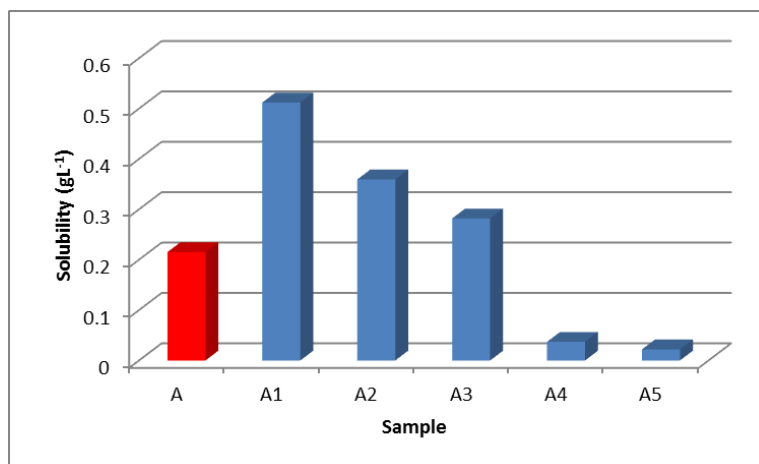


Figure 1-18 Comparison of the solubility of an API (A) with co-crystals A1-A5 (figure adapted from reference).⁴⁴

Recently, Zaworotko *et al.*⁴⁵ improved the aqueous solubility of Meloxicam® by synthesizing co-crystals with a variety of co-formers. Meloxicam is a non-steroidal anti-inflammatory drug (NSAID) used to treat pain which contains a sulfinyl (S=O) group which can act as a hydrogen-bond acceptor, Figure 1.19.

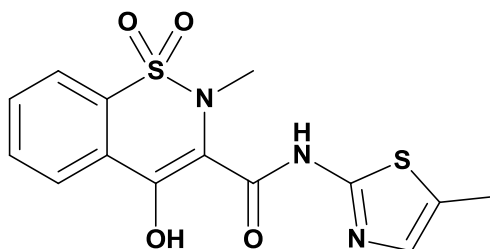


Figure 1-19 Molecular structure of Meloxicam®.

After making co-crystals with various coformers, the aqueous solubility of the new solid forms was studied. Co-crystal 1 (Meloxicam:1-Hydroxy-2-Napthoic acid) shows an improvement in dissolution rate (and therefore bioavailability) over pure Meloxicam. The results from the formation of co-crystals containing API and co-former show improved aqueous solubility. It is therefore important for crystal engineers to understand the nature of

intermolecular interactions so, in principle, any drug with poor physical properties may be transformed into a new solid form with improved physiochemical properties.

1.5 Goals

In order to build multicomponent crystals (co-crystals) in a predictable and controllable way, one needs to understand the nature of fundamental interactions occurring *between* molecules. In order to accomplish this goal, the synthetic landscape for non-covalent interactions needs to be mapped out. In other words, a reliable hierarchy for intermolecular interactions must be established which will allow the crystal engineer to build multicomponent crystals with predictable structures and desired functionality.

As a result, the goals of this thesis are to:

I. Establish if pyrazole···carboxylic acid heterosynthons can be made and are reliable enough for synthesizing co-crystals

Various pyrazole molecules will be synthesized and combined with a library of twenty substituted benzoic acid molecules via melt experiments. The resulting solids will be analyzed using IR spectroscopy to determine if a reaction occurred or not. For those which gave a positive result, they will be converted to solution based experiments in an effort to generate single crystals. The crystal structures will then be analyzed to determine any binding preferences and patterns of intermolecular bonding observed.

II. Test the binding preferences of hydrogen-bond (HB) and halogen-bond (XB) donors with a series of ditopic molecules containing two potential binding sites: pyridine/pyrazole and pyridine/triazole

Ditopic molecules containing both pyridine and pyrazole functional groups will be synthesized using Suzuki-Miyaura cross-coupling reactions. The molecules will be screened with a library of twenty-one carboxylic acids and fourteen halogen-bond (XB) donors. Ditopic pyridine/triazole molecules will be made and combined with a library of twenty acids. Reactions which give a positive result (based on characteristic stretches and shifts in the IR spectrum) will be converted

to solution based experiments to grow single crystals. The structures will be analyzed using X-ray crystallography to search for patterns of intermolecular bonding and bonding preferences.

III. Determine whether hydrogen-bond (HB) and halogen-bond (XB) capping ligands can be used to influence nanoparticle assembly

Nanoparticles will be made and functionalized with hydrogen-bond (HB) and halogen-bond (XB) donor and acceptor groups. The particles will be made and combined to test the viability of HB and XB to influence the assembly of gold nanoparticles. The assemblies will be analyzed using UV-Vis, IR spectroscopy, and TEM.

1.6 References:

-
- ¹ Lehn, J. M. In *Supramolecular Chemistry*, VCH, Weinheim, **1995**.
 - ² Lehn, J. M. *Science*, **2002**, 295(5564), 2400-2403.
 - ³ Dunitz, J. D. In *Perspectives in Supramolecular Chemistry: the Crystal As a Supramolecular Entity*, ed. Desiraju, G. R., Wiley, Amsterdam, **1995**.
 - ⁴ Aakeröy, C. B.; Rajbanshi, A.; Li, Z. J.; Desper, J. *CrystEngComm*, **2010**, 12(12), 4231-4239.
 - ⁵ Scifinder scholar, Copyright © 2013 American Chemical Society.
 - ⁶ Kim, S.; Li, Z.; Tseng, Y.-C.; Nar, H.; Spinelli, E.; Varsolona, R.; Reeves, J. T.; Lee, H.; Song, J. J.; Smoliga, J.; Yee, N.; Senanayake, C. *Org. Proc. Res. & Dev.*, **2013**, 17(3), 540-548; Bolton, O.; Simke, L. R.; Pagoria, P. F.; Matzger, A. J. *Cryst. Growth Des.*, **2012**, 12(9), 4311-4314.
 - ⁷ Yan, Z.; Guang, S.; Xu, H.; Su, X.; Ji, X.; Liu, X. *RSC Adv.*, **2013**, 3(21), 8021-8027.
 - ⁸ Fang, Y.; Murase, T.; Sato, S.; Fujita, M. *J. Am. Chem. Soc.*, **2013**, 135(2), 613-615.
 - ⁹ Hennemann, M.; Murray, J. S.; Politzer, P.; Riley, K. E.; Clark, T. *J. Mol. Model.*, **2012**, 18(6), 2461-2469; Aakeröy, C. B.; Beatty, A. M. *Aust. J. Chem.*, **2001**, 54(7), 409-421.
 - ¹⁰ Aakeröy, C. B.; Desper, J.; Helfrich, B. A.; Metrangolo, P.; Pilati, T.; Resnati, G.; Stevenazzi, A. *Chem. Commun.*, **2007**, 41, 4236-4238.
 - ¹¹ Aakeröy, C. B.; Hitchcock, P. B. *J. Mat. Chem.*, **1993**, 3(11), 1129-1135.
 - ¹² Jin, S.; Guo, M.; Wang, D.; Wei, S.; Zhou, Y.; Zhou, Y.; Cao, X.; Yu, Z. *J. Mol. Struct.*, **2012**, 1020, 70-82.
 - ¹³ Aakeröy, C. B.; Rajbanshi, A.; Desper, J. *Chem. Commun.*, **2011**, 47(41), 11411-11413.
 - ¹⁴ Singh, S.; Aggarwal, A.; Farley, C.; Hageman, B. A.; Batteas, J. D.; Drain, C. M. *Chem. Commun.*, **2011**, 47(25), 7134-7136.
 - ¹⁵ Patra, R.; Titi, H. M.; Goldberg, I. *Cryst. Growth Des.*, **2013**, 13(3), 1342-1349.
 - ¹⁶ Koner, R.; Goldberg, I. *CrystEngComm*, **2009**, 11(7), 1217-1219.

¹⁷ Aakeröy C. B.; Chopade, P. D.; Ganser, C.; Desper, J. *Chem. Commun.*, **2011**, 47(16), 4688-4690.

¹⁸ Some highlighted papers from the work of G. M. J. Schmidt: Harnik, E.; Herbstein, F. H.; Schmidt, G. M. J. *Nature*, 1951, 168, 158-160; Herbstein, F. H.; Schmidt, G. M. J. *Nature*, **1952**, 169, 323-324; Herbstein, F. H.; Schmidt, G. M. J. *Acta Cryst.*, **1955**, 8, 399-405; Bregman, J.; Schmidt, G. M. J. *J. Am. Chem. Soc.*, **1962**, 84, 3785-3786; Cohen, M. D.; Schmidt, G. M. J. *J. Chem. Soc.*, **1964**, 1996-2000; Rabinovich, D.; Schmidt, G. M. J. *Nature*, **1966**, 211(5056), 1391-1393; Leiserowitz, L.; Schmidt, G. M. J. *J. Chem. Soc. A*, **1969**, 16, 2372-2382; Penzien, K.; Schmidt, G. M. J. *Angew. Chemie., Int. Ed. Engl.*, **1969**, 8(8), 608-609.

¹⁹ Schmidt, G. M. J. *Pure Appl. Chem.*, **1971**, 27(4), 647-678.

²⁰ For examples of directed supramolecular assembly (including metals) see the following examples: Aakeröy C. B.; Schultheiss N.; Desper J. *Dalton Trans.*, **2006**, 13, 1627-1635; Aakeröy, C. B.; Scott, B. M. T.; Smith, M. M.; Urbina, J. F.; Desper, J. *Inorg. Chem.*, **2009**, 48(9), 4052-4061; Aakeröy, C. B.; Schultheiss, N.; Desper, J. *Inorg. Chem.*, **2005**, 44(14), 4983-4991; Schmidt, R.; Stolte, M.; Gruene, M.; Wurthner, F. *Macromolecules*, **2011**, 44(10), 3766-3776.

²¹ Aakeröy, C. B.; Seddon, K. R. *Chem. Soc. Rev.*, **1993**, 22, 397-407.

²² Jiang, W.; Tiefenbacher, K.; Ajami, D.; Rebek, J. *Chem. Sci.*, **2012**, 3(10), 3022-3025.

²³ Kubitschke, J.; Javor, S.; Rebek, J. *Chem. Commun.*, **2012**, 48(74), 9251-9253.

²⁴ Ryan, D. A.; Rebek, J. *Analyst*, **2013**, 138(4), 1008-1010.

²⁵ Metrangolo, P.; Resnati, G. *Cryst. Growth Des.*, **2012**, 12(12), 5835-5838.

²⁶ Cariati, E.; Cavallo, G.; Forni, A.; Leem, G.; Metrangolo, P.; Meyer, F.; Pilati, T.; Resnati, G.; Righetto, S.; Terraneo, G.; Tordin, E. *Cryst. Growth Des.*, **2011**, 11(12), 5642-5648.

²⁷ Bruce, D. W.; Metrangolo, P.; Meyer, F.; Pilati, T.; Praesang, C.; Resnati, G.; Terraneo, G.; Wainwright, S. G.; Whitwood, A. C. *Chem. Eur. J.*, **2010**, 16(31), 9511-9524.

²⁸ Baldrighi, M.; Cavallo, G.; Chierotti, M. R.; Gobetto, R.; Metrangolo, P.; Pilati, T.; Resnati, G.; Terraneo, G. *Mol. Pharm.*, **2013**, 10(5), 1760-1772.

²⁹ Nonappa; Lahtinen, M.; Kolehmainen, E.; Haarala, J.; Shevchenko, A. *Cryst. Growth Des.*, **2013**, 13(1), 346-351.

³⁰ Desiraju, G. R. *Angew. Chemie, Int. Ed.*, **1995**, 34(21), 2311-2327.

³¹ Aakeröy, C. B.; Chopade, P. D.; Desper, J. *Cryst. Growth Des.*, **2011**, 11(12), 5333-5336; Dunitz, J. D.; Gavezzotti, A. *Cryst. Growth Des.*, **2012**, 12(12), 5873-5877.

³² Etter, M. C. *Acc. Chem. Res.*, **1990**, 23, 120-126; Etter, M. C.; MacDonald, J. C.; Bernstein, J. *Acta Cryst.*, **1990**, B46(2), 256-262.

³³ Bernstein, J.; Etter, M. C.; MacDonald, J. C. *J. Chem. Soc., Perkin Trans. 2: Phys. Org. Chem.* (1972-1999), 5, 695-698.

³⁴ Aakeröy, C. B.; Salmon, D. J. *CrystEngComm*, **2005**, 7, 439-448.

³⁵ Zhang, G.-C.; Lin, H.-L.; Lin, S.-Y. *J. Pharm. Biomed. Anal.*, **2012**, 66, 162-169.

³⁶ Liu, X.; Lu, M.; Guo, Z.; Huang, L.; Feng, X.; Wu, C. *Pharm. Res.*, **2012**, 29(3), 806-817.

³⁷ Kirchner, M. T.; Blaeser, D.; Boese, R. *Chem. Eur. J.*, **2010**, 16(7), 2131-2146.

³⁸ Aakeröy, C. B.; Desper, J.; Helfrich, B. A. *CrystEngComm*, **2004**, 6(5), 19-24.

³⁹ Seaton, C. C.; Parkin, A.; Wilson, C. C.; Blagden, N. *Cryst. Growth Des.*, **2009**, 9(1), 47-56.

⁴⁰ Luo, Y.-H.; Sun, B.-W. *Cryst. Growth Des.*, **2013**, 13(5), 2098-2106.

⁴¹ Basavoju, S.; Bostroem, D.; Velaga, S. P. *Mol. Cryst. Liq. Cryst.*, **2012**, 562(1), 254-264.

⁴² Kratochvil, B.; Koupilova, I. *Chemické Listy*, **2011**, 105(1), 3-7.

⁴³ Dubey, R.; Pavan, M. S.; Desiraju, G. R. *Chem. Commun.*, **2012**, 48(72), 9020-9022; Tothadi, S.; Desiraju, G. R. *Philos. Trans. of the Royal Soc. A*, **2012**, 370(1969), 2900-2915; Mukherjee, A.; Grobelny, P.; Thakur, T. S.; Desiraju, G. R. *Cryst. Growth Des.*, **2011**, 11(6), 2637-2653.

⁴⁴ Aakeröy, C. B.; Forbes, S.; Desper, J. *J. Am. Chem. Soc.*, **2009**, 131(47), 17048-17049.

⁴⁵ Weyna, D. R.; Cheney, M. L.; Shan, N.; Hanna, M.; Zaworotko, M. J.; Sava, V.; Song, S.; Sanchez-Ramos, J. R. *Mol. Pharm.*, **2012**, 9(7), 2094-2102.

Chapter 2 - Is the pyrazole...carboxylic acid synthon robust enough for driving co-crystal synthesis?

2.1 Introduction

Although crystal structure prediction¹ has yet to be realized for even the simplest compounds, it is important to study intermolecular interactions in solids and to establish a toolbox for building supermolecules.² Gaining control over the composition and dimensionality of supramolecular assemblies³ may allow specific structures to be made⁴ with predictable physical properties.⁵ Therefore, a careful and thorough understanding of how to assemble small molecule 'building blocks' is essential for developing the synthesis of functional materials.⁶

One common intermolecular interaction used for the assembly of building blocks is the hydrogen bond,⁷ which can be formed between an electropositive hydrogen atom and any electronegative element, such as nitrogen, oxygen, or sulfur. A significant number of examples of hydrogen bonds found in crystal engineering occur between pyridine and carboxylic acids; a 2012 CSD search gave over 4560 hits⁸ of this synthon⁹.

The interaction involves a primary O-H...N(py) and, occasionally, a secondary C-H...O contact, Figure 2.1.¹⁰⁻¹¹

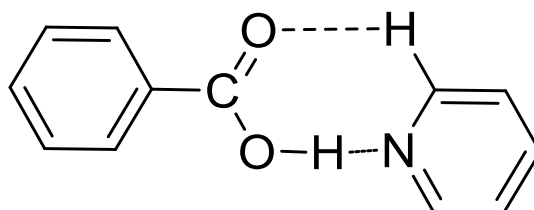


Figure 2-1 The carboxylic acid...pyridine heterosynthon, $R_2^2(7)$.

In order to expand the synthetic toolbox, it is important to explore other N heterocycles containing both a good hydrogen-bond acceptor site (and hydrogen bond donor site), and within this class of compounds pyrazole is particularly intriguing. Found as a backbone of many agrichemicals¹² and as small molecule enzyme inhibitors,¹³ pyrazole provides a scaffold for exploring such interactions. Since the pK_b of the pyridine nitrogen (8.75)¹⁴ is lower than that of

the pyrazole nitrogen (11.5)¹⁵, it is important to know if the charge on the pyrazole is robust enough for driving co-crystal synthesis, Figure 2.2.

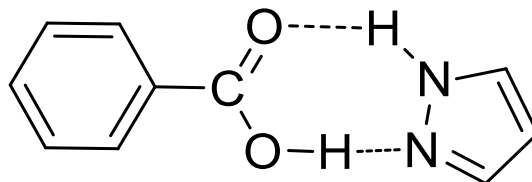


Figure 2-2 The carboxylic acid···pyrazole heterosynthon, $R_2^2(7)$.

Despite looking very similar to the pyridine···carboxylic acid synthon, and having identical graph set notation, $R_2^2(7)$ ¹⁶, there are very few examples that demonstrate pyrazole as an attractive site for making co-crystals¹⁷ and can act as a suitable hydrogen-bond acceptor site with carboxylic acids. Surprisingly, an analysis of the CSD of pyrazole and carboxylic acid structures gives only 92 hits. Careful examination reveals that the majority of structures containing pyrazole are used as ligands in metal coordination complexes¹⁸ and the few structures which do not contain a metal show the tendency to form either trimer¹⁹ and tetramer²⁰ motifs, as opposed to forming dimers in solid-state architectures. This study will address the following questions:

- I. Is there a pyrazole···carboxylic acid synthon robust enough for driving co-crystal synthesis? **Hypothesis:** pyrazole will provide a suitable hydrogen-bond acceptor site N(py) which is strong enough to drive co-crystal synthesis. This will be achieved by combining nine pyrazoles with twenty benzoic acid cofomers.
- II. Can the electrostatic nature of the pyrazole be altered by adding covalent ‘handles’ to the molecular backbone which influence the supramolecular yield? **Hypothesis:** the electronic nature of the pyrazole can be changed by adding electron donating groups (R-X, X=CH₃) and electron withdrawing (R-X, X=Cl, Br, I, NO₂) substituents to the backbone of the pyrazole and will alter the electrostatic nature of the N(py) acceptor site. A higher charge should increase the supramolecular yield.

2.2 Experimental

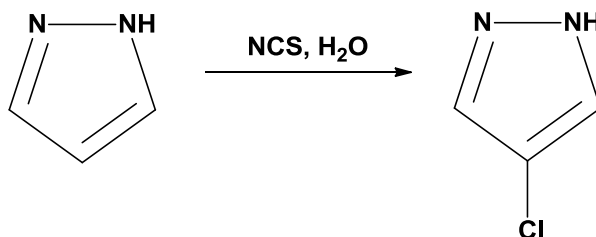
2.2.1 Charge calculations

Molecular electrostatic potential (MEP) surface charge calculations were performed using Spartan (Wavefunction, Inc., Irvine, CA). The molecules were optimized using AM1, with the maxima and minima in the electrostatic potential surface (0.002 e/au isosurface) determined using a positive point charge in the vacuum as a probe.

2.2.2 Covalent synthesis

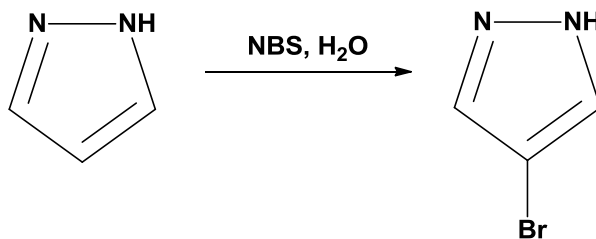
All chemicals were purchased from Aldrich and used without further purification unless otherwise noted. Substituted pyrazoles were synthesized according to published literature procedures.²¹⁻²²⁻²³ NMR data was recorded on a Bruker 200MHz (unless otherwise noted). Melting points were determined on a Fisher-Johns melting point apparatus and are uncorrected.

2.2.2.1 Synthesis of 4-chloro-1H-pyrazole, **1.Cl**



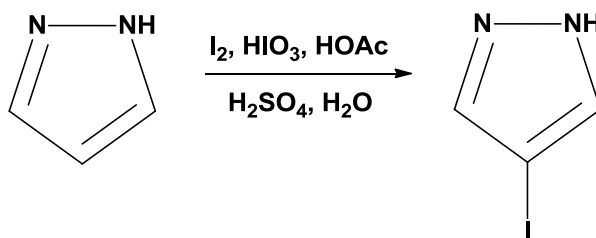
To a round-bottom flask, 1H-pyrazole (0.89g, 13.1mmol) and H₂O (15ml) were added. To this solution, *N*-chlorosuccinimide (NCS, 1.75g, 13.1mmol) was added and the reaction was stirred at room temperature for four hours. The reaction was monitored by ¹H NMR (disappearance of the single C-H proton). Upon completion, CHCl₃ was added to the reaction mixture to create bilayers. The water layer was washed twice with CHCl₃ (15mL), the organic extracts were combined, dried over MgSO₄, and the solvent was removed under vacuum to yield **1** as a white solid (0.66g, 49%). Mp: 73-74°C (lit. 75-76°C).²¹ ¹H NMR (200 MHz, CDCl₃) δ ppm: 9.88 (br. s., 1H), 7.65 (s, 2H), Figure A-1.

2.2.2.2 Synthesis of 4-bromo-1H-pyrazole, 1.Br



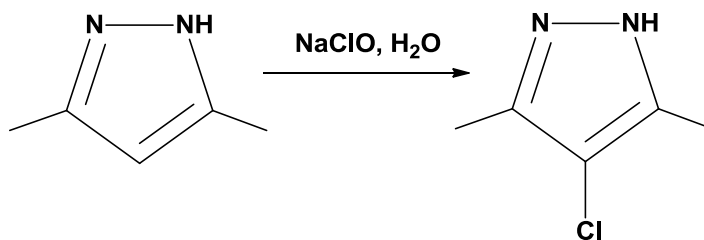
To a round-bottom flask, 1H-pyrazole (0.52g, 7.6mmol) and H₂O (15mL) were added. To this solution, N-bromosuccinimide (NBS, 1.4g, 7.6mmol) was added and 4mL of H₂O was used to wash the NBS off the sides of the flask. The reaction was stirred at room temperature for four hours and monitored by ¹H NMR (disappearance of the single proton). Upon completion, CHCl₃ was added to the reaction mixture to create bilayers. The water layer was washed twice with CHCl₃(15mL), the organic extracts were combined, dried over MgSO₄, and the solvent was removed under vacuum to yield **2** as a white solid (0.84g, 75%). Mp: 89-91 °C (lit. 91-92 °C).²¹ ¹H NMR (δ_H; 200MHz, CDCl₃) δ ppm: 7.61 (s, 2H), Figure A-2.

2.2.2.3 Synthesis of 4-iodo-1H-pyrazole, 1.I



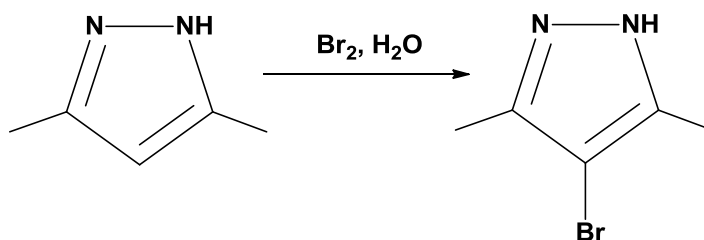
To a round-bottom flask, 1H-pyrazole (0.34g, 5.0mmol) and glacial acetic acid (7.4mL, 129.4mmol) were added. To this solution, I₂ (0.51g, 2.0mmol) was added and the solution turned brown. Next, HIO₃ (0.18g, 1.0mmol) and H₂SO₄ (200μL) were added. The mixture was refluxed with stirring under argon, and the remaining H₂SO₄ (100μL) and deionized water (700μL) were added. The reaction was kept at 70 °C, and the solution turned from pink to colorless after 20 minutes. Saturated NaHCO₃(aq) (1mL) was then added to the refluxing mixture, which was cooled to room temperature. Finally, 20% Na₂CO₃(aq) was added (10mL additions) until no bubbling was observed. CHCl₃ was added to create bilayers (20mL). The water layer was washed three times with CHCl₃ (20mL) and the organic extracts were combined, dried over MgSO₄, and solvent was removed under vacuum to yield **3** as a white solid (0.70g, 72%). Mp: 104-105 °C (lit. 108 °C).²² ¹H NMR (δ_H; 200MHz, CDCl₃) δ ppm: 10.66 (br. s., 1H), 7.66 (s, 2H), Figure A-3.

2.2.2.4 Synthesis of 4-chloro-(3,5-dimethyl)-1H-pyrazole, 2.Cl



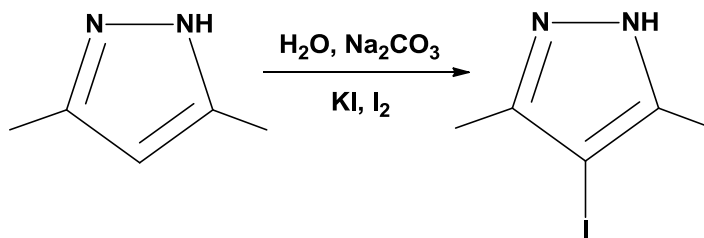
To a 100mL single-neck round bottom flask, 3,5-dimethyl-1H-pyrazole (0.50g, 5.2mmol) and 5.4mL of deionized water were added. A white flocculate was observed, at which point glacial acetic acid (0.81mL, 14.2mmol) was added, which dissolved the white flocculate. To the clear solution, Clorox® Bleach (15mL) was added. A white cloudiness was observed and the mixture was stirred at room temperature for two hours, at which point 3mL of saturated Na₂CO₃(aq) was added to neutralize any remaining acetic acid. Two drops of ammonium hydroxide were then added and the flask was placed in the refrigerator. The white solids were filtered and washed with cold water twice (5mL) to give **4** as a white solid (0.42g, 62%). Mp: 106-108°C (lit. 117-118°C).²³ ¹H NMR (δ_H; 200MHz, CDCl₃) δ ppm: 2.25 (s, 6H), Figure A-4.

2.2.2.5 Synthesis of 4-bromo-(3,5-dimethyl)-1H-pyrazole, 2.Br



To a 100mL single-neck round bottom flask, 3,5-dimethyl-1H-pyrazole (0.55g, 5.8mmol) and 22mL of deionized water were added. The mixture was stirred at room temperature until the solids dissolved, at which point Br₂ (0.3mL, 5.8mmol) was added slowly while stirring. The colorless solution turned brown, and the mixture was then neutralized with NaOH(aq) (4M, 40mL). Brown solids which precipitated were filtered off, and the filtrate was placed in the refrigerator overnight. The filtrate was washed twice with CH₂Cl₂ (50mL), dried over MgSO₄, and the solvent was removed under vacuum to give **5** as tan solids (0.38g, 38%). Mp: 116-119°C (lit. 122°C).²³ ¹H NMR (δ_H; 200MHz, CDCl₃) δ ppm: 2.26 (s, 6H), Figure A-5.

2.2.2.6 Synthesis of 4-iodo-(3,5-dimethyl)-1H-pyrazole, 2.I



To a 250mL three-neck round bottom flask, 3,5-dimethyl-1H-pyrazole (0.51g, 5.3mmol) and Na₂CO₃ (0.30g, 2.8mmol) were added. The solids were then dissolved in 28.2mL of deionized water and the mixture was heated to reflux under dinitrogen. In a separate beaker, KI (1.75g, 10.5mmol) and I₂ (1.31g, 5.16mmol) were dissolved in 4.5mL of deionized water. The KI₃ solution was added dropwise to the dimethylpyrazole solution at a rate of one drop every fifteen seconds. After 25 minutes, a fine white flocculate formed, and the remaining KI₃ solution was added to the mixture. The flask was placed in the refrigerator overnight to help precipitation. The next day, a white flocculate was filtered and washed twice with 15mL of ice water. The filtered solids were then dissolved in 23mL of CH₂Cl₂. The organic layer was washed once with dilute Na₂CO₃(aq), the organic layer was separated, dried over MgSO₄, and concentrated under vacuum to give **6** as a white solid (0.51g, 52%). Mp: 135-136°C. ¹H NMR (δ_H; 200MHz, CDCl₃) δ ppm: 2.27 (s, 6H), Figure A-6.

2.2.2.7 Synthesis of 4-bromo-1H-pyrazole:3,5-dinitrobenzoic acid (1:1), 1.Br:N

To a vial, 4.3 mg (0.029 mmol) of 4-bromo-1H-pyrazole was added along with 1 mL of methanol. To a separate vial, 6.1 mg (0.029 mmol) of 3,5-dinitrobenzoic acid was added along with 1 mL of methanol. The two solutions were combined in a vial, covered with parafilm (one pinhole), and left for slow evaporation. Colorless prisms were obtained after several days. M.p.: 135-140°C.

2.2.2.8 Synthesis of 4-iodo-1H-pyrazole:4-cyanobenzoic acid (1:1), 1.I:H

To a vial, 15.2 mg (0.078 mmol) of 4-iodo-1H-pyrazole was added along with 0.5 mL of methanol. To a separate vial, 11.5 mg (0.078 mmol) of 4-cyanobenzoic acid was added along with 0.5 mL of methanol. The vial containing the acid was heated until fully dissolved, then added to the solution containing the pyrazole. The vial was covered with parafilm (three

pinholes) and left for slow evaporation. Colorless prisms were obtained after several days. M.p.: 189-190°C.

2.2.2.9 Synthesis of 4-iodo-1H-pyrazole:3,5-dinitrobenzoic acid (1:1), 1.I:N

To a vial, 12.6 mg (0.065 mmol) of 4-iodo-1H-pyrazole was added along with 0.5 mL of methanol. To a separate vial, 13.8 mg (0.065 mmol) of 3,5-dinitrobenzoic acid was added along with 0.5 mL of methanol. The two solutions were combined in a vial, covered with parafilm (three pinholes), and left for slow evaporation. Colorless plates were obtained after several days. M.p.: 123-125°C.

2.2.2.10 Synthesis of 4-chloro-3,5-dimethyl-1H-pyrazole:4-hydroxy-3-methoxybenzoic acid (1:1), 2.Cl:B

To a vial, 7.3 mg (0.056 mmol) of 4-chloro-3,5-dimethyl-1H-pyrazole was added along with 200 µL of methanol. To a separate vial, 9.6 mg (0.057 mmol) of 4-hydroxy-3-methoxybenzoic acid was added along with 200 µL of methanol. The two solutions were combined in a vial, covered with parafilm (one pinhole), and left for slow evaporation. Colorless spheres were obtained after several days. M.p.: 205-209°C.

2.2.2.11 Synthesis of 4-chloro-3,5-dimethyl-1H-pyrazole:3,5-dinitrobenzoic acid (1:1), 2.Cl:N

To a vial, 5.3 mg (0.041 mmol) of 4-chloro-3,5-dimethyl-1H-pyrazole was added along with 200 µL of methanol. To a separate vial, 8.9 mg (0.042 mmol) of 3,5-dinitrobenzoic acid was added along with 200 µL of methanol. The two solutions were combined in a vial, covered with parafilm (one pinhole), and left for slow evaporation. Colorless prisms were obtained after several days. M.p.: 156-160°C.

2.2.2.12 Synthesis of 4-bromo-3,5-dimethyl-1H-pyrazole:3,5-dinitrobenzoic acid (1:1), 2.Br:N

To a vial, 5.7 mg (0.033 mmol) of 4-bromo-3,5-dimethyl-1H-pyrazole was added along with 1 mL of methanol. To a separate vial, 7.1 mg (0.033 mmol) of 3,5-dinitrobenzoic acid was added along with 1 mL of methanol. The two solutions were combined in a vial, covered with parafilm (one pinhole), and left for slow evaporation. Colorless plates were obtained after several days. M.p.: 155-158°C.

2.2.2.13 Synthesis of 4-chloro-3,5-dimethyl-1H-pyrazolium:2,4-dinitrobenzoate:4-chloro-3,5-dimethyl-1H-pyrazole (1:1:1), 2.Cl:T

To a vial, 5.6 mg (0.043 mmol) of 4-chloro-3,5-dimethyl-1H-pyrazole was added along with 200µL of methanol. To a separate vial, 9.2 mg (0.043 mmol) of 2,4-dinitrobenzoic acid was added along with 200µL of methanol. The two solutions were combined in a vial, covered with parafilm (one pinhole), and left for slow evaporation. Colorless plates were obtained after several days. M.p. 100-102°C.

2.2.2.14 Synthesis of 4-iodo-3,5-dimethyl-1H-pyrazolium:3,5-dinitrobenzoate (1:1), 2.I:N

To a vial, 5.4 mg (0.024 mmol) of 4-iodo-3,5-dimethyl-1H-pyrazole was added along with 200µL of methanol. To a separate vial, 5.2 mg (0.024 mmol) of 3,5-dinitrobenzoic acid was added along with 200µL of methanol. The two solutions were combined in a vial, covered with parafilm (one pinhole), and left for slow evaporation. Colorless prisms were obtained after several days. M.p. 138-142°C.

2.2.2.15 Synthesis of 1H-pyrazolium:3,5-dinitrobenzoate:3,5-dinitrobenzoic acid (1:1:1), 1.H:N

To a small beaker, 29.1 mg (0.43 mmol) of 1H-pyrazole was added and dissolved in 1 ml of absolute ethanol (200 proof). To a separate beaker, 91.4 mg (0.43 mmol) of 3,5-dinitrobenzoic acid was added and dissolved in 1 ml of absolute ethanol (200 proof). The two solutions were combined in a beaker, covered with parafilm (five pinholes), and left for slow evaporation. Colorless plates were obtained after several days. M.p. 146-148°C.

2.2.2.16 Synthesis of 3,5-dimethyl-1H-pyrazolium:3,5-dinitrobenzoate hydrate (1:1:1), 2.H:N:H₂O

To a small beaker, 27.9 mg (0.29 mmol) of 3,5-dimethyl-1H-pyrazole was added and dissolved in 1 ml of absolute ethanol (200 proof). To a separate beaker, 62.3 mg (0.29 mmol) of 3,5-dinitrobenzoic acid was added and dissolved in 1 ml of absolute ethanol (200 proof). The two solutions were combined in a test tube and left for slow evaporation. Colorless prisms were obtained after several days. M.p. 120-124°C.

2.2.2.17 Synthesis of 1*H*-pyrazolium:2,6-dichlorobenzoate:2,6-dichlorobenzoic acid (1:1:1), 1*H*:*R*

To a test tube, 13.1 mg (0.19 mmol) of 1*H*-pyrazole was added along with 39.3 mg (0.21 mmol) of 2,6-dichlorobenzoic acid. The solids were heated using a heat gun until both components had melted. The melt was allowed to cool to room temperature, yielding colorless plates. M.p.: 71-73°C.

2.2.3 IR

Infrared experiments were collected on a Thermo Scientific Nicolet 380 FT-IR using a ZnSe crystal. The solids obtained from melt (or solution) experiments were analyzed by placing the solid directly on the crystal and performing 32 scans.

2.3 Results

2.3.1 MEP surface calculations

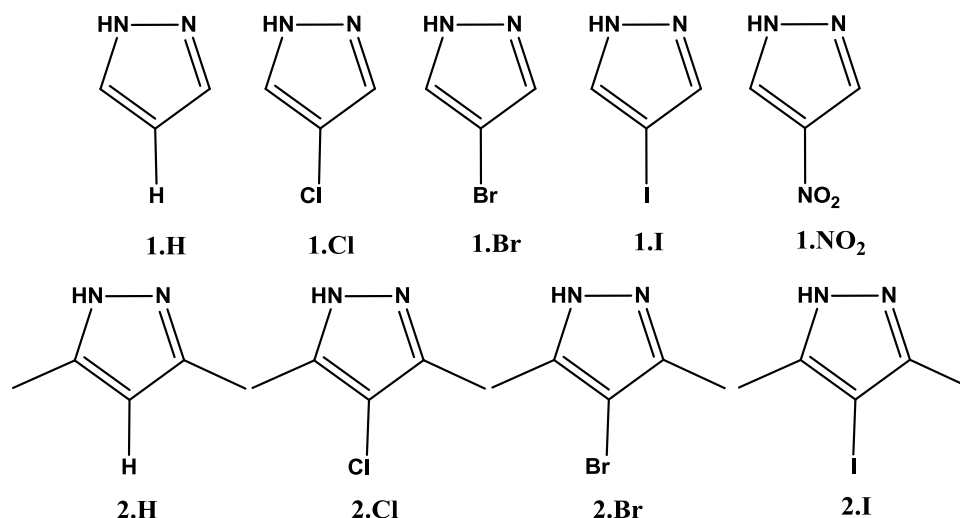
Molecular electrostatic potential (MEP) surface calculations were made in order to rank the strengths of the hydrogen bond donor (H) and acceptor (N) sites. Although a low level of theory is used (AM1)²⁴, PM3 and DFT (B3LYP/6-311+G** level) calculations were also conducted to see if a similar trend in binding site strength site was observed. Previously, Hunter²⁵ and co-workers²⁶ showed that AM1 works well for calculating electrostatic surface energies for small molecules like *N*-methyl acetamide.

Table 2.1 Molecular electrostatic surface potential calculations for the various pyrazoles (AM1, PM3, DFT). Values given in kJ/mol.

Molecule	AM1 (H)	AM1 (N)	PM3 (H)	PM3 (N)	DFT (H)	DFT (N)
1.H	178	-251	156	-307	245	-186
1.Cl	194	-236	167	-289	269	-159
1.Br	200	-230	169	-283	273	-160
1.I	200	-231	161	-282	-	-
1.NO ₂	254	-260	280	-297	315	-162
2.H	171	-256	141	-308	226	-195
2.Cl	188	-238	150	-298	260	-172
2.Br	193	-239	152	-293	253	-171
2.I	191	-237	150	-302	-	-

2.3.2 Covalent synthesis

Nine pyrazole molecules were synthesized with different covalent substituents on the molecular backbone intended to alter the electrostatic potential surface energy of the molecule. The nine pyrazole molecules used are shown in Scheme 1. Six of the nine pyrazoles used were synthesized according to literature procedures, and the results are summarized in Table 2.1.



Scheme 1. The nine pyrazole molecules used in this study.

Table 2.2 ¹H NMR data, yields, and melting points for six pyrazoles synthesized.

Molecule	¹ H NMR values [Lit. value]	Melting point [Lit. value]	% Yield
1.Cl	7.58 (s, 2H, CH) [7.55, s, 2H, CH]	73-74°C [75-76°C] ²¹	49%
1.Br	7.61 (s, 2H, CH) [7.53, s, 2H, CH]	89-91°C [91-92°C] ²¹	30%
1.I	7.65 (s, 2H, CH) [7.64, s, 2H, CH]	104-105°C [108°C] ²²	47%
2.Cl	2.25 (s, 6H, CH ₃) [2.25, s, 6H, CH ₃]	106-108°C [117-118°C] ²³	62%
2.Br	2.26 (s, 6H, CH ₃) [2.26, s, 6H, CH ₃]	116-119°C [122°C] ²³	38%
2.I	2.27 (s, 6H, CH ₃) [2.27, s, 6H, CH ₃]	135-136°C [Not reported]	52%

2.3.3 Infrared data

The pyrazole molecules were screened with twenty carboxylic acids of varying pK_a strength, Table 2.

Table 2.3 Table of aromatic carboxylic acids used in the study.

Label (pKa) ²⁷	Benzoic Acid
A (4.57 +/- 0.10)	4-Hydroxybenzoic acid
B (4.45 +/- 0.10)	4-Hydroxy-3-methoxy benzoic acid
C (4.34 +/- 0.10)	3,5-Dimethylbenzoic acid
D (4.08 +/- 0.10)	3-Hydroxybenzoic acid
E (4.02 +/- 0.10)	4-Iodobenzoic acid
F (3.97 +/- 0.10)	4-Chlorobenzoic acid
G (3.64 +/- 0.10)	3-Cyanobenzoic acid
H (3.54 +/- 0.10)	4-Cyanobenzoic acid
I (3.48 +/- 0.10)	3-Nitrobenzoic acid
J (3.46 +/- 0.10)	3-Bromo-5-iodobenzoic acid
K (3.42 +/- 0.10)	4-Nitrobenzoic acid
L (3.27 +/- 0.10)	2-Fluorobenzoic acid
M (2.97 +/- 0.25)	2-Chlorobenzoic acid
N (2.77 +/- 0.10)	3,5-Dinitrobenzoic acid
O (2.34 +/- 0.10)	2,6-Difluorobenzoic acid
P (2.19 +/- 0.25)	2-Nitrobenzoic acid
Q (1.93 +/- 0.10)	2-Fluoro-6-iodobenzoic acid
R (1.69 +/- 0.10)	2,6-Dichlorobenzoic acid
S (1.60 +/- 0.10)	Pentafluorobenzoic acid
T (1.43 +/- 0.25)	2,4-Dinitrobenzoic acid

The results from the screening experiment are summarized in Table 2.4, and the corresponding supramolecular yield (calculated as the number of positive hits) is given in the last row.

Table 2.4 Summary of prominent IR stretches (cm⁻¹) from the melt experiments between nine pyrazoles and twenty carboxylic acids.

Acids	1.H	1.Cl	1.Br	1.I	1.NO ₂	2.H	2.Cl	2.Br	2.I
A	-	2499, 1897, 1666	2507, 1874, 1674	-	-	2488, 1855, 1679	-	2507, 1897, 1691	-
B	-	-	-	-	-	2496, 1879, 1667	2491, 1878, 1667	2491, 1881, 1671	2448, 1870, 1675
C	-	-	-	-	-	-	2452, 1838, 1671	-	-
D,E, F	-	-	-	-	-	-	-	-	-
G	-	2440, 1862, 1682	2535, 1865, 1693	2535, 1872, 1686	-	-	-	2382, 1870, 1679	-
H	-	2464, 1862, 1729	2396, 1865, 1693	2469, 1885, 1699	-	2503, 1897, 1699	2553, 1893, 1687	2541, 1889, 1675	2357, 1850, 1695
I	2382, 1883, 1695	2436, 1885, 1702	2425, 1862, 1698	2401, 1835,	2491, 1893,	2484, 1891, 1687	2632, 1889, 1720	2448, 1878,	2429, 1889,

				1679	1721			1688	1695
J	2397, 1928, 1690	-	-	2499, 1867, 1675	-	2350, 1858, 1704	2429, 1850, 1708	2468, 1897, 1708	2456, 1862, 1716
K	-	2487, 1874, 1690	2429, 1854, 1690	2417, 1846, 1687	-	-	-	2433, 1893, 1683	2429, 1866, 1683
L	2533, 1912, 1679	2433, 1881, 1694	2495, 1878, 1683	-	-	2476, 1891, 1695	2397, 1881, 1712	2390, 1901, 1720	2417, 1893, 1716
M	2517, 1936, 1679	2515, 1878, 1682	2495, 1881, 1682	-	-	2476, 1904, 1695	2499, 1917, 1679	2511, 1921, 1679	2448, 1885, 1687
N	2436, 1866, 1702	2413, 1854, 1698	2405, 1823, 1691	2413, 1827, 1691	-	2492, 1851, 1683	2519, 1842, 1701	2413, 1889, 1704	2433, 1846, 1698
O	2492, 1932, 1704	-	-	-	-	2521, 1887, 1720	-	-	-
P	2448, 1874, 1702	2526, 1874, 1674	2522, 1885, 1678	-	-	2459, 1842, 1708	-	2554, 1897, 1699	2386, 1901, 1691
Q	2357, 1912, 1720	2464, 1893, 1706	2491, 1893, 1702	2464, 1885, 1704	2546, 1862, 1698	2488, 1887, 1712	2483, 1909, 1712	2358, 1893, 1675	2452, 1909, 1712
R	2440, 1885, 1709	2483, 1893, 1709	2499, 1897, 1713	2415, 1897, 1704	-	2491, 1885, 1708	2476, 1901, 1716	2483, 1881, 1704	2468, 1889, 1708
S	2296, 1932, 1647	2421, 1909, 1702	-	-	-	2435, 1822, 1699	-	-	-
T	2429, 1866, 1713	2425, 1878, 1706	2366, 1881, 1708	2374, 1881, 1709	-	2522, 1893, 1717	2464, 1889, 1704	2456, 1878, 1699	2358, 1885, 1704
Supramolecular yield (%)	11/20 = 55%	13/20 = 65%	12/20 = 60%	12/20 = 60%	2/20 = 10%	14/20 = 70%	11/20 = 55%	14/20 = 70%	12/20 = 60%

2.3.4 Crystal structure of 4-bromo-1H-pyrazole:3,5-dinitrobenzoic acid (1:1), 1.Br:N

The crystal structure determination of **1.Br:N** shows a co-crystal with the intended 1:1 stoichiometry. The acidic protons remain on the two unique carboxylic acids as shown by the significantly different C=O/C-O(H) bond lengths, 1.219(4)/1.325(4) Å, and 1.219(4)/1.312(4) Å, respectively. The driving force for the reaction is the heteromeric O-H...N(pyraz)/N-H...O synthon, resulting in head-to-head dimers, Figure 2.3. These dimers are organized into 1-D chains via C-Br...O(nitro) halogen bonds; r(C-Br...O) is 3.148 Å and 3.028 Å; C-Br...O angle is 157° and 154°, respectively.

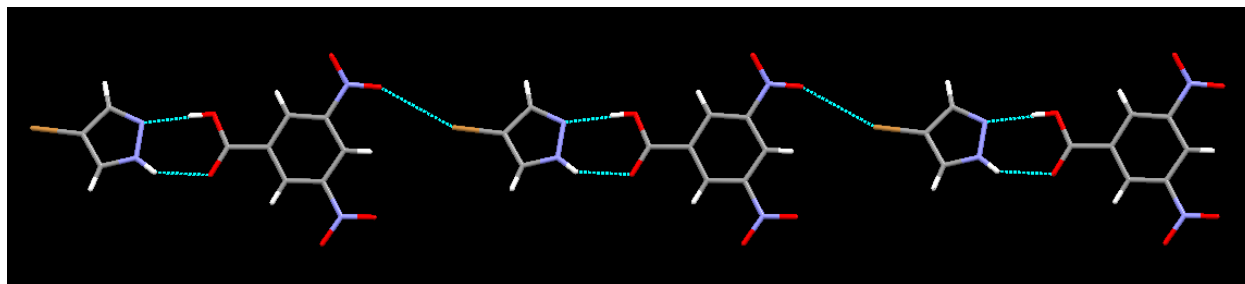


Figure 2-3 Infinite 1-D chain in the crystal structure of **1.Br:N** driven by O-H...N(pyz) and N-H...O synthons. N-O⁻...Br interactions extend the dimers into 1D chains.

2.3.5 Crystal structure of 4-iodo-1H-pyrazole:4-cyanobenzoic acid (1:1), 1.I:H

The crystal structure of **1.I:H** displays a very similar supermolecule as in **1.Br:N**. A head-to-head dimer is constructed from neutral O-H...N(pyz)/N-H...O synthons, Figure 2.4. The dimers are assembled into infinite 1-D chains by CN...I halogen bonds, where the CN...I distance is 3.183 Å with a C-I...N angle of 179°.

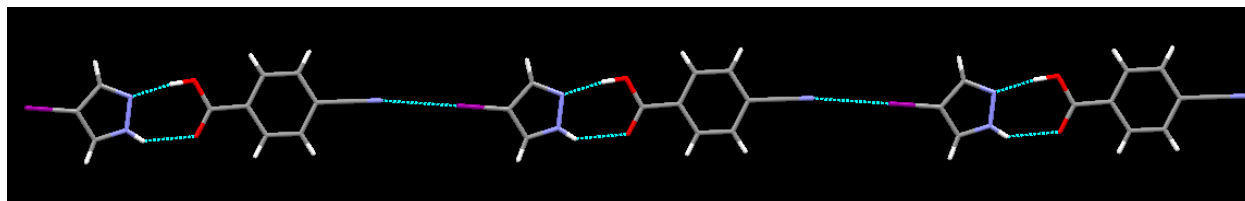


Figure 2-4 Infinite 1-D chain in the crystal structure of **1.I:H** driven by O-H...N(pyz) and N-H...O synthons. C-N...I interactions extend the dimers into 1-D chains.

2.3.6 Crystal structure of 4-iodo-1H-pyrazole: 3,5-dinitrobenzoic acid (1:1), 1.I:N

The crystal structure of **1.I:N** also contains 1-D chains where dimer formation occurs via O-H...N(pyz) and N-H...O interactions. The dimers are connected into 1-D chains through C-H...O synthons. The chains are linked together in a stair-step fashion through I...I (type I)²⁸ halogen bonds, Figure 2.5. The I...I distance is 3.698 Å and the C-I...I angle is 137°.

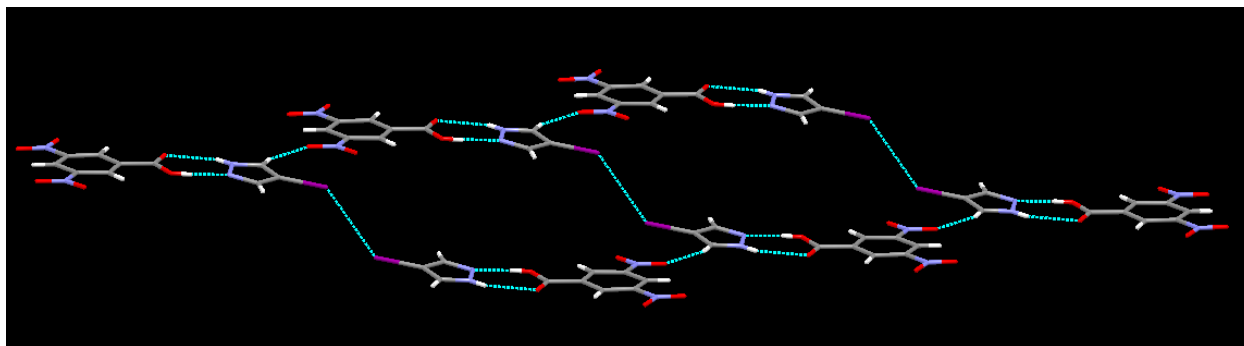


Figure 2-5 An overview of the 2-D layer in the crystal structure of **1.I:N**.

2.3.7 Crystal structure of 4-chloro-3,5-dimethyl-1H-pyrazole:4-hydroxy-3-methoxybenzoic acid (1:1), **2.Cl:B**

The crystal structure of **2.Cl:B** contains head-to-head heterodimers formed via O-H \cdots N(pyz) and N-H \cdots O synthons, Figure 2.6. The N-H proton is bifurcated between the C=O oxygen from one acid and the O-H oxygen from a second symmetry-related neutral acid. The synthons combine to form an extended zig-zag chain.

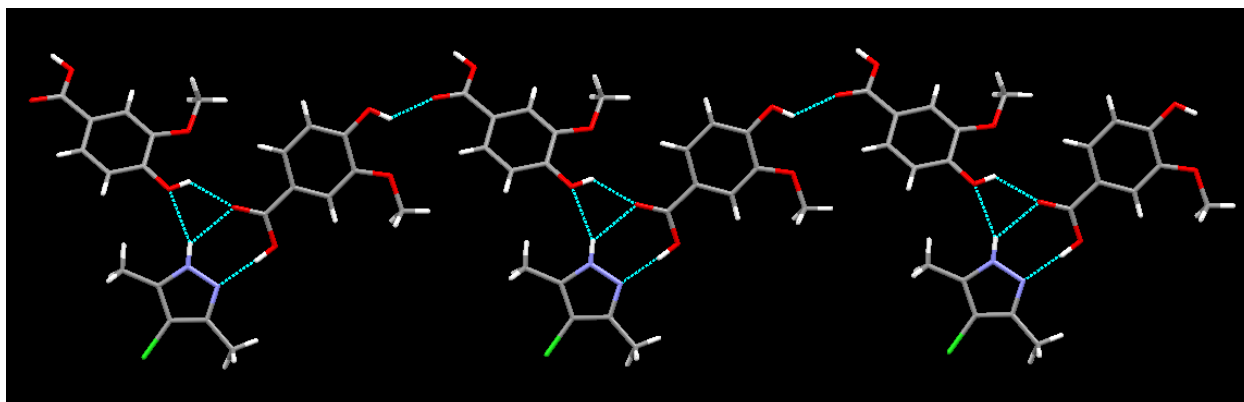


Figure 2-6 Infinite 1-D zig-zag chain in the structure of **2.Cl:B**.

2.3.8 Crystal structure of 4-chloro-3,5-dimethyl-1H-pyrazole:3,5-dinitrobenzoic acid (1:1), **2.Cl:N**

The structure of **2.Cl:N** contains neutral heterodimers formed by O-H \cdots N(pyz) and N-H \cdots O synthons, Figure 2.7. The dimers extend into 1-D chain via C-Cl \cdots O synthons. The C-Cl \cdots O distance is 3.065 Å and the C-Cl \cdots O angle is 170°.

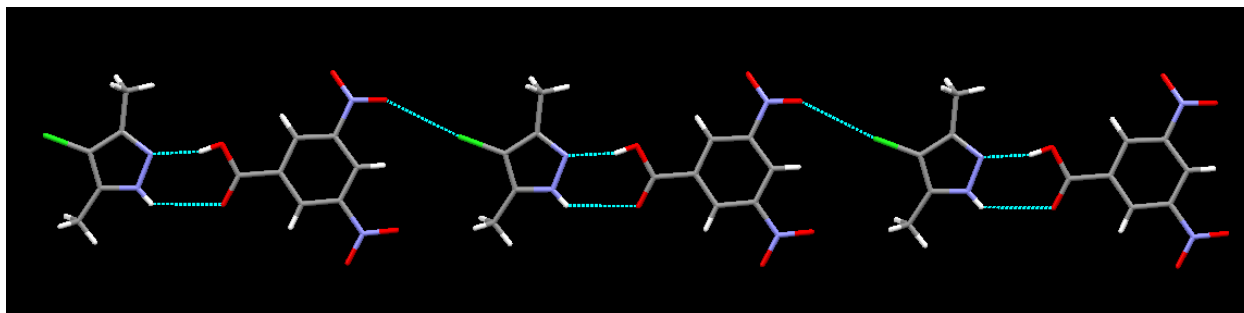


Figure 2-7 1-D chain of in the structure of **2.Cl:N**.

2.3.9 Crystal structure of 4-bromo-3,5-dimethyl-1H-pyrazole:3,5-dinitrobenzoic acid (1:1), 2.Br:N

In the crystal structure of **2.Br:N**, an infinite chain is observed where O-H \cdots N(pyz) and N-H \cdots O synthons drive co-crystal formation, Figure 2.8. The C-Br \cdots O $^-$ distance is 3.022 Å and the C-Br \cdots O $^-$ angle is 174°.

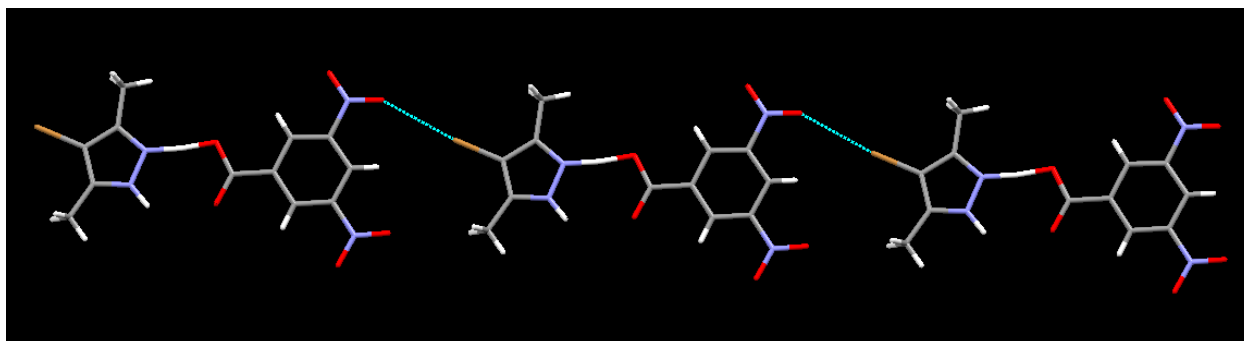


Figure 2-8 1-D chain in the crystal structure of **2.Br:N**.

2.3.10 Crystal structure of 4-chloro-3,5-dimethyl-1H-pyrazolium:2,4-dinitrobenzoate:4-chloro-3,5-dimethyl-1H-pyrazole (1:1:1), 2.Cl:T

In the crystal structure **2.Cl:T**, proton transfer occurred resulting in salt formation. Not only has the proton been transferred from the acid to the base, an additional neutral pyrazole molecule is also included in the lattice, Figure 2.9. The three building blocks are assembled into discrete trimers, driven by N-H \cdots O, N-H \cdots N, and charge-assisted N-H $^+$ \cdots O $^-$ synthons.

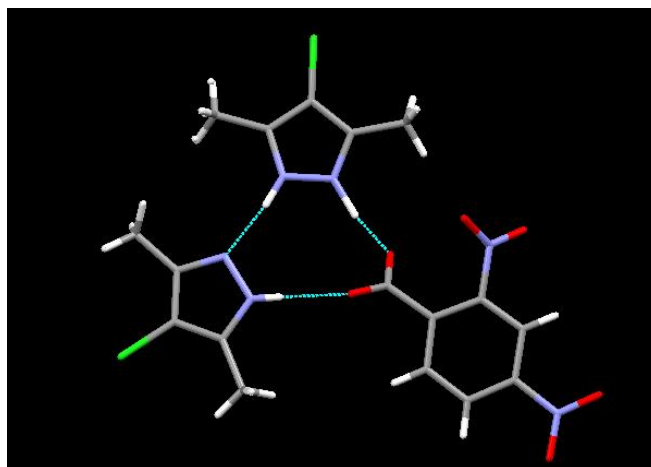


Figure 2-9 A hydrogen-bonded trimer in the crystal structure of 4-chloro-3,5-dimethylpyrazolium:2,4-dinitrobenzoate:4-chloro-3,5-dimethylpyrazole, 1:1:1, **2.CI:T**.

2.3.11 Crystal structure of 4-iodo-3,5-dimethyl-1H-pyrazolium:3,5-dinitrobenzoate (1:1), 2.I:N

The reaction between **2.I** and **N** also results in an ionic compound. A combination of charge-assisted $\text{N-H}^+\cdots\text{O}^-$, $\text{N-H}\cdots\text{O}$, and $\text{N-H}\cdots\text{O}^-$ synthons produce tetramers, Figure 2.10, which are connected into a ladder-like motif via $\text{C-I}\cdots\text{O}$ interactions, with a $\text{C-I}\cdots\text{O}$ distance of 3.089 Å and a $\text{C-I}\cdots\text{O}$ angle of 178°.

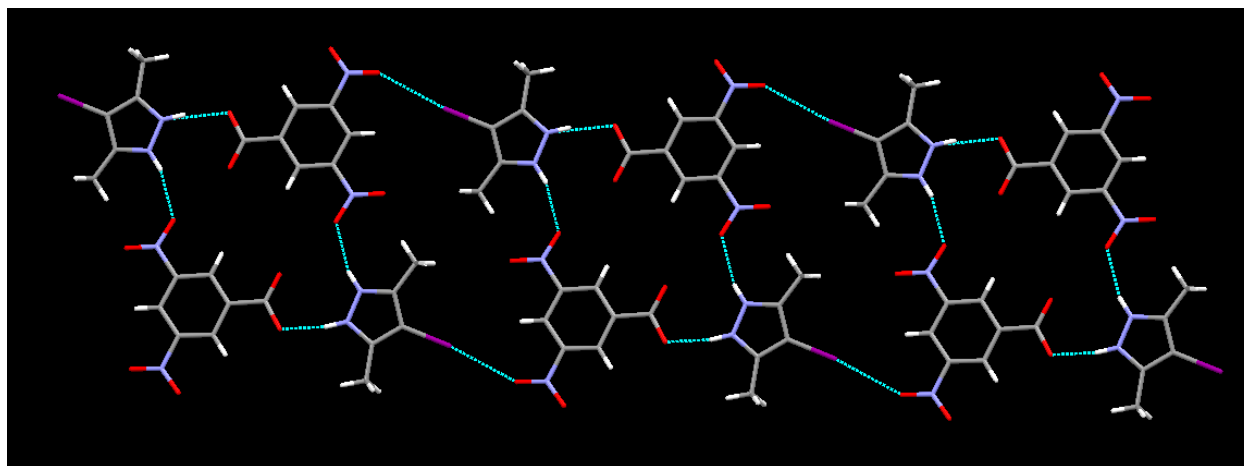


Figure 2-10 Tetramers (subsequently linked into ribbon) formed in the solid product resulting from a combination of **2.I** and **N**.

2.3.12 Crystal structure of 1*H*-pyrazolium:3,5-dinitrobenzoate:3,5-dinitrobenzoic acid (1:1:1), 1*H*:*N*

Figure 2.11 depicts a zig-zag chain formed by charge-assisted N-H⁺···O⁻ synthons in the crystal structure of the ionic compound produced when **1.H** was allowed to react with **N**. The N-H proton is bifurcated between a C=O oxygen from a second *neutral* acid and the carboxylate oxygen directly involved in the hetero dimer. The second neutral acid also forms an O-H···O⁻ synthon to complete the structure.

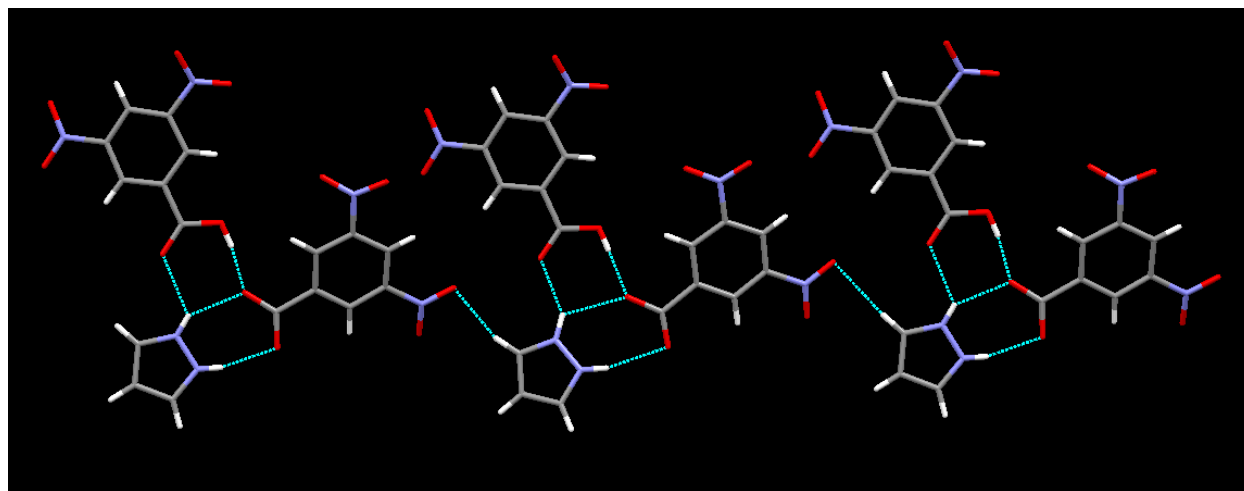


Figure 2-11 A zig-zag chain in the crystal structure of pyrazolium 3,5-dinitrobenzoate 3,5-dinitrobenzoic acid (1:1:1), **1.H**:**N**.

2.3.13 Crystal structure of 3,5-dimethyl-1*H*-pyrazolium:3,5-dinitrobenzoate hydrate (1:1), 2*H*:*N*:*H*₂*O*

The proton transfer from **N** to **2.H** produces the only hydrate in this series. The main feature is a trimer involving all three components, Figure 2.12. The N-H proton interacts directly with the oxygen from water to form a N-H···O_w synthon. The O-H(water)···O(carbonyl) synthon completes the trimer.

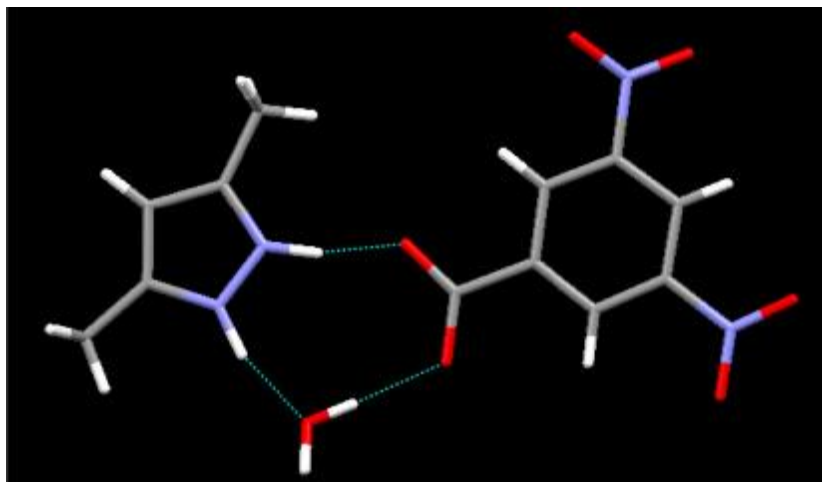


Figure 2-12 A hydrated ion-pair in the crystal structure of pyrazolium:3,5-dinitrobenzoate hydrate (1:1), **2.H:N**

2.3.14 Crystal structure of 1H-pyrazolium:2,6-dichlorobenzoate:2,6-dichlorobenzoic acid (1:1:1), 1.H:R

The reaction between **1.H** and **R** also produces an ionic compound where the main feature of the crystal structure is a tetramer, Figure 2.13, held together by charge-assisted N-H⁺⋯O⁻ synthons.

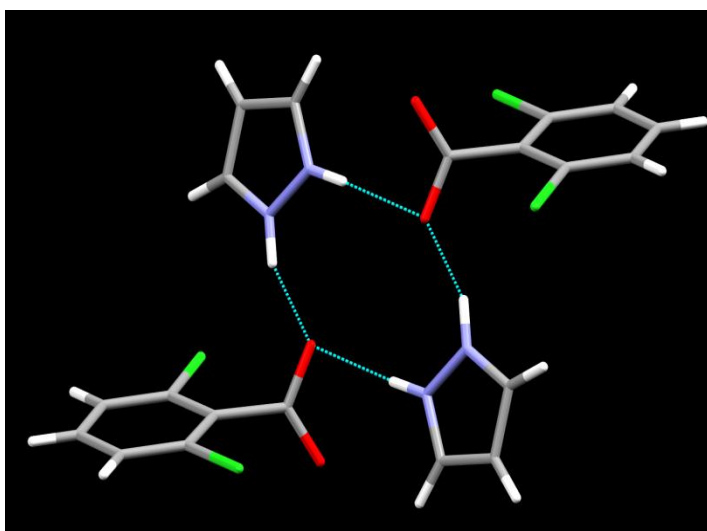


Figure 2-13 Discrete tetramers formed in the crystal structure of **1.H:R**.

All hydrogen bond geometries are listed in Table 2.5.

Table 2.5 Hydrogen bond geometries.

Structure	D-H...A	d(D-H)	d(H...A)	d(D...A)	<(DHA)
1.Br:N	N111-H111...O221	0.87(5)	2.11(5)	2.834(4)	140(4)
	N112-H112...O222	0.75(5)	2.18(5)	2.828(4)	145(5)
	O211-H211...N121	0.88(5)	1.80(5)	2.674(4)	175(5)
	O212-H212...N122	0.89(5)	1.79(5)	2.657(4)	167(5)
1.I:H	O(11)-H(11)...N(22)	0.96(2)	1.70(2)	2.6521(17)	171(2)
	N(21)-H(21)...O(12)	0.79(2)	2.16(2)	2.8225(17)	141(2)
1.I:N	O(11)-H(11)...N(22)	0.87(2)	1.75(2)	2.6225(17)	177(2)
	N(21)-H(21)...O(12)	0.78(2)	2.31(2)	2.9250(17)	136(2)
	O(31)-H(31)...N(42)	0.83(2)	1.84(2)	2.6671(18)	176(2)
	N(41)-H(41)...O(32)	0.76(2)	2.28(2)	2.9050(18)	140(2)
2.Cl:B	N(11)-H(11)...O(22)	0.89(3)	2.18(3)	2.875(2)	136(3)
	O(21)-H(21)...N(12)	0.90(3)	1.76(3)	2.654(2)	174(3)
	O(24)-H(24)...O(22)#1	0.84(4)	2.01(4)	2.636(2)	131(3)
2.Cl:N	N(11)-H(11)...O(22)	0.758(18)	2.619(17)	3.1647(13)	130.6(16)
	O(21)-H(21)...N(12)	0.814(18)	1.810(19)	2.5946(13)	161.6(18)
2.Br:N	N(11)-H(11)...O(22)	0.98(5)	2.49(5)	3.180(5)	128(3)
	O(21)-H(21)...N(12)	1.28(5)	1.30(5)	2.578(4)	173(4)
2.Cl:T	N(11)-H(11)...O(38)	1.15(2)	1.41(2)	2.541(2)	167(2)
	N(12)-H(12)...N(22)	0.92(2)	1.91(3)	2.811(2)	166(2)
	N(21)-H(21)...O(37)	0.78(3)	1.98(3)	2.740(2)	167(3)
2.I:N	N11A H11A O21	0.88	1.85	2.713(6) 3.005(9) 3.024(6) 2.772(7)	168.4
	N11B H11B O21	0.88	2.20		151.1
	N12A H12A O23	0.880.88	2.191.91		158.6
	N12B H12B O23				164.3
1.H:R	N11 H11 O21	0.87(4)	1.94(4)	2.797(4)	166(4)
	N12 H12 O21	0.92(4)	1.78(4)	2.650(4)	158(4)
	O31 H31 O22	0.83(5)	1.75(5)	2.575(4)	171(5)
1.H:N	N11A2-H11A2...O312	0.88	2.30	2.843(17)	119.7
	N12A2-H12A2...O322	0.88	2.22	3.059(17)	160.6
	N11B2-H11B2...O312	0.89(4)	1.73(4)	2.620(3)	178(4)
	N12B2-H12B2...O222	0.83(4)	1.99(4)	2.741(3)	149(3)
	O211-H211...O311	0.86(4)	1.67(4)	2.522(3)	172(3)
	O212-H212...O312	0.79(4)	1.72(4)	2.517(3)	177(4)

2.H:N	N11 H11 O21	0.995(17)	1.595(17)	2.5747(14)	167.2(15)
	N12 H12 O1W	0.967(16)	1.713(16)	2.6490(14)	162.0(15)
	O1W H1A O22	0.890(19)	1.851(19)	2.7390(13)	174.9(17)
	O1W H1B O22	0.888(18)	1.880(18)	2.7681(13)	178.9(18)

2.4 Discussion

2.4.1 Can the charge on the pyrazole backbone be altered by adding covalent ‘handles’?

From the MEP surface charge calculations, all three levels of theory (AM1, PM3, and DFT) give a consistent ranking of hydrogen-bond acceptor ability of the N(py_z) site. The most significant changes in charge were observed for 4-nitropyrazole, which gave a significantly lower charge (-260 kJ/mol) for the N(py_z) acceptor site (and substantial increase in charge for the N-H proton, 254 kJ/mol). The charge calculations do not show a significant difference in N(py_z) acceptor site strength between the halogen and halogen/methyl substituted pyrazoles. When weakly electron withdrawing (and donating) groups were used (R-X, X=Cl, Br, I, CH₃) on the pyrazole backbone, a charge between -231 kJ/mol to -251 kJ/mol was observed.

On the other hand, when a strongly electron withdrawing substituent is added (X=NO₂), the magnitude of charge on the N(py_z) acceptor site increases to -260 kJ/mol. The result demonstrates that even slight covalent alterations to the molecular backbone will have substantial consequences on charge of the N(py_z) acceptor site.

2.4.2 Do the results from the screening experiment corroborate the charge calculations?

From the screening experiments between nine pyrazoles and twenty carboxylic acids, the results indicate that charge plays an important role in determining supramolecular yield. When halogen and methyl covalent handles were added, the charge on the primary hydrogen bond acceptor N(py_z) does not change significantly, and the supramolecular yield was 55-70%. When a strongly electron withdrawing substituent like nitro (X=NO₂) group was added, the negative charge increases on the primary hydrogen bond acceptor site, and subsequently lowers the supramolecular yield to 10%. The results support the view of hydrogen bonds as primarily electrostatic in nature, as changes in the electrostatic charge significantly affect the supramolecular yield.

2.4.3 Co-crystals

Six co-crystals were obtained and all gave the expected stoichiometry (1:1) and the intended chemical composition. As expected, the primary O-H \cdots N(pyrazole) and secondary N-H \cdots O=C interactions drive co-crystal formation. It is noteworthy to point out that pK_a values of the acids play an important role in dictating the outcome. For example, when acids with pK_a values of 2.77 and greater were used, only co-crystal formation was observed.

2.4.4 Salts

Five salts were obtained which gave *unexpected* stoichiometry and unpredictable structural landscapes. When acids with pK_a values of *below* 2.77 were used, only salt formation was observed where the proton from the carboxylic acid was transferred to the nitrogen of the base. The salts display unusual structural landscapes, which involve either water molecules or neutral acids (and bases) becoming part of the main structure. Of those observed, charge-assisted COO⁻ \cdots ⁺H-N were the most common, followed by N-H \cdots N interactions.

2.4.5 Do other nitrogen-based heterocycles display structural unpredictability when proton transfer occurs?

A search of the CSD for pyridinium cations combined with benzoate anions gives 397 hits, out of which structures containing a water, solvent, neutral acid or neutral base molecule totaled 181 (181/397 = 0.455), ~ 46%. This result shows it is not uncommon to observe other molecules, including solvent, in the structure when proton transfer processes occur, as observed in the salts formed between pyrazole and substituted benzoic acids. This result further shows the advantages of co-crystals over salts as far as stoichiometry and composition are concerned.

2.4.3 Is the pyrazole \cdots carboxylic acid synthon robust enough for driving co-crystal synthesis?

Six co-crystals were obtained from solution based experiments from the combination of pyrazole and various benzoic acids, and the expected pyrazole \cdots carboxylic acid synthon occurs 6/6 times (100% supramolecular yield). Great structural consistency was observed in the co-crystals synthesized in this series, demonstrating the usefulness and robustness of the pyrazole \cdots carboxylic acid synthon in forming co-crystals with predictable stoichiometry intended chemical composition, and structural landscape²⁹, Figure 2.14.

Pyrazole + Carboxylic acid

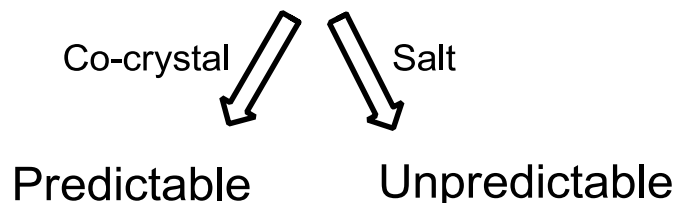


Figure 2-14 Summary of the results obtained from co-crystals and salts.

2.5 References:

-
- ¹ Price, S.L. *Acc. Chem. Res.*, **2009**, *42*(1), 117-126.
- ² Gale, P.A.; Steed, J.W. In *Supramolecular Chemistry: From Molecules to Nanomaterials*, **2012**, *7*, 3563-3586.
- ³ Park, C.; Lee, J.; Kim, C. *Chem. Commun.*, **2011**, *47*(44), 12042-12056.
- ⁴ Gandara, F.; Fortes-Revilla, C.; Snejko, N.; Gutierrez-Puebla, E.; Iglesias, M.; Monge, M. A. *Inorg. Chem.*, **2006**, *45*(24), 9680-9687.
- ⁵ Aitipamula, S.; Wong, A. B. H.; Chow, P. S.; Tan, R. B. H. *CrystEngComm*, **2012**, *14*(24), 8515-8524.
- ⁶ Rancatore, B. J.; Mauldin, C. E.; Frechet, J. M. J.; Xu, T. *Macromolecules*, **2012**, *45*(20), 8292-8299.
- ⁷ Desiraju, G. R. *Cryst. Growth Des.*, **2011**, *11*, 896-898.
- ⁸ Cambridge Structural Database (CSD, version 2012 + in house database).
- ⁹ Desiraju, G. R. *Stimul. Conc. in Chem.*, **2000**, 293-306.
- ¹⁰ Mohamed, S.; Tocher, D. A.; Vickers, M.; Karamertzanis, P. G.; Price, S. L. *Cryst. Growth Des.*, **2009**, *9*, 2881-2889.
- ¹¹ (a) Bhogala, B. R.; Basavoju, S.; Nangia, A. *CrystEngComm*, **2005**, *7*, 551-562. (b) Aakeröy, C. B.; Schultheiss, N. C.; Rajbanshi, A.; Desper, J.; Moore, C. *Cryst. Growth Des.*, **2009**, *9*, 432-441.
- ¹² Vors, J.P.; Gerbaud, V.; Gabas, N.; Canselier, J.P.; Jagerovic, N.; Jimeno, M.L.; Elguero, J. *Tetrahedron*, **2003**, *59*, 555-560.
- ¹³ Li, J.; Jin, H.; Zhou, H.; Rothfuss, J.; Tu, Z. *MedChemComm*, **2013**, *4*(2), 443-449.
- ¹⁴ Linnell, R. *J. Org. Chem.*, **1960**, *25*(2), 290.
- ¹⁵ Petrosyan, V. A.; Burasov, A. V. *Russ. Chem. Bull., Int. Ed.*, **2007**, *56*(11), 2175-2183.
- ¹⁶ (a) Etter, M. C.; MacDonald, J.; Bernstein, J. *Acta Cryst., Sect. B*, **1990**, *B46*, 256-262. (b) Etter, M. C. *Acc. Chem. Res.*, **1990**, *23*, 120-126.
- ¹⁷ (a) Basu, T.; Sparkes, H. A.; Mondal, R. *Cryst. Growth Des.*, **2009**, *9*, 5164-5175; (b) Hager, O.; Llamas-Saiz, A. L.; Foces-Foces, C.; Claramunt, R. M.; Lopez, C.; Elguero, J. *Helv. Chim. Acta*, **1999**, *82*(12), 2213-2230.
- ¹⁸ Perez, J.; Riera, L. *Eur. J. Inorg. Chem.*, **2009**, *33*, 4913-4925.

-
- ¹⁹ Claramunt, R. M.; Garcia, M. A.; Lopez, C.; Elguero, J. *ARKIVOC*, **2005**, 7, 91-101.
- ²⁰ Foces-Foces, C.; Infantes, L.; Aguilar-Parrilla, F.; Golubev, N. S.; Limbach, H.-H.; Elguero, J. *J. Chem. Soc., Perkin Trans.*, **1996**, 3, 349-353.
- ²¹ Zhao, Z.-G.; Wang, Z.-X. *Syn. Commun.*, **2007**, 37, 137-147.
- ²² Vasilevsky, S. F.; Klyatskaya, S. V.; Tretyakov, E. V.; Elguero, J. *Heterocycles*, **2003**, 60, 879-886.
- ²³ Ehlert, M. K.; Storr, A.; Thompson, R. C. *Can. J. Chem.*, **1992**, 70, 1121-1128.
- ²⁴ AM1 calculations were performed using Spartan (Wavefunction, Inc., Irvine, CA). The molecules were optimized using AM1, with the maxima and minima in the electrostatic potential surface (0.002 e/au isosurface) determined using a positive point charge in the vacuum as a probe.
- ²⁵ Hunter, C. A. *Angew. Chem. Int. Ed.*, **2004**, 43, 5310-5324.
- ²⁶ Musumeci, D.; Hunter, C. A.; Prohens, R.; Scuderi, S.; McCabe, J. F. *Chem. Sci.*, **2011**, 2, 883-890.
- ²⁷ Values were obtained from Scifinder scholar, **2013**.
- ²⁸ Pedireddi, V. R.; Reddy, D. S.; Goud, B. S.; Craig, D. C.; Rae, A. D.; Desiraju, G. R. *J. Chem. Sci., Perkin Trans.*, **1994**, 11, 2353-2360.
- ²⁹ Aakeröy, C. B.; Hurley, E. P.; Desper, J. *Cryst. Growth Des.*, **2012**, 12(11), 5806-5814.

Chapter 3 - Structural competition between carboxylic acid···pyridine and carboxylic acid···pyrazole: is there a difference?

3.1 Introduction

In Chapter 2, carboxylic acid···pyrazole interactions were shown to be capable of driving co-crystal formation¹ and to expand on this work, we wanted to determine what would happen in a competitive environment if a second hydrogen-bond acceptor site, pyridine, was added to the *same* molecular backbone. The acid can then choose between two different sites, N(py) or N(pyz), Figure 3.1.

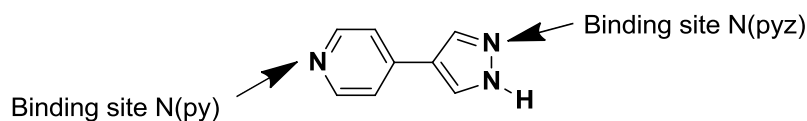


Figure 3-1 Two potential binding sites for an incoming carboxylic acid.

The incoming acid can potentially bind to one site or the other (or both), depending on both electrostatic charge as well as steric factors. Potential supramolecular interactions between the acid and binding sites are shown below, Figure 3.2.

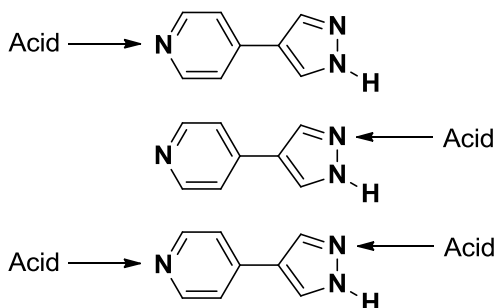


Figure 3-2 Potential supramolecular interactions between acid and N(py) and N(pyz).

When synthesizing co-crystals between carboxylic acids and ditopic molecules (Figure 3.2) it is important to understand where the acid prefers to bind for stoichiometry purposes and in order to predict structure and topology. Balance is exceedingly important when designing new solid forms² of materials, like pharmaceutical drugs, where multiple binding sites frequently exist on the active pharmaceutical ingredient for a cofomer to bind with. Whether a co-crystal or salt³

is obtained, the outcome can have drastic consequences for the physical properties of the solid material, from differences in melting behavior to differences in solubility.⁴ An illustrative example of a pharmaceutical drug with multiple binding sites is Nexium,⁵ Figure 3.3.

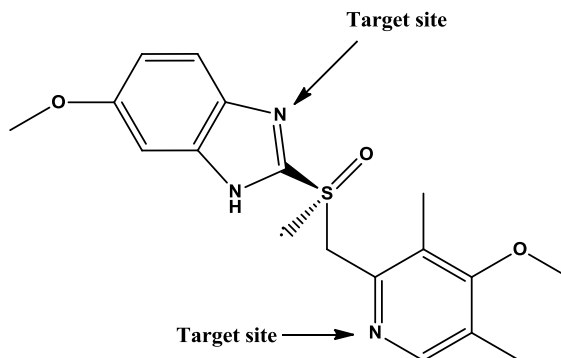


Figure 3-3 Nexium© and potential binding sites for hydrogen bond donors.

This drug contains at least two potential hydrogen-bond acceptor target sites for forming a hydrogen bond with a carboxylic acid-based cofomer. Therefore, it is important to understand binding preferences for stoichiometry purposes during scale-up processes and for control of the structural landscape in crystals.⁶

To examine the binding preferences of carboxylic acids with pyridine and pyrazole, when both functional groups are present on the *same* molecular backbone, ditopic molecules containing both functional groups were synthesized, Figure 3.4.

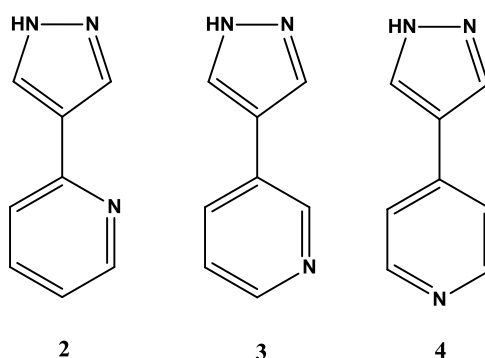


Figure 3-4 Library of isomeric ditopic molecules **2**, **3**, and **4**. The molecules have been named based on the position of the pyridine nitrogen atom.

Although work has been done on metal coordination chemistry of **4** using cobalt and zinc,⁷ there is no CSD data available which examines the binding preferences of carboxylic acids for N(py) or N(pyz) when present together.

To address the competition between N(py) and N(pyz) in the presence of carboxylic acids, charge calculations were performed on the molecules to establish which site, N(py) or N(pyz), has a higher charge and thus can be ranked as the best hydrogen bond acceptor. Solvent assisted grinding using twenty-one carboxylic acids was combined with **2**, **3**, and **4**; results from the IR data which gave a positive result (based on O-H...N stretches from the IR spectra) were then converted to solution experiments to generate single crystals. Single crystal data allow us to make inferences on binding preferences, if the two sites are significantly different in terms of their ability to act as a hydrogen-bond acceptor. A flowchart for the methodology is shown in Figure 3.5.

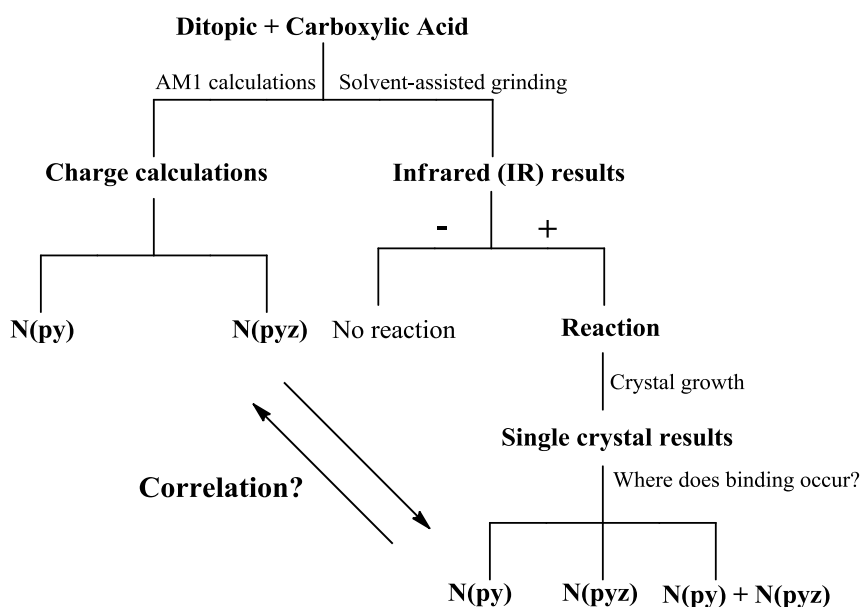


Figure 3-5 Flowchart for determining a correlation between charge and observed structural motifs.

This chapter will address the following questions:

- I. Can charge calculations be used to predict binding preferences? **Hypothesis:** AM1 calculations can be used to give relative strengths of N(py) and N(pyz) hydrogen bond acceptor sites, and the carboxylic acid donor will prefer the site with the highest charge.

- II. Can co-crystal or salt formation be determined from changes in the IR spectrum? **Hypothesis:** Changes in the carbonyl C=O stretch and the presence of broad O-H \cdots N stretches in the 2500 cm⁻¹ and 1900 cm⁻¹ regions indicate a reaction; if the shifts in the C=O are small, co-crystal formation is the likely outcome. If the C=O disappears and two carboxylate COO⁻ stretches appear, salt formation is the likely outcome.
- III. Can we determine binding preferences of carboxylic acids for N(py) or N(pyz) from the single crystal data? **Hypothesis:** Carboxylic acids, when given the choice between N(py) or N(pyz), will choose the site with the highest charge and lowest pK_b value, N(py). However, two possible synthons that can occur are synthon 1 and synthon 2, respectively, Figures 3.6 and 3.7.

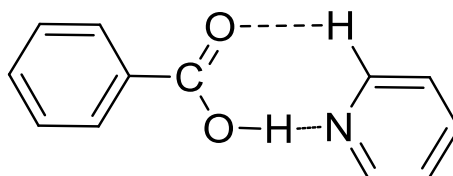


Figure 3-6 The carboxylic acid \cdots pyridine heterosynthon (Synthon 1).

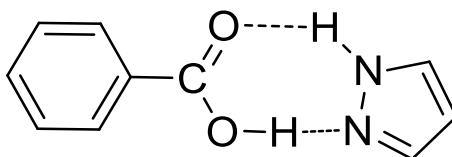


Figure 3-7 The carboxylic acid \cdots pyrazole heterosynthon (Synthon 2).

Despite pyridine being a stronger base, the pyrazole nitrogen has help from a more acidic N-H in a two point contact. This help may tilt the balance and make the pyrazole as competitive as pyridine for an incoming carboxylic acid.

3.2 Experimental

3.2.1 Charge calculations

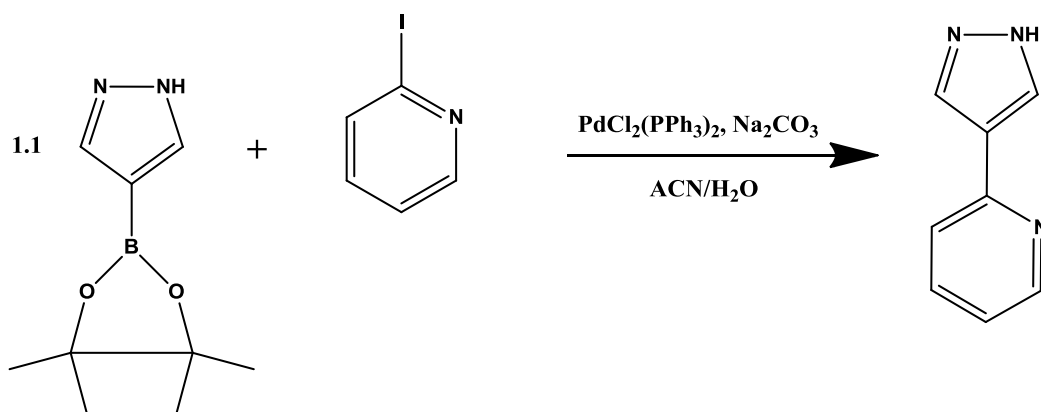
Molecular electrostatic potential (MEP) surface charge calculations were performed using Spartan (Wavefunction, Inc., Irvine, CA). The molecules were optimized using AM1, with

the maxima and minima in the electrostatic potential surface (0.002 e/au isosurface) determined using a positive point charge in the vacuum as a probe.

3.2.2 Covalent synthesis

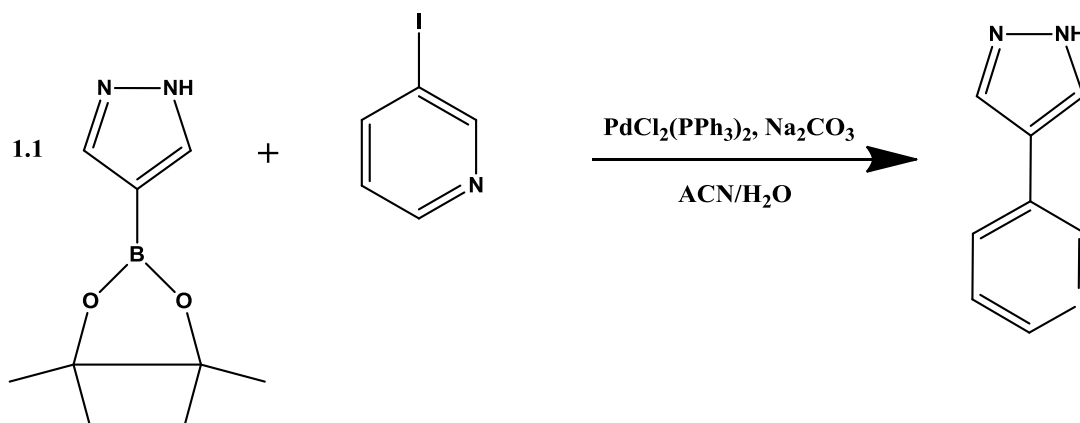
All chemicals were purchased from Aldrich and used without further purification unless otherwise noted. Palladium catalyst was purchased from TCI. ^1H and ^{13}C NMR data were recorded on a Bruker 400 MHz instrument. Melting points were determined on a Fisher-Johns melting point apparatus and are uncorrected.

3.2.2.1 Synthesis of 2-(1H-pyrazol-4-yl)pyridine, 2



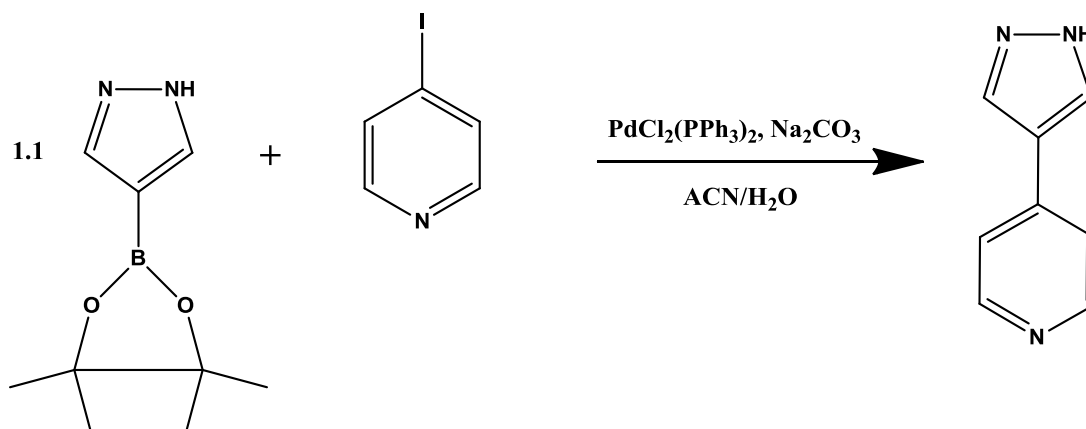
To a clean 250mL round bottom flask, 40mL of deionized water and 40mL of acetonitrile were added. Next, 4-pyrazoleboronic acid pinacol ester (1.02g, 5.3mmol) was added, followed by 2-iodopyridine (0.98g, 4.8mmol). Then, Na_2CO_3 (0.39g, 3.6mmol) and $\text{PdCl}_2(\text{PPh}_3)_2$ catalyst (0.17g, 0.24mmol) were added. The color of the mixture turned yellow/green after the catalyst was added, and most of the color had disappeared after refluxing for 24 hours. The mixture was stirred under dinitrogen at room temperature for 30 minutes, then heated to reflux for 72 hours, upon which the mixture was cooled to room temperature. The crude product was extracted in chloroform, washed once with both water and brine (40mL each), and dried over MgSO_4 . The salt was filtered off, and the filtrate was concentrated to give a pale yellow solid. The solid was purified using column chromatography (silica packed with hexanes, 25% ethyl acetate as eluent, product appears fluorescent blue under UV light). White crystalline solid (0.386g, 55.6%). Mp: 130-133°C. ^1H NMR (400 MHz, CDCl_3) δ ppm: 11.27 (br. s., 1 H), 8.59 (d, $J=0.78$ Hz, 1 H), 8.14 (br. s., 2 H), 7.69 (d, $J=1.56$ Hz, 1 H), 7.52 (d, $J=5.86$ Hz, 1 H), 7.14 (br. s., 1 H), Figure A-7.

3.2.2.2 Synthesis of 3-(1H-pyrazol-4-yl)pyridine, 3



To a clean 250mL round bottom flask, 40mL of deionized water and 40mL of acetonitrile were added. Next, 4-pyrazoleboronic acid pinacol ester (1.90g, 9.77mmol) was added, followed by 3-iodopyridine (1.82g, 8.88mmol). Then, Na_2CO_3 (0.71g, 6.66mmol) and $\text{PdCl}_2(\text{PPh}_3)_2$ catalyst (0.312g, 0.444mmol) were added. The color of the mixture turned yellow/green after the catalyst was added, and most of the color had disappeared after refluxing for 24 hours. The mixture was stirred under dinitrogen at room temperature for 30 minutes, then heated to reflux for 72 hours, upon which the mixture was cooled to room temperature. The crude product was extracted in chloroform, washed once with both water and brine (40mL each), and dried over MgSO_4 . The salt was filtered off, and the filtrate was concentrated to give a brown oil. The oil was purified using column chromatography (silica packed with hexanes, 55% ethyl acetate as eluent, product appears fluorescent blue under UV light). Off-white crystalline solid (0.55g, 42.6%). Mp: 115-117°C. ^1H NMR (400 MHz, CDCl_3) δ ppm: 8.82 (s, 1 H), 8.51 (d, $J=5.08$ Hz, 1 H), 7.93 (s, 2 H), 7.81 (d, $J=7.81$ Hz, 1 H), 7.29 - 7.39 (m, 1 H), Figure A-8.

3.2.2.3 Synthesis of 4-(1H-pyrazol-4-yl)pyridine, 4



To a clean 250mL round bottom flask, 40mL of deionized water and 40mL of acetonitrile were added. Next, 4-pyrazoleboronic acid pinacol ester (0.90g, 4.62mmol) was added, followed by 4-iodopyridine (0.861g, 4.20mmol). Then, Na_2CO_3 (0.334g, 3.15mmol) and $\text{PdCl}_2(\text{PPh}_3)_2$ catalyst (0.147g, 0.210mmol) were added. The color of the mixture turned yellow/green after the catalyst was added, and most of the color had disappeared after refluxing for 24 hours. The mixture was stirred under dinitrogen at room temperature for 30 minutes, then heated to reflux for 72 hours, upon which the mixture was cooled to room temperature. The crude product was extracted in chloroform, washed once with both water and brine (40mL each), and dried over MgSO_4 . The salt was filtered off, and the filtrate was concentrated to give a tan colored solid. The solid was purified using column chromatography (silica packed with hexanes, 55% ethyl acetate as eluent, product appears fluorescent blue under UV light). Yellow crystalline solid (0.114g, 18.7%). Mp: 194-197°C. ^1H NMR (400 MHz, CDCl_3) δ ppm: 10.47 (br. s, 1 H), 8.60 (d, $J=5.86$ Hz, 2 H), 7.99 (s, 2 H), 7.42 (d, $J=5.86$ Hz, 2 H), Figure A-9.

3.2.2.4 Synthesis of 2-(1H-pyrazol-4-yl)pyridine:4-cyanobenzoic acid (1:1), 2:H

To a vial, 2-(1H-pyrazol-4-yl)pyridine (2.4mg, 0.017mmol) was added with 4-cyanobenzoic acid (2.4mg, 0.016mmol). The solids were dissolved in methanol (0.5mL) and left for slow evaporation (loose screw cap). Colorless prisms were obtained after a few days. Mp: 169-171°C.

3.2.2.5 Synthesis of 2-(1*H*-pyrazol-4-yl)pyridine:4-nitrobenzoic acid (1:1), 2:K

To a vial, 2-(1*H*-pyrazol-4-yl)pyridine (2.8mg, 0.019mmol) was added with 4-nitrobenzoic acid (3.3mg, 0.020mmol). The solids were dissolved in methanol (1 mL), heated gently, and left for slow evaporation (loose screw cap). Colorless prisms were obtained after a few days. Mp: 216-217°C.

3.2.2.6 Synthesis of 3-(1*H*-pyrazol-4-yl)pyridine:2,4-difluorobenzoic acid (1:2), 3:M₂

To a vial, 3-(1*H*-pyrazol-4-yl)pyridine (1.0M solution in ethanol, 335μL) was added. In a separate vial, 2,4-difluorobenzoic acid (5.3mg, 0.034mmol) was dissolved in ethanol (0.5mL). The two solutions were combined and left for slow evaporation (parafilm, 1 pinhole). Colorless plates were obtained after a few days. Mp: 105-107°C.

3.2.2.7 Synthesis of 4-(1*H*-pyrazol-4-yl)pyridine:4-nitrobenzoic acid (1:2), 4:K₂

To a vial, 4-(1*H*-pyrazol-4-yl)pyridine (3.7mg, 0.026mmol) was added with 4-nitrobenzoic acid (4.3mg, 0.026mmol). The solids were dissolved in ethanol (0.8mL), heated, then filtered while still hot. The filtrate was left to stand and slowly evaporate (parafilm, 1 pinhole). Gold prisms were obtained after a few days. Mp: 190-192°C.

3.2.2.8 Synthesis of 2-(1*H*-pyrazol-4-yl)pyridinium:2,4-dinitrobenzoate (1:1), 2:U

To a vial, 2-(1*H*-pyrazol-4-yl)pyridine (14.0mg, 0.0964mmol) was added with 2,4-dinitrobenzoic acid (20.0mg, 0.0964mmol). The solids were dissolved in methanol (1.5mL), heated, and left for slow evaporation (loose screw cap). Colorless prisms were obtained after a few days. Mp: 216-218°C.

3.2.2.9 Synthesis of 3-(1*H*-pyrazol-4-yl)pyridinium:2,4-dinitrobenzoate (1:1), 3:U

To a vial, 3-(1*H*-pyrazol-4-yl)pyridine (10mg, 0.069mmol) was added and dissolved in 0.5mL of methanol. To the same vial, 2,4-dinitrobenzoic acid (15.0mg, 0.071mmol) was added. The solution was heated and left for slow evaporation (parafilm, 1 pinhole). Colorless plates were obtained after a few days. Mp: 196-197°C.

3.2.2.10 Synthesis of 4-(1*H*-pyrazol-4-yl)pyridinium:4-cyanobenzoate (1:1), 4:H

To a vial, 4-(1*H*-pyrazol-4-yl)pyridine (10.4mg, 0.0714mmol) was added with 4-cyanobenzoic acid (10.5mg, 0.0714mmol). The solids were dissolved in methanol (1.0mL),

heated, then left to stand and slowly evaporate (loose screw cap). Colorless plates were obtained after a few days. Mp: 185-187°C.

3.2.2.11 Synthesis of 4-(1*H*-pyrazol-4-yl)pyridinium:2,4-dinitrobenzoate dihydrate (1:1:2), 4:U:(H₂O)₂

To a vial, 4-(1*H*-pyrazol-4-yl)pyridine (2.6mg, 0.018mmol) was added with 2,4-dinitrobenzoic acid (3.8mg, 0.018mmol). The solids were dissolved in methanol (0.5mL) and left for slow evaporation (loose screw cap). Colorless prisms were obtained after a few days. Mp: 197-199°C.

3.2.3 IR spectroscopy

Infrared spectra were collected on a Thermo Scientific Nicolet 380 FT-IR using a ZnSe crystal. The solids obtained from grinding (or solution) experiments were analyzed by placing the solid directly on the crystal and performing 32 scans.

3.3 Results

3.3.1 MEP surface calculations

In order to get an idea of the relative strengths of the hydrogen-bond acceptor sites from the ditopic molecules, molecular electrostatic potential (MEP) surface calculations were performed. The two values are used to rank the relative strengths of the pyridine N(py) and pyrazole N(pyz) sites. The MEP surface energies are shown in Table 3.1 and Figure 3.8.

Table 3.1 AM1 Molecular electrostatic surface potential energies for ditopics **2**, **3**, and **4**.

Ditopic molecule	E(Npy) kJ mol ⁻¹	E(Npyz) kJ mol ⁻¹	E(N-H) kJ mol ⁻¹
2	-270	-234	+187
3	-281	-228	+200
4	-276	-226	+205

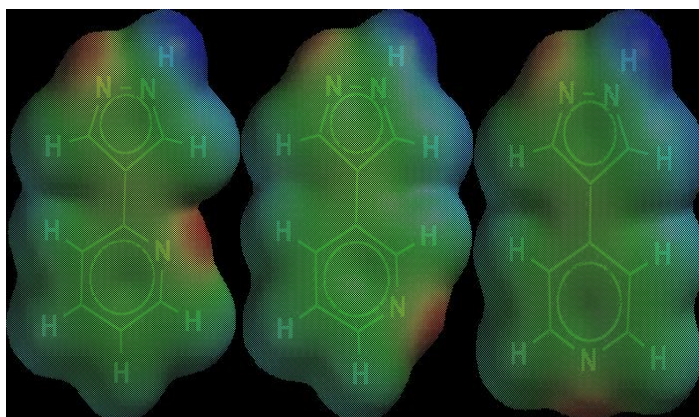


Figure 3-8 MEP surfaces of the ditopic molecules indicating the distribution of charge. Red surfaces indicate hydrogen-bond acceptor sites; blue indicates hydrogen bond donor sites.

3.3.2 Covalent synthesis

Three ditopic molecules were synthesized using a Suzuki-Miyaura cross-coupling reaction and the products were purified using column chromatography. Previous coupling reactions to pyrazole involved multistep synthesis via an aldehyde intermediate⁸ (route 1); coupling a 4-halo pyrazole to pyridine boronic acid did not give the desired product (route 2); however, reversing the substituents by placing the boronic acid substituent on the pyrazole and the halogen on the pyridine gave the direct C-C coupled product in moderate to good yields and reduced the number of steps to one (route 3), Figure 3.9.

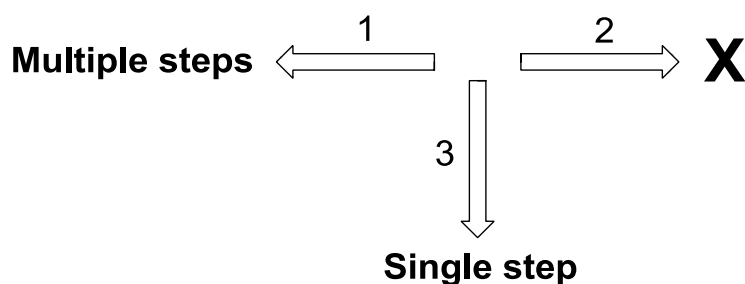


Figure 3-9 Synthetic routes to obtaining the target molecules 2, 3, and 4.

3.3.3 Infrared data

The ditopic molecules were screened with twenty-one carboxylic acids of varying pK_a values and charge using solvent-assisted grinding, Table 3.2.

Table 3.2 Aromatic carboxylic acids used in the study.

Label (pK _a) ⁹	Acid
A (4.57 +/- 0.10)	4-Hydroxybenzoic acid
B (4.45 +/- 0.10)	4-Hydroxy-3-methoxy benzoic acid
C (4.34 +/- 0.10)	3,5-Dimethylbenzoic acid
D (4.08 +/- 0.10)	3-Hydroxybenzoic acid
E (4.02 +/- 0.10)	4-Iodobenzoic acid
F (3.97 +/- 0.10)	4-Chlorobenzoic acid
G (3.64 +/- 0.10)	3-Cyanobenzoic acid
H (3.54 +/- 0.10)	4-Cyanobenzoic acid
I (3.48 +/- 0.10)	3-Nitrobenzoic acid
J (3.46 +/- 0.10)	3-Bromo-5-iodobenzoic acid
K (3.42 +/- 0.10)	4-Nitrobenzoic acid
L (3.27 +/- 0.10)	2-Fluorobenzoic acid
M (3.21 +/- 0.10)	2,4-Difluorobenzoic acid
N (2.97 +/- 0.25)	2-Chlorobenzoic acid
O (2.77 +/- 0.10)	3,5-Dinitrobenzoic acid
P (2.34 +/- 0.10)	2,6-Difluorobenzoic acid
Q (2.19 +/- 0.25)	2-Nitrobenzoic acid
R (1.93 +/- 0.10)	2-Fluoro-6-iodobenzoic acid
S (1.69 +/- 0.10)	2,6-Dichlorobenzoic acid
T (1.60 +/- 0.10)	Pentafluorobenzoic acid
U (1.43 +/- 0.25)	2,4-Dinitrobenzoic acid

3.3.4 Determining co-crystal formation by infra-red (IR) spectroscopy

Using infra-red spectroscopy, it is possible to determine the interaction between a carboxylic acid and an N-heterocycle by the presence of broad stretches in the 2500 cm⁻¹ and 1900 cm⁻¹ region.¹⁰ The broad stretches in this region correspond to O-H...N stretches, and are only present if the two molecules are forming an intermolecular interaction. Furthermore, shifts in the carbonyl (C=O) stretch (normalized against the neutral acid) or the disappearance of the C=O stretch and appearance of two carboxylate COO⁻ stretches indicate co-crystal or salt formation, respectively. An example of an IR spectrum which shows a reaction between acid and base resulting in a co-crystal is shown in Figure 3.10.

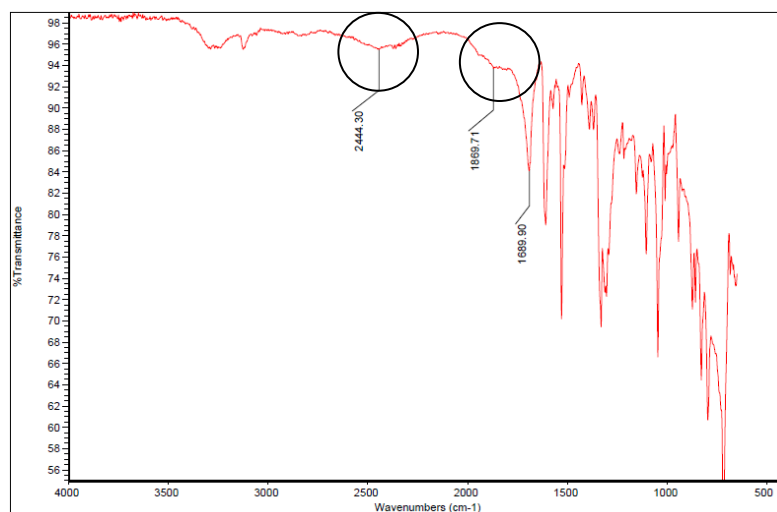


Figure 3-10 IR spectrum of reaction between **4** and **K**. Evidence of O-H...N interactions are circled. Change in the carbonyl C=O stretch is 4 cm⁻¹.

The results from the screening experiments between twenty-one carboxylic acids and ditopics **2**, **3**, and **4** are summarized in Table 3.3, with prominent IR stretches noted. The corresponding supramolecular yield (calculated as the number of positive hits) is given in the last row.

Table 3.3 Summary of prominent IR stretches (cm⁻¹) from the grinding experiments between three ditopic molecules and twenty-one carboxylic acids.

	2	3	4
4-Hydroxybenzoic acid	2487, 1917, 1678	2452, 1928, 1666	2460, 1924, 1659
4-Hydroxy-3-methoxy benzoic acid	No rxn	2565, 1866, 1670	2472, 1952, 1666
3,5-Dimethylbenzoic acid	No rxn	2499, 1913, 1686	2409, 1921, 1670
3-Hydroxybenzoic acid	2581, 1846, 1670	2577, 1846, 1670	2569, 1889, 1651
4-Iodobenzoic acid	2483, 1870, 1682	2546, 1862, 1670	2526, 1862, 1678
4-Chlorobenzoic acid	2479, 1878, 1682	2425, 1921, 1686	2444, 1893, 1686
3-Cyanobenzoic acid	2476, 1866, 1678	2503, 1909, 1670	2460, 1921, 1690
4-Cyanobenzoic acid	2413, 1862, 1698	2433, 1921, 1658, 1424	2460, 2093, 1944, 1665, 1402
3-Nitrobenzoic acid	2413, 1878, 1709	2464, 1905, 1706	2456, 1850, 1690
3-Bromo-5-iodobenzoic acid	2479, 1858, 1706	2476, 1901, 1702	2433, 1858, 1682
4-Nitrobenzoic acid	2436, 1854, 1698	2421, 1932, 1682	2444, 1870, 1690
2-Fluorobenzoic acid	2468, 1885, 1682	2479, 1921, 1698	2620, 2104, 1631, 1377
2,4-Difluorobenzoic acid	2663, 1878, 1690	2452, 1874, 1666	2464, 1960, 1674
2-Chlorobenzoic acid	2479, 1932, 1702	2472, 1917, 1702	2487, 1909, 1627, 1343
3,5-Dinitrobenzoic acid	2448, 2003, 1620, 1430	2835, 1913, 1623, 1425	2538, 2139, 2038, 1631, 1403
2,6-Difluorobenzoic acid	2479, 1940, 1621, 1382	2460, 2167, 1878, 1616, 1378	2456, 1956, 1631, 1385
2-Nitrobenzoic acid	2495, 1928, 1597, 1434	2452, 1901, 1721	2464, 2003, 1698
2-Fluoro-6-iodobenzoic acid	2444, 1901, 1622, 1390	2550, 2116, 1592, 1376	2648, 1995, 1634, 1388

2,6-Dichlorobenzoic acid	2433, 1944, 1641, 1441	2476, 2120, 1952, 1698	2479, 1932, 1631, 1427
Pentafluorobenzoic acid	2491, 2089, 1639, 1403	2433, 2155, 1647, 1623, 1407	2522, 1932, 1604, 1394
2,4-Dinitrobenzoic acid	2472, 2061, 1584, 1373	2464, 2175, 2010, 1620, 1397	2515, 2112, 1631, 1397
Success rate	19/21 = 90%	21/21 = 100%	21/21 = 100%

Co-crystals:

3.3.5 Crystal structure of 2-(1H-pyrazol-4-yl)pyridine:4-cyanobenzoic acid (1:1), 2:H

The crystal structure of **2:H** shows a 1:1 ratio between acid and ditopic molecule and hydrogen bonding occurs between a carboxylic acid and a pyrazole nitrogen atom, giving an O-H...N(pyz) distance of 2.6015(11)Å and an angle of 174(15)°. The acidic proton remains on the carboxylic acid, as evidenced by the C-O/C=O ratio of 1.08. Ditopic molecules are connected into a catemer which forms between the pyrazole N-H proton and a pyridine nitrogen atom, a N-H...N(py) distance of 2.8555(13)Å and an angle of 167(13)°. The N-H proton remains on the pyrazole, as evidenced by a C-N_(py)-C angle of 118(9)°, Figure 3.11.

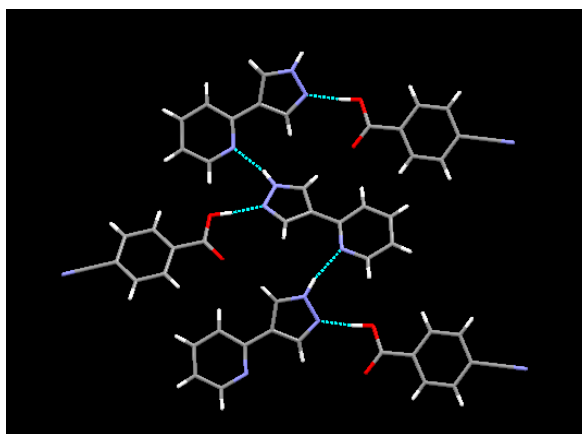


Figure 3-11 Catemer in the crystal structure of **2:H**.

3.3.6 Crystal structure of 2-(1H-pyrazol-4-yl)pyridine:4-nitrobenzoic acid (1:1), 2:K

The crystal structure of **2:K** shows a 1:1 ratio between acid and ditopic molecule where hydrogen bonding occurs between the carboxylic acid and pyrazole nitrogen atom, giving an O-H...N(pyz) distance of 2.588(2)Å and an angle of 167(2)°. The acidic proton remains on the carboxylic acid, as evidenced by the C-O/C=O ratio of 1.09. The ditopic molecules are connected into a catemer through the pyrazole N-H proton and a pyridine nitrogen atom, with a

N-H \cdots N(py) distance of 2.872(3)Å and an angle of 170(2)°. The N-H proton remains on the pyrazole, as evidenced by a C-N_(py)-C angle of 118(18)°, Figure 3.12.

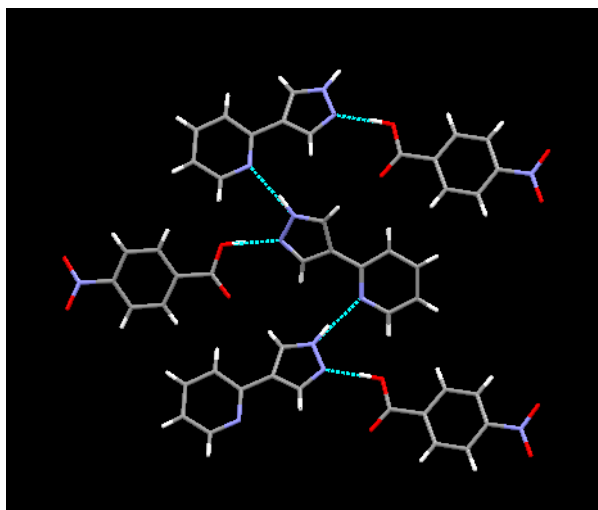


Figure 3-12 Catemer in the crystal structure of **2:K**.

3.3.7 Crystal structure of 3-(1H-pyrazol-4-yl)pyridine:bis-2,4-difluorobenzoic acid (1:2), 3:M₂

The crystal structure of **3:M₂** shows a 1:2 ratio between the ditopic molecule and the acid. Two predominant interactions are observed. At the pyridine site, a two-point contact exists between carboxylic acid and pyridine nitrogen atom, giving an O-H \cdots N(py) distance of 2.662(6)Å and an angle of 152(7)°; the C-H \cdots O=C distance is 2.568Å. The acidic proton remains on the carboxylic acid, and the C-O/C=O ratio is 1.09 and the C-N_(py)-C angle is 118(5)°. On the pyrazole end, a second carboxylic acid bridges two symmetry-related ditopics through the carboxylic acid hydrogen atom and pyrazole nitrogen atom, as well as through the pyrazole N-H proton and carboxylic acid carbonyl interaction, respectively: O-H \cdots N(pyz) distance is 2.693(6)Å and the angle is 139(9)°. The N-H \cdots O=C distance is 2.806(6) and the angle is 141(7)°. The proton remains on the carboxylic acid, as evidenced by the C-O/C=O ratio of 1.06, Figure 3.13.

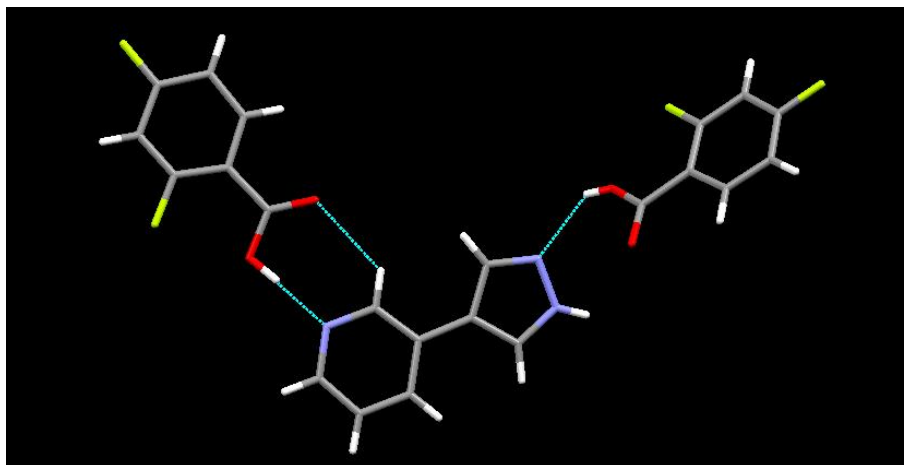


Figure 3-13 Two predominant interactions in the crystal structure of **3:M₂**.

3.3.8 Crystal structure of 4-(1H-pyrazol-4-yl)pyridine:bis-4-nitrobenzoic acid (1:2), **4:K₂**

The crystal structure of **4:K₂** shows a 1:2 ratio between heterocycle and acid. Two predominant interactions are observed. On the pyridine end, a two-point contact exists between a carboxylic acid and a pyridine nitrogen atom, where the O-H...N(py) distance is 2.545(3)Å and the angle is 178(3)°; the C-H...O=C distance is 2.521Å. The acidic proton remains on the carboxylic acid, where the C-O/C=O ratio is 1.06 and the C-N_(py)-C angle is 119(2)°. On the pyrazole end, a second acid forms a hetero synthon with a pyrazole nitrogen atom, and the pyrazole N-H proton interacts with the carbonyl oxygen atom from the carboxylic acid: O-H...N(pyz) distance is 2.672(3)Å and the angle is 175(3)°; N-H...O=C distance is 2.820(3) and the angle is 146(3)°. The ratio of C-O/C=O is 1.07, Figure 3.14.

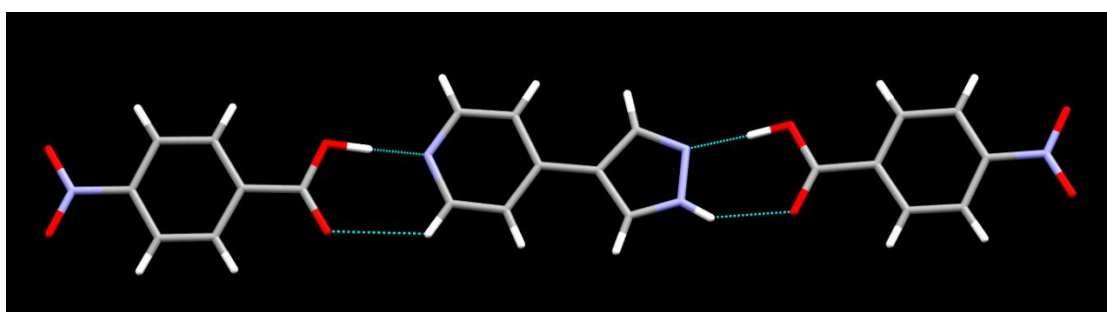


Figure 3-14 Supermolecule formed in the crystal structure of **4:K₂**.

Salts:

3.3.9 Crystal structure of 2-(1H-pyrazol-4-yl)pyridinium:2,4-dinitrobenzoate (1:1), 2:U

In the crystal structure of **2:U** proton transfer occurs between the carboxylic acid and pyridine nitrogen atom, giving a charge-assisted $N^+-H\cdots O^-$ distance of 2.663(3)Å with a $C-N_{(py)}-C$ angle of 123(2)°. The $C-O^-/C-O^-$ carboxylate bond ratio is 1.01, indicating the proton has been transferred. A second charge-assisted $N-H\cdots O^-$ interaction occurs between the pyrazole N-H proton and carboxylate, 2.830(3)Å and 170(3)°, Figure 3.15.

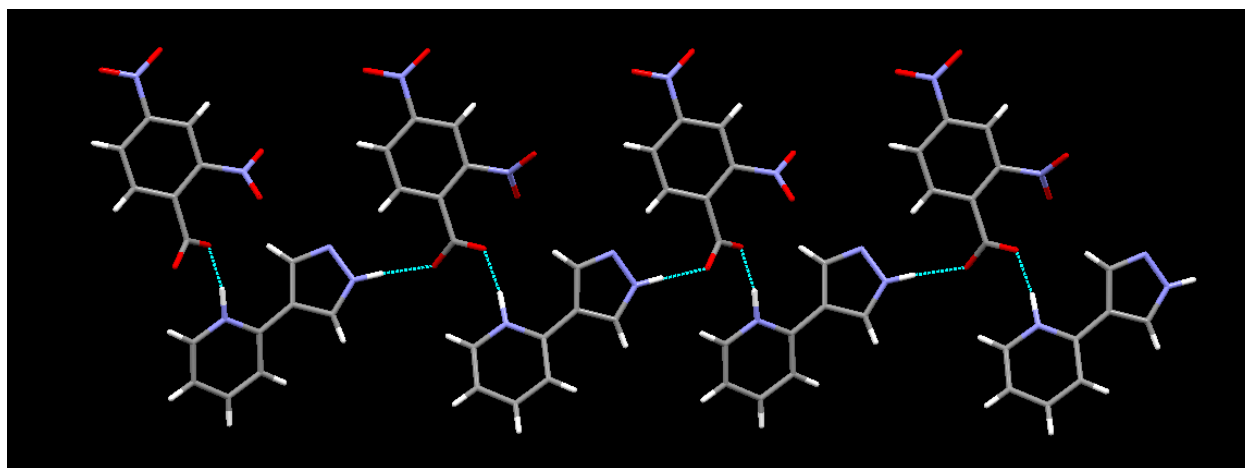


Figure 3-15 Zig-zag chain formed in **2:U**.

3.3.10 Crystal structure of 3-(1H-pyrazol-4-yl)pyridinium:2,4-dinitrobenzoate (1:1), 3:U

In the crystal structure of **3:U** proton transfer occurs between the carboxylic acid and pyridine nitrogen atom, giving a charge-assisted $N^+-H\cdots O^-$ distance of 2.6436(16)Å and an angle of 179(16)°; the $C-N_{(py)}-C$ angle is 120(11)° and $C-O^-/C-O^-$ carboxylate bond ratio is 1.04, indicating the proton has been transferred. A second charge-assisted $N-H\cdots O^-$ interaction occurs between the pyrazole N-H proton and carboxylate, 2.7738(16)Å and 165(17)°, Figure 3.16.

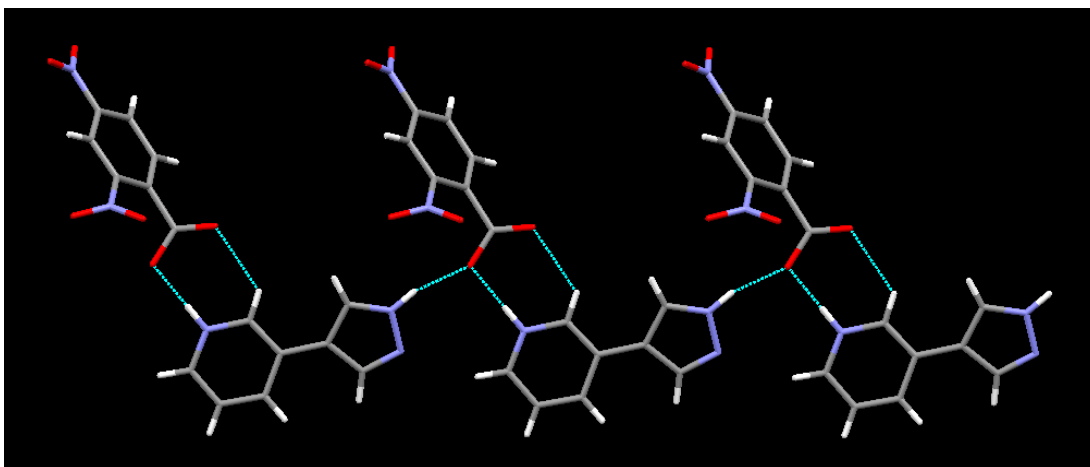


Figure 3-16 Proton transfer from acid to base in the crystal structure of **3:U**.

3.3.11 Crystal structure of 4-(1H-pyrazol-4-yl)pyridinium:4-cyanobenzoate (1:1), **4:H**

The crystal structure of **4:H** shows a zig-zag chain formed through proton transfer from the carboxylic acid to the pyridine nitrogen atom. A carboxylate bridges two ditopic molecules, where charge-assisted $\text{N}^+\text{-H}\cdots\text{O}^-$ distance is 2.5910(11) Å with an angle of 176(13)°. The $\text{C-N}_{(\text{py})}\text{-C}$ bond angle is 121(8)°. The pyrazole N-H proton interacts with a carboxylate, giving an $\text{N-H}\cdots\text{O}^-$ distance of 2.7777(11) Å and an angle of 166(12)°. The $\text{C-O}^+/\text{C-O}^-$ carboxylate bond ratio is 1.04, indicating the proton has been transferred, Figure 3.17.

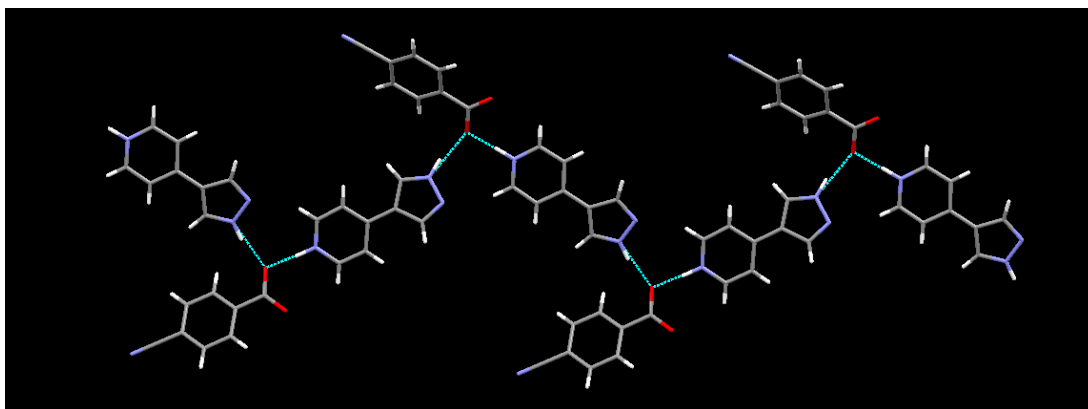


Figure 3-17 Part of the zig-zag chain formed through proton transfer from acid to base in the crystal structure of **4:H**.

3.3.12 Crystal structure of 4-(1H-pyrazol-4-yl)pyridinium:2,4-dinitrobenzoate dihydrate (1:1:2), 4:U:(H₂O)₂

The crystal structure of 4:U:(H₂O)₂ shows a hydrated salt. Proton transfer occurs from the carboxylic acid to a pyridine nitrogen atom, giving a charge-assisted N⁺-H···O⁻ distance of 2.5910(11) Å, 176(13)°. The C-N_(py)-C bond angle is 121(8)°. The carboxylate also interacts with water, where the O_w-H···O distance is 2.7777(11) Å with an angle of 166(12)°. The C-O⁻/C-O⁻ carboxylate bond ratio is 1.04, indicating the proton has been transferred. The pyrazole N-H proton interacts with water through N-H···O_w hydrogen bonds, in addition to O_w-H···N hydrogen bonds with the pyrazole nitrogen atom, Figure 3.18.

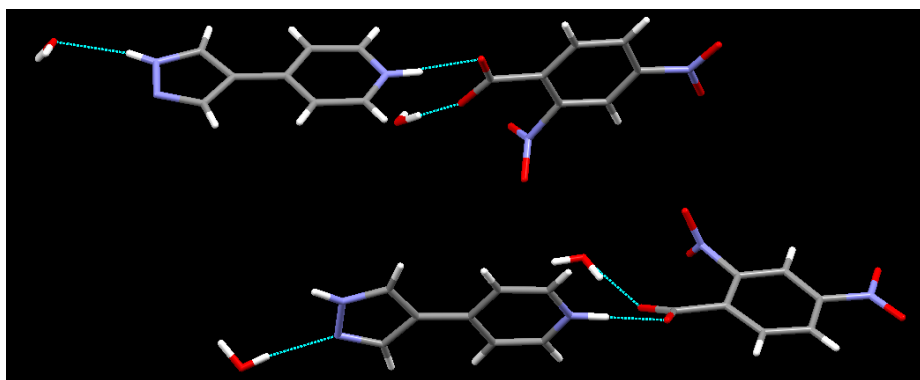


Figure 3-18 Hydrated salt formed in the reaction between 4 and U.

3.4 Discussion

3.4.1 What do the AM1 charge calculations tell us about where binding should take place?

In all cases, the pyridine nitrogen atom, N(py), carries the largest negative charge, with an average AM1 value of -276 kJ/mol (Table 3.1). The pyrazole nitrogen atom, N(pyz), carries a lower negative charge, with an average AM1 value of -229 kJ/mol (Table 3.1). Therefore, we would expect the pyridine nitrogen atom to be the most attractive site for an incoming carboxylic acid or N-H proton, and the best hydrogen bond acceptor; the pyrazole nitrogen atom would be ranked as the second best acceptor site.

The charge on the pyrazole N-H proton carries the largest positive charge, with an average AM1 value of +197 kJ/mol (Table 3.1). Therefore, the N-H proton would be ranked as the best hydrogen bond donor and we would predict the N-H proton to interact with the best acceptor site, N(py). On the other hand, all of the carboxylic acids used carry a lower positive

charge than the pyrazole N-H proton, with values ranging from +130-190 kJ/mol. All acids would be ranked as the second best hydrogen bond donor.

3.4.2 Can we determine co-crystal or salt formation from the IR data?

The IR data show a 90-100% success rate for reactions between twenty-one carboxylic acids and ditopics **2**, **3**, and **4**; this is an increase in the success rate from the system in Chapter 2, which contained *only* pyrazole (and substituted pyrazole). The results show that the addition of a pyridine moiety *increases* the success rate for a reaction (denoted as rxn), suggesting that pyridine is slightly more active than the pyrazole when combined with carboxylic acids. Furthermore, the IR data support our original hypothesis; the addition of a stronger hydrogen bond acceptor site to the pyrazole backbone should increase the supramolecular yield. From Chapter 2, the success rate for a reaction between pyrazole and carboxylic acid was between 55-70%; addition of the pyridine moiety increases the success rate to 90-100%.

To determine unambiguously whether a co-crystal or salt forms requires both IR and single crystal data; therefore, the results presented in Table 3.4 represent a prediction based on changes in the C=O band from the reaction compared to the neutral acid. For co-crystal formation, the C=O band is expected to change slightly. When the acidic proton is transferred from the acid to the base, a carboxylate anion, COO⁻, is expected to form. The C=O band would thus disappear and an asymmetric COO⁻ band combined with a weaker symmetric COO⁻ band is expected to appear.¹¹

Table 3.4 Summary of changes in the carbonyl (C=O) after reaction (rxn).

Acid (C=O)	2			3			4		
	(C=O)	(COO ⁻)	Pred.	(C=O)	(COO ⁻)	Pred.	(C=O)	(COO ⁻)	Pred.
4-Hydroxybenzoic acid (1668)	1678	-	co-crystal	1666	-	co-crystal	1659	-	co-crystal
4-Hydroxy-3-methoxy benzoic acid (1671)	No rxn	-	-	1670	-	co-crystal	1666	-	co-crystal
3,5-Dimethylbenzoic acid (1679)	No rxn	-	-	1686	-	co-crystal	1670	-	co-crystal
3-Hydroxybenzoic acid (1678)	1670	-	co-crystal	1670	-	co-crystal	1651	27	salt
4-Iodobenzoic acid (1667)	1682	-	co-crystal	1670	-	co-crystal	1678	-	co-crystal
4-Chlorobenzoic acid (1678)	1682	-	co-crystal	1686	-	co-crystal	1686	-	co-crystal
3-Cyanobenzoic acid (1683)	1678	-	co-crystal	1670	-	co-crystal	1690	-	co-crystal
4-Cyanobenzoic acid (1691)	1698	-	co-crystal	-	1658, 1424	salt	-	1665, 1402	salt
3-Nitrobenzoic acid (1686)	1709		co-crystal	1706	-	co-crystal	1690	-	co-crystal

3-Bromo-5-iodobenzoic acid (1699)	1706	-	co-crystal	1702	-	co-crystal	1682	-	co-crystal
4-Nitrobenzoic acid (1686)	1698	-	co-crystal	1682	-	co-crystal	1690	-	co-crystal
2-Fluorobenzoic acid (1687)	1682	-	co-crystal	1698	-	co-crystal	-	1631, 1377	salt
2,4-Difluorobenzoic acid (1682)	1690	-	co-crystal	1666	-	co-crystal	1674	-	co-crystal
2-Chlorobenzoic acid (1679)	1702		co-crystal	1702	-	co-crystal	-	1672, 1343	salt
3,5-Dinitrobenzoic acid (1698)	-	1620, 1430	salt	-	1623, 1425	salt	-	1631, 1403	salt
2,6-Difluorobenzoic acid (1686)	-	1621, 1382	salt	-	1616, 1378	salt	-	1631, 1385	salt
2-Nitrobenzoic acid (1671)	-	1597, 1434	salt	1721	-	co-crystal	1698	-	co-crystal
2-Fluoro-6-iodobenzoic acid (1699)	-	1622, 1390	salt	-	1592, 1376	salt	-	1634, 1388	salt
2,6-Dichlorobenzoic acid (1704)	-	1641, 1441	salt	1698	6	co-crystal	-	1631, 1427	salt
Pentafluorobenzoic acid (1709)	-	1639, 1403	salt	-	1623, 1407	salt	-	1604, 1394	salt
2,4-Dinitrobenzoic acid (1716)	-	1584, 1373	salt	-	1620, 1397	salt	-	1631, 1397	salt

From the data in Table 3.4, changes in the C=O which were small were predicted to give a co-crystal. In a few cases, the C=O stretch shifted over 20 wavenumbers, yet the prediction was co-crystal formation based on the overall appearance of the spectrum. When the C=O disappeared, an asymmetric carboxylate (COO⁻) band appeared around 1650-1590 cm⁻¹, combined with a weaker symmetric carboxylate stretch in the 1400 cm⁻¹ region. New bands that appeared were assigned as salt formation.

In a similar study involving 2-aminopyrimidines, Aakeröy *et al.*¹² were able to correlate the difference between co-crystal and salt formation by looking at various changes in the IR spectra. The results showed that co-crystals displayed stretching frequencies around 1700 cm⁻¹ (consistent with neutral acid C=O) and salts displayed specific stretches near 1650 cm⁻¹.

The results in Table 3.4 also indicate that co-crystal formation is the likely outcome when using acids with pK_a values lower than 2-chlorobenzoic acid (pK_a < 2.97). In our system, which is expected to contain either carboxylic acid...pyridine or carboxylic acid...pyrazole interactions, assignments of either co-crystal or salt display a clear cutoff. If we consider the pK_a of the conjugate acid of pyridine (5.25), then the results from Table 3.4 support the ‘rule of 3’¹³ which suggests that a ΔpK_a value between 0 to 3.75 is likely to favor a co-crystal. If the ΔpK_a is greater than 3.75, proton transfer is the likely outcome. As a comparison, the ΔpK_a values were

calculated for the ditopics (using the pK_a of pyridine as the value for the ditopic). A summary of the results is shown in Table 3.5.

Table 3.5 Summary of ΔpK_a and the corresponding structures obtained from the single crystal data. The number of structures is given in parentheses; dash marks indicate no structures.

pK_a of pyridine	pK_a of carboxylic acid	ΔpK_a	Structures
5.25	4.57	0.68	-
5.25	4.45	0.8	-
5.25	4.34	0.91	-
5.25	4.08	1.17	-
5.25	4.02	1.23	-
5.25	3.97	1.28	-
5.25	3.64	1.61	-
5.25	3.54	1.71	Co-crystal (1), Salt (1)
5.25	3.48	1.77	-
5.25	3.46	1.79	-
5.25	3.42	1.83	Co-crystal (2)
5.25	3.27	1.98	-
5.25	3.21	2.04	Co-crystal (1)
5.25	2.97	2.28	-
5.25	2.77	2.48	-
5.25	2.34	2.91	-
5.25	2.19	3.06	-
5.25	1.93	3.32	-
5.25	1.69	3.56	-
5.25	1.6	3.65	-
5.25	1.43	3.82	Salt (3)

Although the pK_a of the pyridine site on the ditopic ligand may vary compared to the pK_a value of pyridine by itself (5.25), the value certainly allows us to verify the ‘rule of 3’ and shows how well it fits with our results. Not surprisingly, the rule of three predicted salt formation for all combinations with 2,4-dinitrobenzoic acid, which corroborates the single crystal results obtained. Moreover, co-crystal predictions also fit with the rule of three. On the other hand, there was one salt structure which did not fit with the prediction.

The importance of forming salts or co-crystals has a large impact on the outcome of pharmaceutical formulations, and liquid forms of pharmaceutical co-crystals at the boundary of salt formation has recently been explored by Rogers *et al.*¹⁴ in addition to a recent paper by MacGillivray *et al.*¹⁵ who looked at supramolecular complexes of sulfadiazine and pyridine at the co-crystal-salt boundary.

3.4.3 Can we group the interactions in the co-crystals and salts obtained from the single crystal data?

Single crystal data confirmed the presence of *both* carboxylic acid...pyridine and carboxylic acid...pyrazole interactions in the structures, suggesting that there is *not* a significant difference between the two acceptor sites. Two groups of interactions were found in the co-crystals as well as the salts, and are described in the following sections.

3.4.3.1 Co-crystals

There are two groups of interactions observed in the four co-crystals. In the first group the carboxylic acid binds to both pyridine and pyrazole nitrogen atoms; the N-H proton is involved in a hetero synthon via N-H...O=C(carbonyl) hydrogen bonds. In the second group the carboxylic acid interacts exclusively with the pyrazole nitrogen atom, forming O-H...N(pyz) hydrogen bonds. The N-H proton forms a N-H...N(py) hydrogen bond to the pyridine nitrogen atom. A summary of the interactions is shown in Figure 3.19.

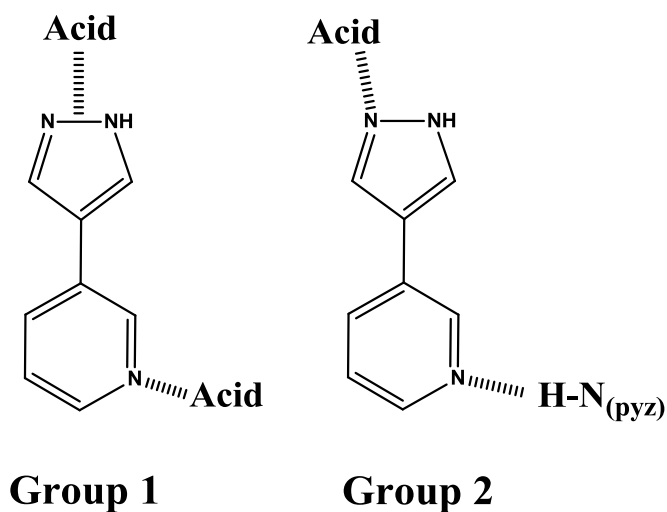


Figure 3-19 Interactions observed in the four co-crystals.

3.4.3.2 Salts

In the four salt structures, proton transfer occurred to the pyridine nitrogen atom. This result is not surprising, considering the pK_b value of pyridine is lower than that of pyrazole (i.e. stronger base) and also indicates the pyridinium ion is more stable than pyrazolium ion. Proton transfer reactions all involved pyridinium...carboxylate charge-assisted synthons. There was one

structure which incorporated water into the crystal lattice, which is not surprising considering carboxylates (COO⁻) are very good hydrogen-bond acceptors.³ This result is consistent with the observations made from Chapter 2, where neutral acids, neutral pyrazole molecules, or water molecules frequently appear in the lattice when proton transfer events take place. A summary of the interactions observed in the co-crystals and salts is shown in Table 3.6.

Table 3.6 Groups of primary interactions between the co-crystals and salts.

<u>Group number</u>	<u>Primary interactions</u>	<u>Co-crystal hits</u>	<u>Salt hits</u>
1	O-H...N(py), N-H...N(py)	2	-
2	O-H...N(py), O-H...N(py) N-H...O=C	2	-
3	N-H ⁺ ... ⁻ O-C, N-H... ⁻ O-C	-	3
4	N-H ⁺ ... ⁻ O-C, N-H...O _w , O _w -H...O, O _w -H...N	-	1

In summary,

- I. Charge calculations can be used to successfully rank the relative strengths of hydrogen-bond donor and acceptor sites.
- II. Co-crystals displayed small changes in the IR spectrum, whereas salt formation resulted in the disappearance of the C=O and appearance of two carboxylate COO⁻ stretches.
- III. Both carboxylic acid...pyridine and carboxylic acid...pyrazole interactions were observed, suggesting that there is *not* a significant difference and carboxylic acid...pyrazole synthons *can* compete with carboxylic acid...pyridine synthons.

3.5 References:

-
- ¹ Aakeröy, C. B.; Hurley, E. P.; Desper, J. *Cryst. Growth Des.*, **2012**, *12*(11), 5806-5814.
 - ² Babu, J. N.; Nangia, A. *Cryst. Growth Des.*, **2011**, *11*(7), 2662-2679.
 - ³ Aakeröy, C. B.; Fasulo, M. E.; Desper, J. *Mol. Pharm.*, **2007**, *4*(3), 317-322.
 - ⁴ Alhalaweh, A.; George, S.; Basavoju, S.; Childs, S. L.; Rizvi, S. A. A.; Velaga, S. P. *Cryst. Growth Des.*, **2012**, *14*(15), 5078-5088.
 - ⁵ <http://en.wikipedia.org/wiki/Esomeprazole>
 - ⁶ Mukherjee A.; Desiraju G. R. *Chem. Commun.*, **2011**, *47*(14), 4090-4092.

⁷ Mulyana, Y.; Kepert, C. J.; Lindoy, L. F.; Parkin, A.; Turner, P. *Dalton Trans.*, **2005**, 9, 1598-1601.

⁸ Delaunay, T.; Es-Sayed, M.; Vors, J. P.; Monteiro, N.; Balme, G. *Chem. Lett.*, **2011**, 40(12), 1434-1436.

⁹ Values were obtained from Scifinder scholar, **2013**.

¹⁰ Lin-Vien, D.; Colthup, N. B.; Fateley, W. G.; Grasselli, J. G. *The Handbook of Infrared and Raman Characteristic Frequencies of Organic Molecules*, © **1991**, Academic Press, Inc.

¹¹ Silverstein, R. M.; Webster, F. X.; Kiemle, D. J. *Spectrometric Identification of Organic Compounds*, 7th edition. © **2005**, Wiley.

¹² Aakeroy, C. B.; Rajbanshi, A.; Li, Z. J.; Desper, J. *CrystEngComm*, **2010**, 12(12), 4231-4239.

¹³ Bhogala, B. R.; Basavoju, S.; Nangia, A. *CrystEngComm*, **2005**, 7, 551-562.

¹⁴ Bica, K.; Shamshina, J.; Hough, W. L.; MacFarlane, D. R.; Rogers, R. D. *Chem. Comm.*, **2011**, 47(8), 2267-2269.

¹⁵ Elacqua, E.; Bucar, D.-K.; Henry, R.F.; Zhang, G. G. Z.; MacGillivray, L. R. *Cryst. Growth Des.*, **2013**, 13(1), 393-403.

Chapter 4 - Are triazoles competitive with pyridine for hydrogen bonds?

4.1 Introduction

The pharmaceutical industry is a multi-billion dollar per year market. Of the many active pharmaceutical ingredients (API's) that are produced, anti-fungal API's are an important class of compounds. Due to such a large market, there is a constant demand for new API's with improved physical properties.

In certain cases, specific anti-fungal API's suffer from poor physical properties, such as aqueous solubility and unwanted behavior during scale-up, to name a few. Poor aqueous solubility is a problem for administering an anti-fungal drug in the body. Anti-fungal API's contain a variety of functional groups, and one group that stands out is triazole, Figure 4.1.

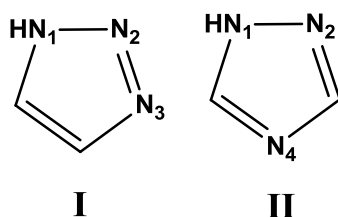


Figure 4-1 Two groups of triazole. (I) 1*H*-1,2,3-triazole. (II) 1*H*-1,2,4-triazole.

The triazole works by inhibiting the biosynthesis of sterols, an important component of cell walls, which results in cell death.¹ Although a large number of anti-fungal active ingredients are used in agricultural applications, they are very important in treating fungal infections in humans.² Within this class of compounds, two commonly used anti-fungal drugs are Fluconazole (I) and Itraconazole (II), Figure 4.2.

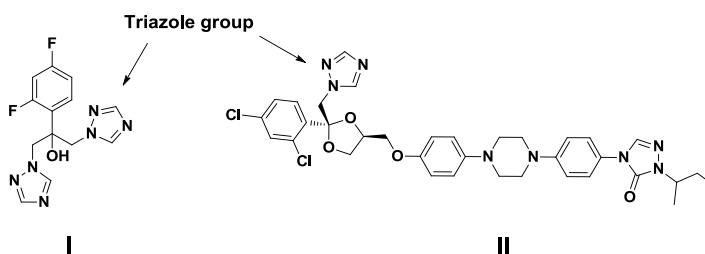


Figure 4-2 (I) Fluconazole® and (II) Itraconazole® highlighting the triazole functional group.

Both fluconazole and itraconazole suffer from poor aqueous solubility,^{3,4} which is a problem when administering the drug to a patient. In order to improve the physical properties of any API, without developing an entirely new library of target compounds, one needs to understand how to make *alternative forms of the API without changing the structure of the molecule*. A few examples of alternative forms of poorly soluble API that were made without changing the molecular structure are *salts*⁵ and *co-crystals*⁶; depending on the application, one or the other (or both) may help overcome some shortcomings (i.e. poor aqueous solubility) from existing API.

In 2003, Remenar *et al.*⁷ synthesized a series of co-crystals Itraconazole API with various di-carboxylic acids in an effort to make alternative solid forms of the drug with improved aqueous solubility. A snapshot of the crystal structure obtained from the Itraconazole:succinic acid co-crystal (2:1) is shown in Figure 4.3.

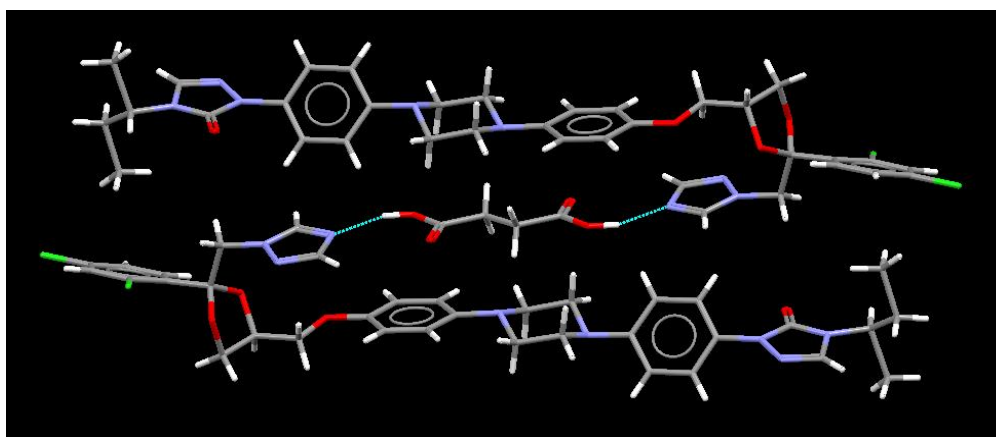


Figure 4-3 Itraconazole:succinic acid co-crystal (2:1).⁷

In the crystal structure, the succinic acid molecule acts as a ‘tether’ which bridges two drug molecules through O-H \cdots N₄(trz) hydrogen bonds. No interaction was observed between N₂(trz) nitrogen, indicating that the N₄(trz) acts as a better hydrogen-bond acceptor site; this observation is not surprising, considering N₄(trz) carries a higher electrostatic charge and is also a better acceptor geometrically for the carboxylic acid, given its position relative to the carboxylic acid groups, Figure 4.4.

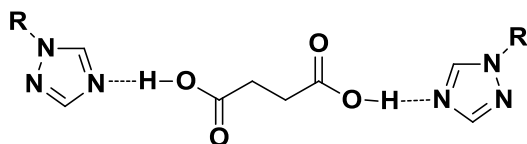


Figure 4-4 Triazole nitrogen position relative to the carboxylic acid.⁷

Although triazole groups are often encountered on the backbone of various anti-fungal API's, pyridine is often seen as well, and both groups are often found on the same molecular backbone. In order to successfully make new solid forms of an API a solid understanding of where co-formers (e.g. carboxylic acids) bind (in the case of co-crystals) or proton transfer may take place (in the case of salt formation) is needed.

As a result, we decided to systematically investigate the supramolecular behavior of carboxylic acids with triazole/pyridine ditopic molecules by synthesizing a library of asymmetric ditopic molecules containing both functional groups, triazole and pyridine (**IV-VII**), Figure 4.5.

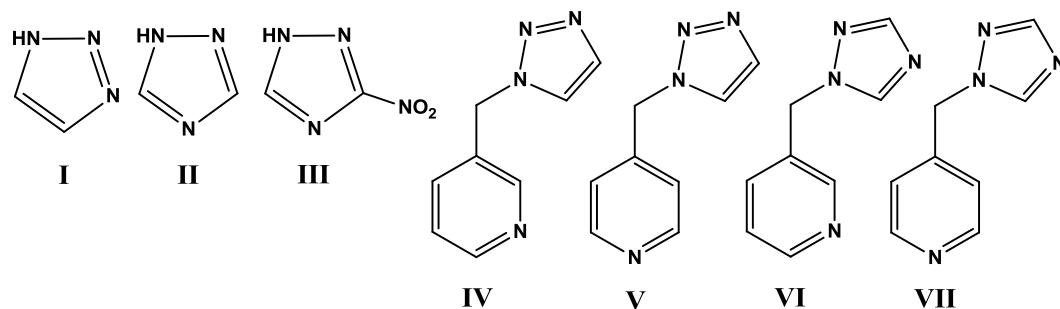


Figure 4-5 Triazole (**I-III**) and triazole/pyridine asymmetric ditopic molecules (**IV-VII**).

Since triazole contains multiple nitrogen atoms, and hence potentially more than one acceptor site, an incoming carboxylic acid could bind in a variety of ways. The potential interactions that could result from a carboxylic acid interacting with 1*H*-1,2,3-triazole (**I**, **II**, **III**) and 1*H*-1,2,4-triazole (**IV**, **V**, **VI**) are shown in Figure 4.6.

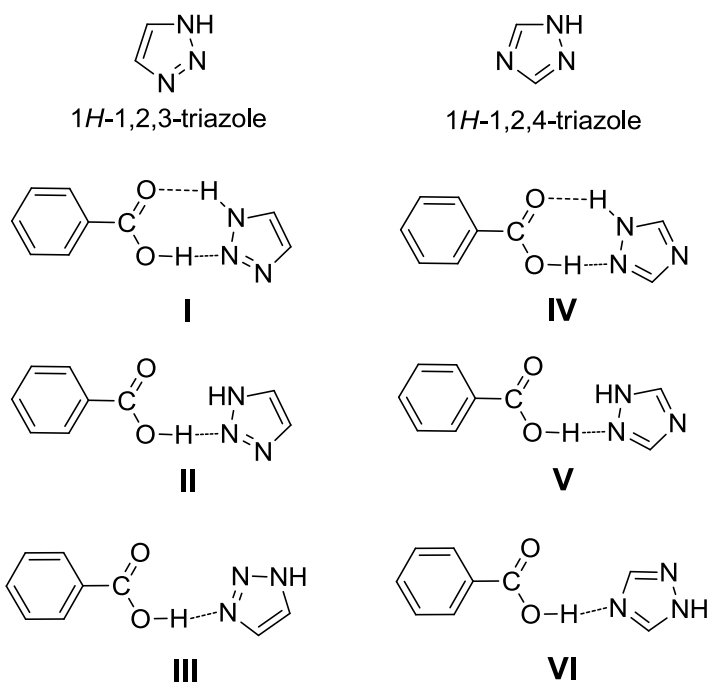


Figure 4-6 Potential interactions between carboxylic acid and triazole molecules. Potential interactions with 1H-1,2,3-triazole (**I,II,III**) and with 1H-1,2,4-triazole (**IV, V, VI**) are shown.

When adding a pyridine moiety to the triazole, the number of potential binding sites increases further; N(py) represents the pyridine site, N₂(trz), N₃(trz), and N₄(trz) represent triazole binding sites. When a carboxylic acid is introduced to the system, the acid now has a choice between multiple sites: a list of potential supramolecular interactions between the carboxylic acid and two of the asymmetric ditopic molecules is shown below (**1-14**), where interactions between acid and 4-((1H-1,2,3-triazol-1-yl)methyl)pyridine are shown in group I, **1-7**; interactions between acid and 4-((1H-1,2,4-triazol-1-yl)methyl)pyridine are shown in group II, **8-14**, Figure 4.7.

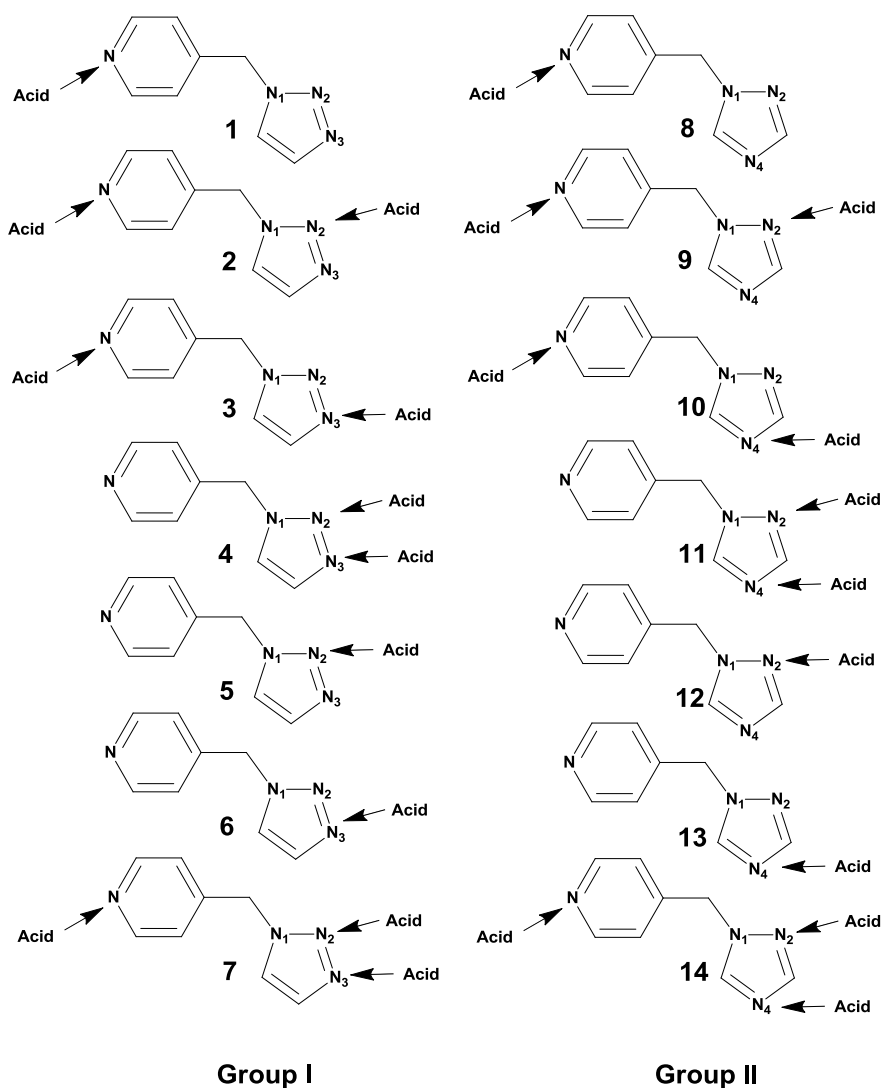


Figure 4-7 Potential binding sites of two of the four triazole/pyridine asymmetric ditopic molecules. Group I: 4-((1*H*-1,2,3-triazol-1-yl)methyl)pyridine. Group II: 4-((1*H*-1,2,4-triazol-1-yl)methyl)pyridine.

To address the competition between N(py), N₂(trz), N₃(trz), and N₄(trz) in the presence of carboxylic acids, charge calculations were performed on the molecules to establish which site, N(py), N₂(trz), N₃(trz), or N₄(trz) carries the highest charge and thus would be ranked as the best hydrogen-bond acceptor. Solvent assisted grinding using the same library of acids from Chapter 2 was combined with triazole and triazole/pyridine asymmetric ditopic molecules **I-VII**; results from the IR spectra which gave a reaction (based on O-H···N) broad stretches in the 2500 cm⁻¹

and 1900 cm^{-1} region were then converted to solution experiments to generate single crystals. Single crystal data allow us to make inferences on binding preferences, if the four sites (N(py), N₂(trz), N₃(trz), or N₄(trz)) are significantly different in terms of their ability to act as a hydrogen-bond acceptor. A flowchart for the approach is shown in Figure 4.8.

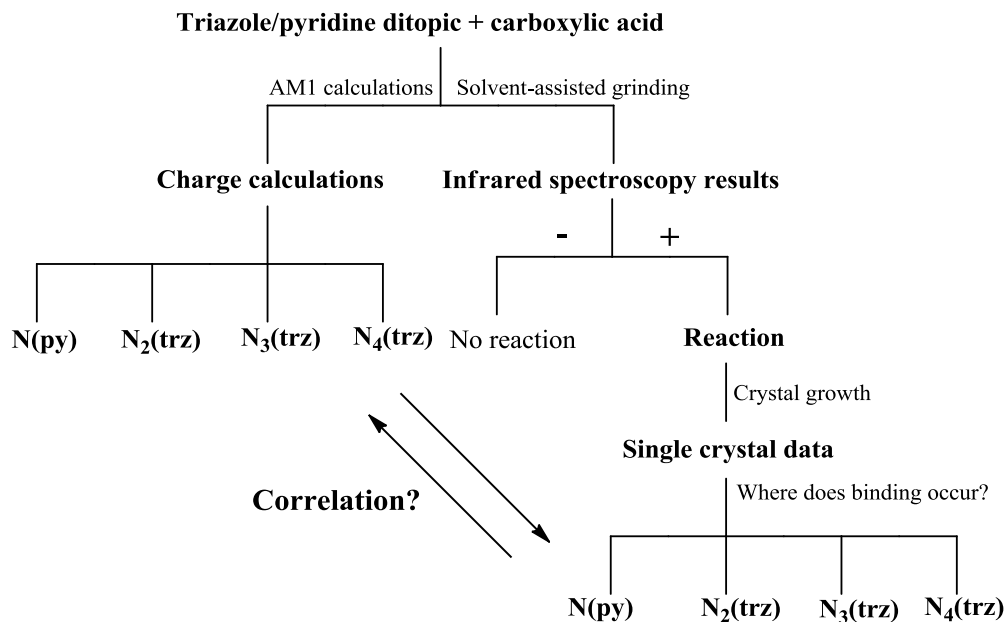


Figure 4-8 Flowchart for determining a correlation between charge calculations, IR spectroscopy results and single crystal data.

None of the proposed molecules in the library have been used for any screening study; in fact, there is only a handful of examples of co-crystals or salts with similar molecules.⁸ Furthermore, there is no study in the literature which systematically examines the binding preferences of carboxylic acids for N(py), N₂(trz), N₃(trz), or N₄(trz) when present in the same system (i.e. same molecular backbone).

The goals of this study are as follows:

- I. Can charge calculations be used to predict binding preferences? **Hypothesis:** AM1 calculations will give relative electrostatic charges of N(py), N₂(trz),

- N₃(trz), and N₄(trz) hydrogen bond acceptor sites and allow us to rank the sites; the carboxylic acid donor will prefer the site which carries the highest charge.
- II. Are there specific handles which can be used to determine reaction or no reaction, *and* co-crystal or salt formation, from changes in the IR spectrum? **Hypothesis:** Changes in the carbonyl C=O stretch and the presence of broad O-H...N stretches in the 2500 cm⁻¹ and 1900 cm⁻¹ regions indicate a reaction; if the shifts in the C=O are small, co-crystal formation is the likely outcome. If the C=O disappears and two carboxylate COO⁻ stretches appear, salt formation is the likely outcome
- III. Can we determine binding preferences of carboxylic acids for N(py), N₂(trz), N₃(trz), or N₄(trz) *in a competitive environment* from the single crystal data? **Hypothesis:** Binding preferences for carboxylic acids, when given the choice between N(py), N₂(trz), N₃(trz), or N₄(trz), will choose the site which carries the highest charge (determined from the AM1 calculations).

4.2 Experimental

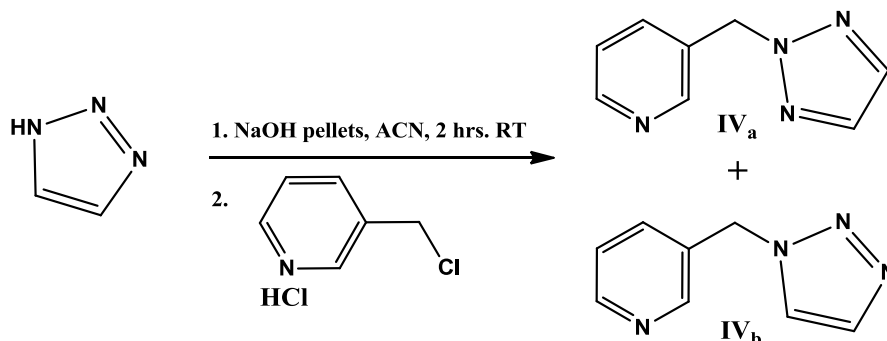
4.2.1 Charge calculations

Molecular electrostatic potential (MEP) surface charge calculations were performed using Spartan (Wavefunction, Inc., Irvine, CA). The molecules were optimized using AM1, with the maxima and minima in the electrostatic potential surface (0.002 e/au isosurface) determined using a positive point charge in the vacuum as a probe.

4.2.2 Covalent synthesis and characterization of products

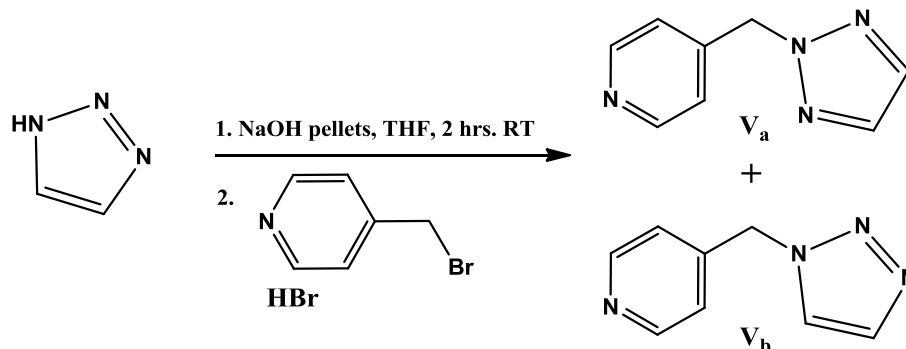
All chemicals were purchased from Aldrich, TCI, and Combi-blocks and used without further purification, unless otherwise noted. ¹H and ¹³C NMR data were recorded on a Bruker 400 MHz instrument. Melting points were determined on a Fisher-Johns melting point apparatus and are uncorrected.

4.2.2.1 Synthesis of 3-((2H-1,2,3-triazol-2-yl)methyl)pyridine and 3-((1H-1,2,3-triazol-1-yl)methyl)pyridine, *IV_a* and *IV_b*



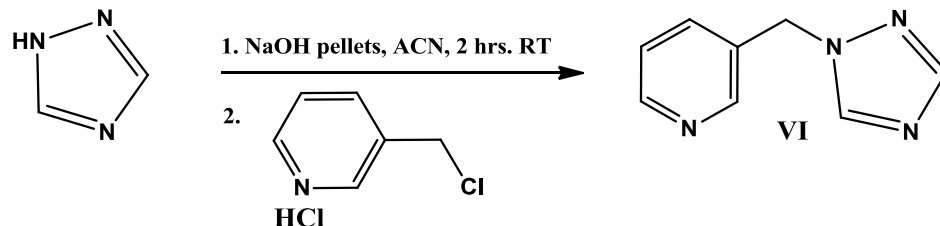
To a round bottom flask, 1H-1,2,3-triazole (2.13g, 30.8mmol) and acetonitrile (ACN, 70mL) were added. To the clear solution, sodium hydroxide pellets (12.35g, 308.8mmol) were added and the mixture was stirred at room temperature for two hours, after which 3-(chloromethyl)pyridine hydrochloride (5.57g, 33.96mmol) was added to the mixture and stirred for an additional 72 hours. The color turned milky orange and the reaction was monitored using TLC and ¹H NMR. Upon completion, water (100mL) was added to dissolve any excess NaOH. Dichloromethane (100mL) was added and the organic layer was separated. The aqueous solution was washed with dichloromethane (4 x 50mL) and once with brine (50mL). The organic extracts were combined, dried over MgSO₄, and concentrated to give a brown oil. From the oil, two isomers were separated using a silica column packed with hexanes (hexanes/ethyl acetate as eluent). The first spot yielded 0.50g of a yellow oil (15% ethyl acetate, 85% hexanes as eluent). The second spot yielded 1.21g of a yellow oil (43% ethyl acetate, 57% hexanes as eluent). **IV_a**: ¹H NMR (400 MHz, CDCl₃) δ ppm: 8.42 - 8.75 (m, 2H), 7.50 - 7.79 (m, 3H), 7.13 - 7.37 (m, 1H), 5.63 (s, 2H), Figure A-10. ¹³C NMR (100 MHz, CDCl₃) δ ppm: 149.98, 149.55, 135.88, 135.06, 131.08, 123.79, 56.14, Figure A-11. **IV_b**: ¹H NMR (400 MHz, CDCl₃) δ ppm: 8.60 (br. s., 2H), 7.73 (s, 1H), 7.47 - 7.63 (m, 2H), 7.30 (d, *J*=3.91 Hz, 1H), 5.59 (s, 2H), Figure A-12. ¹³C NMR (100 MHz, CDCl₃) δ ppm: 150.45, 149.27, 135.88, 134.75, 130.78, 124.17, 123.59, 51.56, Figure A-13.

4.2.2.2 Synthesis of 4-((2H-1,2,3-triazol-2-yl)methyl)pyridine and 4-((1H-1,2,3-triazol-1-yl)methyl)pyridine, V_a and V_b



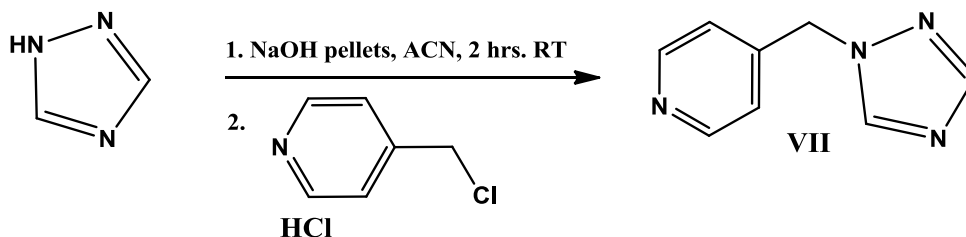
To a round bottom flask, 1H-1,2,3-triazole (0.812g, 11.76mmol) and freshly distilled tetrahydrofuran (THF, 30mL) were added. To the clear solution, sodium hydroxide pellets (4.7g, 117.6mmol) were added and the mixture was stirred at room temperature for two hours, after which 4-(bromomethyl)pyridine hydrobromide (3.27g, 12.93mmol) was added and stirred for an additional 72 hours. THF (10mL) was used to wash the pyridine salt from the sides of the round bottom into the reaction mixture. The mixture turned grey/green in color upon addition and the reaction was monitored using TLC and ^1H NMR. Upon completion, water (30mL) was added to dissolve any excess NaOH pellets. Dichloromethane (30mL) was added and the organic layer separated. The aqueous solution was washed with dichloromethane (4 x 50mL) and once with brine (50mL). The organic extracts were combined, dried over MgSO_4 , and concentrated to give a black oil. From the oil, two isomers were separated using a silica column packed with hexanes (hexanes/ethyl acetate as eluent). The first spot yielded 0.114g of a yellow oil (20% ethyl acetate, 80% hexanes as eluent). The second spot yielded 0.365g of a yellow oil (35% ethyl acetate, 65% hexanes as eluent). V_a : ^1H NMR (400 MHz, CDCl_3) δ ppm: 8.58 (d, $J=5.08$ Hz, 2H), 7.69 (s, 2H), 7.11 (d, $J=5.47$ Hz, 2H), 5.64 (s, 2H), Figure A-14. ^{13}C : (100 MHz, CDCl_3) δ ppm: 150.37, 144.42, 135.28, 122.49, 57.35, Figure A-15. V_b : ^1H NMR (400 MHz, CDCl_3) δ ppm: 8.63 (d, $J=6.25$ Hz, 2H), 7.80 (s, 1H), 7.67 (s, 1H), 7.13 (d, $J=5.47$ Hz, 2H), 5.65 (s, 2H), Figure A-16. ^{13}C : (100 MHz, CDCl_3) δ ppm: 150.67, 143.95, 134.71, 124.16, 122.22, 52.64, Figure A-17.

4.2.2.3 Synthesis of 3-((1H-1,2,4-triazol-1-yl)methyl)pyridine, VI



To a round bottom flask, 1H-1,2,4-triazole (1.64g, 23.7mmol) and acetonitrile (ACN, 40mL) were added. To the clear solution, sodium hydroxide pellets (9.48g, 237mmol) were added along with additional ACN (20mL) and the mixture was stirred at room temperature for two hours, after which 3-(chloromethyl)pyridine hydrochloride (4.28g, 26.1mmol) and additional ACN (20mL) was added to wash the sides of the round bottom and stirred for an additional 72 hours. The color turned milky orange and the reaction was monitored using TLC and ^1H NMR. Upon completion, water (100mL) was added to dissolve any excess NaOH. Dichloromethane (100mL) was added and the organic layer was separated. The aqueous solution was washed with dichloromethane (4 x 50mL) and once with brine (50mL). The organic extracts were combined, dried over MgSO_4 , and concentrated to give a brown oil. The product was isolated using a silica column packed with hexanes (50% ethyl acetate and 50% hexanes as eluent) to give 0.167g (4.4 %) of a yellow oil. **VI**: ^1H NMR (400 MHz, CDCl_3) δ ppm: 8.60 (s, 2H), 8.13 (s, 1H), 7.99 (s, 1H), 7.60 (dd, $J=8.20, 1.95$ Hz, 1H), 7.28 - 7.37 (m, 1H), 5.38 (s, 2H), Figure A-18. ^{13}C : (100 MHz, CDCl_3) δ ppm: 152.65, 150.24, 149.31, 143.35, 135.90, 130.70, 124.06, 51.11, Figure A-19.

4.2.2.4 Synthesis of 4-((1H-1,2,4-triazol-1-yl)methyl)pyridine, VII



To a round bottom flask, 1*H*-1,2,4-triazole (1.65g, 23.9mmol) and acetonitrile (ACN, 40mL) were added. To the clear solution, sodium hydroxide pellets (9.75g, 243.8mmol) were added and the mixture was stirred at room temperature for three hours, after which 4-(chloromethyl)pyridine hydrochloride (4.36g, 26.6mmol) and additional ACN (20mL) was added to wash the sides of the round bottom and stirred for an additional 72 hours. The color turned purple and the reaction was monitored using TLC and ¹H NMR. Upon completion, water (100mL) was added to dissolve any excess NaOH. Dichloromethane (100mL) was added and the organic layer was separated. The aqueous solution was washed with dichloromethane (4 x 50mL) and once with brine (50mL). The organic extracts were combined, dried over MgSO₄, and concentrated to give a black oil. The product was isolated using a silica column packed with hexanes (50% ethyl acetate and 50% hexanes as eluent) to give 0.211g (9.4 %) of an orange oil. **VII:** ¹H NMR (400 MHz, CDCl₃) δ ppm: 8.61 (br. s., 2H), 8.17 (s, 1H), 8.01 (s, 1H), 7.10 (br. s., 2H), 5.38 (s, 2H), Figure A-20. ¹³C: (100 MHz, CDCl₃) δ ppm: 152.77, 150.52, 149.90, 143.85, 122.28, 52.22, Figure A-21.

4.2.2.5 Synthesis of 4-((1*H*-1,2,4-triazol-1-yl)methyl)pyridine:bis(3-nitrobenzoic) acid (1:2),

VII:I₂

To a vial, 4-((1*H*-1,2,4-triazol-1-yl)methyl)pyridine (5.1mg, 0.032mmol) was added followed by a solution of 3-nitrobenzoic acid (5.9mg, 0.035mmol) in methanol (1mL). The solution was heated and left for slow evaporation (loose screw cap). Colorless plates were obtained after a few days. Mp: 94-96°C.

4.2.2.6 Synthesis of 4-((1*H*-1,2,4-triazol-1-yl)methyl)pyridine:bis(4-nitrobenzoic) acid (1:2),

VII:K₂

To a vial, 4-((1*H*-1,2,4-triazol-1-yl)methyl)pyridine (5.1mg, 0.032mmol) was added followed by a solution of 4-nitrobenzoic acid (6.0mg, 0.036mmol) in methanol (1mL). The solution was heated and left for slow evaporation (loose screw cap). Colorless plates were obtained after a few days. Mp: 162-165°C.

4.2.2.7 Synthesis of 4-((1H-1,2,3-triazol-1-yl)methyl)pyridinium:3,5-dinitrobenzoate:3,5-dinitrobenzoic acid hydrate (1:2:1), V:N₂:H₂O

To a vial, 4-((1H-1,2,3-triazol-1-yl)methyl)pyridine (11.0mg, 0.0686mmol) was added followed by a solution of 3,5-dinitrobenzoic acid (14.6mg, 0.0686mmol) in methanol (400μL). The solution was heated and left for slow evaporation (loose screw cap). Colorless prisms were obtained after a few days. Mp: 104-107°C.

4.2.3 IR

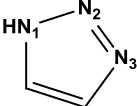
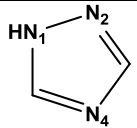
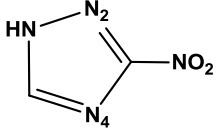
Infrared spectra were collected on a Thermo Scientific Nicolet 380 FT-IR using a ZnSe crystal. The solids (or oily product) obtained from solvent-assisted grinding experiments were analyzed by placing the solid directly on the crystal and performing 32 scans.

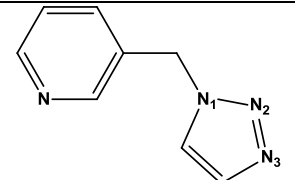
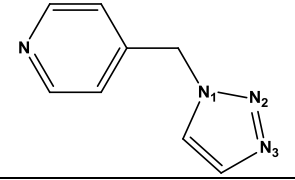
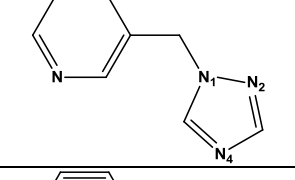
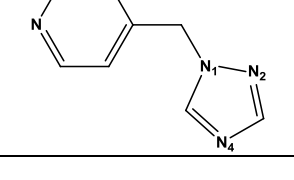
4.3 Results

4.3.1 MEP surface calculations

Molecular electrostatic potential (MEP) surface calculations were made in order to rank the strengths of the hydrogen bond acceptor sites. Although a low level of theory is used (AM1)⁹, this method has proven effective for predicting binding site strengths of various hydrogen-bond acceptor sites. In fact, Hunter¹⁰ and co-workers¹¹ showed that this level of theory works well for calculating electrostatic surface energies for small molecules. The AM1 values for the library of molecules used (**I-VII**) is shown in Table 4.1.

Table 4.1 Molecular electrostatic surface potential (MEP) calculations for the various triazoles and asymmetric ditopic triazole/pyridine molecules. Values are given in kJ/mol.

#	Structure	H-N ₁	N(py)	N ₂ (trz)	N ₃ (trz)	N ₄ (trz)
1		+202	-	-217	-277	-
2		+201	-	-216	-	-280
3		+271	-	-165	-	-238

4		-	-260	-200	-275	-
5		-	-270	-200	-271	-
6		-	-270	-202	-	-288
7		-	-268	-200	-	-280

4.3.2 Covalent synthesis

Four asymmetric ditopic triazole/pyridine molecules were synthesized with different charges on the hydrogen bond acceptor sites, Figure 4.9.

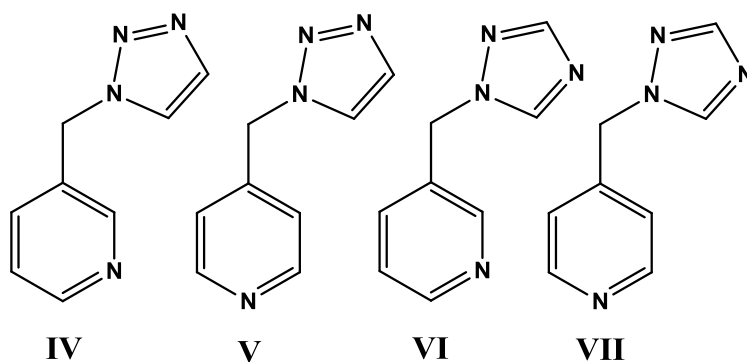


Figure 4-9 The four asymmetric ditopic triazole/pyridine molecules (**IV-VII**) used for screening with carboxylic acids.

4.3.3 Infrared data

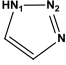
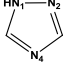
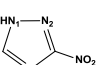
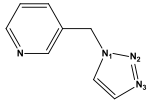
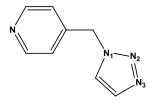
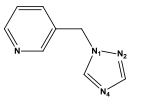
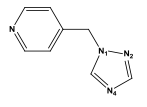
The triazole and ditopic triazole/pyridine molecules were screened with twenty carboxylic acids of varying pK_a strength, Table 4.2.

Table 4.2 Table of aromatic carboxylic acids used in the study.

Label (pKa)	Benzoic Acid
A (4.57 +/- 0.10)	4-Hydroxybenzoic acid
B (4.45 +/- 0.10)	4-Hydroxy-3-methoxy benzoic acid
C (4.34 +/- 0.10)	3,5-Dimethylbenzoic acid
D (4.08 +/- 0.10)	3-Hydroxybenzoic acid
E (4.02 +/- 0.10)	4-Iodobenzoic acid
F (3.97 +/- 0.10)	4-Chlorobenzoic acid
G (3.64 +/- 0.10)	3-Cyanobenzoic acid
H (3.54 +/- 0.10)	4-Cyanobenzoic acid
I (3.48 +/- 0.10)	3-Nitrobenzoic acid
J (3.46 +/- 0.10)	3-Bromo-5-iodobenzoic acid
K (3.42 +/- 0.10)	4-Nitrobenzoic acid
L (3.27 +/- 0.10)	2-Fluorobenzoic acid
M (2.97 +/- 0.25)	2-Chlorobenzoic acid
N (2.77 +/- 0.10)	3,5-Dinitrobenzoic acid
O (2.34 +/- 0.10)	2,6-Difluorobenzoic acid
P (2.19 +/- 0.25)	2-Nitrobenzoic acid
Q (1.93 +/- 0.10)	2-Fluoro-6-iodobenzoic acid
R (1.69 +/- 0.10)	2,6-Dichlorobenzoic acid
S (1.60 +/- 0.10)	Pentafluorobenzoic acid
T (1.43 +/- 0.25)	2,4-Dinitrobenzoic acid

The prominent stretches from the IR are summarized in Table 4.4, showing the presence of broad OH stretches in the 2500 cm^{-1} and 1900 cm^{-1} regions; the corresponding supramolecular yield (calculated as the number of positive hits) is given in the last row to indicate the reactivity.

Table 4.3 Summary of prominent IR stretches for the triazole molecules combined with various carboxylic acids.

Acids	 I	 II	 III	 IV	 V	 VI	 VII
A	-	-	-	2479, 1921, 1670	2550, 1889, 1666	2417, 1874, 1666	2452, 1944, 1666
B	2515, 1831, 1670	2542, 1854, 1670	-	2476, 1874, 1663	2526, 1862, 1674	2503, 1901, 1666	2444, 1893, 1670
C	-	-	-	2569, 1901, 1686	2562, 1874, 1682	2495, 1901, 1682	2515, 1921, 1682
D	-	-	-	2522, 1901, 1694	2577, 1885, 1678	2429, 1854, 1686	2522, 1917, 1694
E	-	-	-	2538, 1905, 1678	2542, 1909, 1670	2542, 1928, 1666	2495, 1893, 1682
F	2831, 1866, 1674	2507, 1905, 1706	-	2491, 1866, 1690	2558, 1924, 1678	2542, 1928, 1674	2401, 1921, 1686
G	-	-	-	2436, 1881, 1682	2581, 1878, 1682	2526, 1905, 1678	2429, 1889, 1698
H	2823, 1878, 1682	2397, 1936, 1702	-	2433, 1897, 1709	2554, 1897, 1690	2421, 1917, 1694	2433, 1897, 1706
I	2468, 1893, 1694	2483, 1878, 1686	-	2444, 1905, 1694	2526, 1913, 1686	2370, 1893, 1686	2390, 1917, 1702
J	-	-	-	2479, 1885, 1690	2526, 1948, 1706	2409, 1881, 1682	2401, 1901, 1682
K	2863, 1854, 1686	2464, 1881, 1702	-	2425, 1905, 1682	2542, 1952, 1690	2390, 1913, 1706	2397, 1909, 1682
L	2827, 1897, 1686	2511, 1897, 1702	-	2468, 1913, 1706	2624, 1913, 1682	2456, 1905, 1698	2472, 1913, 1698
M	-	-	-	2511, 1917, 1686	2538, 1944, 1686	2476, 1909, 1706	2472, 1924, 1698
N	2444, 1975, 1620	2534, 1905, 1694	-	2409, 1924, 1709	2534, 1889, 1694	2448, 1889, 1706	2409, 1921, 1698
O	-	2401, 1924, 1686	-	2476, 1932, 1713	2534, 1952, 1682	2476, 1917, 1709	2487, 1948, 1702
P	2542, 1936, 1678	2483, 1913, 1706	-	2448, 1909, 1709	2538, 1924, 1682	2452, 1913, 1706	2456, 1901, 1709
Q	2487, 1936, 1709	2487, 1932, 1713	-	2444, 1905, 1713	2483, 1921, 1709	2436, 1921, 1706	2464, 1924, 1706
R	2495, 1944, 1709	2499, 1940, 1721	-	2468, 1921, 1713	2491, 1932, 1717	2460, 1921, 1709	2472, 1940, 1713
S	2499, 1901, 1717	2515, 1924, 1717	-	2476, 1913, 1713	2436, 1909, 1717	2464, 1901, 1717	2499, 1924, 1717
T	2526, 1979, 1713	2440, 1936, 1709	-	2448, 1932, 1717	2530, 1924, 1713	2468, 1866, 1682	2487, 1956, 1706
Supramolecular yield (%)	12/20 = 60%	13/20 = 65%	0/20 = 0%	20/20 = 100%	20/20 = 100%	20/20 = 100%	20/20 = 100%

Co-crystals:

4.3.4 Crystal structure of 4-((1H-1,2,4-triazol-1-yl)methyl)pyridine:bis(3-nitrobenzoic acid) (1:2), VII:I₂

The crystal structure of **VII:I₂** shows a 1:2 ratio between ditopic ligand and carboxylic acid. Two predominant interactions are observed. At the pyridine end, a two-point contact exists between carboxylic acid and pyridine nitrogen atom, where O-H...N(py) distance is 2.646(4)Å, 166(2)°; the pyridine C-H interacts with a carbonyl oxygen, and the C-H...O=C distance is 2.654Å. The ratio of C-O/C=O is 1.06 and the C-N_(py)-C angle is 119(3)°, indicating the proton remains on the carboxylic acid. On the triazole end, a second acid forms a single point contact with the triazole nitrogen atom: O-H...N₄(trz) distance is 2.618(12)Å, 167(2)°; the C-N₄-C angle is 103(5)°. The ratio of C-O/C=O is 1.08, indicating the proton remains on the acid, Figure 4.10.

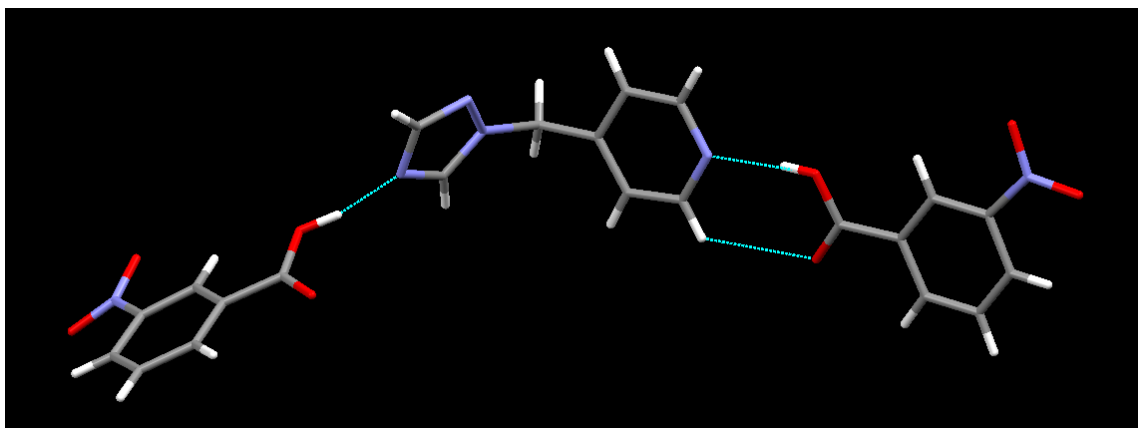


Figure 4-10 The primary interactions observed in the crystal structure of **VII:I₂**.

4.3.5 Crystal structure of 4-((1H-1,2,4-triazol-1-yl)methyl)pyridine:bis(4-nitrobenzoic acid) (1:2), VII:K₂

The crystal structure of **VII:K₂** also shows a 1:2 ratio between ditopic ligand and carboxylic acid. Two predominant interactions are observed. At the pyridine end, a two-point contact exists between carboxylic acid and pyridine nitrogen atom, where O-H...N(py) distance is 2.659(3)Å, 173(2)°; the pyridine C-H interacts with a carbonyl oxygen, and the C-H...O=C distance is 2.557Å. The ratio of C-O/C=O is 1.08 and the C-N_(py)-C angle is 118(2)°, indicating the proton remains on the carboxylic acid. On the triazole end, a second acid forms a two point contact with the triazole base. The triazole nitrogen atom interacts with a carboxylic acid, and a

C-H from triazole interacts with a carbonyl oxygen atom from the acid, respectively: O-H \cdots N₄(trz) distance is 2.673(3)Å, 177(3)°; C-H \cdots O=C distance is 2.661Å. The C-N₄-C angle is 103(2)° and the ratio of C-O/C=O is 1.08, indicating the proton remains in the carboxylic acid, Figure 4.11.

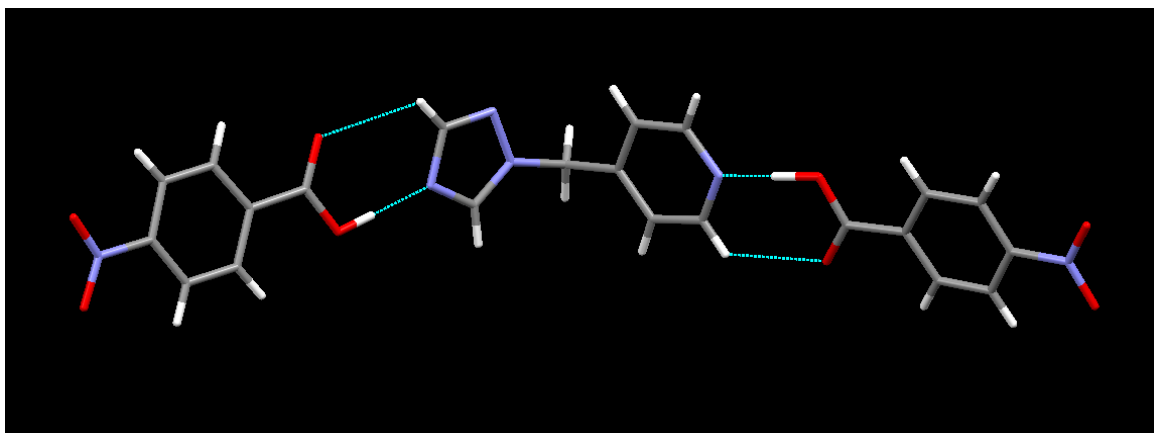


Figure 4-11 The primary interactions observed in the crystal structure of **VII:K₂**.

Salt:

4.3.6 Crystal structure of 4-((1H-1,2,3-triazol-1-yl)methyl)pyridinium:3,5-dinitrobenzoate:3,5-dinitrobenzoic acid hydrate (1:2:1), V:N₂:H₂O

The crystal structure of **V:N₂:H₂O** shows proton transfer from a carboxylic acid to a pyridine nitrogen atom resulting in a hydrated salt, with a charge-assisted N⁺-H \cdots O⁻ distance of 2.5810(18)Å, 176(18)°. The C-N_(py)-C bond angle is 121(14)° and the C-O⁻/C-O⁻ carboxylate bond ratio is 1.02, indicating the carboxylic acid proton has been transferred to the pyridine nitrogen atom. The triazole nitrogen atom (N₃) interacts with water via O-H_w \cdots N₃(trz) hydrogen bonds, where the O-H_w \cdots N₃(trz) distance is 2.7696(19)Å, 177(2)°. The carboxylate interacts with water through charge-assisted O-H_w \cdots O⁻ interactions, where the O-H_w \cdots O⁻-C distance is 2.7276(16)Å, 171(2)°. A neutral acid incorporates itself into the crystal structure via O-H \cdots O_w interactions, where the O-H \cdots O_w distance is 2.5364(16)Å, 172(2)°, Figure 4.12.

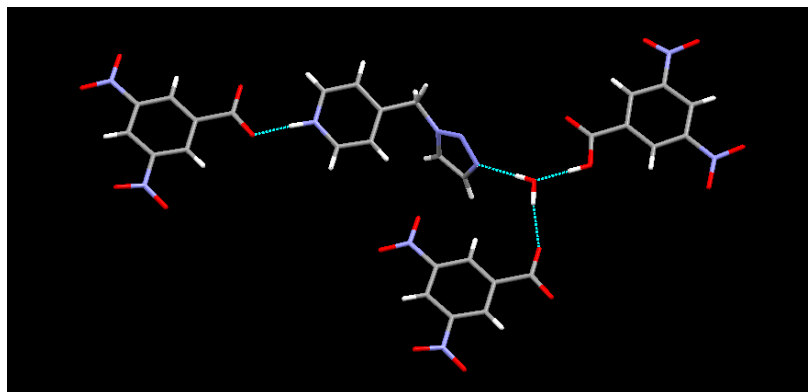


Figure 4-12 The primary interactions observed in the crystal structure of $V:N_2:H_2O$.

4.4 Discussion

4.4.1 What do charge calculations tell us about where binding preferences should be?

Charge calculations were performed on the library of molecules I-VII, Figure 4.13.

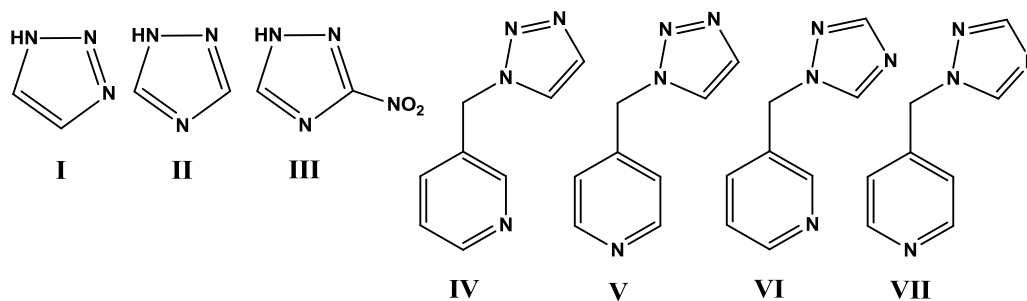


Figure 4-13 Triazole (**I-III**) and triazole/pyridine asymmetric ditopic molecules (**IV-VII**).

The AMI charges for both N_1-H on **I** and **II** are +202 and +201, respectively, indicating very small differences. However, there is a significant difference between the nitrogen atoms on the two triazole molecules. $N_2(trz)$ -217 kJ/mol, and $N_3(trz)$ -277 kJ/mol, respectively. In the case of **II**, the same trend is observed; $N_2(trz)$ is -216 kJ/mol, and $N_4(trz)$ is -280 kJ/mol, respectively. The difference is almost the same as in **I**. This result indicates that in both molecules, **I** and **II**, $N_2(trz)$ should *not* be the preferred hydrogen-bond acceptor site and that both $N_3(trz)$ and $N_4(trz)$ carry a higher charge and should therefore be where a hydrogen-bond donor (e.g. carboxylic acid) would prefer to interact.

When a strongly electron withdrawing nitro group (R-NO₂) is added, **III**, the electrostatic charges change drastically. The N₁-H hydrogen atom goes to +271 kJ/mol, a +70 kJ/mol difference from **I** and **II**. Furthermore, the charge on N₂(trz) drops significantly to -165 kJ/mol, as does N₄(trz) to -238 kJ/mol.

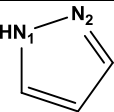
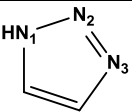
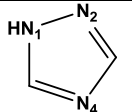
When a third acceptor site is added to the backbone of the triazole molecule via a methylene bridge, there are no significant differences between the N(py) acceptor site compared to either N₃(trz) or N₄(trz). In **IV**, the charge on the N(py) is -260 kJ/mol and N₃(trz) is -275 kJ/mol. The charge on N₂(trz) in this case is -200 kJ/mol, even lower than **I**. The values indicate there may not be a significant difference in binding preference for an incoming hydrogen-bond donor. In the case of **V**, the charge on N(py) is -270 kJ/mol and N₃(trz) is -271 kJ/mol, respectively, indicating both sites should be equally attractive for an incoming acid.

In **VI** and **VII**, respectively, both molecules show a similar trend where N₄(trz) carries a higher charge than N(py). In **VI**, the values are -270 kJ/mol for N(py) and -288 kJ/mol for N₄(trz). In **VII**, the values are -268 kJ/mol for N(py) and -280 kJ/mol for N₄(trz). For **VI** and **VII**, both values of N₂(trz) are around -200 kJ/mol. The results for this set of molecules would predict the binding to occur at N₄(trz), which carries a higher charge over the N(py) in both cases.

4.4.2 Can we determine co-crystal or salt formation from the IR data?

The data from the IR screening show that both triazoles **I** and **II** have very similar reactivity when combined with various carboxylic acids. In the case of **I**, a 60% supramolecular yield was obtained from the solvent assisted grinding experiments with twenty acids of varying strength (12 positive hits / 20 total reactions). In **II**, a 65% yield was obtained upon screening with the same group of acids. The results are not surprising considering the charges on the strongest hydrogen bond acceptor site are nearly identical. The result is consistent with the screening work from Chapter 2 with pyrazole (supramolecular yield of 55%), which carries a slightly lower charge on the primary acceptor, Table 4.4.

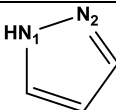
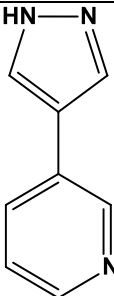
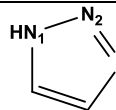
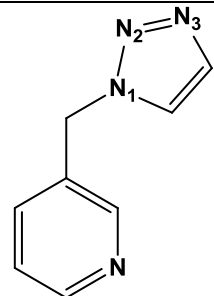
Table 4.4 Summary of charges on pyrazole and the triazole molecules.

Molecule			
Charge on best acceptor (kJ/mol)	-251	-277	-280
Supramolecular yield (%)	55%	60%	65%

On the other hand, the results for **III** (the nitro analog) are completely different. No reactions were observed, and despite the large increase in charge on the N₁-H (+70 kJ/mol) from **I** and **II**, the supramolecular yield *decreases*, indicating the balance between an increase in charge on the hydrogen and a lowering of charge on both nitrogen acceptors is not sufficient to drive any supramolecular reaction, Table 4.4.

When a pyridine moiety is introduced and both pyridine and triazole are part of the same molecular backbone, the supramolecular yield *increases*. This indicates that pyridine is a better acceptor to triazole, despite the two having similar charges. The results follow the same trend as noted in Chapter 3; introducing a pyridine moiety (and subsequently a higher charge on the acceptor site) to the pyrazole backbone also gave an *increased* supramolecular yield, Table 4.5.

Table 4.5 Summary of the results obtained from different chapters.

Chapter #	Ch. 2	Ch. 3	Ch. 4	
Molecule				
Supramolecular yield (%)	55%	100%	60%	100%

The increase in supramolecular reactivity for the pyrazole case can be explained by the fact that adding a group with a higher charge increases the supramolecular yield, but the same

argument does not hold true for the triazole case (since the triazole nitrogens N₃(trz) and N₄(trz) actually carry the same or higher charge in molecules **I**, **II**, **IV-VII**).

The additional C-H···O=C interaction present in carboxylic acid···pyridine synthons may push the balance to favor the pyridine side; triazole does have an aromatic C-H group to make a C-H···O=C interaction, but the geometry around that site is very different and therefore may not stabilize the interaction as much as the two-point contact to pyridine.

4.4.3 Can we group the interactions in the co-crystals and salts from the single crystal data?

Two co-crystals and one salt were obtained, and the co-crystals show structural consistency. The salt, on the other hand, displayed unpredictable chemical composition and structural landscape, consistent with the results obtained from Chapters 2 and 3.

4.4.3.1 Co-crystals

Both co-crystals obtained (2/2) display the same 1:2 ratio between ditopic molecule and carboxylic acid. The structures both show the expected O-H···N(py) interaction, as well as an O-H···N₄(trz) interaction, Figure 4.14.

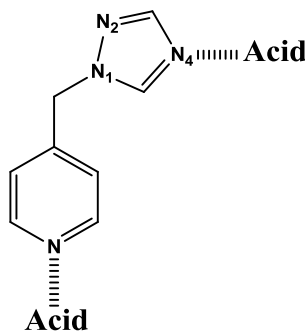


Figure 4-14 Primary interactions observed in the co-crystals obtained.

4.4.3.2 Salt

In the crystal structure of **V** + **N**, the proton is transferred to the pyridine nitrogen atom over the two triazole acceptor sites, N₂(trz) and N₃(trz). Both N(py) and N₃(trz) carry nearly identical charges, but the proton is transferred to the site with the lower pK_b value, N(py), Figure 4.15.

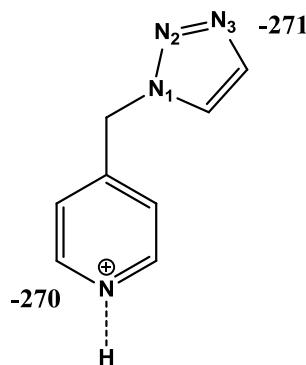


Figure 4-15 Proton transfer to the N(py) site in the salt formed between **V** and **N**.

So, how do we explain the proton being transferred to the N(py) and not the N₃(trz)? A search of the CSD of other ditopic molecules containing pyridine and triazole shows the following results. First, there are no other structures in the database containing the asymmetric ditopic molecule presented. Second, there are a number of structures, (ABIYEP, BIYROQ, CUVMEM, CUVMIQ, CUVMOW, JINQAZ, KASMEW, VABLOZ) where proton transfer occurs to the pyridine 100% of the time over the triazole, Table 4.6.

Table 4.6 Summary of relevant structures

CSD code	ABIYEP	BIYROQ	FOPHEY	FOPHIC	IKALUC
Proton transfer	N(py)	N(py)	N(py)	N(py)	N(py)

CIPCUA and UGARUP are two examples of a triazole being protonated instead of pyridine, which we would not predict based on pK_b values. ZAPMIO protonation occurs at N₂ over N₄.

This result is not surprising, considering the pyridine has a lower pK_b value compared to the 1,2,4-triazole. The data also indicate that the pyridinium cation is more stable than the triazolium cation. When proton transfer takes place, it is not uncommon to find water or neutral molecules in the crystalline lattice. Carboxylates are very good hydrogen-bond acceptors, and show a propensity to attract a wide variety of hydrogen-bond donors. This is also consistent with Chapters 2 and 3, where the formation of salts displays unpredictable landscape and topology.¹²

In summary,

- I. Triazole *can* compete with pyridine for carboxylic acids.

- II. The screening results give the same success rates for the triazoles (60-65%) compared to pyrazole (55-65%) from Chapter 2; the asymmetric ditopic triazole/pyridine gives similar success rates (100%) as ditopic pyrazole/pyridine (90-100%) from Chapter 3.
- III. Carboxylic acids can bind equally well to N(py) or N₄(trz) and display binding motifs **1** and **10** from Figure 4.7, shown in Figure 4.16 below.

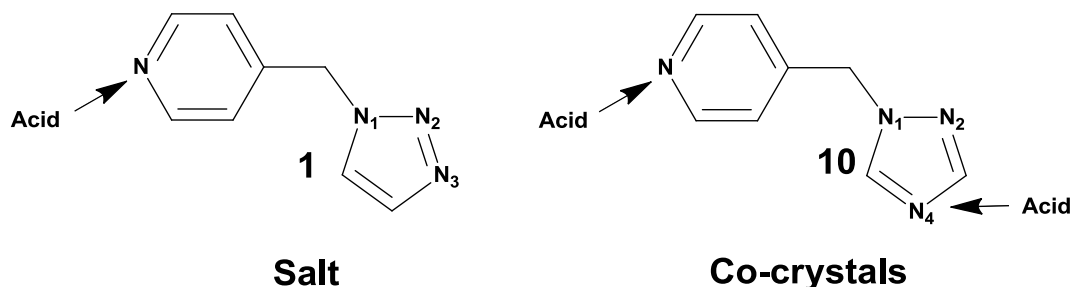


Figure 4-16 Two groups of interactions, **1** and **10**, observed from the potential interactions listed in Figure 4.7.

4.5 References:

-
- ¹ Thompson III, G. R.; Cadena, J.; Patterson, T. F. *Clin. Chest Med.*, **2009**, *30*, 203–215.
- ² Tang, H.; Zheng, C.-H.; Ren, X.-H.; Liu, J.; Liu, N.; Lv, J.-G.; Zhu, J.; Zhou, Y.-J. *Chin. Chem. Lett.*, **2013**, *24*(3), 219-222.
- ³ Taupitz, T.; Dressman, J. B.; Buchanan, C. M.; Klein, S. *Eur. J. Pharm. Biopharm.*, **2013**, *83*(3), 378-387.
- ⁴ Kastelic, J.; Hodnik, Z.; Sket, P.; Plavec, J.; Lah, N.; Leban, I.; Pajk, M.; Planinsek, O.; Kikelj, D. *Cryst. Growth Des.*, **2010**, *10*(11), 4943-4953.
- ⁵ Bolla, G.; Nangia, A. *Cryst. Growth Design*, **2012**, *12*(12), 6250-6259.
- ⁶ Upadhyay, N.; Shukla, T. P.; Mathur, A.; Manmohana; Jha, S. K. *Int. J. Pharm. Sci. Rev. Res.*, **2011**, *8*(1), 144-148; Maddileti, D.; Jayabun, S. K.; Nangia, A. *Cryst. Growth Design*, **2013**, *ahead of print*.
- ⁷ Remenar J. F; Morissette S. L; Peterson M. L; Moulton B.; MacPhee J. M.; Guzman H. R.; Almarsson O., *J. Am. Chem. Soc.*, **2003**, *125*(28), 8456-8457.
- ⁸ CSD searches revealed 41 hits for the 1*H*-1,2,3-triazole and 192 hits for the 1*H*-1,2,4-triazole. Only a few co-crystals with carboxylic acids were found: CSD ref codes CINCAE, EVIMIF, GUZDEL, IQIHEW, IQIHEW01.
- ⁹ AM1 calculations were performed using Spartan (Wavefunction, Inc., Irvine, CA). The molecules were optimized using AM1, with the maxima and minima in the electrostatic potential

surface (0.002 e/au isosurface) determined using a positive point charge in the vacuum as a probe.

¹⁰ Hunter, C.A. *Angew. Chem. Int. Ed.*, **2004**, *43*, 5310-5324.

¹¹ Musumeci, D.; Hunter, C. A.; Prohens, R.; Scuderi, S.; McCabe, J. F. *Chem. Sci.*, **2011**, *2*, 883-890.

¹² Aakeröy, C. B.; Fasulo, M. E.; Desper, J. *Mol. Pharm.* **2007**, *4(3)*, 317-322.

Chapter 5 - Halogen-bonding (XB) with ditopic pyridine/pyrazole: Are halogen-bonds competitive with hydrogen-bonds?

5.1 Introduction

The halogen-bond (XB), a term first used by J. M. Dumas¹ to describe complexes formed between CCl₄, CBr₄, SiCl₄, and SiBr₄ with pyridine, anisole, tetrahydrofuran, tetrahydropyran, and di-*n*-butylether in organic solvents, is a non-covalent intermolecular interaction between an electronegative atom like nitrogen or oxygen (Lewis base) and a covalently bound halogen atom.² The XB has emerged as a reliable tool for the crystal engineer to design functional materials³ and supramolecular complexes and networks⁴ with predictable topologies⁵, ranging from sensors⁶ to applications in medicinal chemistry and biology.⁷

Halogen bonded ‘addition complexes’ have been known since the mid-19th century, and were first reported by Guthrie⁸ in 1863 where he described the interaction of a Lewis base with a dihalogen (H₃N···I₂). Over thirty years later in 1896, Remsen and Norris⁹ followed that work by studying amines and adducts formed with bromine and chlorine. XB investigations in the early 20th century began with the work of Benesi and Hildebrand¹⁰ involving spectrophotometric investigation of iodine interactions with aromatic hydrocarbons (benzene). Hassel¹¹ worked on crystalline compounds formed between various Lewis bases and dihalogens in the 1950’s and 1960’s, for which he was subsequently jointly awarded the Nobel prize with Derek H. R. Barton in 1969.¹² The early work of Bent¹³, Laurence¹⁴, Pennington¹⁵, and Klemperer¹⁶ (to name a few) all enabled the field to see substantial growth before the beginning of the 21st century. Since then, Metrangolo and Resnati have led the way in understanding halogen bonding and its applications in the field of crystal engineering.¹⁷

The directionality of the XB is attributed to the presence of a sigma hole¹⁸, which is an area of positive charge on an outer ‘electron depleted’ *p* orbital on iodine.¹⁹ The name is a result of the sigma hole being an extension of the C-I sigma bond between carbon and iodine. A simple picture of this phenomenon is illustrated using carbontetrafluoride, where replacing one of the fluorine atoms with a halogen, beginning with chlorine, bromine and iodine creates a positive electrostatic tip on the halogen atom. The electron withdrawing effects induced by the fluorine atoms on the halogen atom increases going from chlorine to bromine to iodine; the most

pronounced effect is felt by iodine, which displays the biggest sigma hole (largest blue lobe), Figure 5.1.

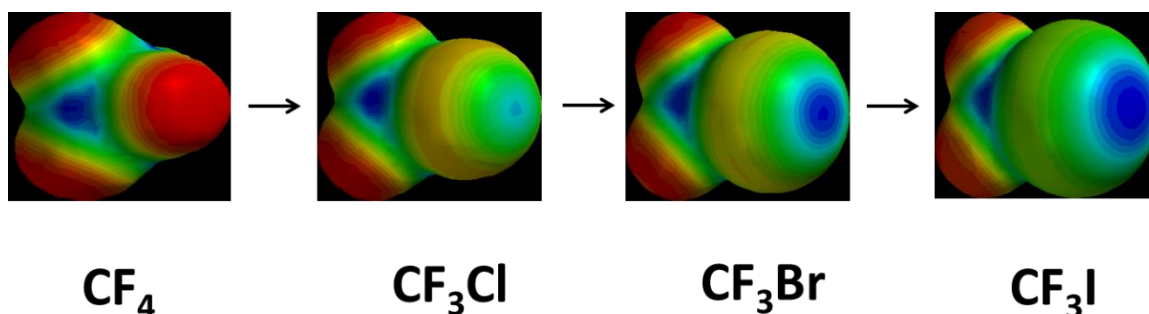


Figure 5-1 Increase in the size of the sigma hole. Red indicates areas of negative charge; blue indicates areas of positive charge (figure adapted from reference).²⁰

Iodine has a larger sigma hole than either bromine or chlorine, and the electrostatic potential around the end of the iodine (and bromine, to a lesser extent) is positive and carries a positive quadrupole moment.²¹ As a result, fluorinated iodine and fluorinated bromine are commonly used as XB donors. A simple schematic of a XB bond between a nitrogen atom electron lone pair (Lewis base) and a ‘sigma hole’ from an iodine atom is shown in Figure 5.2.

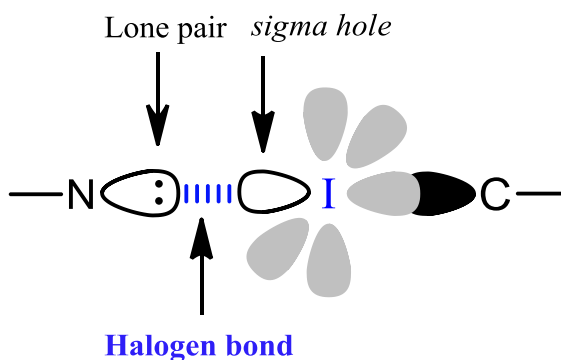


Figure 5-2 Halogen-bonding (XB) interaction between nitrogen and iodine.

Why has XB become so popular among crystal engineers and, can it compete with hydrogen bonds (HB)? First, halogen bonding is both strong (in a non-covalent context) and directional²², with energies on the order of 20-160 kJ/mol.²³ Legon *et al.*²⁴ has shown that these energies are similar to those observed for hydrogen bonds. There is strong evidence to suggest that XB’s are competitive with HB’s,²⁵ and XB’s have even been claimed to represent “a world

parallel to hydrogen bonding^{27,26} and can be used to design useful materials, from polymeric liquid crystals²⁷, inorganic coordination complexes²⁸, and supramolecular gels.²⁹

Crystal engineers have recognized XB as a useful tool for the assembly of various solid-state architectures containing both aromatic and non-aromatic perfluoroalkanes. Some examples of the use of iodoperfluoroalkanes for halogen-bond driven co-crystal synthesis^{30-31,32} is shown below, Figure 5.3.

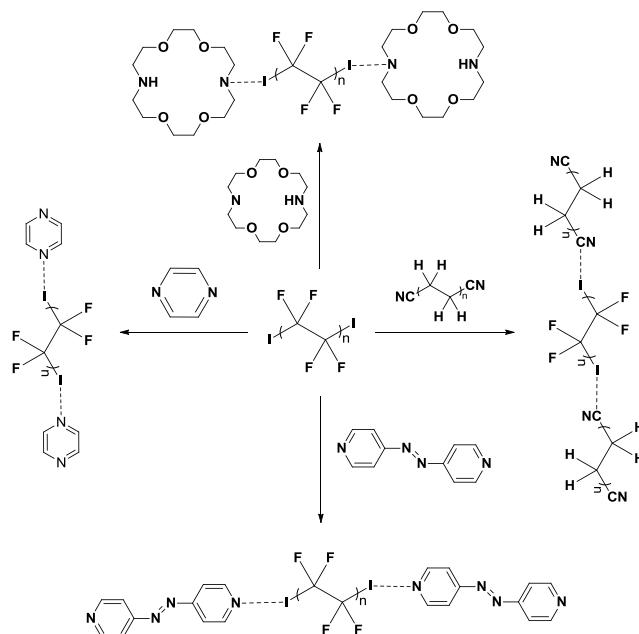


Figure 5-3 Halogen-bonding (XB) interaction between IPFA's and aromatic and aliphatic nitrogen compounds (figure adapted from reference).³³

Despite the fact that the examples in Figure 5.3 all contain $I \cdots N(\text{py})$ or $I \cdots N(\text{amine})$ halogen bonds, it has yet to be established if halogen bonds to a pyrazole nitrogen atom, $N(\text{pyz})$, can be formed. In fact, a recent search of the CSD shows no hits for XB's to a pyrazole nitrogen atom. Furthermore, it is important to establish if XB's and HB's may be used together to give reliable and predictable synthons used for making supramolecular structures.

Thus, if halogen bonds are electrostatic in nature, akin to hydrogen bonds, then there should be similarities when forming XB's to pyridine and pyrazole. Since we already established that reliable hydrogen bonds can be formed to both pyridine and pyrazole nitrogen atoms from the work in Chapter 3, we wanted use the same methodology to screen a library of XB donors

with pyrazole and pyridine/pyrazole based acceptor molecules. Density functional theory (DFT) calculations will replace AM1 because a higher level of theory is required for calculating electrostatic potentials of halogen-containing molecules. The resulting solids from the grinding experiments were analyzed using IR spectroscopy, and each peak from the XB donor was carefully scrutinized to determine any shifts. Those solids which gave a reaction were then converted to single crystal experiments in an effort to generate single crystals. From the single crystal data, inferences about binding preferences were made, following the same process used in Chapters 2-4. A flowchart displaying the method is shown in Figure 5.4.

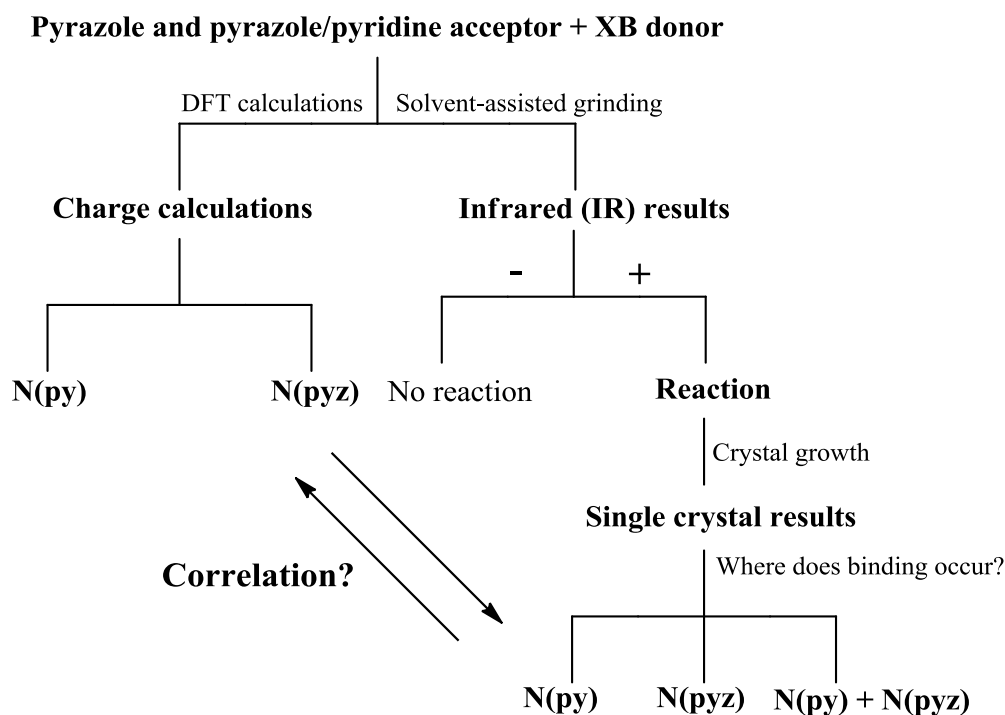


Figure 5-4 Flowchart for determining a correlation between charge calculations and single crystal results.

This chapter will attempt to answer the following questions:

- I. Do iodine-based XB donors show a higher success rate than bromine-based XB donors when screened with N(pyz) and N(py) acceptor molecules? **Hypothesis:** Iodine donors will show a higher success rate compared to bromine. CSD results indicate that iodine is better suited for XB interactions with Lewis bases.

- II. Is the pyrazole nitrogen atom, N(py_z), a suitable halogen-bond acceptor? **Hypothesis:** The pyrazole nitrogen atom, N(py_z), will be a suitable XB acceptor.
- III. Are halogen bonds competitive with hydrogen bonds? **Hypothesis:** XB to N(py_z) or N(py) should be able to compete with N-H hydrogen bonds to the acceptor sites. The following XB donors and acceptors will be used, Tables 5.1 and 5.2.

Table 5.1 Library of halogen-bond (XB) acceptors used in the screening.

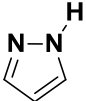
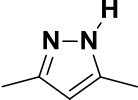
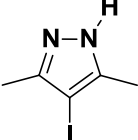
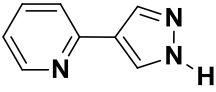
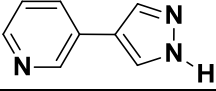
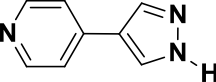
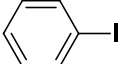
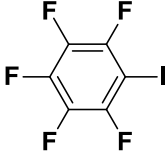
<u>Name</u>	<u>Abbreviation</u>	<u>Structure</u>
1 <i>H</i> -Pyrazole	P	
3,5-Dimethyl-1 <i>H</i> -pyrazole	DMP	
4-Iodo-3,5-dimethyl-1 <i>H</i> -pyrazole	DMP-I	
2-(1 <i>H</i> -Pyrazol-4-yl)pyridine	2	
3-(1 <i>H</i> -Pyrazol-4-yl)pyridine	3	
4-(1 <i>H</i> -Pyrazol-4-yl)pyridine	4	

Table 5.2 Library of halogen bond (XB) donors used in the screening.

	<u>Name</u>	<u>Abbreviation</u>	<u>Structure</u>
<u>Iodine-based XB donors</u>	Iodobenzene	IB	
	Iodopentafluorobenzene	IPFB	

	1,4-diiidotetrafluorobenzene	DITFB	
	1,2-diiidotetrafluorobenzene	1,2-DITFB	
	1,2-diiidotetrafluoroethane	1,2-DITFE	
	1,4-diiidooctafluorobutane	1,4-DIOFB	
	1,6-diiidoperfluorohexane	1,6-DIPFH	
	2,2',3,3',5,5',6,6'-octafluoro-4,4'-diiido-1,1'-biphenyl	4,4'-DIOFBP	
<u>bromine-</u> <u>based XB</u> <u>donors</u>	bromobenzene	BB	
	bromopentafluorobenzene	BPFB	
	1,4-dibromotetrafluorobenzene	DBTFB	
	1,2-dibromotetrafluorobenzene	1,2-DBTFB	
	1,3-dibromotetrafluorobenzene	1,3-DBTFB	
	2,2',3,3',5,5',6,6'-octafluoro-4,4'-dibromo-1,1'-biphenyl	4,4'-DBOFBP	

5.2 Experimental

5.2.1 Charge calculations

Molecular electrostatic potential (MEP) surface charge calculations were performed using Spartan (Wavefunction, Inc., Irvine, CA). The molecules were optimized using DFT at the B3LYP/6-311+G** level.

5.2.2 Synthesis of 3-(1*H*-pyrazol-4-yl)pyridine:1,4-diiodooctafluorobutane (4:1), 3₄:1,4-DIOFB

To a vial, 1,4-diiodooctafluorobutane (65.5mg, 0.1443mmol) was added followed by 0.5mL of methanol. Next, 3-(1*H*-pyrazol-4-yl)pyridine (21.0mg, 0.1443mmol) was added to the same vial. The solution was heated and left for slow evaporation (loose screw cap). Colorless rods were obtained after a few days. Mp: 113-115°C.

5.2.3 Synthesis of 3-(1*H*-pyrazol-4-yl)pyridine:1,6-diiodoperfluorohexane (4:1), 3₄:1,6-DIPFH

To a vial, 1,6-diiodoperfluorohexane (18.3mg, 0.033mmol) was added followed by 0.5mL of methanol. Next, 3-(1*H*-pyrazol-4-yl)pyridine (4.8mg, 0.033mmol) was added to the same vial. The solution was heated and left for slow evaporation (loose screw cap). Colorless rods were obtained after a few days. Mp: 107-108°C.

5.2.4 Synthesis of 4-(1*H*-pyrazol-4-yl)pyridine:1,2-diiodotetrafluoroethane (2:1), 4₂:1,2-DITFE

To a vial, 1,2-diiodotetrafluoroethane (51.8mg, 0.146mmol) was added followed by 0.5mL of methanol. Next, 4-(1*H*-pyrazol-4-yl)pyridine (21.0mg, 0.146mmol) was added to the same vial. The solution was heated and left for slow evaporation (loose screw cap). Bronze plates were obtained after a few days. Mp: turns opaque at 90°C.

5.2.5 Synthesis of 4-(1*H*-pyrazol-4-yl)pyridine:1,4-diiodooctafluorobutane (5:3), 4₅:1,4-DIOFB₃

To a vial, 1,4-diiodooctafluorobutane (51.6mg, 0.114mmol) was added followed by 0.5mL of methanol. Next, 4-(1*H*-pyrazol-4-yl)pyridine (16.5mg, 0.114mmol) was added to the same vial. The solution was heated and left for slow evaporation (loose screw cap). Colorless prisms were obtained after a few days. Mp: turns opaque at 85°C.

5.2.6 Synthesis of 2-(1H-pyrazol-4-yl)pyridine:1,4-diiidotetrafluorobenzene (1:1), 2:1,4-DITFB

To a vial, 1,4-diiidotetrafluorobenzene (12.5mg, 0.031mmol) was added followed by 0.5mL of methanol. Next, 2-(1H-pyrazol-4-yl)pyridine (4.3mg, 0.030mmol) was added to the same vial. The solution was heated and left for slow evaporation (loose screw cap). Colorless prisms were obtained after a few days. Mp: 140-143°C.

5.2.7 Synthesis of 3-(1H-pyrazol-4-yl)pyridine:1,4-diiidotetrafluorobenzene (1:1), 3:1,4-DITFB

To a vial, 1,4-diiidotetrafluorobenzene (12.5mg, 0.031mmol) was added followed by 0.5mL of methanol. Next, 3-(1H-pyrazol-4-yl)pyridine (4.4mg, 0.030mmol) was added to the same vial. The solution was heated and left for slow evaporation (loose screw cap). Colorless prisms were obtained after a few days. Mp: 135-140°C.

5.2.8 Synthesis of 4-(1H-pyrazol-4-yl)pyridine:1,4-diiidotetrafluorobenzene (2:1), 4₂:1,4-DITFB

To a vial, 1,4-diiidotetrafluorobenzene (10.2mg, 0.0254mmol) was added followed by 0.5mL of methanol. Next, 4-(1H-pyrazol-4-yl)pyridine (3.7mg, 0.0254mmol) was added to the same vial. The solution was heated and left for slow evaporation (loose screw cap). Colorless rods were obtained after a few days. Mp: 101-105°C.

5.2.7 IR spectroscopy

Infrared spectra were collected on a Thermo Scientific Nicolet 380 FT-IR using a ZnSe crystal. The solids obtained from solvent-assisted grinding experiments (and solution-based experiments) were analyzed by placing the solid directly on the crystal and performing 128 scans. Melting points were determined on a Fisher-Johns melting point apparatus and are uncorrected.

5.3 Results

5.3.1 DFT calculations

Density functional theory (DFT) calculations were made in order to rank the strengths of XB acceptor and donor molecules, Tables 5.3 and 5.4.

Table 5.3 Summary of DFT charges (kJ/mol) on the pyridine nitrogen atom (N(py), red), pyrazole nitrogen atom (N(pyz), orange) and pyrazole N-H hydrogen atom (blue).

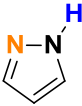
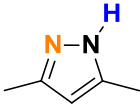
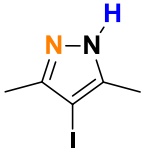
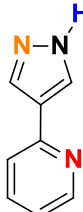
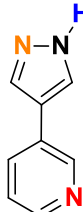
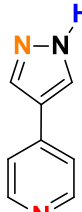
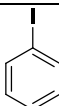
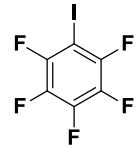
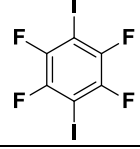
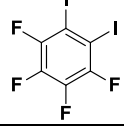
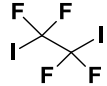
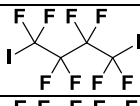

					
N(pyz) = -185 N-H = +239	N(pyz) = -195 N-H = +225	N(pyz) = -195 N-H = +225	N(pyz) = -178 N(py) = -144 N-H = +245	N(pyz) = -168 N(py) = -191 N-H = +271	N(pyz) = -161 N(py) = -193 N-H = +274

Table 5.4 Summary of charges for the iodine donors

	Name	Abbreviation	Structure	Charges
Iodine donors	Iodobenzene	IB		+103
	Iodopentafluorobenzene	IPFB		+166
	1,4-Diiodotetrafluorobenzene	DITFB		+169
	1,2-Diiodotetrafluorobenzene	1,2-DITFB		+163
	1,2-Diiodotetrafluoroethane	1,2-DITFE		+164
	1,4-Diiodooctafluorobutane	1,4-DIOFB		+171
	1,6-Diiodoperfluorohexane	1,6-DIPFH		+169

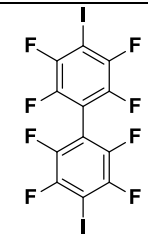
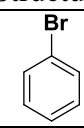
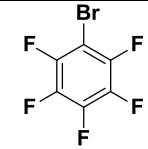
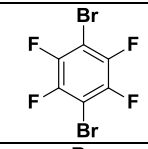
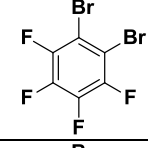
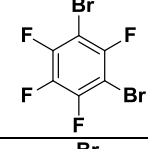
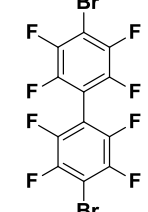
	2,2',3,3',5,5',6,6'- Octafluoro-4,4'-diiodo- 1,1'-biphenyl	4,4'-DIOFBP		-
--	--	-------------	---	---

Table 5.5 Summary of charge for the bromine donors

	Name	Abbreviation	Structure	Charges
Bromine donors	Bromobenzene	BB		+63
	Bromopentafluorobenzene	BPFB		+143
	1,4- Dibromotetrafluorobenzene	DBTFB		+140
	1,2- Dibromotetrafluorobenzene	1,2-DBTFB		+137
	1,3- Dibromotetrafluorobenzene	1,3-DBTFB		+140
	2,2',3,3',5,5',6,6'- Octafluoro-4,4'-dibromo- 1,1'-biphenyl	4,4'-DBOFBP		+142

5.3.2 IR spectroscopy

A library of six XB acceptor molecules containing pyrazole or pyrazole/pyridine (Table 5.1) were screened with fourteen halogen-bond donor molecules containing both activated and unactivated (as control) iodine and bromine, Table 5.2. The combinations which gave a reaction, based on shifts in the XB donor bands, were converted to solution based experiments. The values of the bands after the grinding are tabulated in Table 5.6.

Table 5.6 Summary of 84 solvent-assisted grinding experiments. XB donors are listed in the left hand column; XB acceptors are top row.

XB donors	Pyrazole	DMP	DMP-I	2	3	4
Iodobenzene (1571, 1471, 1438, 1058, 1014, 997, 727, 684)	no rxn	no rxn	no rxn	no rxn	no rxn	no rxn
IPFB (1509, 1489, 1081, 1001, 974, 805)	no rxn	no rxn	no rxn	(1512, 1482, 1088, 989, 957, 779)	(1502, 1477, 1079, 995, 971, 795)	(1504, 1481, 1073, 1001, 969, 808)
1,4-DITFB (1459, 1430, 1355, 1215, 986, 969, 941, 759)	no rxn	no rxn	no rxn	(1456, 1430, 1351, 1211, 982, 967, 939, 750)	(1455, 1427, 1356, 1211, 973, 935, 756)	(1452, 1430, 1355, 1217, 983, 958, 934, 759)
1,2-DITFB (1490, 1439, 1110, 1024, 814, 773)	no rxn	(1483, 1420, 1304, 1105, 1024, 1008, 777)	no rxn	(1482, 1435, 1101, 1021, 812, 776)	(1482, 1433, 1107, 1021, 812, 772)	(1481, 1437, 1100, 1016, 807, 763)
1,2-DITFE (1206, 1153, 1100, 973, 834, 694, 636)	no rxn	(1201, 1127, 1092, 975, 802, 698)	(1198, 1163, 1074, 968, 832, 681)	(1202, 1136, 974, 827, 701)	(1200, 1149, 1077, 966, 827, 698)	(1201, 1158, 1092, 972, 833, 691, 633)
1,4-DIOFB (1192, 1134, 1103, 1088, 1039, 888, 764, 718, 696, 634)	no rxn	no rxn	(1161, 1103, 1076, 1036, 886, 764, 714, 689)	(1197, 1116, 1075, 1038, 889, 776, 741, 703, 676)	(1193, 1133, 1108, 1087, 1041, 889, 764, 723, 704, 633)	(1176, 1124, 1045, 868, 757, 716, 687, 629)
1,6-DIPFH (1199, 1141, 1086, 927)	(1214, 1131, 1091, 923)	(1208, 1145, 1086, 838)	(1164, 1128, 1076, 909)	(1216, 1129, 1081, 931)	(1210, 1148, 1089, 928)	(1209, 1132, 1078, 920)
4,4'-DPDIOF (1471, 1219, 984, 975, 954, 716)	no rxn	no rxn	no rxn	no rxn	no rxn	no rxn
Success rate (%)	1/8 = 12.5%	3/8 = 37.5%	3/8 = 37.5%	6/8 = 75%	6/8 = 75%	6/8 = 75%
Bromobenzene (1575, 1472, 1440, 1067, 1018, 1000, 902, 730, 682, 669)	no rxn	no rxn	no rxn	no rxn	no rxn	no rxn
BPFB (1499, 1091, 1005, 978, 834, 615)	no rxn	no rxn	no rxn	(1523, 1089, 990, 956, 827)	(1514, 1030, 947, 793)	(1512, 1103, 1001, 955, 832)
1,4-DBTFB (1494, 1449, 1235, 990, 954, 788)	no rxn	14823, 1420, 1308, 1027, 1008, 777)	no rxn	no rxn	no rxn	no rxn
1,2-DBTFB (1499, 1457, 1118, 1035, 847, 802)	(1500, 1464, 1134, 1029, 837, 752)	(1483, 1462, 1149, 1028, 841, 779)	(1463, 1407, 1075, 1033, 765)	(1478, 1431, 1117, 1024, 829, 775)	(1486, 1448, 1151, 1029, 838, 794)	(1513, 1428, 1101, 1027, 834, 813)
1,3-DBTFB (1484, 1446, 1082, 893, 743, 702)	no rxn	(1421, 1304, 1153, 1027, 1008, 840, 778, 737)	(1573, 1408, 1304, 1161, 1075, 1033, 765)	no rxn	no rxn	(1513, 1428, 1103, 899, 683, 660)
4,4'-DPDBOF (1467, 1238, 993, 958, 866, 720)	no rxn	no rxn	no rxn	no rxn	no rxn	no rxn
Success rate (%)	1/6 = 16.7%	3/6 = 50%	2/6 = 33.3%	2/6 = 33.3%	2/6 = 33.3%	3/6 = 50%

5.3.3 Crystal structure of 3-(1H-pyrazol-4-yl)pyridine:1,4-diiodooctfluorobutane (4:1), 3₄:1,4-DIOFB

The crystal structure of **3₄:1,4-DIOFB** displays a combination of hydrogen and halogen bonds. A hydrogen bond forms between the pyrazole nitrogen atom and the pyrazole N-H proton to make a catemer on both sides: on one side, the N-H···N(pyz) distance is 2.8027(16), angle is 178(17)°; on the second side, the N-H···N(pyz) distance is 2.9385(15)Å, angle is 161(16)°. A halogen bond occurs between the pyridine nitrogen atom and iodine atom, giving a C-I···N distance of 2.781Å and a C-I···N angle of 173°, Figure 5.5

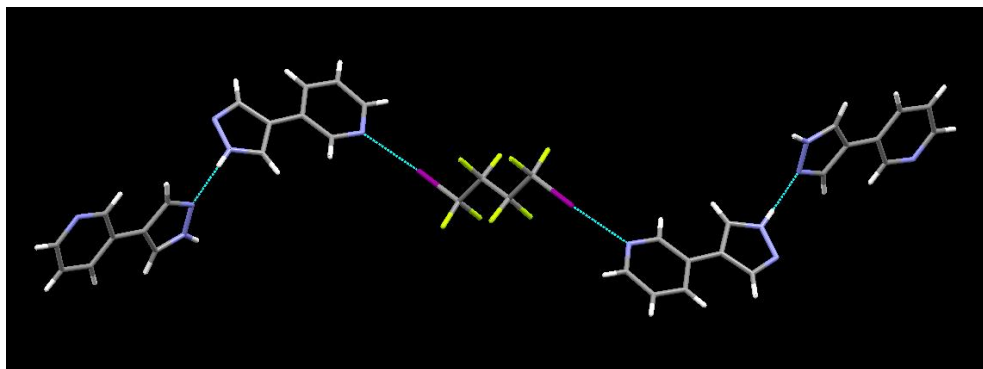


Figure 5-5 Primary interactions in the crystal structure of **3₄:1,4-DIOFB**.

5.3.4 Crystal structure of 3-(1H-pyrazol-4-yl)pyridine:1,6-diiodoperfluorohexane (4:1), 3₄:1,6-DIPFH

The crystal structure of **3₄:1,6-DIPFH** displays a combination of hydrogen and halogen bonds. A hydrogen bond occurs between the pyrazole nitrogen atom and the pyrazole N-H proton to make a catemer on both sides: on one side, the N-H···N(pyz) distance is 2.800(3)Å, angle is 170(3)°; on the second side, the N-H···N(pyz) distance is 2.942(3)Å, angle is 162(2)°. A halogen bond occurs between the pyridine nitrogen atom and iodine atom, giving a C-I···N distance of 2.786Å and a C-I···N angle of 175°, Figure 5.6

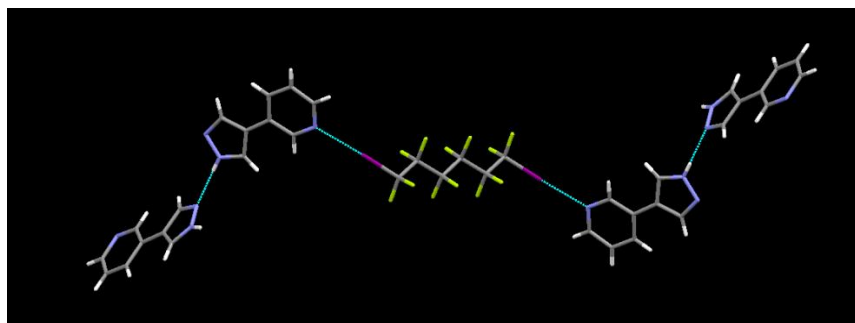


Figure 5-6 Primary interactions in the crystal structure of **3₄:1,6-DIPFH**.

5.3.5 Crystal structure of 4-(1H-pyrazol-4-yl)pyridine:1,2-diiodotetrafluoroethane (2:1), 4₂:1,2-DITFE

The crystal structure of **4₂:1,2-DITFE** shows 1-D chains connected via N-H···N(py) hydrogen bonds. The N-H···N(py) distance is 2.838(3)Å and the N-H···N(py) angle is 168(3)°. The N-H proton remains on the pyrazole as evidenced by the C-N_(py)-C bond angle of 116(19)°. The chains are connected via C-I···N(py) halogen bonds; C-I···N(py) distance is 2.839Å and the C-I···N(py) angle is 173°, Figure 5.7.

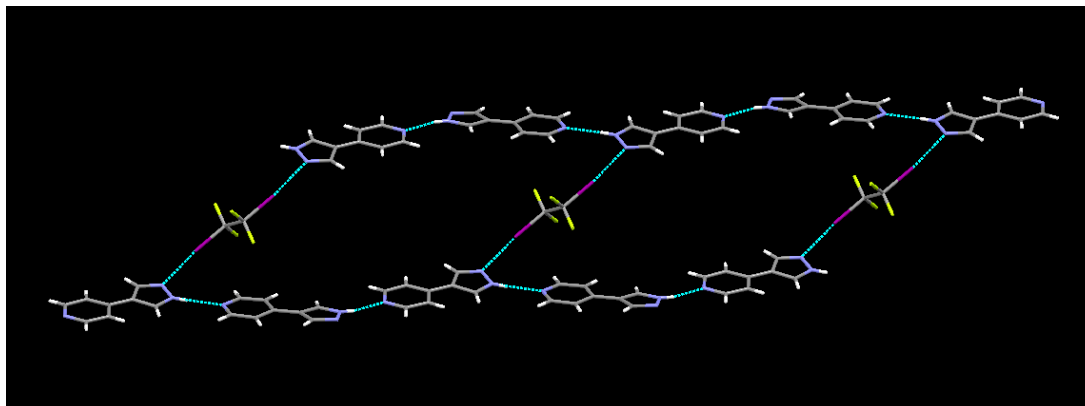


Figure 5-7 Primary interactions in the crystal structure of **4₂:1,2-DITFE**.

5.3.6 Crystal structure of 4-(1H-pyrazol-4-yl)pyridine:1,4-diiodooctafluorobutane (5:3), 4₅:1,4-DIOFB₃

The crystal structure of **4₅:1,4-DIOFB₃** displays a combination of hydrogen and halogen bonds. Two sets of hydrogen bonds occur. In the first set, a hydrogen bond occurs between the pyridine nitrogen atom and the pyrazole N-H proton; the N-H···N(py) distance is 3.195(12)Å and the N-H···N(py) angle is 165(3)°. The proton remains on the pyrazole as evidenced by the C-N_(py)-C bond angle of 119(9)°. In the second set, a hydrogen bond occurs between the pyrazole nitrogen atom and the pyrazole N-H proton; the N-H···N(py) distance is 2.886(13) Å and gives an angle of 176(3)°. There are three sets of halogen bonds. In the first set, a pyridine nitrogen atom interacts with an iodine atom; C-I₁···N(py) distance is 2.743Å and the C-I₁···N(py) angle is 177°; in the second set, C-I₂···N(py) distance is 2.758Å and the C-I₂···N(py) angle is 174°; in the third set, the pyrazole nitrogen atom interacts with an iodine atom, giving a C-I₃···N(py) distance is 2.845Å and the C-I₃···N(py) angle is 174°, Figure 5.8.

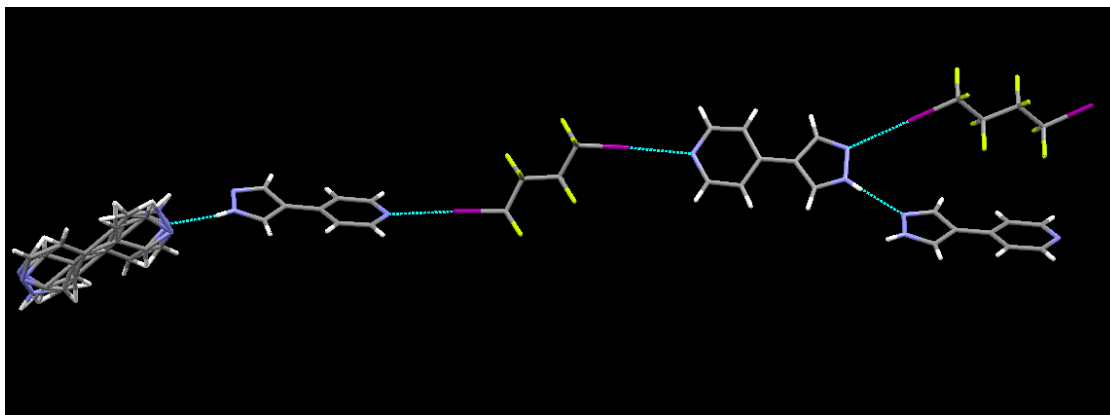


Figure 5-8 Primary interactions in the crystal structure of **4₅:1,4-DIOFB₃**.

5.3.7 Crystal structure of 2-(1*H*-pyrazol-4-yl)pyridine:1,4-diiodotetrafluorobenzene (1:1), 2:1,4-DITFB

The crystal structure determination of **2:1,4-DITFB** displays a supermolecule formed by the combination of hydrogen and halogen bonds. A hydrogen bond occurs between the pyridine nitrogen atom and pyrazole N-H proton, where the N-H \cdots N(py) distance is 2.872(3)Å and the N-H \cdots N(py) angle is 159°. The proton remains on the pyrazole as evidenced by the C-N_(py)-C bond angle of 118(2)°. A halogen bond occurs between the pyrazole nitrogen atom and iodine atom, giving a C-I \cdots N(pyz) distance of 2.799Å and a C-I \cdots N(py) angle of 177°. The second iodine atom shows no short or long range contacts, Figure 5.9.

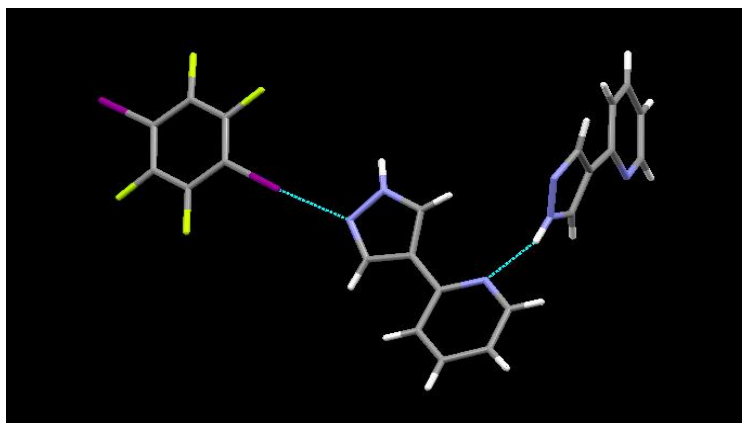


Figure 5-9 Primary interactions in the crystal structure of **2:1,4-DITFB**.

5.3.8 Crystal structure of 3-(1*H*-pyrazol-4-yl)pyridine:1,4-diiodotetrafluorobenzene (1:1), 3:1,4-DITFB

The crystal structure determination of **3:1,4-DITFB** displays a supermolecule formed by the combination of hydrogen and halogen bonds. A hydrogen bond occurs between the pyridine nitrogen atom and pyrazole N-H proton, where the N-H...N(py) distance is 2.830(4)Å and the N-H...N(py) angle is 174(4)°. The N-H proton remains on the pyrazole as evidenced by the C-N_(py)-C bond angle of 118(3)°. A halogen bond occurs between the pyrazole nitrogen atom and iodine atom, giving a C-I...N(py) distance of 2.738Å and a C-I...N(py) angle of 174°. The second iodine atom shows no short or long range contacts, Figure 5.10.

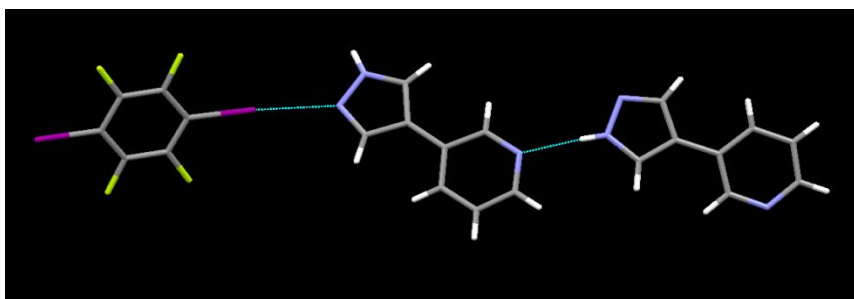


Figure 5-10 Primary interactions in the crystal structure of **3:1,4-DITFB**.

5.3.9 Crystal structure of 4-(1*H*-pyrazol-4-yl)pyridine:1,4-diiodotetrafluorobenzene (2:1), 4₂:1,4-DITFB

The crystal structure determination of **4₂:1,4-DITFB** displays a chain formed by hydrogen and halogen bonds. A hydrogen bond occurs between the pyrazole nitrogen atom and the N-H proton, where the pyrazole forms a catemer; the N-H...N(py) distance is 2.979(2)Å and the N-H...N(py) angle is 168(3)°. The halogen bond occurs between the pyridine nitrogen atom and iodine atom, giving a C-I...N(py) distance of 2.806Å and a C-I...N(py) angle of 179°, Figure 5.11.

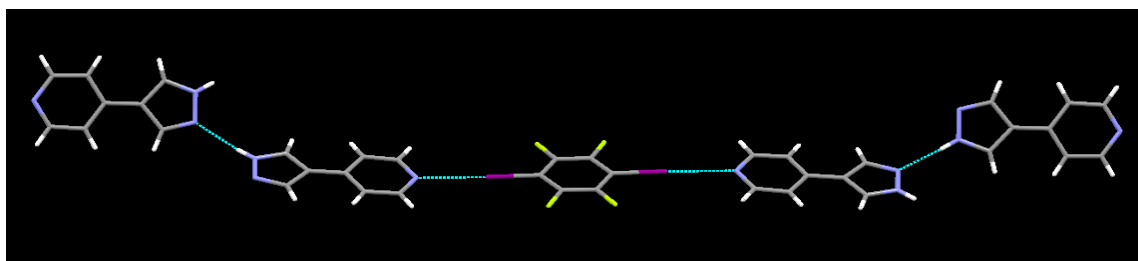


Figure 5-11 Primary interactions in the crystal structure of **4₂:1,4-DITFB**.

5.4 Discussion

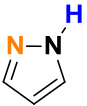
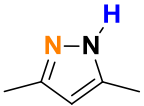
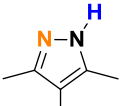
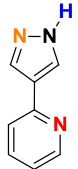
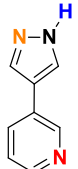
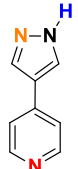
5.4.1 What do the DFT calculations tell us about ranking the acceptors and donors?

From the DFT calculations, it is possible to rank the strengths of the XB acceptors and donors, and formulate hypotheses regarding binding preferences.

First, the XB acceptors contain two possible binding sites, N(py) and N(pyz). The DFT calculations for the pyrazole molecules used (**P**, **DMP**, and **DMP-I**) all show the pyrazole nitrogen atom, N(pyz), to be similar in value, ranging from -185 kJ/mol (for **P**) to -195 kJ/mol (for **DMP** and **DMP-I**). These values indicate that the three pyrazole molecules should display similar reactivity when combined with various XB donor molecules.

When a pyridine moiety is introduced in ditopic molecules **2**, **3**, and **4**, the charge on the N(pyz) is lowered in each case. In **2**, the charge drops to -178 kJ/mol, whereas in **3** and **4** the charge lowers to -168 kJ/mol and -161 kJ/mol, respectively. The values indicate the addition of a pyridine moiety withdraws electron density from the N(pyz), and thereby lowers its charge. On the other hand, the charge on the N(py) site shows that in ditopic **2** the N(pyz) outranks the N(py), -178 kJ/mol vs. -144 kJ/mol. The pyridine nitrogen atom, being in the **2** position, is sterically hindered compared to the **3** and **4** isomers, and as a result the charge is less than the pyrazole nitrogen atom. On the other hand, the N(py) outranks the N(pyz) in **3** and **4**. For **3**, the values are -191 kJ/mol vs. -168 kJ/mol. For **4**, the values are -193 kJ/mol vs. -161 kJ/mol. It is noteworthy that the charge on the N(py) in **3** and **4** differs by only 2 kJ/mol, Table 5.7.

Table 5.7 Summary of charges on the pyrazole and pyrazole/pyridine XB acceptor molecules.

					
P	DMP	DMP-I	2	3	4
N(pyz) = -185 N-H = +239	N(pyz) = -195 N-H = +225	N(pyz) = -195 N-H = +225	N(pyz) = -178 N(py) = -144 N-H = +245	N(pyz) = -168 N(py) = -191 N-H = +271	N(pyz) = -161 N(py) = -193 N-H = +274

When ranking the XB donors in the system, it is clear that the iodine donors carry higher charges than bromine donors. The range for the iodine donors is 163-171 kJ/mol. For the bromines, the range is 137-143 kJ/mol. Furthermore, activation of the iodine and bromine displays the effects of adding electron-withdrawing fluorine atoms to the ring. The charges on the non-activated iodobenzene and bromobenzene are 103 kJ/mol and 63 kJ/mol, respectively. The activated forms (substituting hydrogen atoms for fluorine atoms) are 166 kJ/mol and 143 kJ/mol, respectively, Table 5.8.

Table 5.8 Range of charges on the iodine and bromine XB donors. IPFB = iodopentafluorobenzene. BPFB = bromopentafluorobenzene.

<u>Iodine range</u>	<u>Bromine range</u>	<u>Activated</u>	<u>Non-activated</u>
163-171 kJ/mol	137-143 kJ/mol	Iodopentafluorobenzene (166 kJ/mol)	Iodobenzene (103 kJ/mol)
-	-	Bromopentafluorobenzene (143 kJ/mol)	Bromobenzene (63 kJ/mol)

The N-H proton on the pyrazole displays the highest positive electrostatic potential, and outranks all the XB donor molecules. For the pyrazole N-H, the values range from 225 kJ/mol to 239 kJ/mol. In the ditopics, the values are even higher, ranging from 245 kJ/mol to 274 kJ/mol. The values in every case outrank the XB donor by ~80-100 kJ/mol, and the pyrazole N-H is expected to compete with the XB donors for the N(py) and N(py₂) XB acceptor sites.

5.4.2 Does iodine show a higher success rate than bromine from the IR spectra results?

From the results of the IR data, the supramolecular yield from the reactions between various pyrazole molecules and iodine and bromine donors is around the same percentage. For P, a 12.5% success rate was obtained for reactions with iodine donors; bromine donors were slightly higher at 16.7%. For DMP, a similar trend was observed; reactions with iodine donors gave a supramolecular yield of 37.5%, and those with bromine was slightly higher at 50%. For DMP-I, the reactions with iodine and bromine donors were essentially the same value. For the iodine donors, 37.5% supramolecular yield was obtained; for the bromine, 33.3% supramolecular yield was obtained.

When a pyridine group is introduced as in **2**, **3**, and **4**, the supramolecular yield increases for the iodine donors and stays about the same for the bromine donors. In the cases of 2,3,4, the

supramolecular yield jumps to 75%; the bromine values were 33.3%, 33.3%, and 50%, Table 5.9.

Table 5.9 Summary of supramolecular yields obtained from the screening experiments.

Donors	P	DMP	DMP-I	2	3	4
Iodine	13%	38%	38%	75%	75%	75%
Bromine	17%	50%	33%	33%	33%	50%

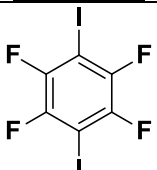
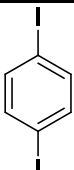
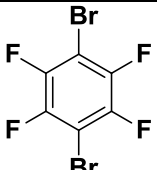
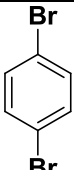
The results show the halogen bonds to the pyrazole nitrogen atom are feasible, and the data also suggest that iodine...pyridine interactions are more favorable than bromine...pyridine interactions. A recent search using 1,4-DITFB and 1,4-DBTFB (as XB donors) and pyridine confirms that more structures containing iodine...pyridine interactions (as opposed to bromine...pyridine) are found, Table 5.10.

Table 5.10 Summary of hits found in CSD.

Interaction	C-I...N(py)	C-Br...N(py)
# of CSD hits	50	11

Moreover, pyrazole and pyrazole/pyridine ditopic acceptors display no activity with the unactivated XB donor molecules. The importance of activating the halogen is further highlighted by a recent CSD search which shows no hits for both 1,4-diiodobenzene and 1,4-dibromobenzene, Table 5.11.

Table 5.11 Summary of CSD results for co-crystals of 1,4-diiodobenzene vs. 1,4-diiodotetrafluorobenzene.

<u>Name</u>	<u>Activated</u>	<u>Non-activated</u>
Structure		
# of CSD hits	112	0
Structure		
# of CSD hits	18	0

5.4.3 Is the pyrazole nitrogen atom suitable for forming XB's based on the single crystal results?

From the single crystal data, it is clear that both nitrogen atoms, N(py) and N(pyz), can form XB interactions with activated iodine donor atoms. A summary of the observed synthons in the crystal structures is shown below, Table 5.12.

Table 5.12 Summary of the observed interactions in the crystal structures.

Synthons	3 + 1,4-DIOFB	3 + 1,6-DIPFH	4 + 1,2-DITFE	4 + 1,4-DIOFB	2 + 1,4-DITFB	3 + 1,4-DITFB	4 + 1,4-DITFB
C-I...N(py)	√	√		√			√
C-I...N(pyz)			√	√	√	√	
N-H...N(py)			√	√	√	√	
N-H...N(pyz)	√	√		√			√

From the single crystal results, two groups of interactions are observed, and both contain hydrogen and halogen bonds. In group 1, an iodine atom interacts with a pyridine nitrogen atom, and a pyrazole N-H proton interacts with a pyrazole nitrogen atom. The two interactions together were observed in three structures (3/7). In group 2, an iodine atom interacts with a pyrazole nitrogen atom, and a pyrazole N-H proton interacts with a pyridine nitrogen atom. The two interactions together were also observed in three structures (3/7), Figure 5.12.

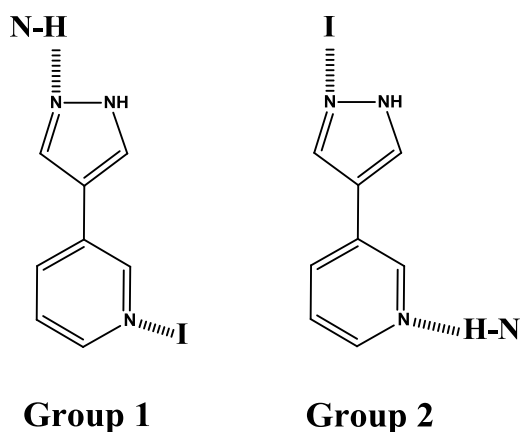


Figure 5-12 The two groups of interactions observed in the crystals.

It is therefore not surprising that in one crystal structure (1/7), both groups of synthons (Group 1 and Group 2) were observed. The results clearly show that the pyrazole nitrogen atom is a suitable XB acceptor, and can compete with the pyridine nitrogen atom for XB interactions.

When XB donors are combined with a molecule containing pyridine or pyrazole nitrogen acceptor atoms, then there is the likelihood of either interaction occurring.

In support of these findings a recent example from the literature shows that both synthons can work together to form infinite chains.³⁴ For example, the primary interactions observed in the crystal structure formed between 2-amino-3,5-dibromopyrazine and 1,4-diiodotetrafluorobenzene displays an infinite chain assembled through the interplay of hydrogen and halogen bonds, Figure 5.13.

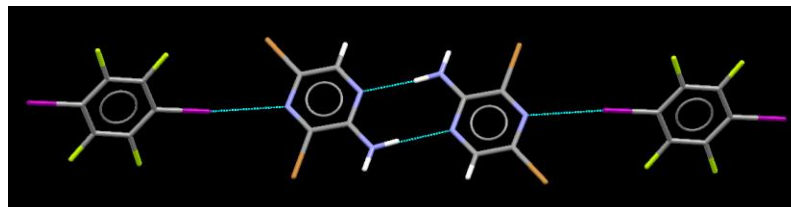


Figure 5-13 The primary interactions observed in the crystals structure of 2-amino-3,5-dibromopyrazine:1,4-DITFB displaying the hydrogen and halogen bonds.³⁴

In summary,

- I. Iodine based XB donors show an overall higher success rate than bromine donors for a reaction to occur when combined with a library of ditopic pyrazole/pyridine XB acceptors (52% vs. 36%); the pyrazole acceptors, P, DMP, and DMP-I, show little difference in supramolecular yield when combined with iodine or bromine XB donors.
- II. The pyrazole nitrogen atom, N(pyz), can act as a suitable XB acceptor.
- III. Two groups of synthons were observed in the crystal structures, Group 1 and Group 2, and both groups display an interplay of hydrogen and halogen bonds, respectively.

5.5 References:

¹ a) Dumas, J. M.; Geron, C.; Peurichard, H.; Gomel, M. *Bull. Soc. Chim. Fr.*, **1976**, 5-6 (1), 720-728; b) Dumas, J. M.; Kern, M.; Janier-Dubry, J. L. *Bull. Soc. Chim. Fr.*, **1976**, 11-12 (1), 1785-1790; c) Dumas, J. M.; Peurichard, H.; Gomel, M. *J. Chem. Res. (S)*, **1978**, 2, 54-55.

-
- ² a) Metrangolo, P.; Resnati, G. *Chem. Euro. J.*, **2001**, *7* (12), 2511-2519; b) Politzer, P.; Murray, J. S. *ChemPhysChem.*, **2013**, *14*(2), 278-294.
- ³ Lemouchi, C.; Vogelsberg, C. S.; Zorina, L.; Simonov, S.; Batail, P.; Brown, S.; Garcia-Garibay, M. A. *J. Am. Chem. Soc.*, **2011**, *133*(34), 13765.
- ⁴ Rissanen, K. *CrystEngComm*, **2008**, *10*, 1107-1113.
- ⁵ Ding, X.; Tuikka, M.; Haukka, M. Recent Advances in Crystallography: Chapter 7 (Halogen bonding in crystal engineering) **2012**, 143-168, DOI: 10.5772/48592.
- ⁶ Yan, D.; Bucar, D.-K.; Delori, A.; Patel, B.; Lloyd, G. O.; Jones, W.; Duan, X. *Chem. Eur. J.*, **2013**, *ahead of print*.
- ⁷ Wilcken, R.; Zimmermann, M. O.; Lange, A.; Joerger, A. C.; Boeckler, F. M. *J. Med. Chem.*, **2013**, *56*(4), 1363-1388.
- ⁸ Guthrie, F. *J. Chem. Soc.*, **1863**, *16*, 239-244.
- ⁹ Remsen, I.; Norris, J. F. *Am. Chem. J.*, **1896**, *18*, 90-95.
- ¹⁰ Benesi, H. A.; Hildebrand, J. H. *J. Am. Chem. Soc.*, **1949**, *71*, 2703-2707.
- ¹¹ O. Hassel, O.; Rømming, C. *Q. Rev. Chem. Soc.*, **1962**, *16*, 1-18.; Hassel, O. *Science*, **1970**, *170*, 497-502.
- ¹² http://www.nobelprize.org/nobel_prizes/chemistry/laureates/1969/hassel-bio.html
- ¹³ Bent, H. A. *Chem. Rev.*, **1968**, *68*, 587-648.
- ¹⁴ Ouvrard, C.; Le Questel, J.-Y.; Berthelot, M.; Laurence, C. *Acta Crystallogr., Sect. B: Struct. Sci.*, **2003**, *59*, 512-526.
- ¹⁵ Pennington, W. T.; Hanks, T. W.; H. D. Arman, H. D. *Halogen Bonding: Fundamentals and Applications*, ed. Metrangolo, P.; Resnati, G., **2008**, pgs. 65-104, Springer books, Berlin.
- ¹⁶ a) Novick, S. E.; Janda, K. C.; Klemperer, W. *J. Chem. Phys.*, **1976**, *65*, 5115-5121; b) Baiocchi, F. A.; Dixon, T. A.; Klemperer, W. *J. Chem. Phys.*, **1982**, *77*, 1632-1638.
- ¹⁷ For some highlighted papers from P. Metrangolo and G. Resnati on XB and applications in supramolecular chemistry and crystal engineering, see the following: Metrangolo, P.; Meyer, F.; Pilati, T.; Resnati, G.; Terraneo, G., *Angew. Chemie, Int. Ed.*, **2008**, *47*(33), 6114-6127; Metrangolo, P.; Resnati, G.; Pilati, T.; Biella, S. *Structure and Bonding* (Berlin, Germany), **2008**, *126*, 105-136;
- ¹⁸ a) Politzer, P.; Murray, J. S.; Clark, T. *Phys. Chem. Chem. Phys.* **2010**, *12*(28), 7748-7757; b) Brinck, T.; Murray, J. S.; Politzer, P. *Int. J. Quantum. Chem.* **1992**, *44*, 57-64.
- ¹⁹ Alkorta, I.; Elguero, J.; Del Bene, J. E. *J. Phys. Chem. A.*, **2013**, *117*(23), 4981-4987.
- ²⁰ Clark, T.; Hennemann, M.; Murray, J. S.; Politzer, P. *J. Mol. Mod.* **2007**, *13*(2), 291-296; Politzer, Peter; Lane, Pat; Concha, Monica C.; Ma, Yuguang; Murray, Jane S. *J. Mol. Mod.* **2007**, *13*(2), 305-311.
- ²¹ Stone, A. J. *J. Am. Chem. Soc.*, **2013**, *135*(18), 7005-7009.
- ²² Saccone, M.; Cavallo, G.; Metrangolo, P.; Pace, A.; Pibiri, I.; Pilati, T.; Resnati, G.; Terraneo, G. *CrystEngComm*, **2013**, *15*(16), 3102-3105.
- ²³ Energy of XB vs. HB
- ²⁴ a) Legon, A. C. *Phys. Chem. Chem. Phys.*, **2010**, *12*(28), 7736-7747; b) Legon, A. C. *Angew. Chemie, Int. Ed.*, **1999**, *38*(18), 2687-2714.
- ²⁵ Metrangolo, P.; Resnati, G. *Science*, **2008**, *321*(5891), 918-919.
- ²⁶ Metrangolo, Pierangelo; Neukirch, Hannes; Pilati, Tullio; Resnati, Giuseppe *Acc. Chem. Res.*, **2005**, *38*(5), 386-395.
- ²⁷ Cho, C. M.; Wang, X.; Li, J. J.; He, C.; Xu, J. *Liquid Crystals*, **2013**, *40*(2), 185-196.

-
- ²⁸ Smart, P.; Bejarano-Villafuente, A.; Brammer, L. *CrystEngComm*, **2013**, *15(16)*, 3151-3159.
- ²⁹ Lorenzo Meazza, L.; Foster, J.A.; Fucke, K.; Metrangolo, P.; Resnati, G.; Steed, J.W. *Nature Chemistry*, **2013**, *5*, 42-47.
- ³⁰ Cardillo, P.; Corradi, E.; Lunghi, A.; Valdo Meille, S.; Messina, Teresa M.; Metrangolo, P.; Resnati, G. *Tetrahedron*, **2000**, *56(30)*, 5535-5550.
- ³¹ Metrangolo, P.; Pilati, T.; Resnati, G.; Stevenazzi, A. *Chem. Commun.*, **2004**, *13*, 1492-1493.
- ³² Fox, D.; Metrangolo, P.; Pasini, D.; Pilati, T.; Resnati, G.; Terraneo, G. *CrystEngComm*, **2008**, *10(9)*, 1132-1136.
- ³³ Aakeröy, C. B.; Chopade, P. D. In *Supramolecular Chemistry: From Molecules to Nanomaterials*, © **2012**, Vol. 6, pgs. 2975-2992, John Wiley and Sons Ltd., ISBN: 978-0-470-74640-0.
- ³⁴ Aakeröy, C. B.; Chopade, P. D.; Desper, J. *Cryst. Growth Des.*, **2011**, *11(2)*, 5333-5336.

Chapter 6 - Can hydrogen-bonds (HB) and halogen-bonds (XB) influence nanoparticle assembly?

6.1 Introduction

In Chapters 2-5, supramolecular synthons were used to construct multicomponent crystals. The synthons consisted of, in some cases, a combination of hydrogen and halogen bonds, both of which are considered fairly strong¹ and directional² ‘non-covalent’ electrostatic interactions which have been used for the assembly of small molecules.³ On the other hand, what if the same non-covalent interactions could be used to influence the assembly of much larger nanoparticles, Figure 6.1?

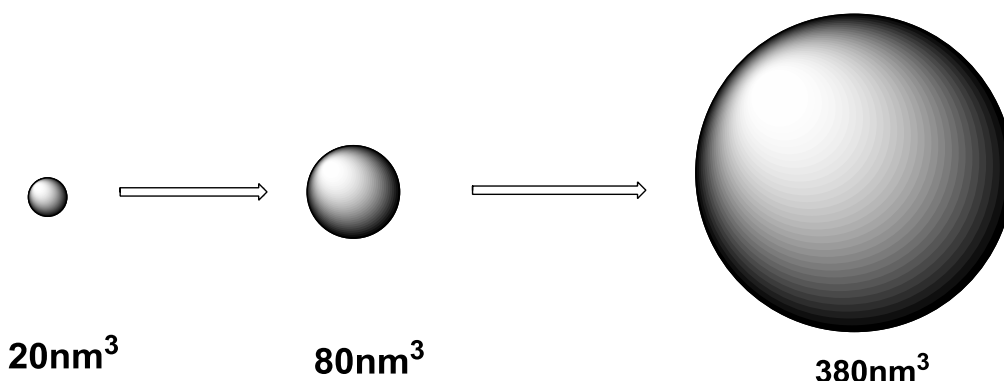


Figure 6-1 Relative volumes of nanoparticles ($\sim 380\text{nm}^3$) compared to molecules ($\sim 20\text{nm}^3$) and coordination complexes ($\sim 80\text{nm}^3$).

The first report of colloidal gold was made by Antonii⁴ and came in the early 17th century. However, the first *synthesis* was described by Faraday⁵ in the mid-19th century, and describes the reduction of ionic gold to give nanoparticles.

Since then, there has been an enormous amount of research on gold nanoparticles⁶ and nanomaterials in general.⁷ Nanomaterials are attractive for a number of reasons, and particular focus has been in their use in medicine⁸, environmental remediation⁹, and optical imaging.¹⁰

Nanoparticles are made up of clusters of atoms which can be stabilized by long alkyl chains which can directly influence their solubility.¹¹ The alkyl chains serve two purposes; first,

they contain an end which can coordinate to the surface of the nanoparticle. Second, they contain an ‘inert’ end which is typically a methyl group. The alkyl ligands can ‘interdigitate’, and space the particle cores, where the chains interact via van der Waals interactions, Figure 6.2.

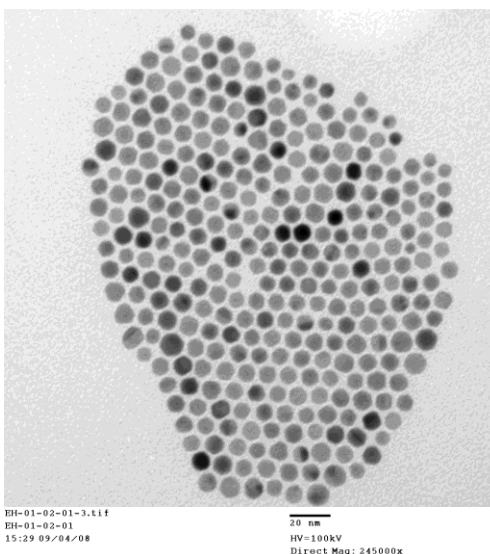


Figure 6-2 Arrangement of nanoparticles observed in dodecylamine functionalised gold nanoparticles.

The properties of the nanoparticles and their ordered structures is dependent on both capping ligand¹² and interparticle distance.¹³ Ligands containing thiol (R-SH) groups form stronger interactions with the gold surface compared to ligands containing an amine (R-NH₂) group¹⁴, and ligands are designed with this in mind. Furthermore, capping ligands terminated with hydrogen bond donor (or acceptor) groups¹⁵ have been used for the construction of supramolecular assemblies.

In 2010, the first report of a supramolecular assembly containing halogen bonds and gold nanoparticles was made. In this work, van der Boom *et al.*¹⁶ showed that *N*-oxide based ligands could be used to cap the nanoparticles and form halogen-bond interactions with bipyridyl-based organic linkers, Figure 6.3.

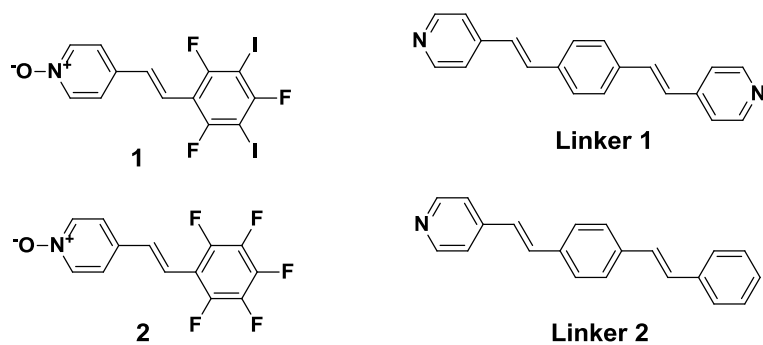


Figure 6-3 Ligands (1 and 2) and linkers (1 and 2) used in the halogen-bond assembly of nanoparticles.¹⁶

When the XB donor particles were combined with the linkers, the particles formed dense aggregates and fractal networks. The results clearly demonstrated particle aggregation was influenced by XB interactions between XB donor (nanoparticle) and XB acceptor (bi-pyridyl linker). It is not surprising that C-I \cdots N interactions were able to accomplish this goal, considering the number of examples in the CSD¹⁷ where this synthon is used to drive co-crystal formation.¹⁸ Therefore, when designing new ligands for potential HB and XB interactions, the ligands should display the following features:

- I. An aliphatic chain terminated with a sulfur functionality (thiol or disulfide).
- II. A hydrogen bond (HB) and halogen-bond (XB) acceptor moiety (i.e. nitrogen).
- III. A HB and XB donor moiety (i.e. hydrogen and iodine, respectively).

Data in the CSD has shown the versatility of pyridine as a halogen bond acceptor, and recent examples of XB to pyridine confirm the utility of this synthon.¹⁹ In addition to pyridine, imidazole-based acceptors have proven useful for forming XB with activated iodine atoms.²⁰ Therefore, capping ligands containing an imidazole-based acceptor (I) and activated iodine donor (II) were synthesized, Figure 6.4.

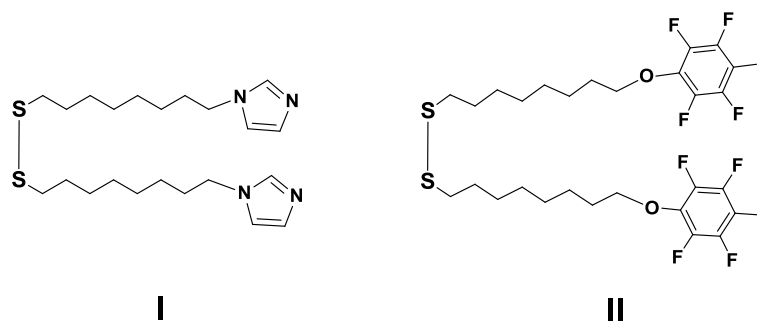


Figure 6-4 Target ligands **(I)** bis(8-imidazol-1-yl)octyl)disulfide, **(IM)**; **(II)** bis(8-(2,3,5,6-tetrafluoro-4-iodophenoxy)octyl)disulfide, **(XBD)**.

Gold nanoparticles were synthesized using inverse micelle method following the method developed by Stoeva et. al.²¹ The particles were then subjected to digestive ripening²² (purification procedure), and then a ligand exchange reaction. The exchange ligands were prepared using traditional organic synthetic techniques. The exchanged particles were washed with Toluene, dried, and re-dispersed in a polar solvent. The particles were then analysed using TEM and IR, and combined with other particles containing complementary functional groups. The combined samples were analyzed using TEM, dried and the residue analyzed using IR, Figure 6.5

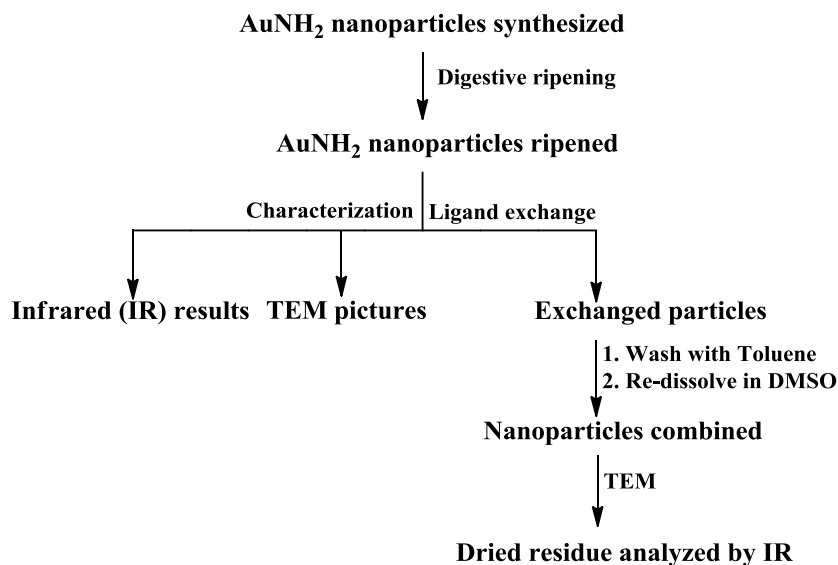


Figure 6-5 Flowchart for synthesis and characterization of gold nanoparticles.

This chapter will attempt to answer the following questions:

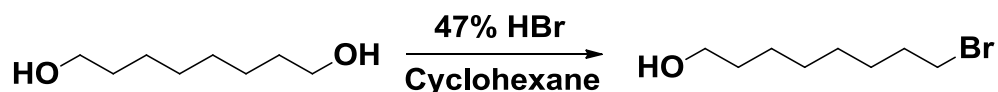
- I. Can suitable capping ligands for functionalizing the surface of gold nanoparticles be synthesized and used to make nanoparticles?
- II. Can nanoparticles be synthesized with HB and XB capping ligands?
- III. Can HB and XB interactions influence the assembly of nanoparticles?

6.2 Experimental

6.2.1 Synthesis

All chemicals were purchased from Sigma-Aldrich unless otherwise noted and used without further purification. Glassware used for making nanoparticles was cleaned using the following procedure: 1) Scrub with soap and water. 2) Rinse with aqua regia (3:1 HCl:HNO₃). 3) Rinse with concentrated H₂SO₄. 4) Dip glassware in base bath. 5) Rinse with deionized water. 6) Oven dry overnight. Melting points were determined on a Fisher-Johns melting point apparatus and are uncorrected. UV-Vis data were collected on a Shimadzu UV-1650PC spectrophotometer. Infrared experiments were collected on a Thermo Scientific Nicolet 380 FT-IR using a ZnSe crystal. Transmission electron microscopy (TEM) images were collected using a Siemens CM-100 electron microscope. IR Samples for TEM were prepared by placing a 2 μ L drop of the colloidal solution on a Formvar carbon copper grid on 400 mesh copper grids (FCF400-Cu) purchased from Electron Microscopy Sciences (Hatfield, PA). The grids were allowed to dry at room temperature (for toluene samples) and dried using a heat gun (for DMSO samples).

6.2.1.1 Synthesis of 1-bromooctan-8-ol, 6.1



To a round bottom flask, 1,8-octanediol (5.90g, 40.4mmol) and cyclohexane (105mL) were added. To the biphasic mixture, 47% HBr (27mL) was added and the mixture was stirred at reflux for 6 hours. Upon completion, the reaction mixture was cooled to room temperature, diluted with hexanes, and small amounts of aqueous Na₂CO₃ was added in small amounts until most of the bubbling ceased. The aqueous layer was separated, and the organic layer was washed with aqueous Na₂CO₃ (3 x 50mL), saturated NaCl (1 x 50mL), dried over MgSO₄ and reduced to

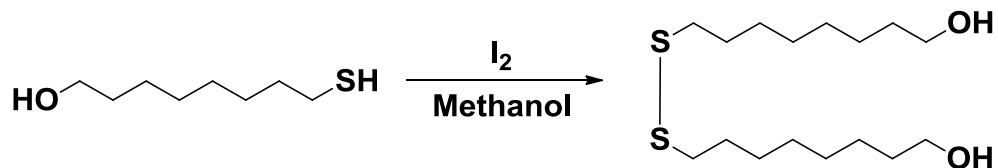
a light yellow oil (4.55g, 54%). ^1H NMR (400 MHz, CDCl_3) δ ppm: 3.61 (t, $J=6.64$ Hz, 2H), 3.39 (t, $J=6.83$ Hz, 2H), 1.70 - 1.91 (m, 4H), 1.53 (d, $J=6.64$ Hz, 4H), 1.20 - 1.45 (m, 4H), Figure A.22.

6.2.1.2 Synthesis of 1-mercaptooctan-8-ol, 6.2



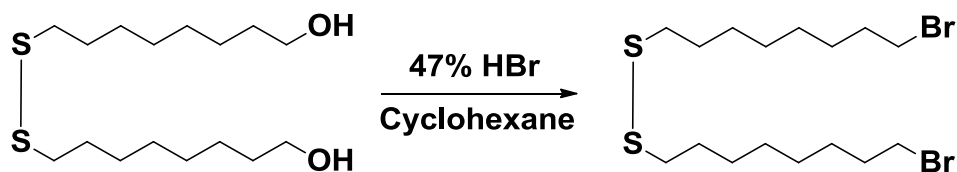
To a round bottom flask, **6.1** (4.76g, 22.76mmol) and 200 proof ethanol (150mL) were added. To the solution, thiourea (3.59g, 47.12mmol) was added and the reaction refluxed for 3 hours, at which point, 10% NaOH (75mL) was added and the reaction refluxed for a further 2 hours. The reaction was cooled to room temperature and the pH adjusted to 2-3 with 2M HCl. The acidic solution was washed with dichloromethane (3 x 100mL), the organic extracts combined, dried over MgSO_4 and reduced to an off-white solid/colorless oil (3.33g, 90%). ^1H NMR (400 MHz, CDCl_3) δ ppm: 3.65 (t, $J=6.44$ Hz, 2H), 2.41 - 2.57 (m, 2H), 1.45 - 1.64 (m, 4H), 1.17 - 1.43 (m, 8H), Figure A.23.

6.2.1.3 Synthesis of bis(8-hydroxyoctyl)disulfide, 6.3



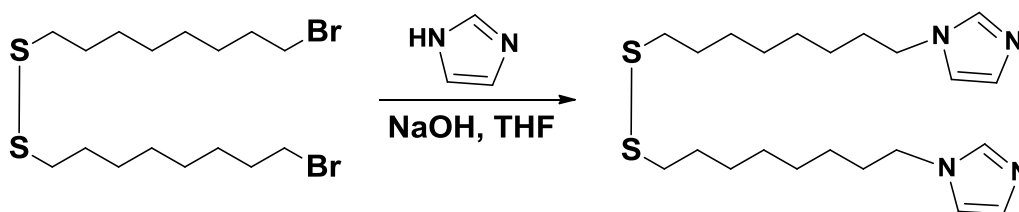
To a round bottom flask, **6.2** (3.33g, 20.5mmol) and methanol (27mL) were added. Once in solution, a saturated solution of iodine (~30mL) was added drop wise until the solution remained orange/yellow. The reaction was then quenched with 10% NaHSO_3 (75mL) and dichloromethane (75mL). The organic layer was extracted and the aqueous layer was washed with dichloromethane (4 x 50mL). All organic extracts were combined, dried over MgSO_4 and reduced to a white solid. The solids were dried under high vacuum for 20 minutes. (2.41g, 73%). Mp: 41-44°C. ^1H NMR (400 MHz, CDCl_3) δ ppm: 3.61 (t, $J=6.44$ Hz, 4 H), 2.66 (t, $J=7.22$ Hz, 4H), 1.64 (dd, $J=13.86, 6.83$ Hz, 4H), 1.56 (br. s., 4H), 1.22 - 1.44 (m, 16H), Figure A.24.

6.2.1.4 Synthesis of bis(8-bromooctyl)disulfide, 6.4



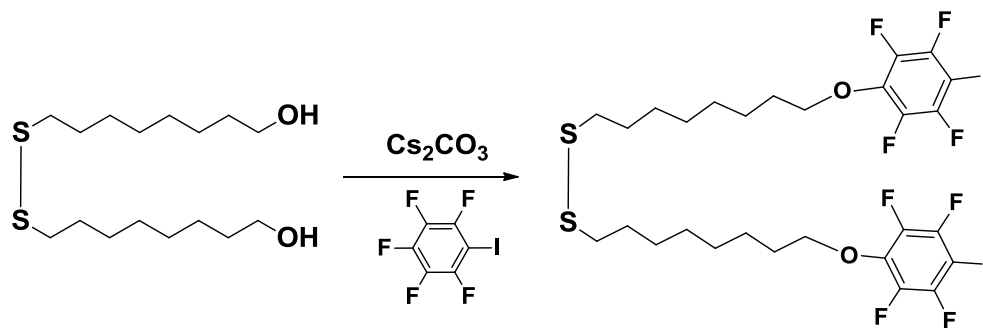
To a round bottom flask, **6.3** (3.11g, 9.64mmol) and cyclohexane (80mL) were added. Once in solution, 47% HBr (80mL) was added and the reaction refluxed for 24 hours, at which point a second portion of 47% HBr (80mL) was added and the reaction refluxed for an additional 24 hours. Upon completion, the reaction was cooled to room temperature and diluted with hexanes (100mL). The aqueous layer was separated, and the organic layer was then washed with aqueous NaHCO₃ (4 x 100mL) and saturated NaCl (1 x 100mL), separated, dried over MgSO₄ and reduced to a yellow liquid (2.81g, 65%). ¹H NMR (400 MHz, CDCl₃) δ ppm: 3.41 (t, *J*=7.42 Hz, 4H), 2.68 (t, *J*=6.83 Hz, 4H), 1.78 - 1.95 (m, 4H), 1.62 - 1.74 (m, 4H) 1.22 - 1.52 (m, 16H), Figure A.25.

6.2.1.5 Synthesis of bis(8-imidazol-1-yl)octyl)disulfide, 6.5



To a round bottom flask, imidazole (2.20g, 32.3mmol) and dry THF (100mL) were added. Once in solution, NaOH pellets (3.18g, 79.5mmol) were added and the reaction stirred for 2 hours at room temperature. Upon completion, **6.4** (3.48g, 7.76mmol) in dry THF (100mL) was added and the reaction stirred for 4 days at room temperature. Upon completion, H₂O (100mL) was added to dissolve NaBr and NaOH and the aqueous layer was saturated with NaCl. The THF layer was extracted, dried over MgSO₄ and reduced to a yellow oil. The yellow oil was dissolved in ethyl acetate (50mL) and washed with 1M NaOH(aq) (3 x 50mL). The organic layer was removed, dried over MgSO₄ and reduced to a yellow oil (1.76g, 54%). ¹H NMR (400 MHz, CDCl₃) δ ppm: 7.39 (s, 1H), 6.97 (s, 1H), 6.84 (s, 1H), 3.85 (t, *J*=7.03 Hz, 4H), 2.60 (t, *J*=7.03 Hz, 4H), 1.47 - 1.81 (m, 8H), 1.04 - 1.41 (m, 16H), Figure A-26.; ¹³C NMR (δ_H; 100 MHz, CDCl₃) δ ppm: 137.18, 129.39, 118.97, 47.18, 39.14, 31.20, 29.25, 29.17, 29.09, 28.48, 26.62, Figure A-27.

6.2.1.6 Synthesis of bis(8-(2,3,5,6-tetrafluoro-4-iodophenoxy)octyl)disulfide, 6.6



To a round bottom flask, **6.3** (0.211g, 0.654mmol) and Cs₂CO₃ (0.448g, 1.37mmol) were added. The mixture was warmed just above room temperature and stirred under nitrogen for two days, at which point Iodopentafluorobenzene (0.42g, 1.43mmol) was added. The reaction was stirred and heated around 40°C for an additional 24 hours, at which point a second addition of Cs₂CO₃ (0.460g, 1.41mmol) and Iodopentafluorobenzene (0.43g, 1.46mmol) were added. The reaction was stirred and heated for an additional 24 hours, then cooled to room temperature. The reaction was diluted with CH₂Cl₂ (40mL) and H₂O (40mL). The aqueous layer was removed, and the organic layer was washed with aqueous NaCl (2 x 50mL), separated, dried over MgSO₄ and reduced to a brown liquid. The product was isolated using a silica column packed with hexanes (100% hexanes as eluent) to give a yellow/orange oil (0.129g, 23%). ¹H NMR (400 MHz, CDCl₃) δ ppm: 4.23 (t, *J*=6.44 Hz, 4H), 2.68 (t, *J*=7.42 Hz, 4H), 1.58 - 1.93 (m, 8H), 1.15 - 1.54 (m, 16H), Figure A-28; ¹⁹F NMR (δ_H; 376.3 MHz, CDCl₃) δ ppm: -154.78 (s, 4F), -121.99 (s, 4F), Figure A-29.

6.2.1.7 Synthesis of dodecylamine functionalised gold nanoparticles, 7

To a clean, dry, 50mL Erlenmeyer flask, didodecyldimethylammonium bromide (DDAB) (1.62g, 3.50mmol) was dissolved in freshly distilled toluene (10mL). AuCl₃ (0.0340g, 0.112mmol) was added to the mixture and the resulting orange/red solution was sonicated until AuCl₃ was dissolved. Argon was bubbled through the orange/red solution for one hour, at which point aqueous NaBH₄ (36μL of a 9.4M solution) was added to the solution while stirring under Argon. The color changes from orange/red to yellow to deep red/purple. The red/purple solution was stirred under Argon for a further 15min to ensure complete reduction before being transferred into a clean, dry, 40ml vial. Dodecylamine (0.81g, 1474.37mmol) was then added neat to the vial and shaken vigorously for five minutes. The red/purple solution was diluted with absolute

ethanol (28mL) and shaken for one minute. The mixture settled overnight, and the ethanol/toluene/DDAB mixture was removed from the vial using a Pasteur pipette. The particles were covered in aluminum foil and dried under high vacuum for 15 minutes.

6.2.1.8 Digestive ripening of gold nanoparticles, 8

The dried particles, **7**, were re-dissolved in dry toluene (15mL) to give a red/purple solution. The solution was transferred to a clean, dry 50mL round bottom flask containing a stirbar, and excess dodecylamine (0.81g, 1474.37mmol) was added. The reaction vessel was covered in aluminum foil (to block light) and heated to reflux under argon for 90 minutes. The red/purple solution was cooled to room temperature, transferred to a clean 40mL vial, and diluted with absolute ethanol (28mL). The mixture settled overnight, and the ethanol/toluene/Dodecylamine mixture was removed from the vial using a Pasteur pipette. The particles were covered in aluminum foil and dried under high vacuum for 15 minutes. *The dried particles were stored under argon and wrapped in aluminum foil.*

6.2.1.9 Ligand exchange of gold nanoparticles, 9

The dried, digestively ripened particles were redispersed in toluene (15mL) with sonication and heating. The exchange ligand (11-mercaptoundecanoic acid (**MUA**), 0.195g, 0.893mmol; bis(8-imidazol-1-yloctyl)disulfide (**IM**) 0.377g, 0.893mmol; 1,2-bis(8-(2,3,5,6-tetrafluoro-4-iodophenoxy)octyl)disulfide (**XBD**), 0.777g, 0.893mmol) was added to the solution neat and shaken for five minutes resulting in precipitation and a red/purple to purple color change. The particles were allowed to settle and the toluene was removed using a Pasteur pipette. The particles were washed with toluene (2x15mL) and dissolved in DMSO with heating and sonication.

6.3 Results

6.3.1 TEM image of dodecylamine functionalized AuNP's

The TEM image of dodecylamine functionalized AuNP's shows a nanoparticle superlattice containing particles uniform in size and shape. The particles are ~7-8nm in diameter with an average interparticle spacing of ~1.5nm, Figures 6.6 and 6.7.

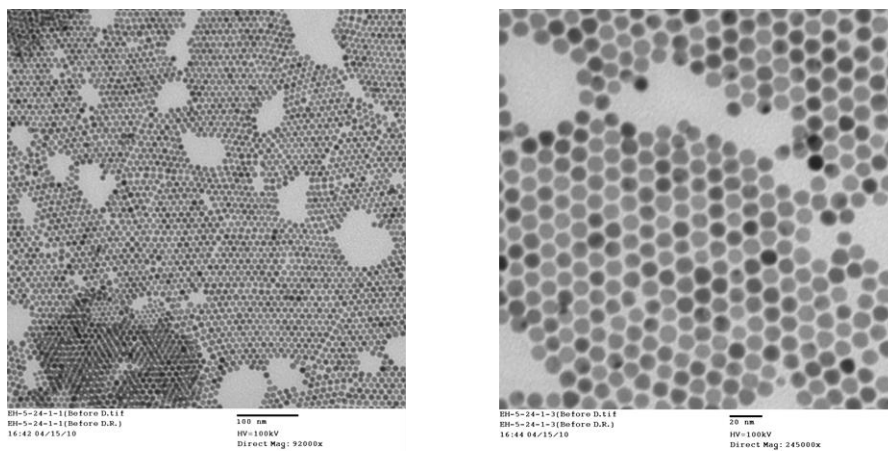


Figure 6-6 TEM image of dodecylamine functionalized AuNP's. (I) magnification = 92,000x; scale = 100nm (II) magnification = 245,000x; scale = 20nm.

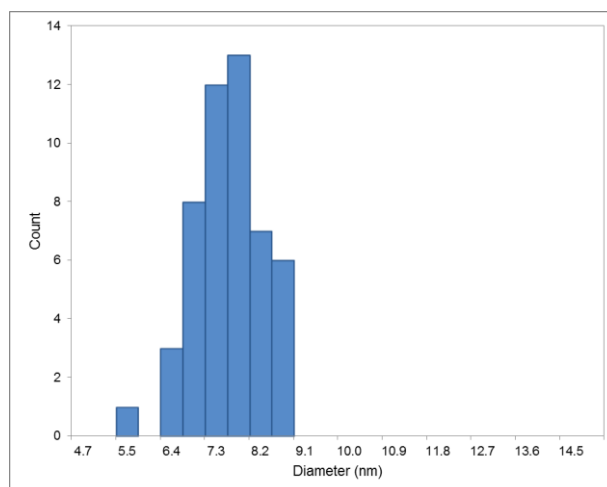


Figure 6-7 Histogram of dodecylamine functionalized AuNP's.

6.3.2 TEM image of 11-mercaptoundecanoic acid (MUA) functionalized AuNP's

The TEM image of 11-mercaptoundecanoic acid (MUA) functionalized AuNP's shows a fractal network. The particles are ~7-8 nm in diameter with an average interparticle spacing of ~2nm, Figures 6.8 and 6.9.

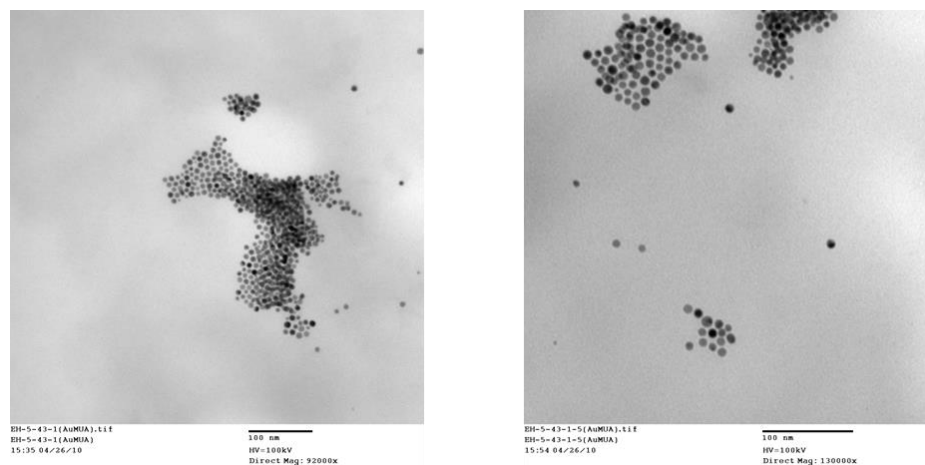


Figure 6-8 TEM image of 11-mercaptopundecanoic acid (MUA) functionalized AuNP's. (I) magnification = 92,000x; scale = 100nm (II) magnification = 130,000x; scale = 100nm.

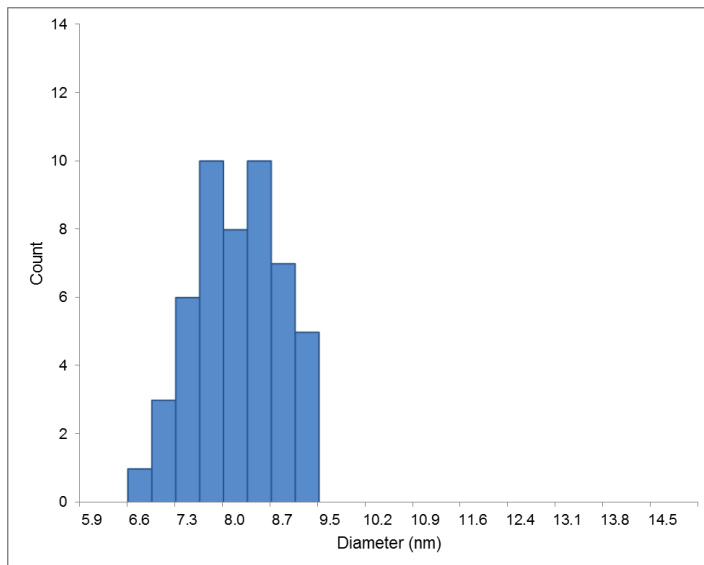


Figure 6-9 Histogram of 11-mercaptopundecanoic acid (MUA) functionalized AuNP's.

6.3.3 TEM image of bis(8-imidazol-1-yloctyl)disulfide functionalized AuNP's

The TEM image of bis(8-imidazol-1-yloctyl)disulfide functionalized AuNP's shows clusters of particles. The particles are ~7-8 nm in diameter with an average interparticle spacing of ~1.7 nm, Figures 6.10 and 6.11.

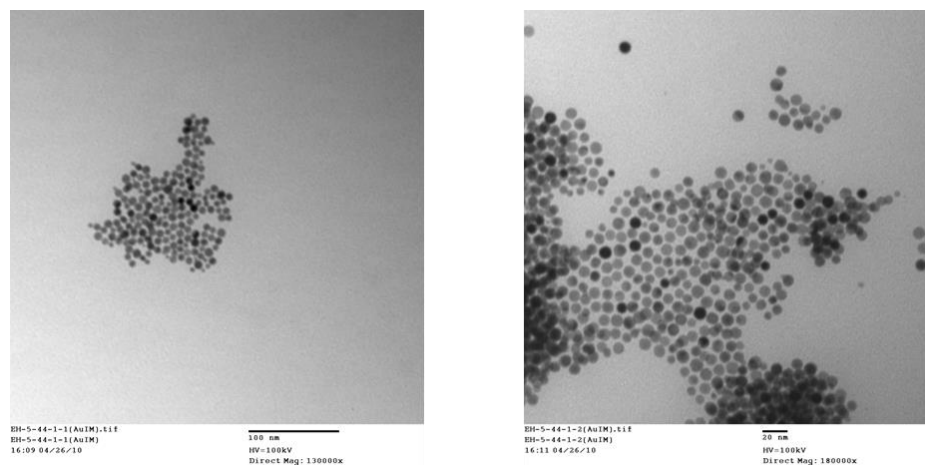


Figure 6-10 TEM image of bis(8-imidazol-1-yl)octyl disulfide functionalized AuNP's. (I) magnification = 130,000x; scale = 100nm (II) magnification = 180,000x; scale = 20nm.

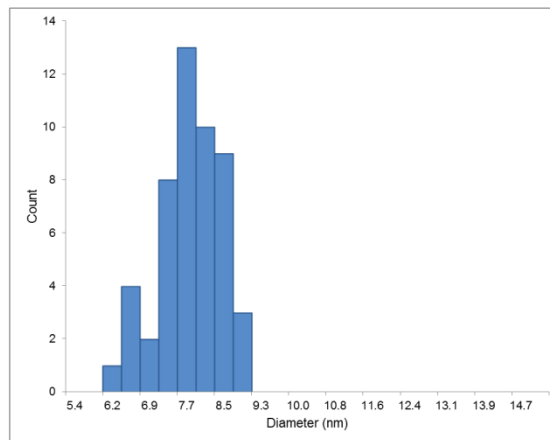


Figure 6-11 Histogram of bis(8-imidazol-1-yl)octyl disulfide (DS-IM) functionalized AuNP's.

6.3.4 TEM image of bis(8-(2,3,5,6-tetrafluoro-4-iodophenoxy)octyl)disulfide functionalized AuNP's

The TEM image of bis(8-(2,3,5,6-tetrafluoro-4-iodophenoxy)octyl)disulfide functionalized AuNP's shows clusters of particles. The particles are ~9-11 nm in diameter with an average interparticle spacing of ~1.7nm, Figures 6.12 and 6.13.

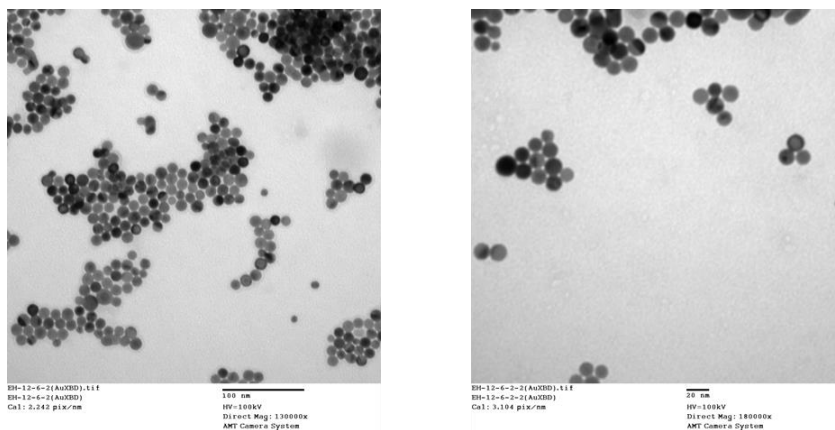


Figure 6-12 TEM image of bis(8-(2,3,5,6-tetrafluoro-4-iodophenoxy)octyl)disulfide functionalized AuNP's. (I) magnification = 130,000x; scale = 100nm (II) magnification = 180,000x; scale = 20nm.

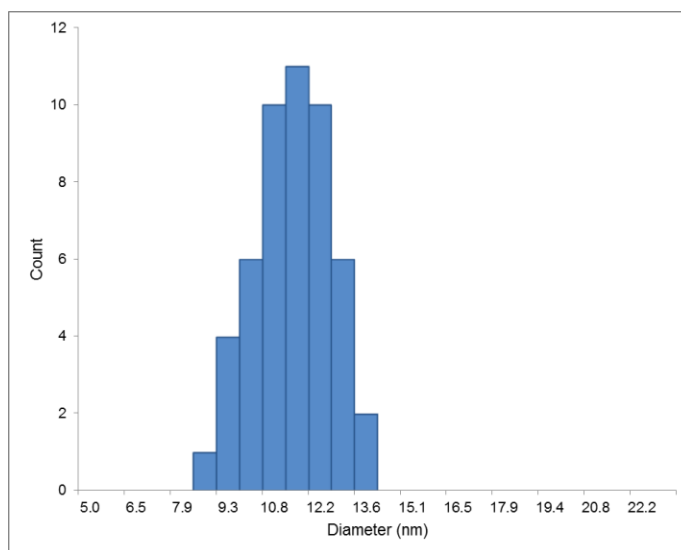


Figure 6-13 Histogram of bis(8-(2,3,5,6-tetrafluoro-4-iodophenoxy)octyl)disulfide functionalized AuNP's.

6.3.6 TEM image of 11-mercaptoundecanoic acid (MUA) functionalized AuNP's + bis(8-imidazol-1-yl)octyl)disulfide functionalized AuNP's

The TEM image of 11-mercaptoundecanoic acid (MUA) functionalized AuNP's combined with bis(8-imidazol-1-yl)octyl)disulfide functionalized AuNP's shows fractal aggregates of particles, Figure 6.14.

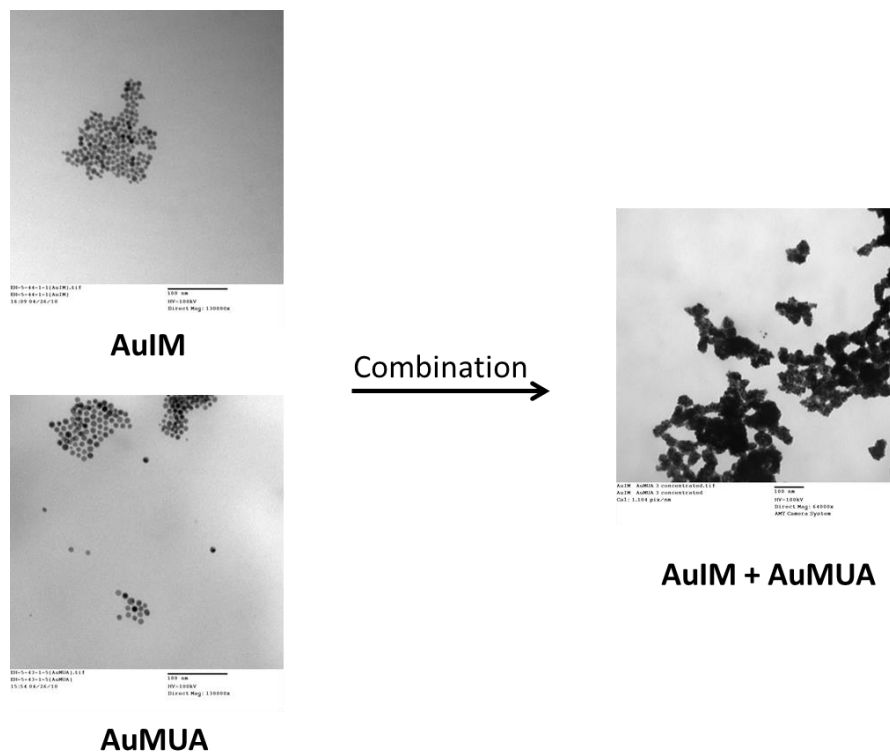


Figure 6-14 TEM image of 11-mercaptopundecanoic acid (MUA) functionalized AuNP's combined with bis(8-imidazol-1-yl)octyl)disulfide functionalized AuNP's. (I) magnification = 130,000x; scale = 100nm (II) magnification = 180,000x; (III) magnification = 64,000x; scale = 20nm.

6.3.7 TEM image of bis(8-(2,3,5,6-tetrafluoro-4-iodophenoxy)octyl)disulfide functionalized AuNP's + bis(8-imidazol-1-yl)octyl)disulfide functionalized AuNP's

The TEM image of bis(8-(2,3,5,6-tetrafluoro-4-iodophenoxy)octyl)disulfide combined with bis(8-imidazol-1-yl)octyl)disulfide functionalized AuNP's shows fractal aggregates of particles, Figure 6.15.

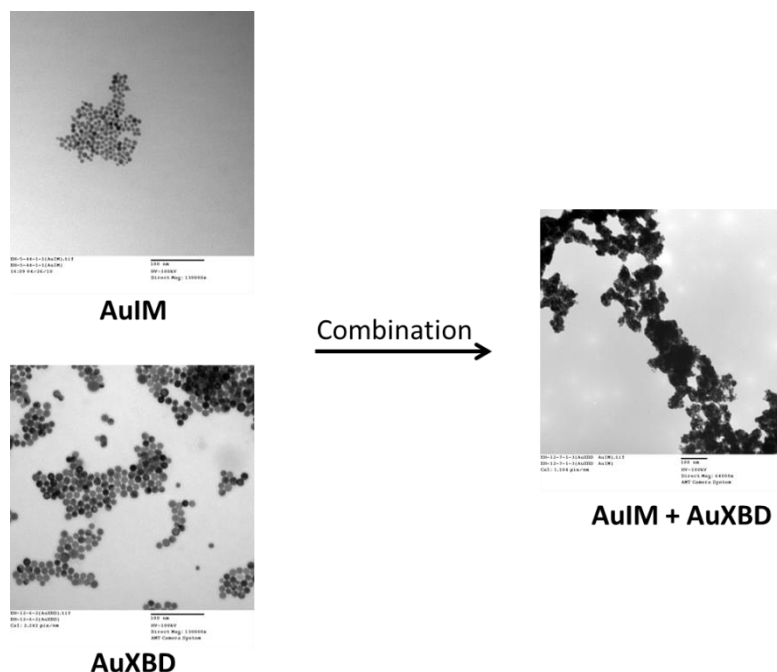


Figure 6-15 TEM image of bis(8-(2,3,5,6-tetrafluoro-4-iodophenoxy)octyl)disulfide combined with bis(8-imidazol-1-yl)octyl)disulfide functionalized AuNP's. (I) magnification = 130,000x; scale = 100nm (II) magnification = 180,000x; scale = 20nm.

6.3.7 Determining nanoparticle 'communication' using infra-red (IR) spectroscopy

IR spectroscopy is a useful tool for examining various spectroscopic bands from specific ligands and looking at shifts caused by nanoparticle interaction. In the system containing 11-mercaptopundecanoic acid (MUA) gold nanoparticles combined with bis(8-imidazol-1-yl)octyl)disulfide gold nanoparticles, O-H...N hydrogen bonds are expected to form between the capping ligands. Two broad bands at 2500 cm^{-1} and 1900 cm^{-1} , representing changes in the OH stretch, as well as changes in the position of the carbonyl C=O may give an indication that the ligands (and hence the nanoparticles) are interacting, Figure 6.16.

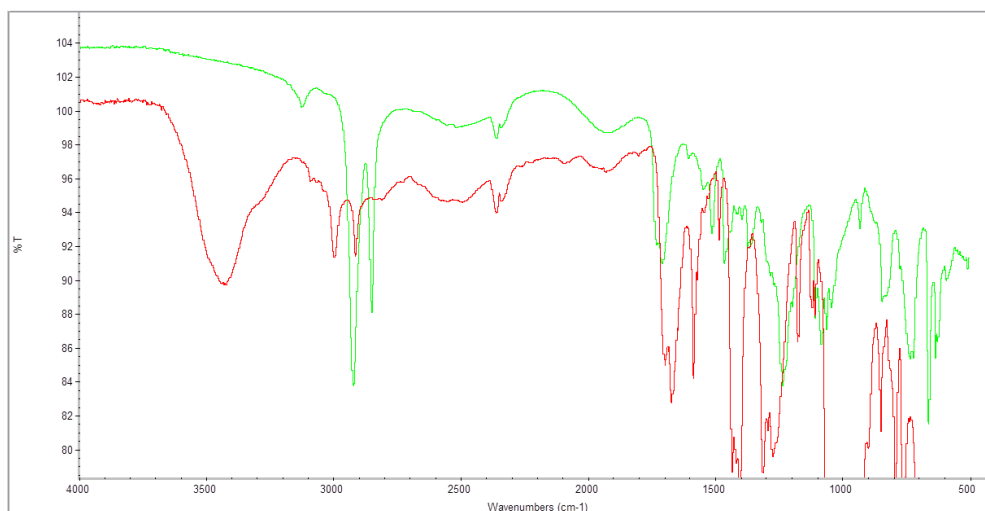


Figure 6-16 IR spectrum of 11-mercaptopundecanoic acid (MUA) capping ligand combined with bis(8-imidazol-1-yl)octyl)disulfide capping ligand (green scan, top). AuIM nanoparticles combined with AuMUA nanoparticles showing the O-H···N hydrogen bonds (red scan, bottom).

In the system containing bis(8-(2,3,5,6-tetrafluoro-4-iodophenoxy)octyl)disulfide nanoparticles combined with bis(8-imidazol-1-yl)octyl)disulfide nanoparticles, C-I···N halogen bonds are expected to form between the capping ligands, Figure 6.17.

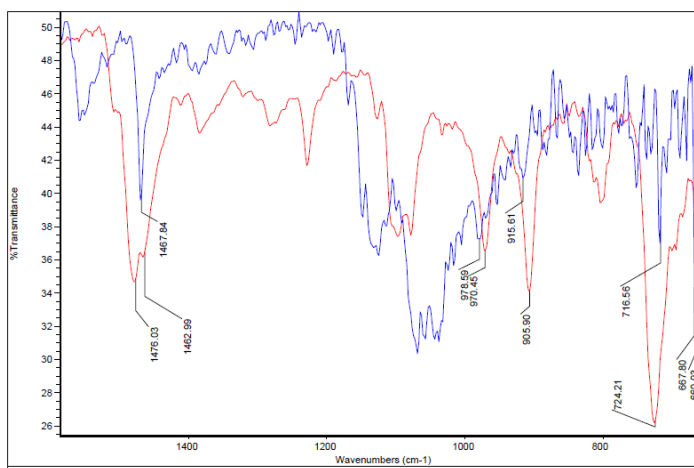


Figure 6-17 IR spectrum comparison of bis(8-(2,3,5,6-tetrafluoro-4-iodophenoxy)octyl)disulfide neat ligand (red scan, top) versus the combination of bis(8-imidazol-1-yl)octyl)disulfide and bis(8-(2,3,5,6-tetrafluoro-4-iodophenoxy)octyl)disulfide gold nanoparticles (purple scan, bottom).

6.4 Discussion

6.4.1 Examining the effect of digestive ripening

Gold nanoparticles were heated in the presence of excess ligand (dodecylamine) to obtain well defined, monodisperse particles. Although the theory of how digestive ripening works²³ is still a topic for debate, the utility of this method for the purification of dodecylamine gold nanoparticles is not. Pictures of the particles before and after digestive ripening, highlighting the differences in particle shape and arrangement is shown in Figure 6.18.

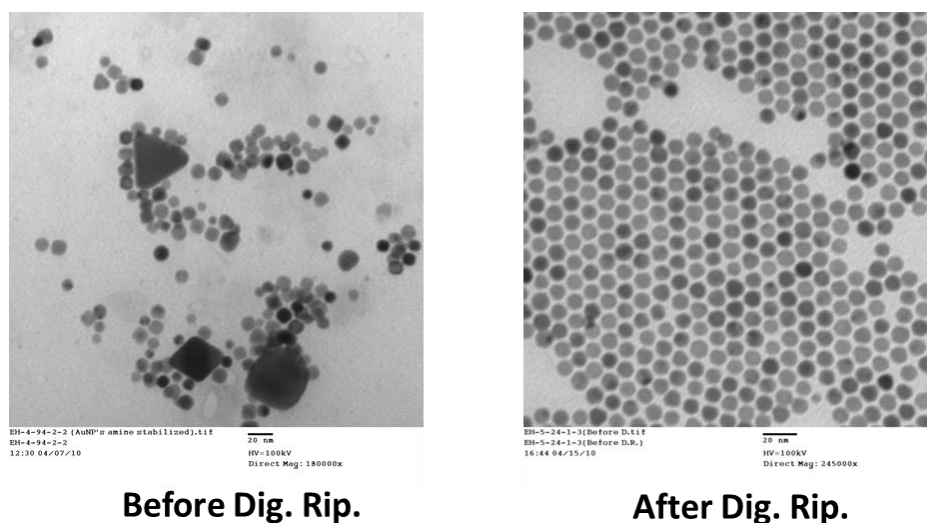


Figure 6-18 TEM images of dodecylamine particles. (I) before digestive ripening and (II) after digestive ripening; magnification = 92,000x; scale = 100nm.

6.4.2 Examining the effect of ligand exchange

Ligand exchange reactions were carried out on digestively ripened dodecylamine gold nanoparticles (AuNH_2) with the following ligands: 11-mercaptoundecanoic acid (**MUA**); bis(8-imidazol-1-yl)octyl)disulfide (**IM**); bis(8-(2,3,5,6-tetrafluoro-4-iodophenoxy)octyl)disulfide (**XBD**). The TEM images of the exchanged particles are shown in Figure 6.19.

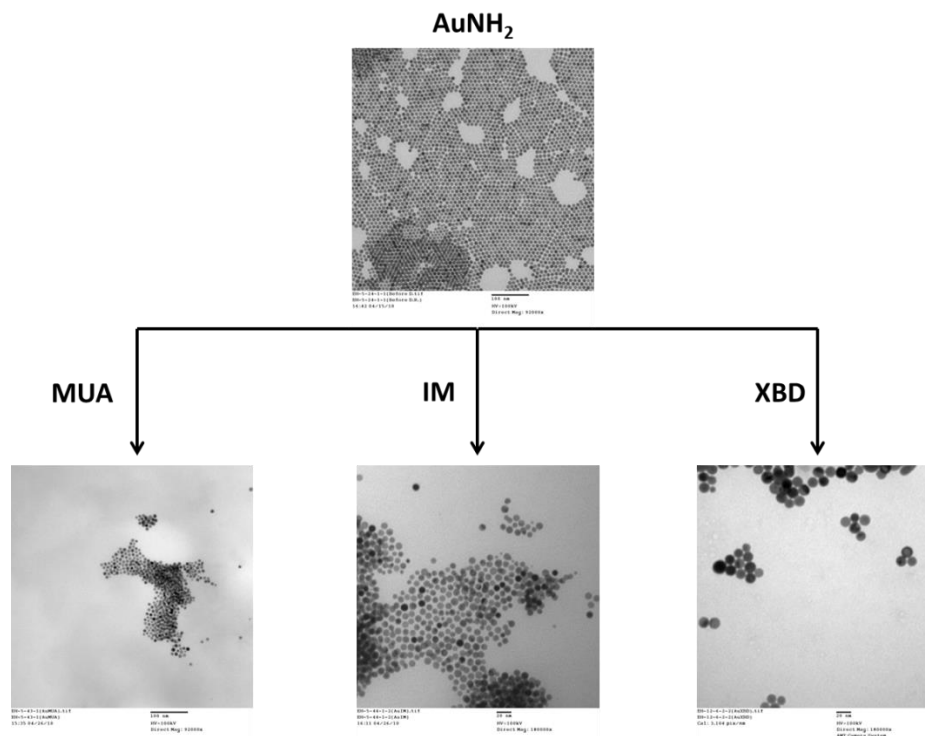


Figure 6-19 TEM images of dodecylamine particles before and after ligand exchange. (I) 11-mercaptopundecanoic acid (MUA); (II) bis(8-imidazol-1-yl)octyl)disulfide (IM); (III) bis(8-(2,3,5,6-tetrafluoro-4-iodophenoxy)octyl)disulfide (XBD); magnification = 92,000x; scale = 100nm.

6.4.3 Examining interparticle distances

The distances between the as-prepared gold nanoparticles were measured and recorded in Table 6.1. The ligands containing an inert end (e.g methyl group) are expected to give a different spacing compared to a non-inert end (e.g carboxylic acid). Since the acid may be able to form a homomeric acid···acid interaction, the interparticle spacing is slightly larger compared to the methyl-terminated particles. The particles terminated with imidazole (AuIm) or tetrafluoroiodobenzene (AuXBD) give interparticle spacing distances that are intermediate from the methyl and carboxylic acid capped particles. A possible explanation for this is the ligands do not interdigitate like in AuNH₂ since they are not inert and thus do not allow the ligands to interact as much. On the other hand, the particles are not capable of forming a homomeric tip to tip interaction, as may be the case in AuMUA. Therefore, their interparticle distance lies between the two values (1.5 and 2.0) of the AuNH₂ and AuMUA, respectively, Table 6.1.

Table 6.1 Comparison of the interparticle distance between gold nanoparticles.

AuNP	AuNH ₂	AuMUA	AuIM	AuXBD	AuMUA + AuIM	AuXBD + AuIM
Interparticle spacing	~1.5	~2.0	~1.7	~1.7	-	-

6.4.4 Examining interparticle ‘communication’

Interparticle communication was determined by examining both the TEM images and the IR spectrum obtained from the dried residue of the combination experiments between different nanoparticles.

To determine if particle aggregation could take place by adding two different (i.e. different functionalized particles), AuIM was combined with AuNH₂ to see if particle ‘communication’ was taking place. The particles are not expected to communicate, since the capping ligands do not contain complementary functional groups. The images from the combination experiments are shown in Figure 6.20.

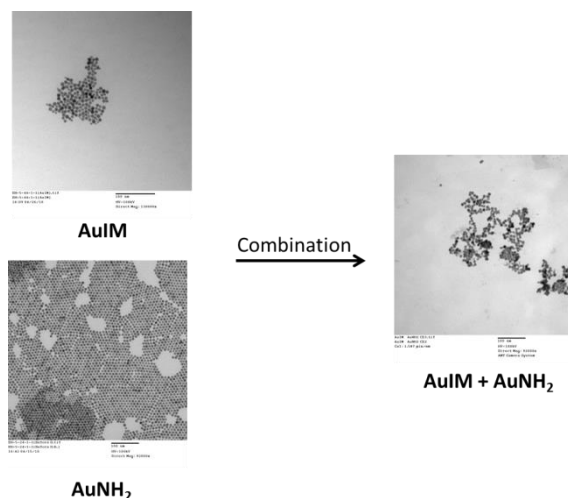


Figure 6-20 TEM images of the combination of AuIM + AuNH₂.

As observed in the combination image, there is no evidence for the formation of dense clusters from the combination of the two non-complementary particles. This result eliminates the possibility of particle aggregation being caused by adding two separate particles together.

When AuNH₂ is replaced with AuMUA, O-H···N hydrogen bonds form between the particles, resulting in dense aggregate formation. Furthermore, the IR data support the formation of HB between particles, as evidenced by the two broad stretches in the 2500 cm⁻¹ and 1900 cm⁻¹ regions.

To test the ability of halogen bonds to influence particle assembly, AuNH₂ was replaced with AuXBD, which is capable of forming XB with AuIM. From the TEM images, dense clusters of particles formed, indicating the XB can influence the assembly of particle formation. The IR results show slight shifts in the bands, supporting the XB influence on particle assembly. To further support the observations, a comparison of Van der Boom's XB assembly compared with our XB assembly is displayed in Figure 6.21.

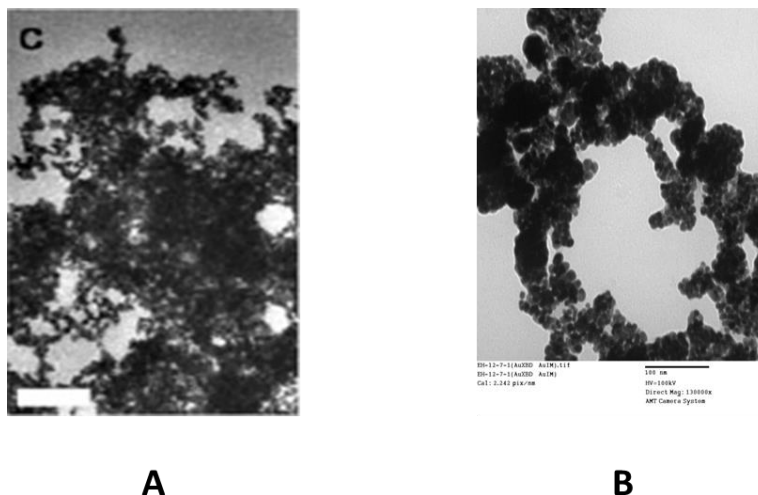


Figure 6-21 TEM images of Van der Boom's particles (A) and the particles obtained in this study (B), both influenced by XB interactions.

In summary,

- I. Suitable capping ligands for functionalizing the surface of gold nanoparticles have been synthesized.
- II. Nanoparticles can be made with hydrogen-bond (HB) and halogen-bond (XB) functionalized capping ligands.
- III. Relatively weak non-covalent interactions are capable of influencing the assembly of nanoparticles into clusters.

6.5 References:

- ¹ Metrangolo P.; Neukirch H.; Pilati T.; Resnati G. *Acc. Chem. Res.*, **2005**, *38*(5), 386-395.
- ² Politzer, P.; Murray, J. S.; Clark, T. *Phys. Chem. Chem. Phys.*, **2013**, *15*(27), 11178-11189.
- ³ Aakeröy, C. B.; Chopade, P. D.; Desper, J. *Cryst. Growth Des.*, **2011**, *11*(12), 5333-5336;
Aakeröy, C. B.; Desper, J.; Helfrich, B. A.; Metrangolo, P.; Pilati, T.; Resnati, G.; Stevenazzi, A. *Chem. Commun.*, **2007**, *41*, 4236-4238.
- ⁴ Antonii, F. *Panacea Aurea-Auro Potabile*, Bibliopolio Frobeniano, Hamburg, **1618**.
- ⁵ Faraday, M. *Philos. Trans. R. Soc. London*, **1857**, 147, 145.
- ⁶ Mieszawska, A. J.; Mulder, W. J. M.; Fayad, Z. A.; Cormode, D. P. *Mol. Pharm.*, **2013**, *10*(3), 831-847.
- ⁷ Coll, C.; Bernardos, A.; Martinez-Manez, R.; Sancenon, F. *Acc. Chem. Res.*, **2013**, *46*(2), 339-349.
- ⁸ Lohse, S. E.; Murphy, C. J. *J. Am. Chem. Soc.*, **2012**, *134*(38), 15607-15620.
- ⁹ Jiang, W.; Chen, X.; Niu, Y.; Pan, B. *J. Hazard. Mat.*, **2012**, *243*, 319-325.
- ¹⁰ Xiao, L.; Wei, L.; Cheng, X.; He, Y.; Yeung, E. S. *Anal. Chem.*, **2011**, *83*(19), 7340-7347.
- ¹¹ Lohman, B. C.; Powell, J. A.; Cingarapu, S.; Aakeröy, C. B.; Chakrabarti, A.; Klabunde, K. J.; Law, B. M.; Sorensen, C. M. *Phys. Chem. Chem. Phys.*, **2012**, *14*(18), 6502-6506.
- ¹² Lewandowski, W.; Jatzcak, K.; Pocięcha, D.; Mieczkowski, J. *Langmuir*, **2013**, *29*(10), 3404-3410.
- ¹³ Hermes, J. P.; Sander, F.; Peterle, T.; Cioffi, C.; Ringler, P.; Pfohl, T.; Mayor, M. *Small*, **2011**, *7*(7), 920-929.
- ¹⁴ Leifert, A.; Pan-Bartnek, Y.; Simon, U.; Jahnen-Dechent, W. *Nanoscale*, **2013**, *5*(14), 6224-6242.
- ¹⁵ For examples of hydrogen-bond nanoassemblies, see the following: Huang, K.; Renault, O.; Simonato, J.-P.; Grevin, B.; Rouviere, E.; De Girolamo, J.; Reiss, P.; Demadrille, R.; Benmansour, H. *J. Phys. Chem. C*, **2009**, *113*(51), 21389-21395; Yu, X.; Samanta, B.; Xu, H.; Arumugam, P.; Ofir, Y.; Jordan, B. J.; Rotello, V. M. *Small*, **2009**, *5*(1), 86-89.
- ¹⁶ Shirman, T.; Arad, T.; van der Boom, M. E. *Angew. Chemie.*, **2010**, *49*(5), 926-929.
- ¹⁷ Cambridge structural database (CSD), version 2012.
- ¹⁸ For examples of C-I...N halogen bonds, see the following: Vartanian, M.; Lucassen, A. C. B.; Shimon, L. J. W.; van der Boom, M. E. *Crystal Growth Des.*, **2008**, *8*(3), 786-790; Lucassen, A. C. B.; Karton, A.; Leitus, G.; Shimon, L. J. W.; Martin, J. M. L.; Van der Boom, M. E. *Crystal Growth Des.*, **2007**, *7*(2), 386-392; Lucassen, A. C. B.; Zubkov, T.; Shimon, L. J. W.; van der Boom, M. E. *CrystEngComm*, **2007**, *9*(7), 538-540.
- ¹⁹ Priimagi, A.; Cavallo, G.; Metrangolo, P.; Resnati, G. *Accts. Chem. Res.*, *Ahead of Print*.
- ²⁰ For examples of XB to imidazole-based acceptors, see CBA in house database.
- ²¹ Stoeva, S. I.; Zaikovski, V.; Prasad, B. L. V.; Stoimenov, P. K.; Sorensen, C. M.; Klabunde, K. J. *Langmuir*, **2005**, *21*(23), 10280-10283.
- ²² Prasad, B. L. V.; Stoeva, S. I.; Sorensen, C. M.; Klabunde, K. J. *Chem. Mater.*, **2003**, *15*(4), 935-942; Prasad, B. L. V.; Stoeva, Savka I.; Sorensen, Christopher M.; Klabunde, Kenneth J.

Langmuir, **2002**, *18*(20), 7515-7520; Stoeva, S.; Klabunde, K. J.; Sorensen, C. M.; Dragieva, I. *J. Am. Chem. Soc.*, **2002**, *124*(10), 2305-2311.

²³ Klabunde, K. J.; Sorensen, C. M.; Stoeva, S. I.; Prasad, B. L. V.; Smetana, A. B.; Lin, X.-M. In *Metal Nanoclusters in Catalysis and Materials Science: The Issue of Size Control*, **2008**, 233-249. Edited by Corain, B.; Schmid, G.; Toshima, N.

Appendix A - ^1H , ^{13}C and ^{19}F NMR

Figure A-1. ^1H NMR of 1.Cl

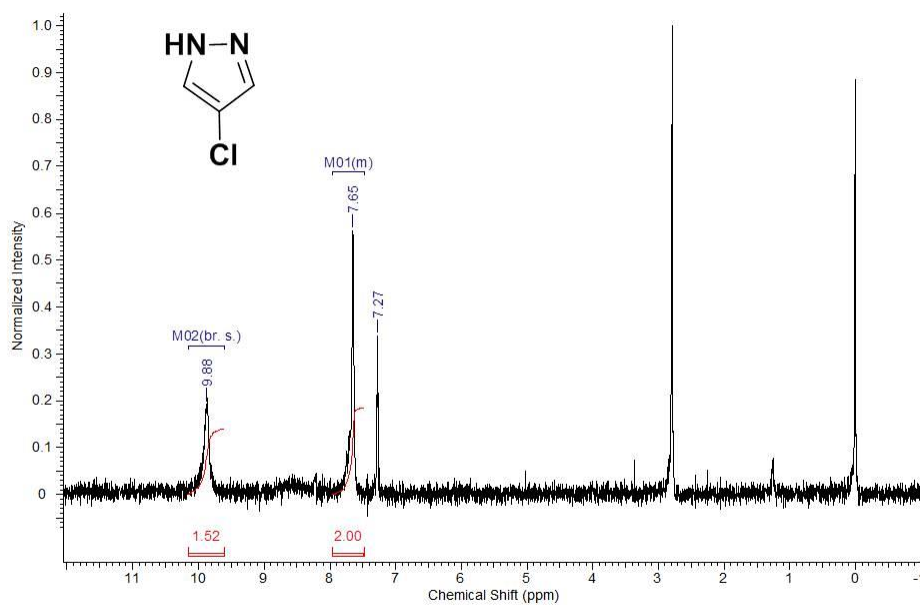


Figure A-2. ^1H NMR of 1.Br

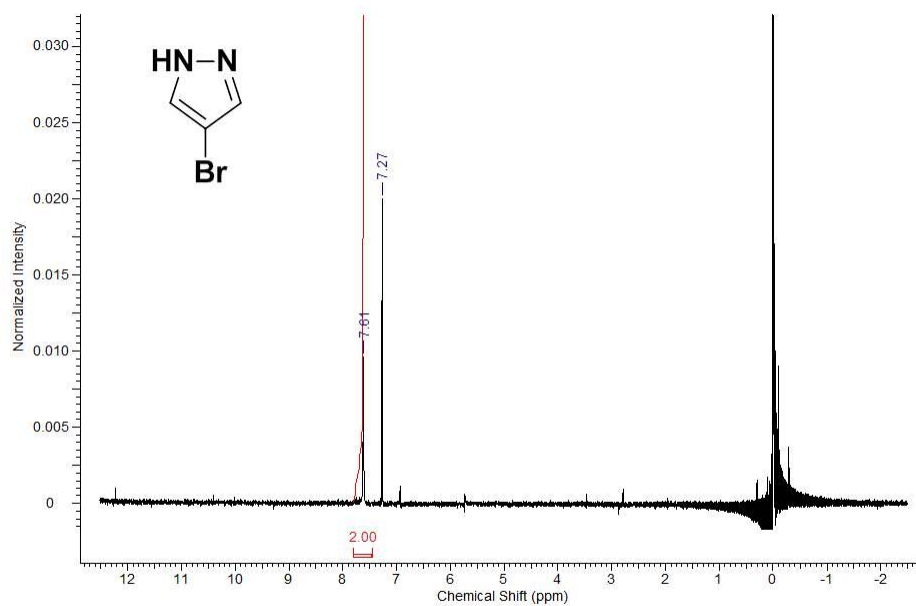


Figure A-3. ^1H NMR of 1.I

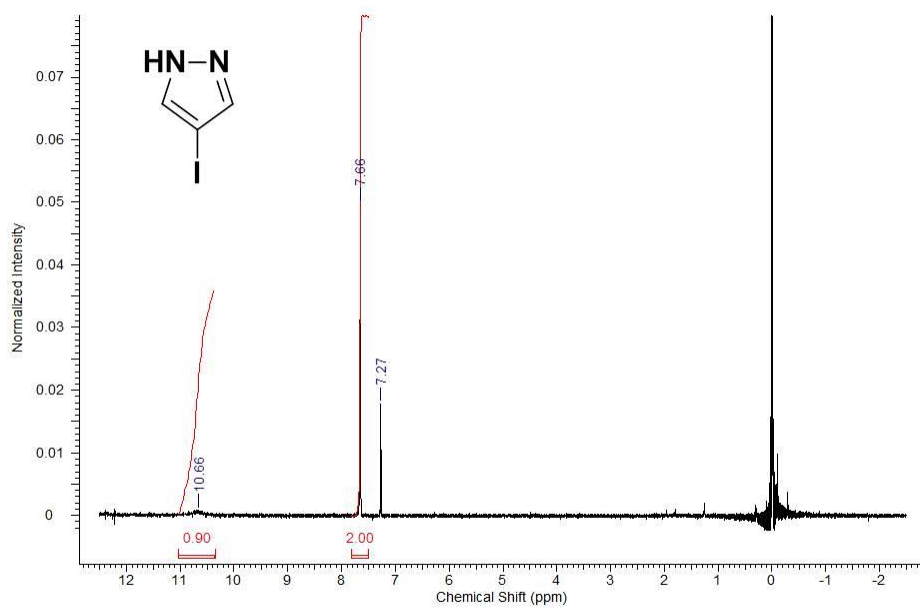


Figure A-4. ^1H NMR of 2.Cl

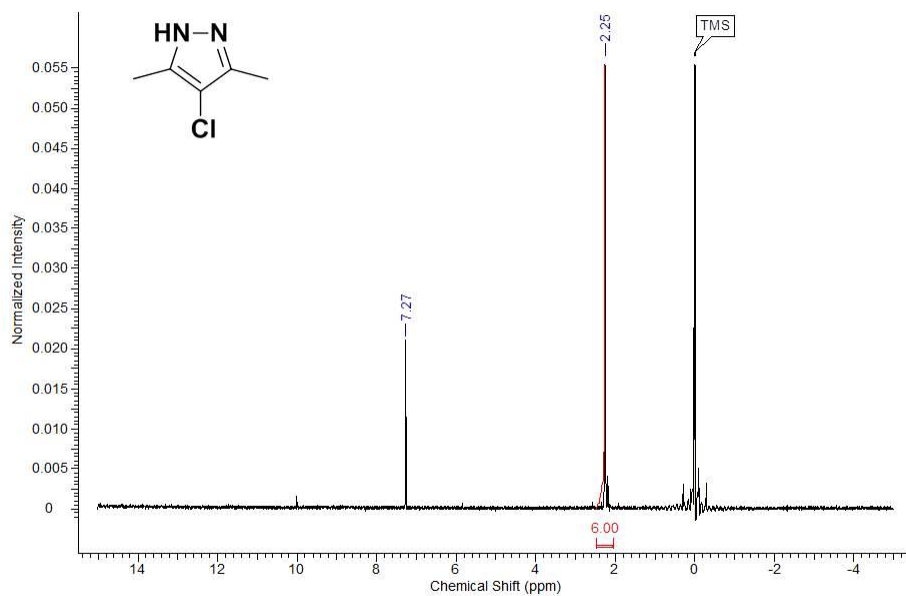


Figure A-5. ^1H NMR of 2.Br

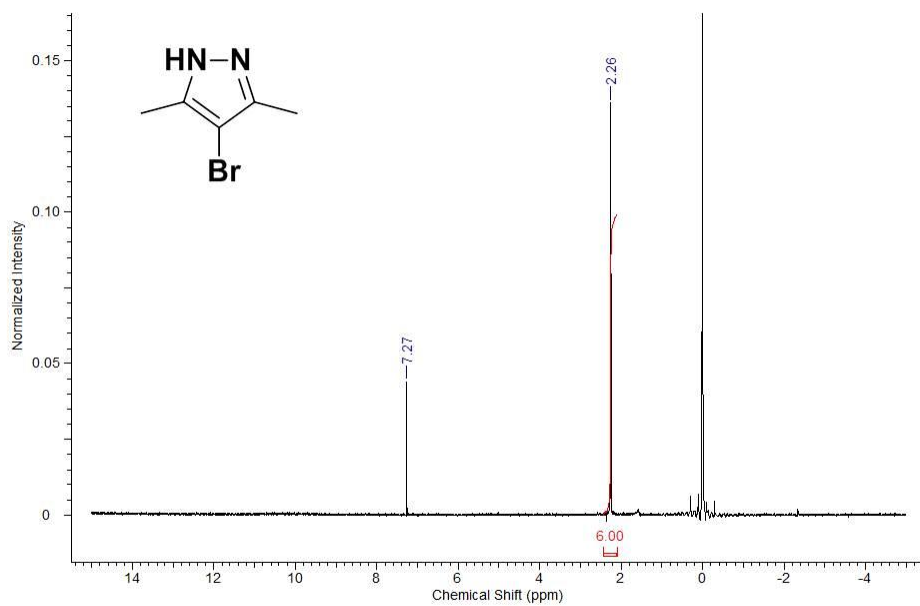


Figure A-6. ^1H NMR of 2.I

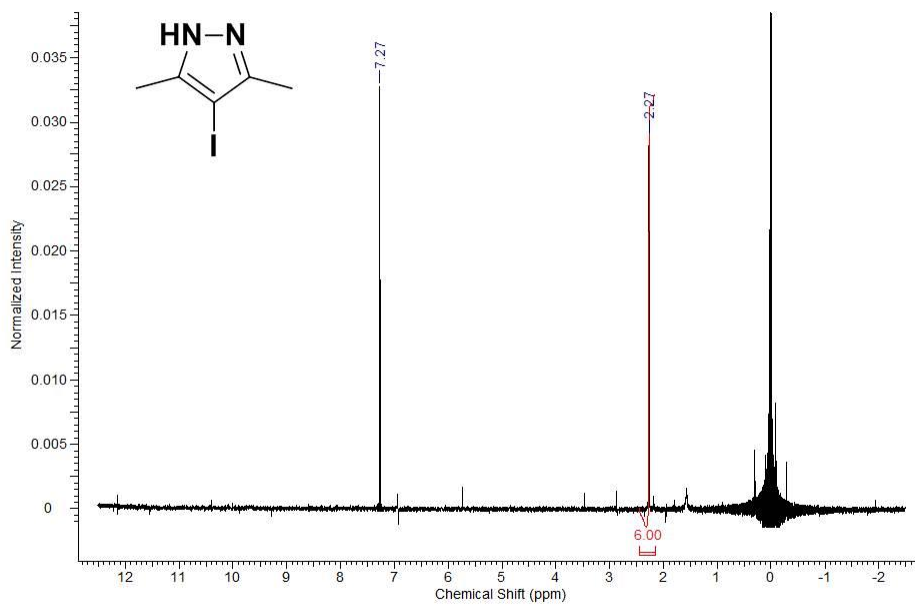


Figure A-7. ^1H NMR of 2

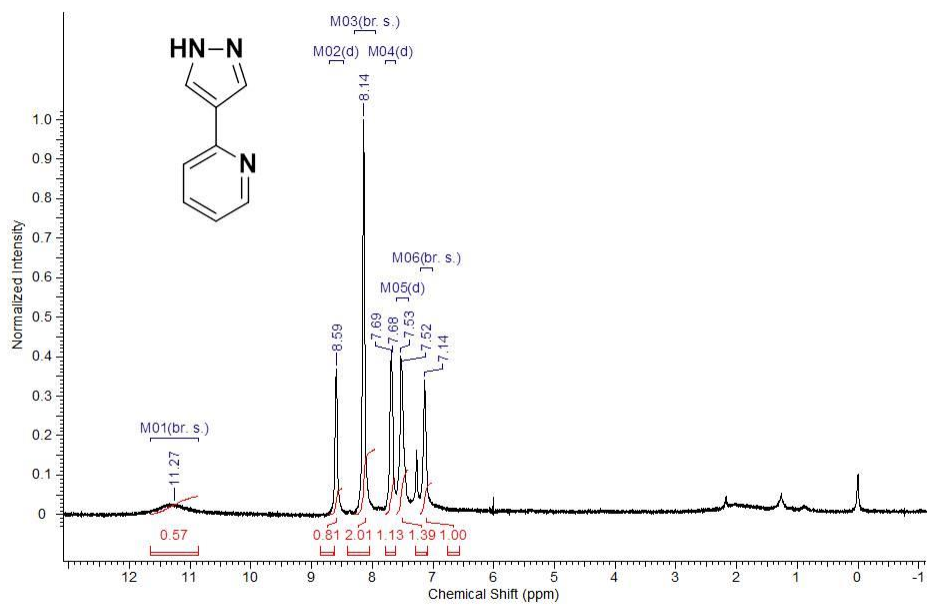


Figure A-8. ^1H NMR of 3

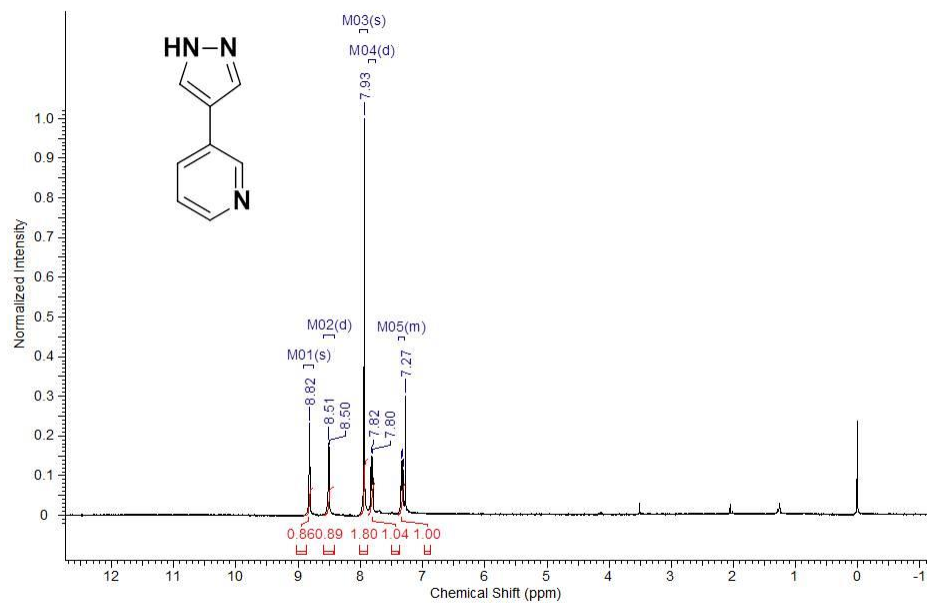


Figure A-9. ¹H NMR of 4

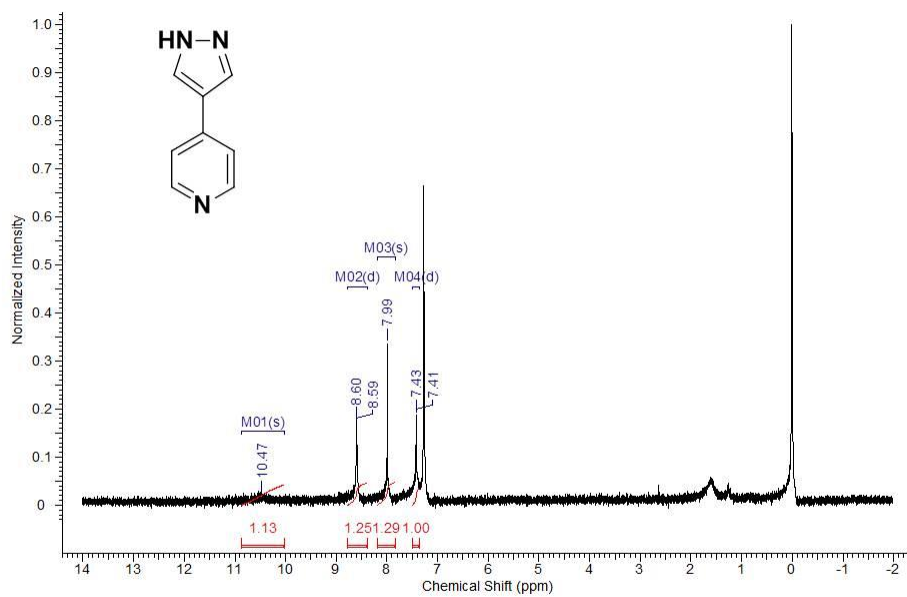


Figure A-10. ^1H NMR of IV_a

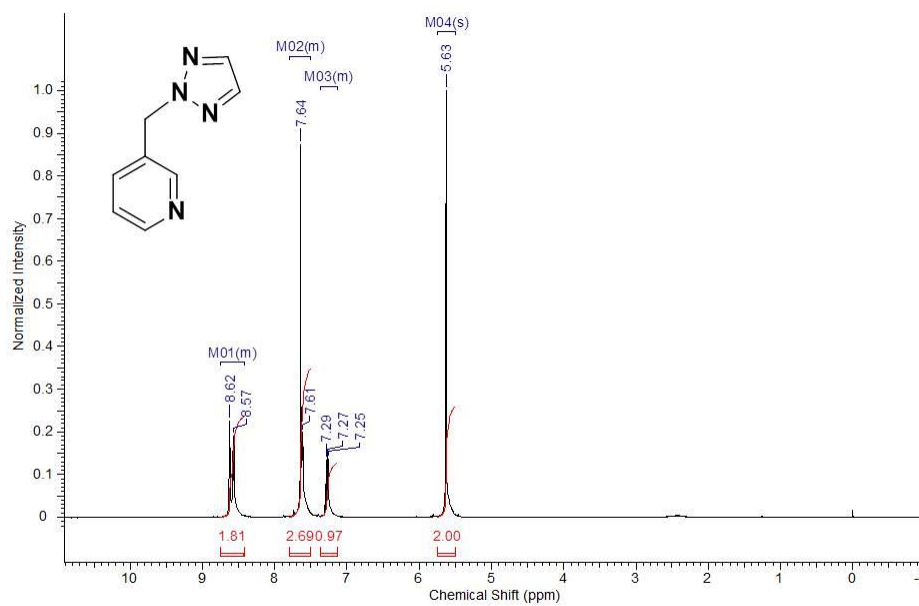


Figure A-11. ^{13}C NMR of IV_a

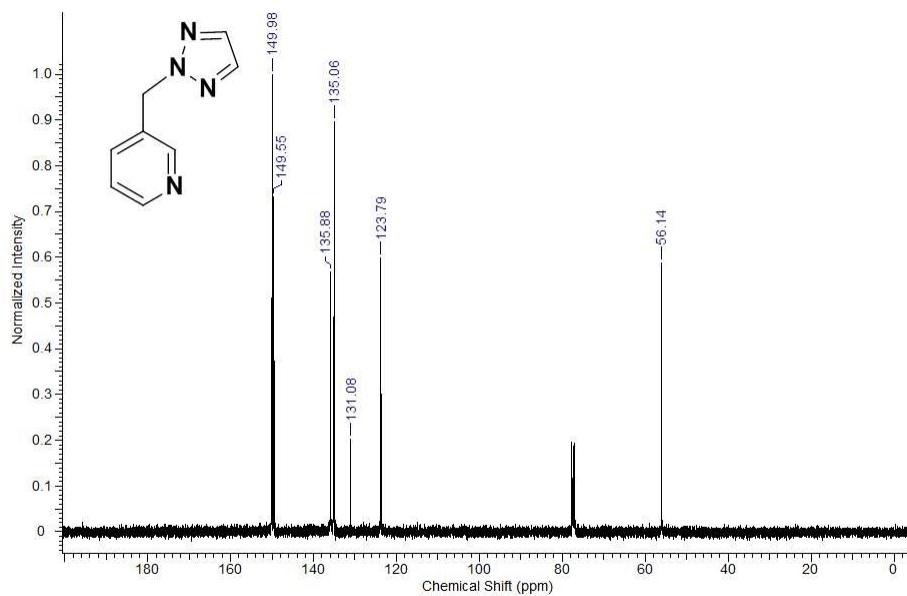


Figure A-12. ^1H of IV_b

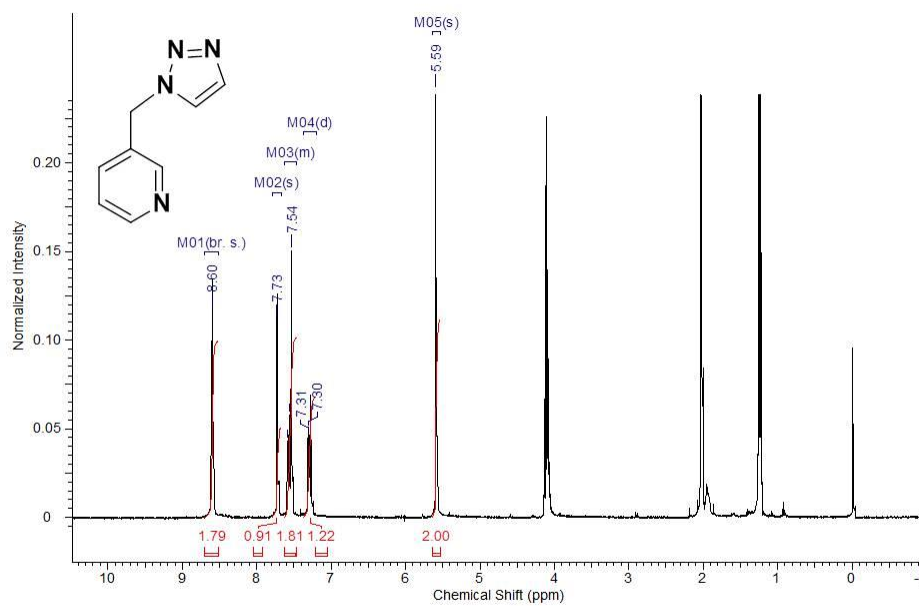


Figure A-13. ^{13}C NMR of IV_b

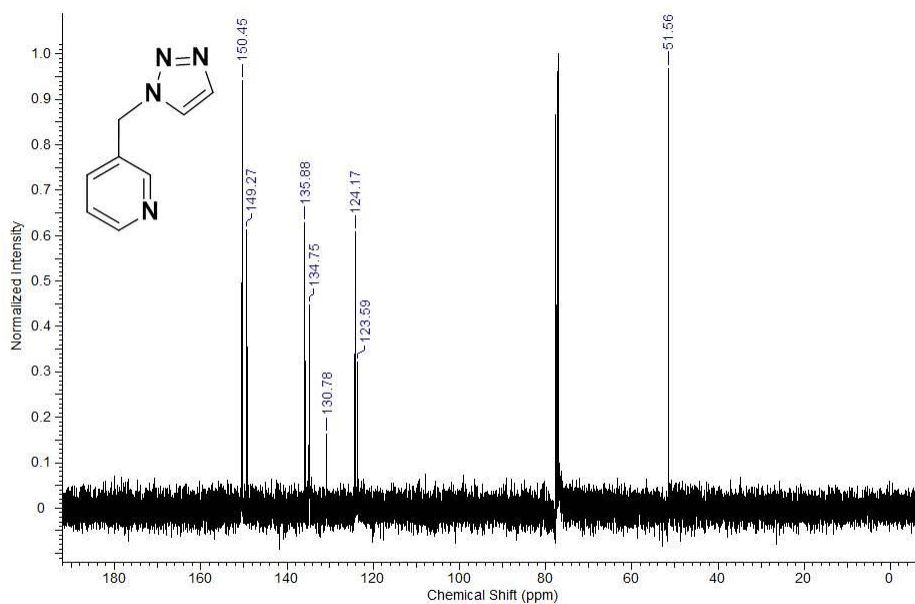


Figure A-14. ^1H NMR of V_a

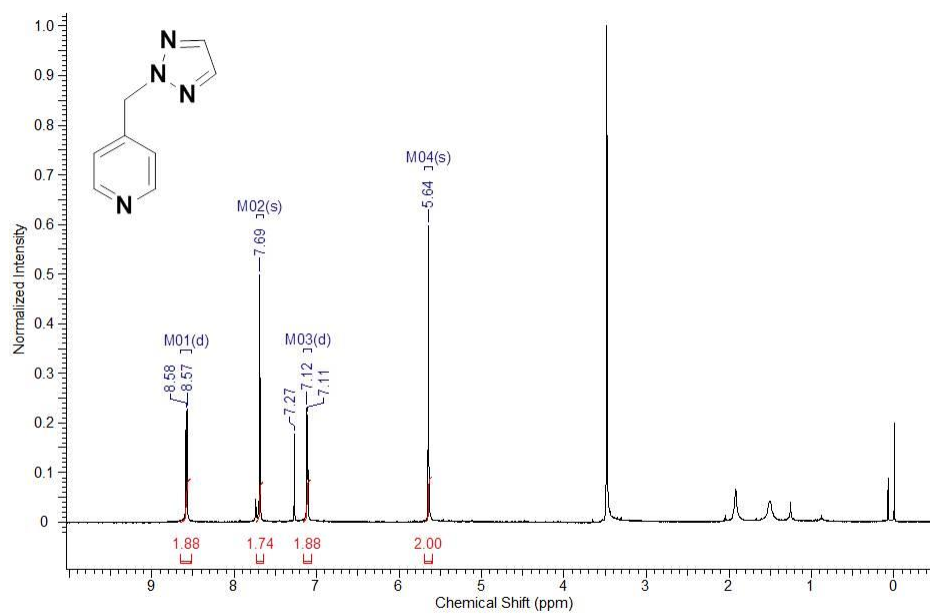


Figure A-15. ^{13}C NMR of V_a

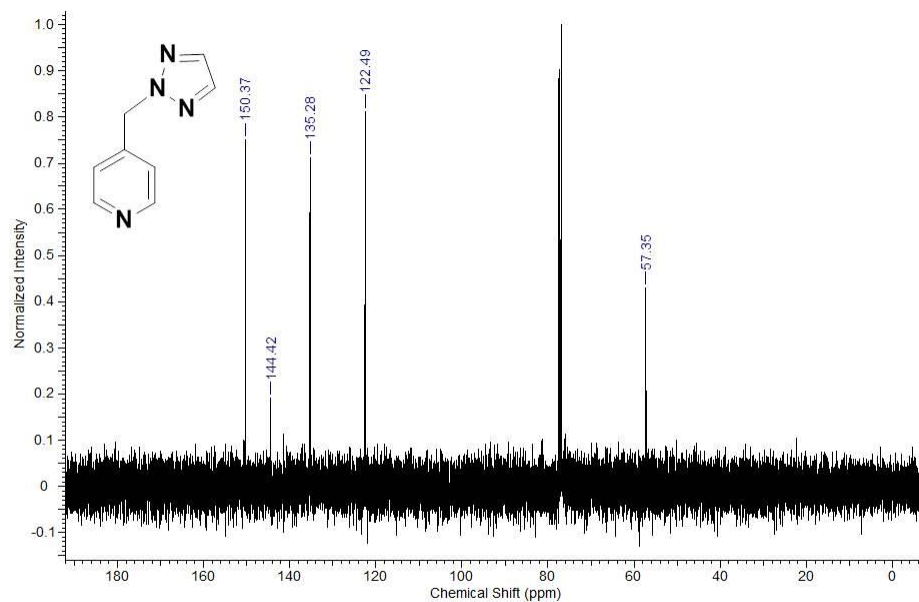


Figure A-16. ^1H NMR of V_b

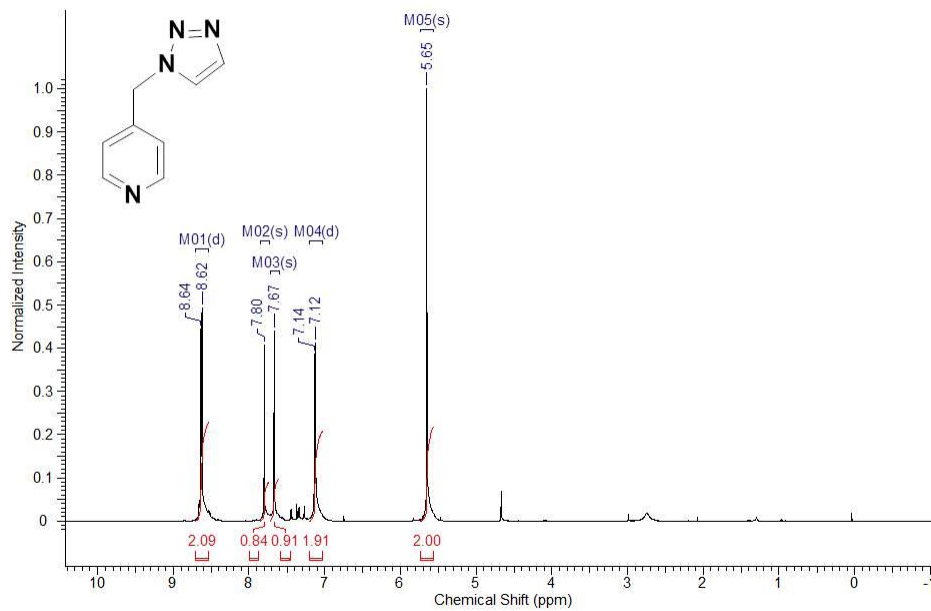


Figure A-17. ^{13}C NMR of V_b

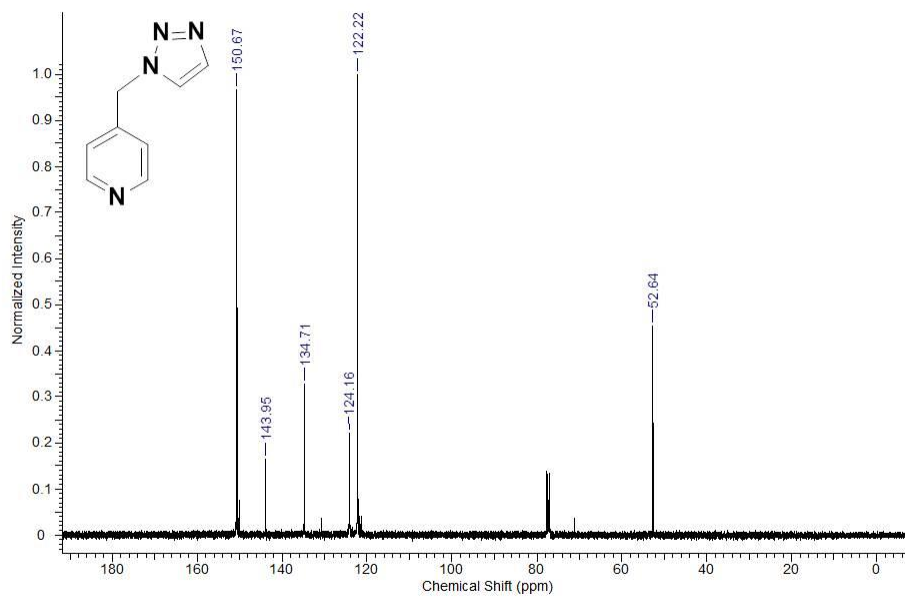


Figure A-18. ^1H NMR of VI

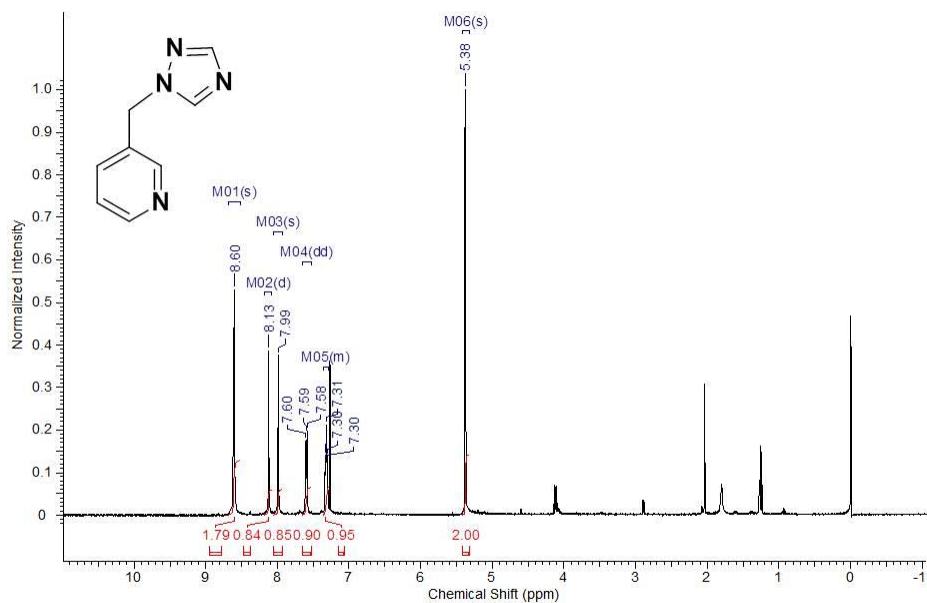


Figure A-19. ^{13}C NMR of VI

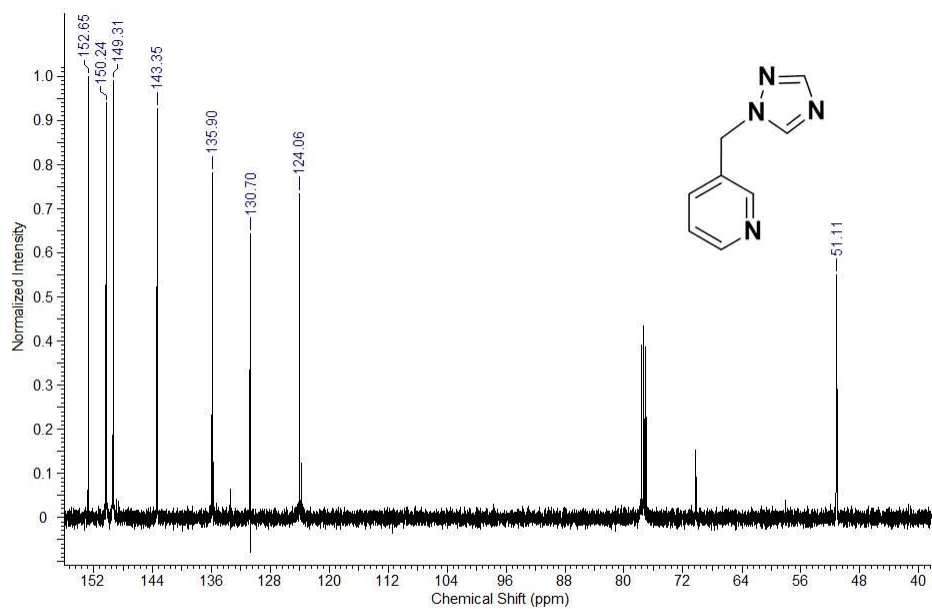


Figure A-20. ^1H NMR of VII

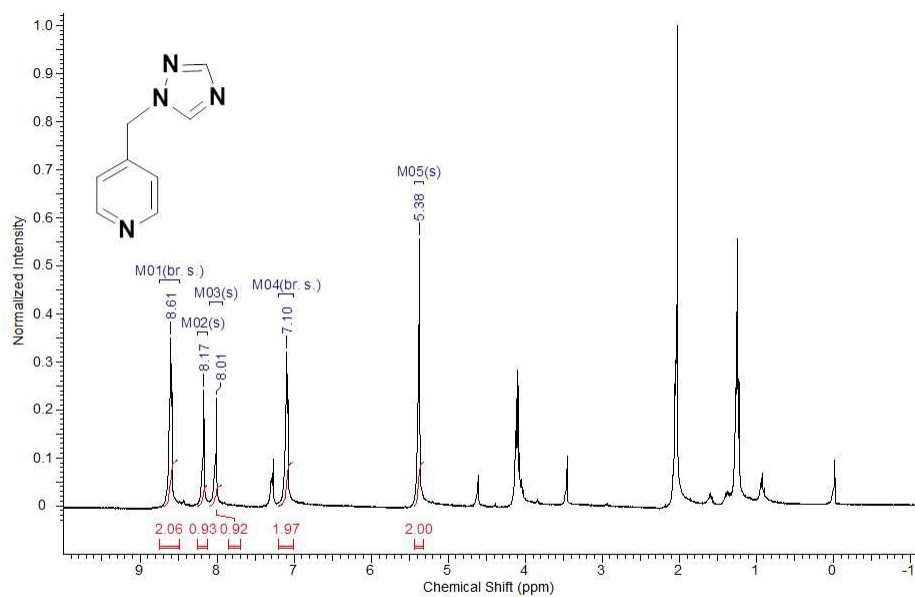


Figure A-21. ^{13}C NMR of VII

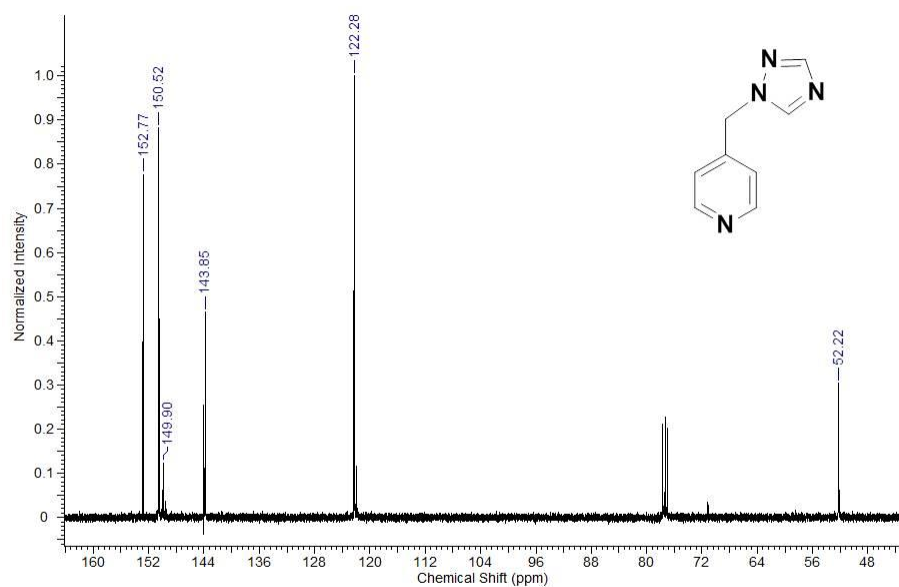


Figure A-22. ^1H NMR of 6.1

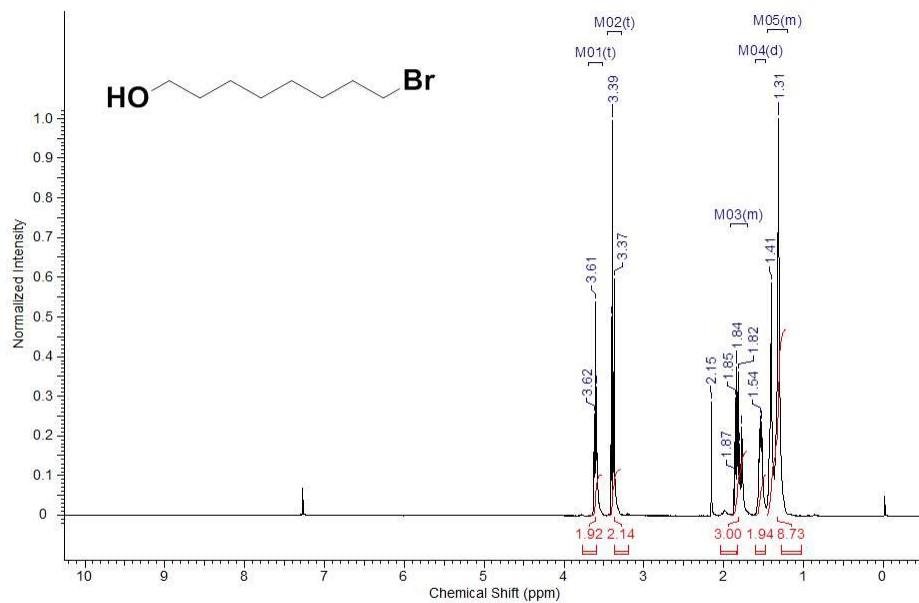


Figure A-23. ^1H NMR of 6.2

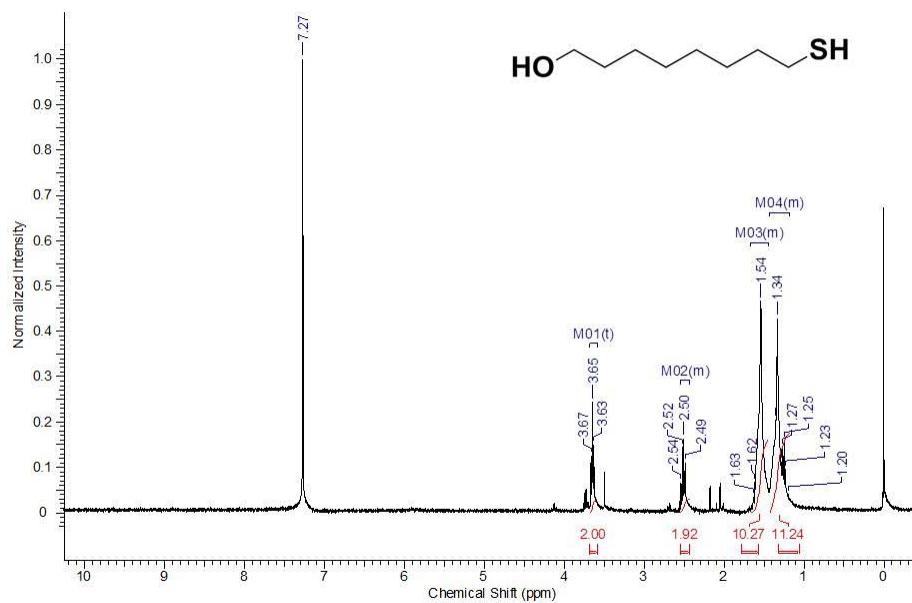


Figure A-24. ^1H NMR of 6.3

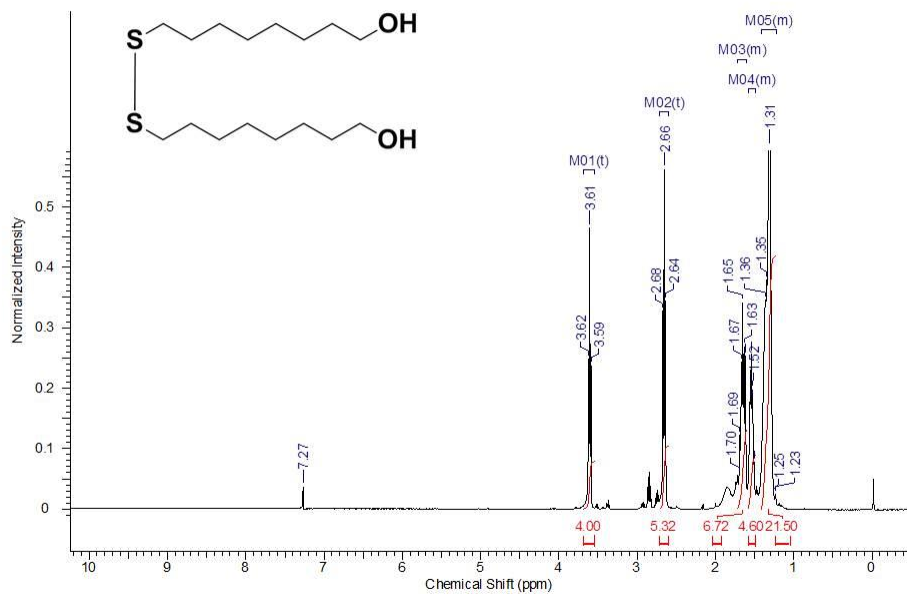


Figure A-25. ^1H NMR of 6.4

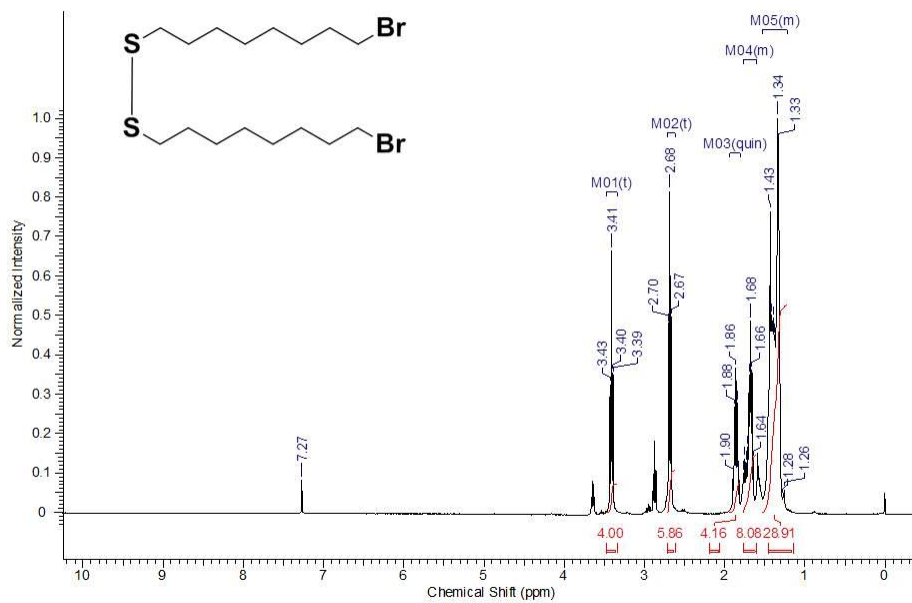


Figure A-26. ^1H NMR of 6.5

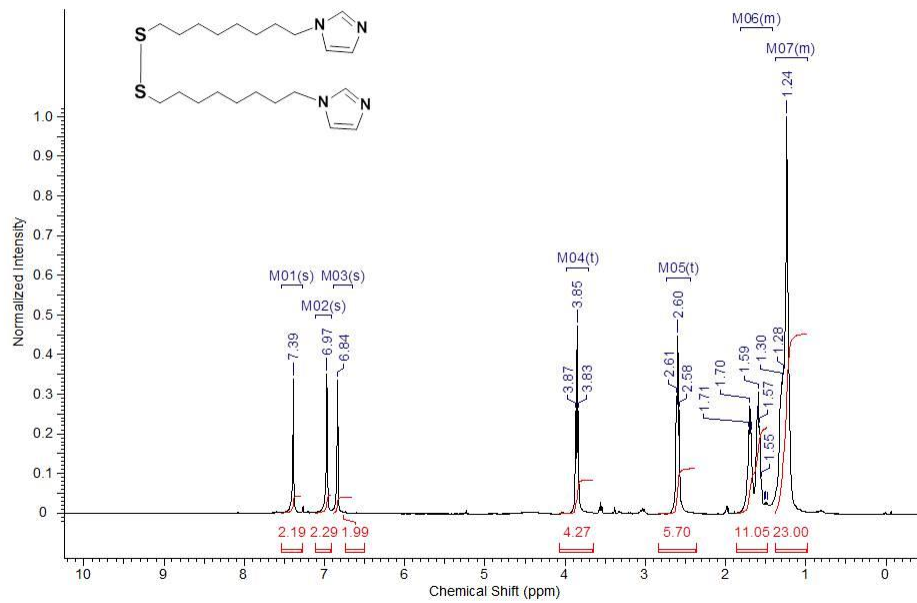


Figure A-27. ^{13}C NMR of 6.5

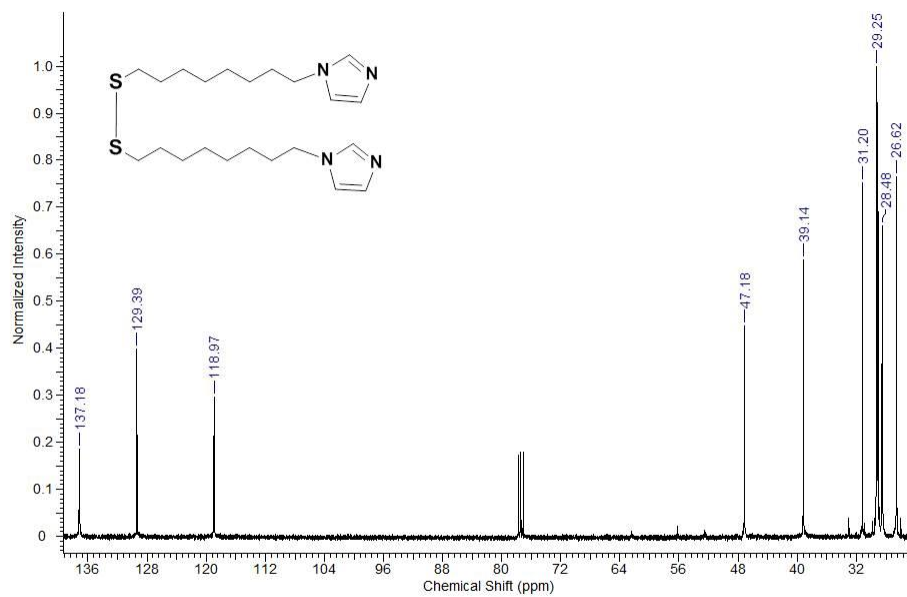


Figure A-28. ^1H NMR of 6.6

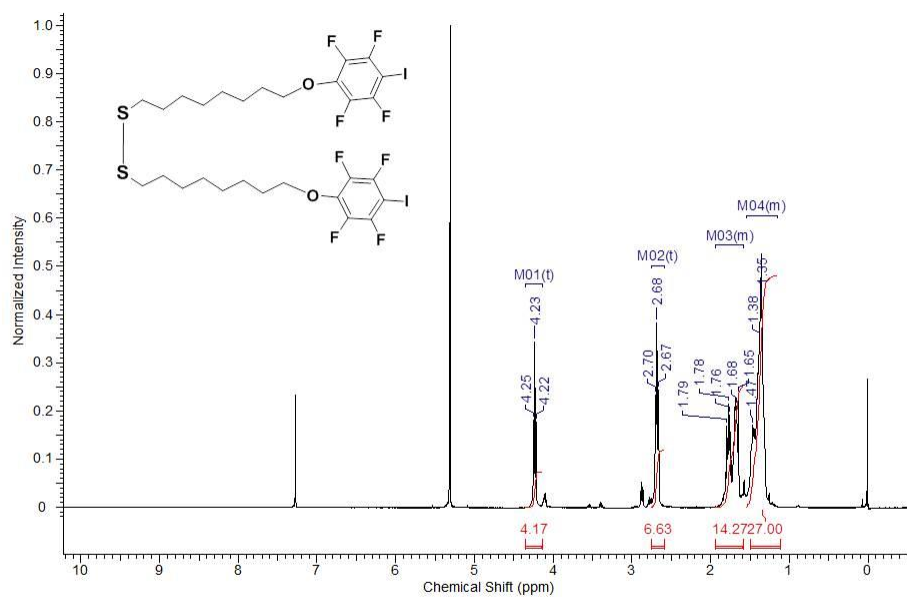


Figure A-29. ^{19}F NMR of 6.6

